STRATEGIES TO IMPROVE THE BIOACTIVTY OF COBALT CHROMIUM MOLYBDENUM USING SURFACE MODIFICATION TECHNIQUES

A thesis submitted by

Niall James Logan

For the degree of Doctor of Engineering to

University College London

2016

Department of Chemistry

Faculty of Mathematical and Physical Sciences

University College London

STATEMENT

I, Niall James Logan confirm that the work presented in this thesis is my own. Where information has been derived from other sources, I confirm that this has been identified in the thesis.

ABSTRACT

Titanium and its alloys are widely accepted as the current gold standard for orthopaedic and dental applications due to its good biocompatibility. Other materials, such as the cobalt alloy, cobalt chromium molybdenum (CoCrMo), can often be preferred due to its mechanical strength and resistance to wear, but despite these advantageous properties, CoCrMo does not have the biocompatibility of titanium alloys. This project examined novel strategies of enhancing the biocompatibility of CoCrMo. Firstly this involved coating the surface of CoCrMo in a thin, durable, layer of anatase titanium oxide (TiO_2) using atmospheric pressure chemical vapour deposition (CVD). TiO_2 is the same oxide layer as found on titanium and its alloys, and consequently, markers of osteogenic differentiation and adhesion were enhanced ($p < 0.05$) in human mesenchymal stem cells on TiO_2 surfaces *in vitro*. This early data implied that there was an enhanced rate of bone formation occurring on TiO_2 coated surfaces. Following this, functionalization of the TiO_2 layer using a process called ultraviolet photofunctionalization was investigated. Whilst the majority of cellular processes were not affected, markers of cell adhesion were significantly improved on functionalised surfaces. Ultraviolet photofunctionalization of the TiO_2 coated CoCrMo caused the substrates to transition from hydrophobic to superhydrophilic, which resulted in enhanced cell retention due to larger cells with increased actin and vinculin expression ($p < 0.05$). The topographical effect of CoCrMo was then examined by creating four topographies, ranging from smooth to moderately rough (SMO, AE, SLA50, SLA250). It was found that the moderately rough SLA250 surface was advantageous for osteogenic applications, by enhancing the osteogenic differentiation and retention of human mesenchymal stem cells ($p < 0.05$). Lastly, the combination of the topographically modified SLA250 surface and the TiO_2 coating was investigated. It was of interest to ascertain if the TiO_2 CoCrMo SLA surface could stimulate a similar cellular response to titanium SLA. It was found that a large amount of cellular processes were similar between all groups, although markers of osteogenic differentiation were significantly enhanced on the TiO_2 SLA CoCrMo surface to a comparable level as seen on titanium SLA ($p < 0.05$). This data implies that the application of the TiO_2 SLA surface to implants formed of CoCrMo, could promote enhanced bone formation and ultimately lead to reduced healing times following surgery and increased implant stability.

ACKNOWLEDGEMENTS

I would like to thank my primary supervisor Dr Peter Brett for his valuable guidance, input and interest throughout the entirety of my EngD, which without his expert opinion would have ended up a much more difficult process. I feel I am a better scientist having worked with Peter the past few years.

I would also like to thank my secondary supervisor Dr Laurent Bozec, who despite having a lesser role in my experimental work, always had a genuine interest in my personal wellbeing.

Alison Cross and Carlos Sotelo-Vasquez deserves special thanks for having spent many of their valuable hours, monotonously coating and checking many discs of titanium oxide coated cobalt.

I would also like to thank my colleagues at the Eastman Dental Institute who have made working in the department a real pleasure. Specifically, I'd like to thank the technicians Mr George Georgiou and Dr Graham Palmer who always helped out when I was trying to get to grips with a new piece of equipment. Dr Nicola Mordan also deserves a special mention as she was always there to give out valuable advice as I taught myself fluorescence microscopy.

As my EngD was sponsored by Corin Ltd, I'd like to thank those who I worked closely with including Simon Collins, Leona Morton and Alison Traynor.

Of course I would like to thank my parents whose support and encouragement has been with me always, but this was even more apparent during my doctorate.

Lastly, I'd like to thank my fiancé Orla who was always there to support me, listen to me and encourage me; for that I am truly grateful.

PUBLICATIONS AND CONFERENCE ABSTRACTS

Publications

Niall Logan, Laurent Bozec, Alison Traynor, Peter Brett "Mesenchymal stem cell response to topographically modified CoCrMo." Journal of Biomedical Materials Research Part A, 2015, DOI: 10.1002/jbm.a.35514

Niall Logan, Anas Sherif, Alison Cross, Simon Collins, Alison Traynor, Laurent Bozec, Ivan Parkin, Peter Brett, "TiO_2 coated CoCrMo: Improving the osteogenic differentiation and adhesion of mesenchymal stem cell in vitro." Journal of Biomedical Materials Research Part A, 2015. 103(3): p. 1208-1217.

Niall Logan, Alison Cross, Alison Traynor, Laurent Bozec, Ivan Parkin, Peter Brett, "Mesenchymal stem cell response to UV-photofunctionalized TiO_2 coated CoCrMo." RSC Advances, 2014, 4, 59847-59857. doi:10.1039/C4RA11524D

Niall Logan and Peter Brett, "The Control of Mesenchymal Stromal Cell Osteogenic Differentiation through Modified Surfaces," Stem Cells International, vol. 2013, Article ID 361637, 10 pages, 2013. doi:10.1155/2013/361637

Conference abstracts

"Mesenchymal stem cell response to UV photofunctionalized cobalt chromium molybdenum" – Orthopaedic Research Society – Las Vegas 28th-31st March 2015. Poster Presentation.

"The effects of cobalt chromium molybdenum surface topography on mesenchymal stem cells *in vitro*" – Orthopaedic Research Society – Las Vegas 28th-31st March 2015. Poster Presentation.

"Titanium oxide coated cobalt-chromium-molybdenum: Improving the osteogenic response of mesenchymal stem cells *in vitro*" – European Society for Biomaterials – Liverpool 31st August – 3rd September 2014. Poster Presentation.

"Titanium oxide coated cobalt-chromium-molybdenum; Improving the osteogenic differentiation of mesenchymal stem cells *in vitro*" – World Conference on Regenerative Medicine – Leipzig 23rd-25th October 2013. Oral Presentation.

TABLE OF CONTENTS

LIST OF FIGURES

LIST OF TABLES

LIST OF ABREVIATIONS

AFM	Atomic force microscopy
Al_2O_3	Aluminium oxide
ALP	Alkaline phosphatase
AM	Acetomehtylester
BMP	Bone morphogenic protein
BSP	Bone sialoprotein
CCMT	Cobalt chromium molybdenum coated with titanium oxide
CoCrMo	Cobalt chromium molybdenum
Con A	Concanavalin A
CVD	Chemical vapour deposition
DAPI	4′,6-Diamidino-2-phenylindole dihydrochloride
DMEM	Dulbecco's Modified Eagle's Medium
DMP1	Dentin matrix protein 1
DMSO	Dimethyl sulfoxide
E	Elastic modulus
ECM	Extracellular matrix
EDTA	Elthylenediaminetetraactic acid
EDX	Energy dispersive x-ray
ELISA	Enzyme linked immunosorbent assays
FBS	Foetal bovine serum
FGF	Fibroblast growth factor
FTIR	Fourier transform infrared spectroscopy
GM	Growth media

GPa	Gigapascal
H^+-ATPase	H+-adenosine triphosphatase
H_2SO_4	Sulfuric acid
HCl	Hydrochloric acid
ICP-MS	Inductively coupled plasma mass spectroscopy
IDGF	Insulin derived growth factor
keV	Kilo-eletronvolts
MAO	Micro arc oxidation
MCS-F	Macrophage colony stimulating factor
MEM-α	Minimum essential media α
mL	Millilitre
MS	Mass spectrometer
MSC	Mesenchymal stem cell
N	Newtons
nm	Nanometres
OM	Osteogenic media
PBS	Dulbecco's phosphate buffered saline
PDGF	Platelet derived growth factor
PFA	Paraformaldehyde
PI	Propidium iodide
PMMA	Polymethylmethacrylate
QMF	Quadrupole mass filter
R_a	Arithmetic average roughness
RANKL	Receptor activator of nuclear factor kappa-B ligand

RF	Radio frequency
RPM	Revolutions per minute
Runx	Runt related factors
RT	Room temperature
SEM	Scanning electron microscopy
SiC	Silicon carbide
SLA	Sand blasted acid etched
TCP	Tissue culture plastic
TGF-β	Transforming growth factor beta
Ti-6Al-4V	Titanium aluminium vanadium
THA	Total hip arthroplasty
TJA	Total joint arthroplasty
TKA	Total knee arthroplasty
UHMWPE	Ultra high molecular weight polyethylene
USA	United States of America
UV	Ultraviolet
XRD	X-ray diffraction

LIST OF REAGENTS/KITS/CHEMICALS

Product	**Supplier**	**Code**
ALP assay	Abcam	ab83369
Vinculin antibody	Abcam	ab18058
AlamarBlue	AbD Serotec	BUF012A
Nitric acid	BDH	19088 5E
Triton X-100	BDH	30632 4N
Calcium Assay kit	Bio Assay Systems	DICA-900
Tip-less cantilevers	Bruker	NP-010
250µm blasting media	Cobra	15851005
50µm blasting media	Cobra	15941205
DMEM	Gibco	31885-023
FBS	Gibco	10270-106
MEM-α	Gibco	22571-020
Trypsin/EDTA	Gibco	R-001-100
Alexa fluor 488 Phalloidin	Life Technologies	A12379
Alexa fluor 488 goat anti-mouse	Life Technologies	A11001
Alexa fluor 568 goat anti-mouse	Life Technologies	A11031
Live/Dead kit	Life technologies	R37601
Propidium iodide	Life Technologies	P3566
OsteoImage kit	Lonza	PA-1503
PBS	Lonza	17-512F

Ethanol	Millipore	108543
Glass beads	Polysciences	07666
L-ascorbic acid	Sigma-Aldrich	A8960
β-glycerol phosphate	Sigma-Aldrich	G9891
DAPI	Sigma-Aldrich	D9542
Dexamethasone	Sigma-Aldrich	D9402
DMSO	Sigma-Aldrich	D2650
Goat serum	Sigma-Aldrich	G9023
Hexamethyldisilazane	Sigma-Aldrich	379212
Hydrochloric acid	Sigma-Aldrich	258148
Isopropanol	Sigma-Aldrich	190764
Paraformaldehyde	Sigma-Aldrich	P6148
Penicillin-streptomycin	Sigma-Aldrich	P0781
Serum free media	Sigma Aldrich	14571C
Sulfuric acid	Sigma-Aldrich	320501
Type I COL antibody	Sigma-Aldrich	C2456
1000 SiC paper	Struers	40400011
DP-Lubricant Blue	Struers	40700006
DP-Suspension P 3µm	Struers	40600251
MD Dac	Struers	40500071
SpeciFix-20	Struers	40200048

CHAPTER ONE:

INTRODUCTION

1. LITERATURE REVIEW

1.1. BONE

Bone is a highly vascular, constantly changing, mineralised connective tissue that is significant for its resilience and hardness. The specialised tissue consists of cells embedded in an organic matrix, which is rich in inorganic mineral (Aiello and Dean, 1990). The primary function of bone is to provide mechanical support, as well as offer internal support in the form of providing attachment sites for muscles and protective cavities to shield vital organs such as the heart and lungs. To successfully fulfil these roles bone needs to be stiff enough to resist deformation, yet flexible enough to absorb energy from movements, resulting in the need for a complex internal structure which varies considerably with age and site. Accompanying these mechanical requirements is also the need for haematopoiesis and maintenance of calcium homeostasis (Fuchs, 2009).

1.1.1. BONE ANATOMY

What gives bone its unique structural properties is its anatomy and the different forms of bone tissue present in the skeleton. There are two types of bone tissue, each with the same matrix composition but drastically different function and structure. These two distinct types of bone tissue are known as cortical and trabecular bone. Approximately 80% of the total skeletal mass is made up of cortical bone, which has low porosity and high matrix mass per unit volume. These features allow cortical bone to contribute to the mechanical role of bone, as it can cope with high compressive forces. Although cortical bone appears to be a solid mass, it does contain microscopic pores that constitute around 10% of its volume, that allow for the delivery of nutrients and vascular supply. Due to the features of cortical bone, it is distributed primarily within long bones of the skeleton. There are three distinct regions of long bones; the proximal and distal epiphyses, the diaphysis, and the metaphysis. Cortical bone is prominently featured in the diaphysis region, as it forms a thick cortical shell, known as the cortex, which surrounds the medullary canal filled with bone marrow. This structure provides the bone with great strength and rigidity, alongside the lightness that is required for movement. Towards the metaphysis and epiphyses regions, cortical bone thins and trabecular bone becomes prominent. Trabecular bone has extremely high porosity with the total bone volume

consisting of 50-90% pores. With an almost sponge-like resemblance, it is formed of trabeculae, which are an orderly arranged network of horizontal and vertical rod and plate like structures that create a porous network. This porous structure only provides approximately one tenth the compressive strength of cortical bone, although trabecular bone has a different primary function to cortical bone. The high porosity results in an increase in surface area which helps facilitate calcium homeostasis and haematopoiesis. Trabecular bones unique internal structure also helps contribute to the mechanical role of bone, by evenly distributing load and absorbing energy (Fuchs, 2009). This is particularly important in the vicinity of joints where trabecular bone is prominently found. It is important to note that trabecular bone has been observed to be lost earlier than cortical bone (Riggs et al., 2008), which contributes to cases of osteoporosis in sites such as the femoral neck. Bone strength in these regions is influenced by trabecular connectivity, which when lost, leaves the region mechanically weak (Fuchs, 2009).

1.1.2. BONE CELLS

1.1.2.1. OSTEOBLASTS

Osteoblasts are mononuclear cells that contain a large circular nucleus and have high internal concentrations of rough endoplasmic reticulum, mitochondria, actin and Golgi apparatus. They originate from mesenchymal stem cells (MSCs) found in bone marrow which are stimulated to form into osteoprogenitor cells via a differentiation process. Numerous factors can then further induce the differentiation of these osteoprogenitor cells into osteoblasts, such as, interleukins, bone morphogenic proteins (BMP), platelet-derived growth factor (PDGF), insulin derived growth factor (IDGF), fibroblast growth factor (FGF) and transforming growth factor-β (TGF-β). Osteoblast internal cytoskeletal proteins, such as actin, help to preserve the structural integrity of the cell whilst assisting in cell attachment and movement. The primary function of osteoblasts is to secrete and deposit an extracellular matrix (ECM), which can eventually become mineralised bone tissue. Osteoblasts primarily secrete an organic matrix, in the form of an osteoid that can consist of type I collagen, osteocalcin, osteopontin, osteoprotegrin, proteoglycans and growth factors such as BMPs (Jayakumar and Di Silvio, 2010). Osteoblasts can then consequently assist in the mineralisation of the osteoid, which involves increased alkaline

phosphatase (ALP) activity (Golub and Boesze-Battaglia, 2007), saturation of ECM fluids at specific zones such as calcium nucleation sites, and the production of osteocalcin, which helps increase the local calcium concentration via actively binding to calcium. Furthermore, the release of matrix vesicles containing ALP and pyrophosphatase help new crystal formation, with ALP raising the local phosphate concentration and pyrophosphatase acting as an anti-inhibitory for the process by degrading pyrophosphate, a key regulator of calcification (Golub, 2009).

1.1.2.2. OSTEOCYTES

Osteocytes make up 90% of bone cells found in the adult skeleton and are derived from osteoblasts. As osteoblasts on the surface of the tissue secrete osteoid, they connect with already embedded cells and eventually become engulfed in osteoid, and are then referred to as osteoid-osteocytes. When the osteoid becomes mineralised, these cells then become mature osteocytes which interconnect with one another by long dendritic processes that travel along small tunnels known as canaliculi. This novel feature allows for the communication of signals between osteocytes, as well as the ability to communicate with cells on the bone surface and in the marrow (Bonewald, 2007). It was widely believed that osteocytes were passive cells but it is now thought that osteocytes play the role of a mechanosensor, transforming mechanical forces into biochemical signals capable of triggering bone resorption or formation (Chen et al., 2010b). Osteocytes may also play a role in mineral metabolism, as it has been shown that the deletion or mutation of dentin matrix protein 1 (DMP1), a molecule highly expressed in osteocytes, resulted in hypophosphatemic rickets in a mice model (Feng et al., 2006).

1.1.2.3. OSTEOCLASTS

Osteoclasts, the primary cell involved in bone resorption, are large multinucleated cells derived from the macrophage linage. For macrophages to become osteoclasts, MSCs and osteoblasts must be present, as these accessory cells express the molecules, receptor activator of nuclear factor kappa-B ligand (RANKL) and macrophage colony stimulating factor (M-CSF), necessary for osteoclastogenesis to occur. The primary role of

osteoclasts within the body is the resorption of bone, which is a complex multistep process of removing bone tissue. Once the differentiated osteoclasts attach to the bone tissue via anchoring proteins, they have the ability to polarise their cellular membrane to form a ruffled membrane, were it is believed this ruffling effect may represent the transportation of acidifying vesicles into the plasma membrane. The osteoclast then generates its own microenvironment via a sealing zone, which forms a ring, primarily made of f-actin, around the ruffled membrane. This isolated microenvironment can then begin to be demineralised by the rapid release of protons, a process mediated by H^+-adenosine triphosphatase (H^+-ATPase) in the ruffled membrane, which leads to the secretion of HCl, lowering the pH in the microenvironment to ~4.5. Demineralised organic matrix can then begin to be degraded by the lysosomal enzyme cathepsin K, with the products of the degeneration being endocytosed and released at the cell surface (Teitelbaum, 2000). Further functions of osteoclasts in bone tissue are currently being debated, which include modulation of differentiation of other cells, regulation of the movement of hematopoietic cells from bone marrow to bloodstream, and participation in immune responses (Boyce et al., 2007).

1.1.3. STEM CELLS

The role of MSCs in bone repair is well documented, with the term, 'stem cell', referring to elements capable of self-renewal, proliferation, differentiation and regeneration of tissues *in vivo* (Baldini, 2009). Primarily there are three main groups of stem cells, which are known as embryonic, adult and the more recent, induced pluripotent stem cells. Embryonic stem cells are derived from the inner cell mass of a blastocyst and have the potential to differentiate into cells of any desired linage. However, there are strict regulations in place for the use of embryonic stem cells, as well as moral and ethical issues, which are based around when the cells are harvested, the embryo does not survive (Cogle et al., 2003). Induced pluripotent and adult stem cells are not surrounded with the same controversy as embryonic stem cells as they do not involve the destruction of an embryo. Induced pluripotent stem cells are typically adult stem cells that have been genetically reprogrammed i.e. forced to change from their multipotent state to a pluripotent form (Takahashi et al., 2007). Induced pluripotent stem cells have great potential in the field of regenerative medicine and tissue engineering, although the

research is still in its infancy and there are questions regarding the safety of this cell type, as studies have reported potential carcinogenic behaviour (Gutierrez-Aranda et al., 2010). Adult stem cells, the group which MSCs belong to, are located and isolated from healthy adult tissues, such as bone marrow and are multipotent, due to their ability to differentiate into the different linages of the parent tissue; For example, bone marrow derived stem cells have the ability to differentiate along the osteogenic, chondrogenic and adipogenic linages. MSCs are adult non-haematopoietic stromal stem cells that have the capability to proliferate through multiple passages whilst maintaining their characteristics and differentiate into the various specialist cell types of their parent linage (Pittenger et al., 1999). MSCs can be found at various sources such as bone marrow, periosteum, adipose tissue, vessel walls, synovial fluid, muscle tissue, tendon and skin (Wang et al., 2013b). The role of MSCs in bone repair is to target and colonise the site of injury where repair is necessary, then differentiate along their osteogenic linage, forming osteoprogenitor cells and eventually mature osteoblasts capable of depositing new bone tissue.

1.1.4. CELLULAR PROCESSES

1.1.4.1. OSTEOGENESIS

The mechanisms of osteogenic differentiation in MSCs are thought to be similar to the events during normal skeletal development through embryogenesis (Deschaseaux et al., 2009). Transcription factor Runx2, of the runt related factors family (Runx), is widely accepted to be the master switch for early osteogenesis, triggering MSCs to form into osteoprogenitor cells. In Runx2 knockout mice ($Runx2^{-/-}$), ossification was completely missing due to the absence of mature osteoblasts, highlighting the importance of this gene for early osteogenesis (Komori et al., 1997). Runx2 is not solely responsible for the osteogenic differentiation of MSCs. Osterix is another transcription factor which acts downstream of Runx2 and is just as important for bone formation. Whereas Runx2 is responsible for the MSC to osteoprogenitor transition, osterix is responsible for converting theses osteoprogenitor cells into fully functioning osteoblasts (Cohen, 2006). In osterix null mice ($Osterix^{-/-}$) various osteoblastic markers were shown to be affected, including reduced type 1 collagen, and no expression of osteopontin, osteocalcin, bone sialoprotein (BSP) and osteonectin (Nakashima et al., 2002). Other factors that are

important for osteogenesis include the Wnt canonical signalling pathway, found to trigger osteoprogenitor proliferation and up-regulate osteogenic genes (Chen and Alman, 2009, Liu et al., 2009), and BMPs, multifunctional growth factors belonging to the TGF-β family (Chen et al., 2004).

1.1.4.2. CELL ADHESION

MSCs are an adherent cell type that require anchorage to a surface or material before they are capable of proliferation or differentiation. For this to transpire, physical interactions that allow the cell to communicate with its outside microenvironment must occur, where signals can then be translated into cellular processes such as adhesion or migration. Known as focal adhesions, these large molecular complexes link the cell to its microenvironment and involve numerous components that must work coherently. Focal adhesions are based around a transmembrane α – β integrin that binds to the extracellular matrix of the cells external microenvironment (Lo, 2006). Integrins do not contain actin binding sites, therefore the signals from the microenvironment must be mediated through regulatory and structural proteins. One protein of significance in focal adhesion formation and regulation is vinculin. Specifically, it has been found that the head region of vinculin can regulate integrin dynamics and clustering, whereas the tail region is a binding site for the cytoskeletal protein actin (Humphries et al., 2007). It is the tail region of vinculin that links the protein to the mechanotransductive components of the cell. Vinculin does not bind directly to the integrin, but through the proteins talin and paxillin, which play a role in recruiting focal adhesion kinase (FAK), an important receptor and regulator of cell adhesion and motility (Mitra et al., 2005). FAK also plays a role in the phosphorylation of the α-actinin protein which binds to vinculin and also crosslinks actin fibres, securing them to the focal adhesion complex. Other integrin associated proteins in found focal adhesions include PINCH and Src, which play a role in relaying signals from the extracellular microenvironment to downstream effectors (Wu, 2007). It is the complex system found at focal adhesions that allows for processes such as cell adhesion and motility onto functional biomaterial surfaces, such as those found in hip and knee arthroplasty devices.

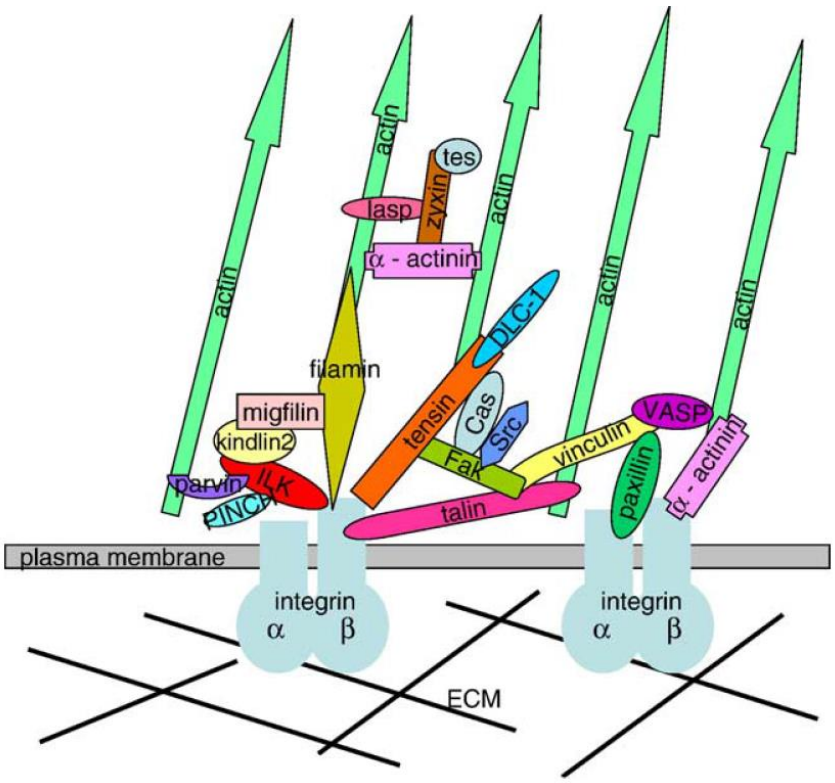

Figure 1 A schematic of the components that work coherently in focal adhesion complexes, taken from (Lo, 2006).

1.2. TOTAL JOINT ARTHROPLASTY

The role of a total hip or knee arthroplasty device is to return a joint to its full working function by replacing any diseased or compromised tissues, therefore reducing or relieving any prior pain and improving the patient's quality of life. The need for total joint arthroplasty (TJA) procedures can arise from numerous degenerative diseases such as osteoarthritis, which affects the articulating cartilage and subchondral bone, resulting in stiff painful joints. TJA devices are formed of biomaterials which can be described as either natural or synthetic materials that are used to create implants or structures, to replace a lost tissue or organ within the body, therefore restoring the original form and function. It is common in the field of orthopaedics for two or more different classes of biomaterial to be grouped together to form a medical device, as each class has individual strengths and weaknesses due to their different compositions and properties (Hoffman, 2004).

1.2.1. TOTAL HIP REPLACEMENT

THA devices are comprised of two major components: a femoral component, composed of a long stem with a femoral head, and an acetabular component, consisting of a mechanically strong outer cup with an inset internal bearing surface designed to receive the articulating head of the femoral component. The femoral stem is formed of metal such as titanium alloy. The use of titanium as a biomaterial dates back to the 1930s (Gonzalez-Carrasco, 2009), but it was the creation of the alloy Ti-6Al-4V in the 1950s that significantly increased the popularity of the material. Ti- 6Al-4V lent itself nicely to the biomedical industry due to its high corrosion resistance and excellent biocompatibility, and was used in surgical implants by the 1960s (Geetha et al., 2009). What makes titanium alloys more advantageous for medical applications, is the materials ability to promote osseointegration, which is the formation of a direct interface between the implant surface and bone without the need for connective soft tissue (Puleo and Nanci, 1999). Osseointegration was discovered in 1952 by Per-Ingvar Brånemark of Sweden during an experiment designed to study blood flow in the bone tissue of rabbits. Viewing chambers formed of titanium were implanted directly into the fibula and when the time came to remove the chambers, the bone had integrated completely with the titanium (Branemark, 1983). Brånemark later went on to further investigate this finding which resulted in the implementation of osseointegration into dental implants by the 1960s (Laney et al., 1986). It is this heightened biocompatibility that gives titanium alloy its distinct advantage over other metallic biomaterials, and when combined with titanium's low density and potential to be greatly strengthened by alloying and thermo-mechanical processing, makes it highly favourable for biomedical applications such as the femoral component of a THA device.

The head of the femoral component experiences continuous cyclic loading and must have excellent wear resistance to prevent the formation of wear debris within the joint and is usually formed of metal or ceramics, such as alumina or zirconia composites. Ceramics are highly stiff, inert materials which have superior wear resistance over other classes of biomaterials. Despite this, ceramic biomaterials are limited in their use, due to their brittleness which can make them prone to cracks and fractures. Zirconia does not have the same low fracture toughness as alumina, although suffers from an undesirable aging

process due to hydrothermal degradation. Development of composite ceramic materials consisting of both zirconia and alumina have shown increased performance leading to their further application in arthroplasty devices (Kluess, 2008).

The acetabular component outer shell is commonly metal, such as titanium alloy, with the internal bearing surface formed of either ultra-high molecular weight polyethylene (UHMWPE) or composite ceramic due to their excellent resistance to wear, although sometimes can also be formed of metal. UHMWPE is a polymer which has been used for over 30 years as the lining of the acetabular component in total hip arthroplasty (THA) devices, due to its mechanical strength, biocompatibility and low rate of wear. UHMWPE's resistance to wear is of great importance as the component undergoes persistent cyclic loading and wear debris created over time can migrate causing inflammation and potentially cause the device to fail (Katti, 2008). Efforts to improve the properties of UHMWPE are on-going and it has been observed that γ irradiation can improve wear resistance via crosslinking and increased crystallinity (Endo et al., 2001). The combination of biomaterial classes at this articulating interface is an important topic in the field of tribology. The history of THA shows the first metal-on-metal implant pioneered by George Kenneth McKee in the 1950s who adopted stainless steel and later CoCrMo materials in his devices (McKee and Watson Farrar, 1966). These were quickly over shadowed by John Charnley's metal-on-polymer low friction arthroplasty device which utilised a polymer insert with an extremely low coefficients of friction, which went on to be the gold standard for at least half a century (Charnley, 1961).

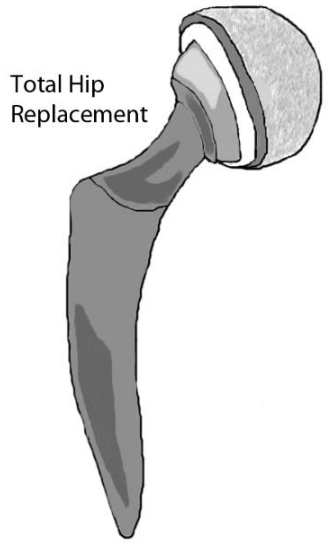

Figure 2 Illustration of a total hip replacement device, consisting of the femoral and acetabular components

1.2.2. TOTAL KNEE REPLACEMENT

TKA has been very successful for the past 40 years at helping relieve the pain of patients suffering from diseases such as osteoarthritis. Their design is more complex than THA as the knee is a more intricate joint, highly dependent on support from soft tissues such as ligaments, which play a role in resisting dislocation and general stability. It is the condition of the ligaments which play a part in selecting the specific components of TKA as they vary in their level of constraint; as a knee joint that has suffered significant damage and has lax ligaments, will required a prosthesis which is more constrictive to prevent failure and dislocation. A TKA device is usually comprised of three main components: a femoral component, a tibial component, and a patellar component. Due to the harsh load bearing environment of the knee joint, metals such as CoCrMo are preferred due to their mechanical strength and high fracture toughness. The most common cobalt alloy used for biomedical application is CoCrMo, also known as vitallium, which was first introduced in 1936 by Venable and Stuck (Gonzalez-Carrasco, 2009). Containing 28wt% chromium, 6wt% molybdenum, CoCrMo is extensively used in components of artificial knees due to its excellent fatigue strength and hardness. The alloy is fabricated by one of two methods; cast or wrought. Cast alloys are simpler to form as it only requires the alloy to be cast into shape, which is useful for more complex shaped components, whilst wrought alloys are processed by hot or cold forging and due to the plastic deformation that occurs, have superior mechanical strength. The exposure of tissues to migrating metallic ions created from corrosion of CoCrMo is still a present concern (Keegan et al., 2008) although vitallium contains chromium element to provide stability against various forms of corrosion. One of the primary reasons for CoCrMo application in TKA is the materials high resistance to wear. CoCrMo can be polished to a mirror finish and subsequently used as a bearing surface between the femoral and tibial components. Due to the complexity of the knee joint, total joint replacement is not always necessary. Unicondylar devices are often preferred as they only replace the lateral components of the knee. By only resurfacing the femoral and tibial condyle, this method helps keep the surrounding ligaments and cartilage, which would've been mostly removed in a full TKR (Sangiorgio, 2013). Whilst CoCrMo does provide excellent mechanical properties and is highly advantageous when used as a bearing surface in TKA, it does not have the same osteogenic biocompatibility as found on titanium alloys, and therefore would benefit from new strategies for improving its biological response *in vivo*.

1.2.3. TJA DEMAND

Overall health in the UK has improved drastically with life expectancy having increased by an average of 4.2 years from 1990-2010 (Murray et al., 2013). Continuous improvements in diagnostic and therapeutic techniques mean it is highly likely this value will increase further in the coming decades. As a consequence of this, the healthcare industry is coming under increased pressure trying to cope with the demand of a growing elderly population. TJA procedures are no exception. Recently, the National Joint Registry reported a 7.5% increase in the amount of THA procedures performed in the UK between 2011 and 2012 (86,488 from 80,314) (Borroff et al., 2014). The same pattern was observed for TKA, which saw a 7.3% rise over the same time period (90,842 from 84,653). At present, the National Joint Registry does not account for all of the procedures carried out in the entire UK, but the trend of an annual increase in the amounts of TJA procedures performed is clear (Culliford et al., 2010). This trend is not limited to the UK, as in the United States of America (USA) it is projected that between 2005 and 2030, the amount of annual THA procedures is set to increase from 209,000 to 572,000, whilst TKA is projected to see an even greater increase, rising from 450,000 procedures to 3,481,000 (Kurtz et al., 2007a). Similar patterns were observed during a recent global survey of primary and revision TKA, which concluded that the total amount of procedures had increased drastically over the past decade (Kurtz et al., 2011).

A growing elderly population is not the sole reason behind this trend. The amounts of young patients (< 65 years old) receiving TJA in the USA was studied and it was found that the population group is also increasing. In 1993, the percentage of TJA performed in those under the age of 65 was 25% and 32% for primary and revision surgeries. By 2006 this had risen to 40% and 45%, and is predicted to increase further with young patients becoming the majority by the year 2030 (Kurtz et al., 2009). The underlying cause behind this increase in TJA in younger patients is unclear, but national patterns of obesity and the effectiveness of TJA may be contributing factors.

In regards to the efficacy of TJA, a recent study carried out in the USA was able to show that TKA procedures were a cost effective method of increasing function and reducing pain in the knee, even at both high and low levels of improvement (Waimann et al., 2014). Indirect costs, such as time lost out of work were also included in the study. Analysis

into the UK's TJA services also found that the treatment is extremely effective both clinically and in cost (Jenkins et al., 2013).

Even though THA and TKA are widely accepted as an effective means of improving the function of a diseased or damaged joint, a study which looked at the cost effectiveness of modern implants against older designs, found that there was no statistical difference between the two chosen implants (Hamilton et al., 2013). The study was based on quality adjusted life years, which quantify the benefits of surgical intervention by measuring change in health related quality of life, but the method did not take into account any improvement to the function of the joint which should be an important factor when measuring the efficacy of TJA. Despite this, the fact that no significant difference was observed between the modern and older design implant shows that there is still room for improvement in TJA device design.

1.2.1. TJA FIXATION METHODS

1.2.1.1. BONE CEMENT

Bone cement has been used for the past 50 years to anchor orthopaedic devices in place; with the primary function of filling the space between the device and bone, creating a working interface designed to optimism the distribution of stresses and load from the prosthesis into the surrounding bone tissue. In cushioning and evenly distributing the forces at the bone-implant interface, this helps to increase the longevity of the device and prevent failure mechanisms such as fatigue fractures. The most commonly used bone cements are based on polymethylmethacrylate (PMMA), which is comprised of a polymer powder and liquid monomer. PMMA bone cement is formed by the radical polymerisation of the methylmethacrylate, which can be a highly exothermic reaction, resulting in the temperature of the cement increasing drastically. Despite these thermal reactions only taking place for a brief time, it has been reported to cause thermal necrosis of the surrounding bone tissue. Another issue surrounding the use of bone cement is polymerisation shrinkage after curing. During the reaction, methylmethacrylate monomers combine forming long polymers, which can result in volume shrinkage of 3-5%, which can sometimes the affect stability of the device. Furthermore, cement removal

during revision surgery is a difficult process, which when combined with other factors has led to the increasing popularity of cementless fixation methods.

1.2.1.2. CEMENTLESS FIXATION

The primary goal of cementless fixation for use in orthopaedics is to improve the longevity of the implant, whilst not having the issues which arise from the use of bone cement, such as thermal necrosis and cement removal during revision surgeries. The principles of cementless fixation that are required for the implants success include, adequate initial stability, the implants ability to promote osseointegration and suitable mechanical properties. Unlike cemented fixation, where bone cement is used to fill the gap formed between the implant and the bone; in cementless fixation, initial stability is achieved by having the forces required to dislodge the components, being equal to or less than the physiological forces holding the component in place. This involves having an initial tight fit, achieved by either the use of surgical screws or a press-fit configuration. An example of the press-fit model would be the acetabular component of a THA device, where the reamed diameter of the area to receive the component is slightly smaller than the diameter of the actual cup itself. Following this initial contact, the bone-implant interface is the ideal environment for osseointegration to occur, allowing the direct integration of the implant to the surrounding bone tissue, highlighting the importance of selecting biomaterials capable of promoting an enhanced osteogenic response following surgery. Furthermore, the mechanical properties of the materials which form the implant are extremely important in cementless fixation, as the removal of bone cement inhibits the implants ability to evenly transfer the load from the joint into the bone, which can result in failure of the joint (Cross, 2008b). The effectiveness of cementless fixation is demonstrated in the field of dentistry, as all dental implants are secured using cementless techniques.

1.2.2. CEMENTED VERSUS CEMENTLESS IMPLANTS

Cemented or cementless fixation is still being debated as to which technique is the optimal fixation method in TJA that can deliver improved performance and longevity of the

device. In a recent systematic review by (Abdulkarim et al., 2013), meta-analysis of all randomised clinical controlled trials, where cemented was compared against uncemented THAs, was completed. It was found that there was no significant difference between the two groups when assessing implant survival rates or post-operative complications. Improved short term clinical outcomes, such as better pain scores, were observed in cemented implants, and it was concluded that cemented was similar if not superior to uncemented THR. The limitation of *Abdulkarim et al's* study was the relativity short follow up time, which ranged from 2 to 8 years. In an earlier systematic review that assessed 20 cemented versus cementless fixation THA studies, (Morshed et al., 2007) found that whilst the meta-analysis failed to demonstrate overall superiority of either method, cemented fixation showed greater survival rates in some subsets of the study population and should be chosen in place of uncemented. A review of cemented versus uncemented hemiarthoplasty for displaced femoral neck fractures, found that after a meta-analysis of eight eligible studies, that there was no significant difference between the two groups in regards to survival rates, mortality or post operational complications (Luo et al., 2011). However, as in *Abdulkarim et al's* review, there was a significant difference observed in regards to pain scores. Residual pain at 1 year was found to be 23.6% in cemented devices, compared to 34.4% for uncemented. Considering the similarities between the two methods in regards to device mortality, it was concluded that the improvement in pain scores using cemented fixation merited that cemented fixation should be preferred over uncemented. Whilst cemented fixation can improve short term pain scores, if a revision is required, working with a cemented device can prove to be difficult when trying to expose new bone tissue for the replacement device. This issue is not present to the same extent in uncemented devices as there is no bone cement that has to be removed by the surgeon. Considering this, as the demand for TJA increases with younger patients potentially outliving the lifespan of their devices, uncemented fixation may be more suitable for younger patients who have a higher chance of revision surgery in the future. Cemented fixation may be best suited to those who are less likely to require a revision and could benefit from the improved pain scores, such as the elderly.

1.2.3. FAILURE MECHANISMS

There are multiple factors which play a role in how a patient responds to an implant, such as the topography, energy, chemistry and composition of the implant, each of which as individually is important as each other. For example, a device may be engineered to have a surface topography ideal for the deposition and formation of new bone tissue, although if the chemical composition of the surface is not accepted by the hosts cells, an inflammatory response can be triggered which may lead to joint failure (Revell, 2008). Fibrous encapsulation is an example of such a response, which can occur when fibrous tissue forms over the surface of the implant as a method of protection, in an attempt to isolate the implant from the host. The fibrous capsule can become thick under certain conditions and lead to loosening of the implant and clinical failure (Long, 2008). To prevent this undesirable response, implants are usually designed out of materials that promote an interfacial response and form direct contact between the tissue and implant, although other failure mechanisms can still occur.

1.2.3.1. STRESS SHIELDING

Biologically active bone is an extremely complex material and one of the key challenges posed to modern implantable materials, is to mimic the mechanical properties of bone. As bone is in a constant state of renewal, it is continually remodelling and this allows bone to react to the external stresses of surrounding environment (Burke, 2008). The remodelling and regenerating properties of bone can be directly related to loading (Cross, 2008a). As stated by Wolff's law: bone subjected to stress or loading will regenerate and bone that is not subjected to stress will atrophy. This is clinically apparent in arthritic joints, where the formation of osteophytes occur due to the increased stress caused at the interface, leading to hypertrophy of the bone (Burke, 2008). For orthopaedic applications, stress in the proximal femur is shared by the metal implant and the host's bone. Therefore, an implantable material that does not have similar mechanical properties to bone may lead to an un-physiological distribution of force transmission at the bone-implant interface. This mismatch in mechanical properties will result in bone resorption and is known as "Stress shielding". In implant technology, stiffness is one of the most important mechanical terms. It is a material property that is defined by the resistance of

an elastic body to deformation or deflection by an applied force. Young's modulus of elasticity, *E* (Elastic modulus), is a measurement of stiffness, and is a ratio of the rate of change of stress (force per area) against strain (deformation) in units of gigapascals (GPa) (Cross, 2008a). The elastic modulus of bone varies, depending on the direction and type of bone, ranging from 4-30GPa (Katz, 1980). Ideally the implantable metal should have an identical elastic modulus to that of bone, to allow the native bone to support as much of the patients weight as possible, but this comprises other important mechanical properties required by the material. Currently titanium and its alloys are most suited as they have a much lower elastic modulus of around 110 GPa (Gotman, 1997) and would therefore keep stress shielding to a minimum. Stress shielding is a prominent factor when choosing cemented or cementless fixation, as the elastic modulus of bone cement is approximately 2400 MPa (Webb and Spencer, 2007) which is considerably closer to the modulus of bone tissue, which can vary from 4-30 GPa (Katz, 1980). The surrounding bone cement can therefore act as an elastic interlayer between the bone and metal implant, allowing for an even transfer of the load and prevention of bone resorption. In contrast, when cementless stems are used in the distal femur of patients, stress shielding is highly likely to occur, as found in a study which observed severe and mild bone resorption in 24% and 76% of the joints assessed, respectively (Yamada et al., 2009). Despite the presence of stress shielding, it was found that the survivorship of cementless acetabular and femoral components after 20 years was still 85.8% and 97.8%, respectively. This data suggests that whilst some stress shielding may occur in cementless fixation devices, the overall survivorship is still relatively high, justifying their use in modern day prosthesis.

1.2.3.2. MICROMOTION

Closely related to material stiffness and stress shielding is the issue of micromotion. When an implant undergoes loading, specifically not long after implantation, small movements can occur between the implant and the surrounding bone. If these movements are excessive, they can prevent integration of the bone with the biomaterial at the bone-implant interface, therefore inhibiting osseointegration (Cross, 2008a). The influence of material stiffness on stress distribution and micromotion at the interface was researched by Simon *et al* (Simon et al., 2003), and it was found that the low stiffness material

showed better stress distribution, but un-expectantly showed more micromotion. This highlighted the importance of having biomaterials with the correct mechanical properties to withstand the deformation that can occur from physiological loading. Specifically for long implants, such as the femoral stem of THA where increased elasticity would result in repetitive deformation, excessive micromotion and ultimately failure of the joint (Cross, 2008a).

1.2.3.3. WEAR

Wear is also one of the major problems associated with failure of orthopaedic devices and can be defined as "The removal of material caused by the contact and relative motion between two surfaces". The underlying cause of wear is always the same: if two components are placed in contact with one another, with a low nominal stress between them, then high local stresses will exist, owning to the fact that no surface is perfectly flat. It is at these points of contact when relative motion occurs, shearing forces will cause small particles of wear debris to break free (Taylor, 2009). Wear most commonly materialises at the interface between the femoral head and acetabular cup, but can arise at multiple interfaces on an orthopaedic device. McKellop (McKellop, 1995) classified the different wear interfaces into four different modes shown below.

Table 1 The different modes of wear possible in TJA (McKellop, 1995).

MODE	**INTERFACE**	**EXAMPLE**
Mode 1	Surfaces that are normally supposed to articulate	Metal femoral head and polyethylene insert
Mode 2	One normal side of articulation against another side that should not normally articulate	Metal femoral head burrows through polyethylene and articulates against the backing of the acetabular cup
Mode 3	When a third body particle interposes itself in a joint	Metallic/bone particles or broken wires that migrate to the total hip articulation site
Mode 4	Two surfaces that are not meant to undergo relative motion	The polyethylene insert of the acetabular cup rotating against the metal shell

The consequences of wear in TJA are severe. As wear proceeds, the tolerances between articulating surfaces become heavily altered, which may lead to changes in function, range of motion, biomechanics and even dislocation. The physiochemical properties of important features such as bearings and surface coatings may also become altered in the presence of wear. Lastly, the result of wear, being the wear and particle debris, can generate a foreign body inflammatory response, periprosthetic osteolysis, aseptic loosening or a pathological fracture (Burke, 2008). It is these clinical consequences that are fuelling the progression of TJAs that have minimal wear so that they can hope to last the lifespan of aging patients.

1.2.3.4. CORROSION

As with the concern over wear on orthopaedic devices, corrosion is also a problem. Corrosion is a complex, multifactorial, electrochemical phenomenon that primarily causes the degradation of the material within the body. Degradation of metal-alloys within the body is undesirable for two reasons: the structural integrity of the implant may decrease, and the release of by products which may be harmful to the host and cause adverse biological reactions (Jacobs et al., 1998). It is no surprise that corrosion of metals and alloys occur in the human body, as it is an extremely harsh environment. The metallic materials have to withstand an oxygenated saline solution with a salt content of around 0.9%, at pH of approximately 7.4 and temperature of 37˚C/98.4˚F (Kamachimudali et al., 2003). It is the organic substances, ions and dissolved oxygen contained in this unforgiving environment that makes it electrochemically reactive to metals. A metals tendency to corrode depends on its electrode potential, with some metals chemically inert such as Au and Pt, and others quite reactive such as Ti, Al, Cr and Co. It is the high reactivity of Ti and Co alloys that make them more desirable for orthopaedic applications. Without the presence of an aqueous solution such as that found in the human body, a form of corrosion known as dry corrosion occurs, when the metal interacts with air. Upon exposure to air, some metals almost immediately form an oxide layer on their surface, approximately a few nanometres thick. This oxide layer on the surface of the metal acts as a passivating layer, preventing the release of electrons and metallic ions from the surface. This layer also serves to prevent any aqueous corrosion occurring within the body and in turn helps to prevent leaching of any potentially harmful ions (White, 2009). The oxide layer may protect the metal implant up to a point, but it does not protect it completely. Proteins, bacteria and cells may upset the equilibrium of reactions, altering pH and electrode potential and reduce the amount of oxygen available to maintain the layer leading to different forms of corrosion. Fretting corrosion is when the oxide layer is continuously removed and reformed in a cyclic process and can lead to the gradual wear of the surface of the implant. Pitting corrosion can cause holes that form in the oxide layer at weak points that cannot be reformed. Lastly, stress corrosion attacks the oxide layer at its weakest points when in the presence of an applied load and can cause cracks that may lead to failure of the device (White, 2009). All the above forms of corrosion highlight the complexity of the interface that occurs between bone and implant surface.

1.2.4. DENTAL IMPLANTS

It should be highlighted that implants used for TJA share numerous similarities with implants found in dentistry. Both share a primary of function of replacing diseased or damaged tissue with a device that is suitable to fulfil the role of the tissue being replaced, both biologically and mechanically. Whilst TJA devices replace the components of a joint, such as the knee or hip, dental implants replace the function of a tooth, and are usually integrated with the bone of the jaw and support a dental prosthesis such as a crown. Both forms of implant must secure adequate osseointegration with the surrounding native bone following surgery, therefore there is considerable overlap in the research of these two individual, but similar fields of medicine. As in orthopaedics, titanium is the gold standard material for dental applications and is widely used in many forms of dental implant (Fandridis and Papadopoulos, 2008). Numerous methods of surface modification and functionalisation are applied to dental implants, similar to those found used in TJA devices (Giannoni et al., 2009).

1.3. BIOMATERIAL SURFACE MODIFICATION

One of the main methods of preventing possible failure mechanisms and to increase the performance of orthopaedic devices is to modify the materials out of which the devices are made. Whilst modifying the composition of the materials can affect the mechanical properties, modification of the material surface can allow for an increase in implant performance whilst retaining the advantageous mechanical properties (Logan and Brett, 2013). Ideally, if the surface of an implant can be modified to promote an environment that can stimulate an enhanced osteogenic response, this should lead to a faster rate of bone deposition and increased levels of osseointegration. In turn, this could result in faster healing times and prevent failure mechanisms such as micromotion. Bioinert materials such as the cobalt alloy vitallium, rely heavily on surface modification, such as bioactive coatings to stimulate an osteoconductive and osteoinductive microenvironment post implantation.

1.3.1. CALCIUM PHOSPHATE BASED SURFACE MODIFICATION

One of the most effective and widely used surface treatments for CoCrMo orthopaedic devices in industry is hydroxyapatite. The material does not exhibit the mechanical properties required to be used as a bulk material in orthopaedic and dental devices, although the bioactive ceramic has excellent potential for use as a coating, considering that it mimics the natural composition of bone (Surmenev et al., 2014). The first and one of the most common methods of depositing hydroxyapatite onto orthopaedic biomaterials is plasma spraying (De Groot et al., 1987), although a variety of deposition techniques can be used, such as pulsed laser deposition (Komath et al., 2011, Koch et al., 2007), ion beam assisted deposition (Choi et al., 2000, Cui et al., 1997) and radio frequency magnetron sputtering (Yamashita et al., 1994, Wolke et al., 1994). It is thought that hydroxyapatite coatings can stimulate an osteoconductive response in the local microenvironment following implantation, depicted below in figure ??. The theory, first described by (Rahbek et al., 2000), states that a change in the surrounding pH levels causes the dissolution of calcium and phosphate ions, which then reprecipitate onto the surface and incorporate into apatite crystals which can stimulate chemotaxis. This increase in cellular response has been observed in *in vitro* biological trials using a variety of osteogenic cells, which have shown enhanced cell adhesion, proliferation and differentiation when on hydroxyapatite based films (Junker et al., 2009, Sima et al., 2010, Hong et al., 2010, Sato et al., 2008, Dimitrievska et al., 2011).

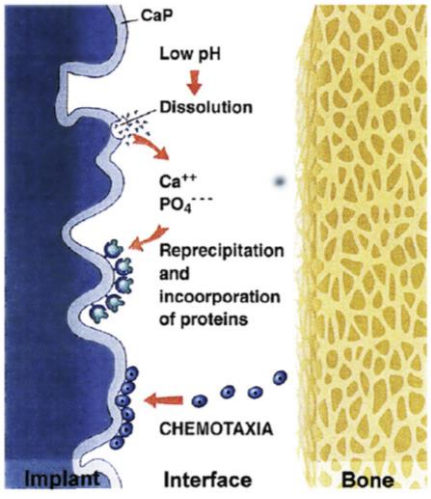

Figure 3 Potential method of osteoconduction stimulated by hydroxyapatite based coatings in orthopaedic applications. Image taken from (Surmenev et al., 2014).

However, despite the beneficial performance of hydroxyapatite based coatings *in vitro*, the performance of implants in *in vivo* clinical studies has been inconsistent. Hydroxyapatite coatings on THA devices have shown good rates of survival with a rate of 97% after 11 years (Geesink, 2002), although several recent orthopaedic clinical studies have shown that there is no clear benefit to using hydroxyapatite coatings in either acetabular cups or femoral stems of THR devices (Lazarinis et al., 2011, Lazarinis et al., 2010, Camazzola et al., 2009, Gandhi et al., 2009, Stilling et al., 2009). Furthermore, for the acetabular cup specifically, those coated with hydroxyapatite have been reported to be inferior to uncoated cups, citing that hydroxyapatite particles that dissociate from the implant can lead to increased wear and aseptic loosening of the device (Stilling et al., 2009). Another factor in regards to the efficacy of the coatings, particularly for plasma sprayed hydroxyapatite, is due to variation in the dissolution rates between different phases that comprise the coating, the coating can be at risk of delamination (Le Guehennec et al., 2007). New coatings with increased stability and longevity may be more suitable at improving the performance of orthopaedic devices at the bone-implant interface.

1.3.2. TIO2 BASED SURFACE MODIFICATION

In contrast to hydroxyapatite based coatings which are advantageous due to their similarity to natural bone, one type of surface modification which has grown in popularity due to the beneficial properties of titanium alloys, is the use of titanium oxide (TiO_2). TiO_2 is the thin (3-7 nm) naturally occurring oxide layer found on the surface of titanium and its alloys (Textor, 2001). It is understood that the advantageous properties of titanium and its alloys can be accounted this surface oxide layer of TiO_2. Consequently, efforts have been made to thicken or deposit additional TiO_2 onto titanium as well as other biomaterials, using a wide variety of different techniques, although the majority of methods are still in the early stages of research and not in commercial use. A number of methods which utilise TiO_2 based surface modification are detailed below.

1.3.2.1. MICRO ARC OXIDATON

Modification of titanium substrates by way of micro-arc oxidation (MAO), also known as plasma electrolyte oxidation, results in the formation of a porous layer of TiO_2 on the substrate surface. Application of an applied voltage over a certain threshold to a titanium substrate submerged in an electrolyte, results in the dielectric breakdown of the surface TiO_2 layer. At this moment, OH ions in the electrolyte and Ti ions from the material move in opposite directions and rapidly reform as TiO_2 in a porous and well adhered layer (Nie et al., 1999). By altering the applied voltage the characteristics of the oxide layer can be varied, resulting in changes to the surface morphology and crystallinity (Li et al., 2004, Chen et al., 2010a). Titanium substrates that have undergone MAO have been shown to be biologically advantageous for osteogenic applications, via enhanced levels of bone tissue formation *in vivo* (Ma et al., 2008, Zhou et al., 2014). In addition, further modification to the implant surface can be achieved by the incorporation of Ca and P ions into the oxide layer by controlling the composition of the electrolyte, and have shown excellent levels of biocompatibility (Ishizawa and Ogino, 1995, Li et al., 2004, dos Santos et al., 2014). Application of MAO TiO_2 layers containing Ca and P onto rough sandblasted substrates have shown improved tribo-mechanics (Szesz et al., 2014, Wang et al., 2014a). MAO TiO_2 layers can also be functionalised using mircoRNAs increasing the osteogenic activity of rat MSCs (Wu et al., 2013). Interestingly, application of MAO is not restricted solely to titanium substrates, as the biocompatibility of cobalt chrome was shown to be enhanced following an initial coating of Ti by electron beam deposition and subsequent MAO treatment (Han et al., 2009).

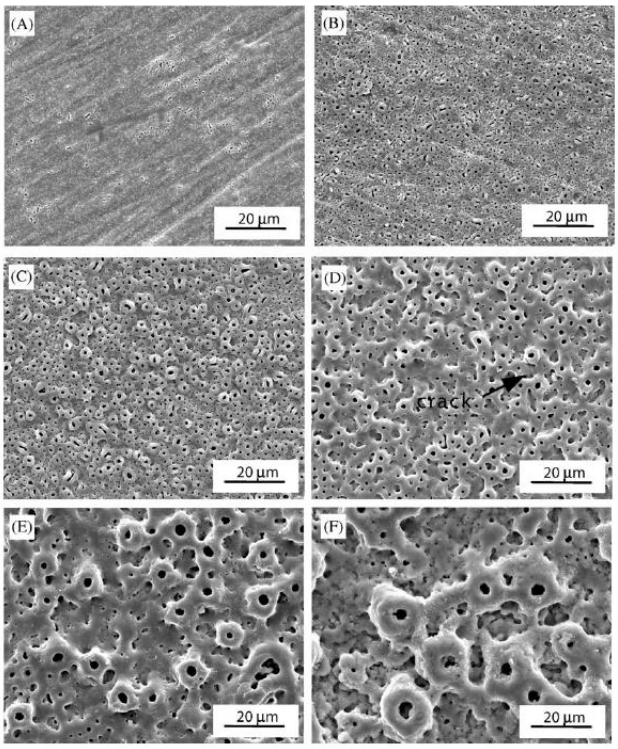

Figure 4 SEM images of titanium substrates modified by MAO at different voltages. Taken from.(Li et al., 2004).

1.3.2.2. SOL GEL COATINGS

Sol gel dip coating is an effective method of producing thin film metal oxide layers on a substrate. For TiO_2 sol gel coatings, the wet chemical process involves the use of a titanium organic precursor and an organic solvent, where controlling the temperature at which the coating is performed can affect crystallinity and phase. The excellent corrosion resistance of titanium can be accounted to its surface oxide layer and is potentially transferrable to TiO_2 coated materials. Using a Sol-gel dip coating method, TiO_2 coated CoCrMo was shown to improve the cytocompatibility of the material by preventing the release of potentially harmful ions such as cobalt and chromium (Tsaryk et al., 2013). Similarly, the titanium alloy Ti6Al4V, was shown to have reduced vanadium ion release following TiO_2 sol gel coating (Hoffmann et al., 2007), whilst a combination of MAO and TiO_2 sol-gel coating significantly improved the corrosion resistance of magnesium (Shi et al., 2009). By improving the cytocompatibility of biomaterials via increasing corrosion resistance, an improvement in biological response can be observed. Sol gel TiO_2 coated 316L stainless steel stimulated such a response in the form of superior cell

morphology and proliferation, whilst also inhibiting any inflammatory response *in vivo* (Marycz et al., 2014). The use of sol gel TiO_2 coatings for soft tissue applications have also been investigated, where it was found that nanoporous sol-gel coated dental implants enhanced soft tissue attachment in both a beagle and rat model (Rossi et al., 2008, Areva et al., 2004). Furthermore, the application of TiO_2 sol gel coatings as an osteogenic enhancer has been shown to promote superior cell response in MC3T3-E1 and MG63 cells (Advincula et al., 2006, Singh, 2011). Methods to further increase the efficacy of sol gel coatings via functionalisation have shown that TiO_2 coatings that were irradiated with UV light enhanced apatite formation (Guo et al., 2010), whilst doping the coating with nickel stimulated a significant improvement in cell response (Dhayal et al., 2012).

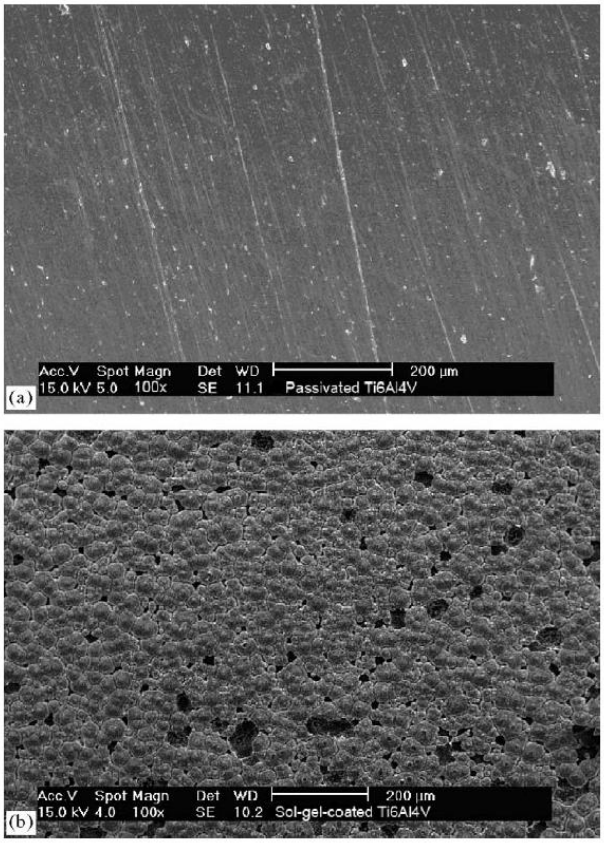

Figure 5 SEM images showing morphologies of control titanium surface above, with a 5 layer sol gel coating below. Taken from (Advincula et al., 2006).

1.3.2.3. SPUTTER DEPOSITION

The application of thin, well adhered TiO_2 films can be achieved onto substrates by sputter deposition techniques. Using molten TiO_2 nanoparticles, thin films can be deposited onto titanium substrates with thickness ranging from 300 picometres to 6.3 nanometres. These thin films of TiO_2 were shown to have no effect on the topography of the titanium substrate, but significantly improved the proliferation and differentiation of rat bone marrow derived cells (Sugita et al., 2011). Using the same deposition technique, the TiO_2 coating stimulated a superior cell response in muscle skeletal cells, in the form of increased cell proliferation, adhesion, attachment, gene expression and collagen production (Ishizaki et al., 2011). A different method of sputter deposition is DC magnetron coating. By using a titanium target in a gas chamber containing a ratio of O_2 and Ar, application of a current for a determined time can result in the formation of TiO_2 on the substrate surface. Such thin films of TiO_2 have been shown to be advantageous for osteogenic applications by enhancing the formation of hydroxyapatite in simulated body fluid and phosphate buffered saline (Kasemanankul et al., 2009, Brohede et al., 2009). Variations in the deposition parameters, such as the Ar to O2 gas flow ratio, are influential on the bioactivity of the TiO_2 layer by affecting hydroxyapatite formation and morphology (Lilja et al., 2011). In addition to enhancing hydroxyapatite formation, these TiO_2 films formed on titanium by way of DC magnetron sputtering have been reported to be extremely well adhered to the substrate which is highly important in regards to the longevity of implantable devices (Brohede et al., 2009).

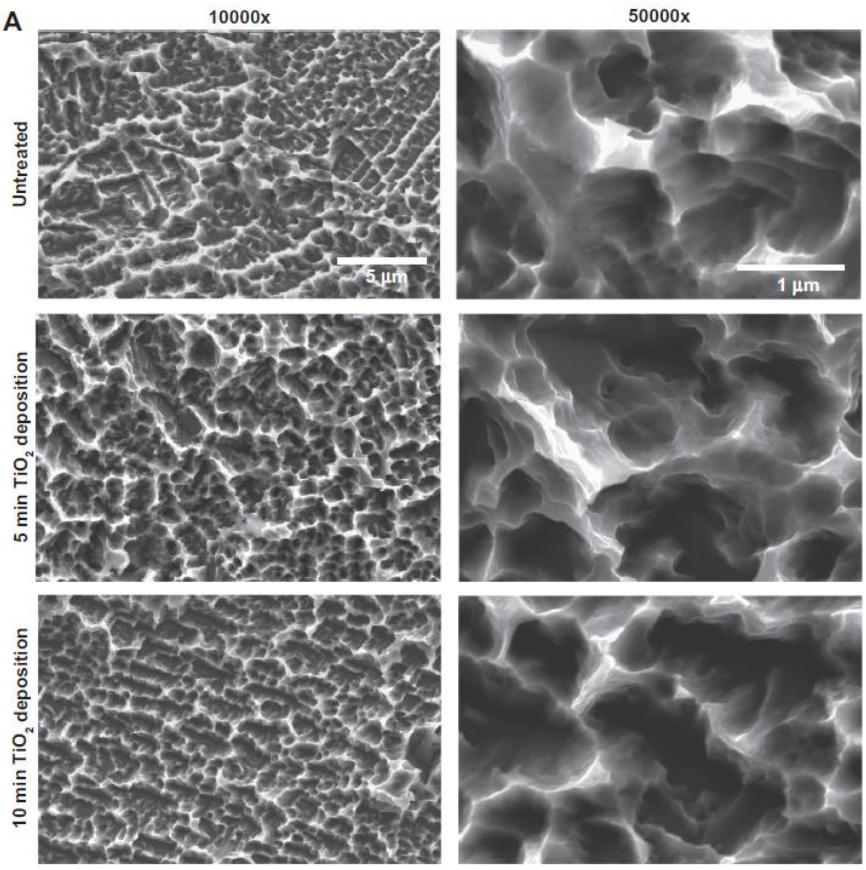

Figure 6 SEM images showing that nanometre thin sputter coatings do not significantly change the morphology of acid etched substrates despite enhancing cell response. Taken from (Ishizaki et al., 2011).

1.3.2.4. TIO2 NANOTUBES

One method of applying additional TiO_2 to the surface of titanium and its alloys whilst also creating a unique topography with distinct and controllable features, is the use of nanotubes. TiO_2 nanotubes can be grown onto the surface of titanium by an electrochemical anodization method, involving a titanium plate as the anode and a platinum sheet as the cathode, with both submersed in a fluoride based electrolyte solution. By altering the supplied voltage and duration, the system can determine the height and diameter of the nanotubes (Brammer et al., 2012). It has been reported that the dimensions of TiO_2 nanotubes are heavily influential on cell response. Nanotubes of diameter, 30, 50, 70 and 100 nanometres (nm) were studied and it was found that whilst the smaller diameter tubes promoted good cell adhesion, they lacked differentiation ability. The larger diameter nanotubes promoted cell elongation and enhanced levels of osteogenic differentiation in MSCs (Oh et al., 2009). In a similar study, it was concluded

that TiO_2 nanotubes with smaller diameters were preferable, as low levels of mineralisation and greater cell apoptosis was observed on large diameter nanotubes (Park et al., 2007). *Park et al* went on to conclude that 15 nm was the optimal size for TiO_2 diameter (Park et al., 2009). Whilst the application of nanotubes holds great potential (Mashinchian et al., 2015), more studies need to be performed to ascertain the optimal dimensions considering the contradictory results in the literature. Furthermore, functionalisation of TiO_2 nanotube surfaces with BMPs have been shown to enhance cell behaviour compared to untreated nanotubes, signifying that there is potential to improve upon the nanotube response alone (Lai et al., 2011, Park et al., 2012).

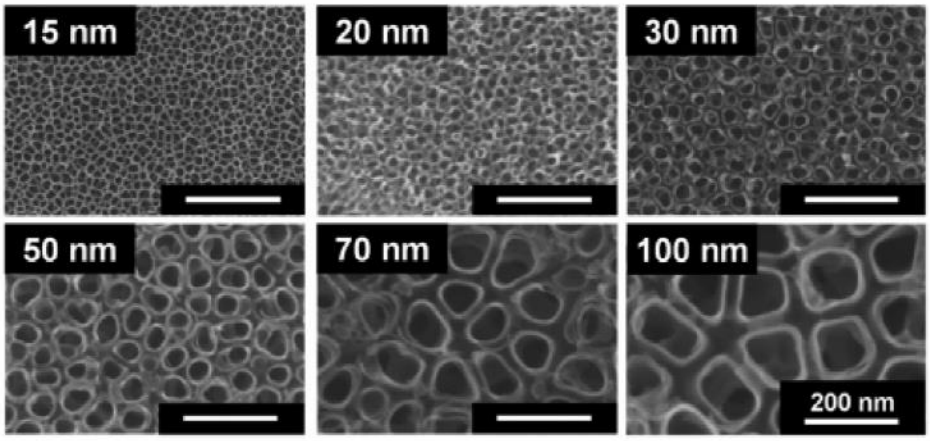

Figure 7 Variation in TiO_2 nanotube dimensions grown on titanium substrates. Image taken from (Park et al., 2007).

1.3.2.5. CHEMICAL VAPOUR DEPOSITION

One potential method of capable of depositing thin and durable TiO_2 coatings is chemical vapour deposition (CVD). CVD can be defined as the deposition of a solid on a heated surface from a chemical reaction in the vapour phase (Pierson, 1999). It is a method appropriate for manufacturing coatings that can contain most metals as well as some non-metallic compounds such as silicon or carbon. CVD is used in a number of applications, such as in the manufacture of semiconductors, coating of tools and bearings, self-cleaning windows, and optoelectronics, although as of yet has not been utilised as a method of coating orthopaedic implant materials. The process of CVD includes the introduction of gaseous compounds into heated chamber, where a reaction occurs and due to the transfer of energy, a solid is deposited onto the target, whilst simultaneously creating gas by-

products. This resultant solid is the desired coating and its composition is dependent on the gaseous compounds used during the reaction. For example, to create a TiO_2 solid film, the compounds would include titanium tetrachloride and ethyl acetate (Cross et al., 2012). By selecting the appropriate input gaseous compounds, the resultant coating can be controlled to contain desired elements and compositions (Pierson, 1999). This degree of control over the composition of the coating could be highly advantageous if the process were to be applied for orthopaedic applications, as compounds beneficial to the osteogenesis process could be applied. Another advantageous property of the CVD process, which merits its potential use in the field of orthopaedics, is the process is not restricted to a line of sight deposition like most coating techniques, such as sputter coating. CVD technology allows for complicated 3-dimensional configurations with deep recesses and holes to be coated with relative ease. In the field of orthopaedics, where implants are complex shapes commonly modified with sophisticated surface topographies, the CVD method of surface modification could be extremely useful, ensuring that the entire implant receives a sufficient coated. Further advantages of the CVD process include a high deposition rate, and no requirement for expensive vacuum equipment as the process can be performed at atmospheric pressure, which ultimately reduces time, cost and complexity.

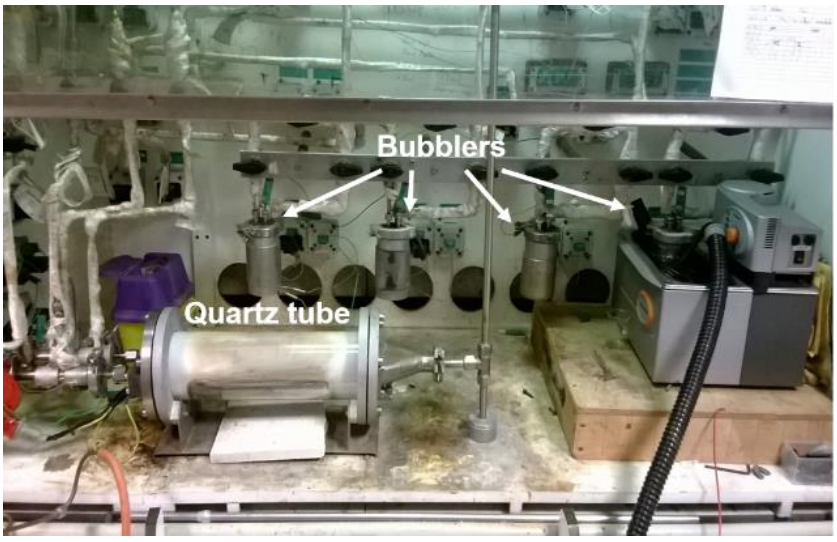

Figure 8 A image of an atmospheric pressure CVD system, containing a quartz tube as the reaction chamber and bubbles to heat the individual gaseous compounds before deposition.

1.3.3. TOPOGRAHICAL SURFACE MODIFICATION

One of the most influential and commonly used methods of improving implant performance is topographical surface modification. There are many widely used physical methods of creating surface morphologies that are capable of improving bone response, as it is believed that osteogenic cells are more favourable to roughened surfaces compared to smooth (Brett et al., 2004). The commercial sandblasted acid-etched (SLA) topography created by Straumann (Walderberg, Switzerland) is one of the best and most widely used topographies on titanium dental implants. Created by a combination of sandblasting using large grit aluminium oxide particles, followed by acid etching using a mixture of HCl and H_2SO_4, the topography has features on both the micro and nano scale. The SLA surface is moderately rough (R_a approximately 1.5 μm) which is within the range described as optimal for enhancing bone formation (Wennerberg and Albrektsson, 2009). Mirco-rough implant surfaces, such as SLA, are thought to stimulate osteoblasts to create a osteogenic microenvironment (Boyan et al., 2003), which can lead to increased bone to implant contact, when compared to smooth surfaces *in vivo* (Shalabi et al., 2006). Due to the surface properties of SLA having the potential to enhance bone formation, healing times from implant placement to implant loading can be significantly reduced. The successful use of SLA implants in early loading clinical long term studies has been widely demonstrated (Cochran et al., 2011, Cochran et al., 2007, Gallini et al., 2004, Bornstein et al., 2005, Roccuzzo et al., 2008). Furthermore, in large, 10 year follow up studies, the long term reliability of the SLA surface was demonstrated by high survival rates in patients, ranging from 95.1% to 100% (Buser et al., 2012, Fischer and Stenberg, 2012, Roccuzzo et al., 2014). The application of topographies, such as the SLA surface, onto bioinert orthopaedic materials like CoCrMo, may potentially be a method of improving the osteoconductive and osteoinductive properties of the material.

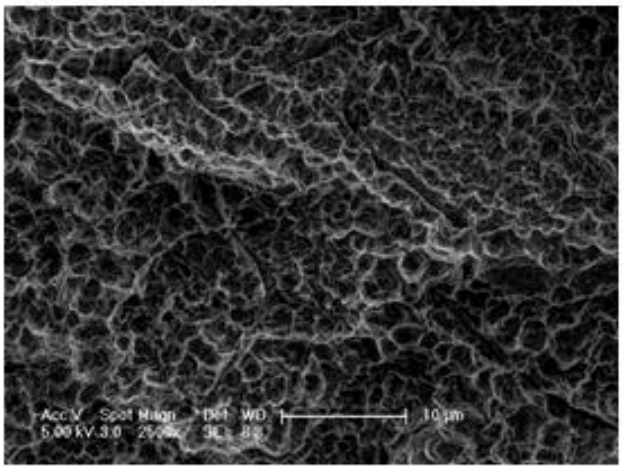

Figure 9 Example of the surface morphology of SLA titanium. Scale bar = 10 µm. Image taken at the Eastman Dental Institute

1.4. AIM AND HYPOTHESES

The aim of this thesis is to develop surface modification strategies, including CVD coatings, functionalisation of CVD coatings, and surface topographies, for the orthopaedic implant material CoCrMo that have the potential to enhance the adhesion and rate of osteogenic differentiation in human MSCs. These approaches could be applied to CoCrMo orthopaedic devices used in total knee and hip replacement surgeries where enhanced bone formation is desirable to improve implant stability and reduce healing times post-surgery.

The hypotheses explored in this thesis are:

1. The addition of a CVD TiO_2 coating onto the surface of smooth CoCrMo would improve cellular markers of osteogenic differentiation and adhesion in human MSCs when compared to uncoated CoCrMo.
2. UV photofunctionalization of the TiO_2 coated CoCrMo would increase cell adhesion, proliferation and ostoegenic differentiation in human MSCs when compared to non-UV TiO_2 coated CoCrMo.
3. The application of a SLA topography onto CoCrMo would stimulate increased calcium and hydroxyapatite formation from human MSCs when compared to smooth CoCrMo.
4. Coating the surface of SLA CoCrMo in a layer of TiO_2 using CVD would increase cellular markers of osteogenic differentiation and adhesion in human MSCs when compared to uncoated SLA CoCrMo.

CHAPTER TWO:

MESENCHYMAL STEM CELL RESPONSE TO TiO_2 COATED COBALT CHROMIUM MOLYBDENUM

2. INTRODUCTION

Advances in diagnostic and therapeutic techniques have resulted in a growing elderly population within the UK and other countries (Murray et al., 2013). As a result of this, the number of TJA procedures performed is predicted to rise significantly by the year 2030 (Kurtz et al., 2007a), which will have a substantial impact on the health industry both clinically and economically (Kurtz et al., 2007b). To counter this situation, current generation orthopaedic devices must be improved and developed to increase longevity and reduce healing times following surgery.

The current material of choice for both orthopaedic and dental applications is titanium alloy (Geetha et al., 2009). This is due to the materials many desirable properties which include, mechanical strength, resistance to corrosion and wear, and its ability to promote osseointegration (Branemark, 1983). Despite these advantageous properties, titanium alloy cannot always be used and other more mechanically strong materials such as CoCrMo are often preferred. For example, CoCrMo is used widely in TKA as its excellent resistance to wear allows the material to be used as a bearing surface. Whilst CoCrMo may be mechanically strong it does not have the same level of biocompatibility as titanium alloy (Sinha et al., 1994).

Following the implantation of an orthopaedic device, the surrounding tissues and cells do not come into contact with the bulk material of the implant, but are instead mediated by its surface. Titanium oxide (TiO_2) is a naturally occurring oxide layer found on the surface of titanium and its alloys. At approximately 3-7 nm thin, this self-repairing, durable oxide layer could play an important role in bone healing, by mediating the events that take place at the cell-implant interface, such as protein adsorption, cell adhesion and differentiation (Textor, 2001).

This section of the project aimed to investigate whether coating the bio inert material, CoCrMo, in a layer of anatase TiO_2 by way of atmospheric CVD, could improve the bioactivity of the material. Human MSCs isolated from the bone marrow of the iliac crest were used for the investigation. MSCs are multipotent cells which have the capability to differentiate into adipocytes, chondrocytes and osteoblasts (Pittenger et al., 1999). It is widely accepted that following orthopaedic implantation, MSCs are one of the first cell types recruited to such sites, where they can then colonise onto the surrounding surfaces and differentiate into osteoblasts capable of facilitating in bone formation and healing

(Davies, 1998, Davies, 2003). Markers of cell proliferation, adhesion and differentiation were studied to assess the osteogenic capability of uncoated CoCrMo, TiO_2 coated CoCrMo (CCMT) and titanium discs (Ti). Surface characterisation of all the substrates was also performed which included surface wettability, topography and SEM analysis.

The hypothesis explored in this chapter is:

1. The addition of an anatase TiO_2 layer created by CVD onto the surface of CoCrMo can generate the increased osteogenic differentiation of human MSCs, to a comparable level as that observed on a titanium positive control surface.

2.1. MATERIALS AND METHODS

2.1.1. SAMPLE PREPARATION

Discs formed of CoCrMo (Cr 26-30, Mo 5-7) were supplied by Corin Ltd (Cirencester, UK). Each disc had a machined finished (Figure 10 A) and dimensions of 15 mm Ø, 1mm thickness. To create a smooth surface on the discs, free of any influence of surface topography, the discs were ground and polished to a mirror finish (Figure 10 B). Individual discs were mounted and fixed on resin bases (SpeciFix-20, Struers, 40200048) using araldite rapid for 30 minutes (Figure 10 C). Once the discs were securely fixed in place, the exposed surface was manually ground to remove the machined finish using a LaboForce-1 grinding machine (Struers) with silicon carbide (SiC) #1000 grit paper (Struers, 40400011) at 300 revolutions per minute (rpm) lubricated with H_2O. The discs were rinsed using $_{dd}H_2O$, transferred to a RotoForce-1 polishing machine (Struers) and polished for 4.5 minutes at a force of 30 Newtons (N) using MD Dac (Struers, 40500071) with DP-Suspension P 3µm (Struers, 40600251). The discs were lubricated during the polishing procedure using DP-Lubricant Blue (Struers, 40700006). Following this, discs were mechanically removed from the resin bases, sonicated for 15 minutes in isopropanol followed by $_{dd}$H2O at room temperature (RT) and air dried. Commercially pure Ti (Cp-Ti) discs were provided by Institut Straumann AG (Walderberg, Switzerland). A detailed description of the Straumann manufacturing process can be found in (Rupp et al., 2006). In brief, Ti discs were punched out of sheets of commercially pure titanium and were ground using diamond paste in oil and SiO_2 suspension.

2.1.2. SAMPLE PASSIVATION AND STERILISATION

Before discs were used for cell culture experiments they underwent a sterilisation procedure. CoCrMo, CCMT and Ti discs were immersed in nitric acid (0.1 N, BDH, 19088 5E) for 10 minutes as a passivation step in order to clean and reduce the effect of external environment factors. The procedure can thicken the protective outer oxide layer and reduce corrosion and the release of potentially harmful ions from the surface (Brune et al., 1984). Lastly, substrates were washed in $_{dd}H_2O$, air dried in a sterile environment

and then irradiated with UV light for 20 minutes on each side prior to use (BONMAY, BR-506).

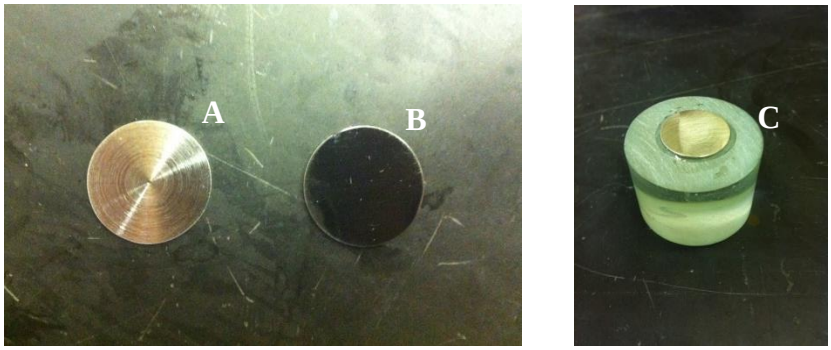

Figure 10 CoCrMo discs supplied with a machined finish (A), and a smooth, mirrored finish following grinding/polishing procedure (B). (C) shows how each disc was individually mounted on a resin base.

2.1.3. CHEMICAL VAPOUR DEPOSITION

***Performed by Alison J Cross, Department of Chemistry, UCL.**

Atmospheric pressure CVD was used to create a thin coating of TiO_2 on smooth CoCrMo discs. Titanium tetrachloride ($TiCl_4$) and ethyl acetate were used in the procedure, previously developed to coat steel substrates and glass (Cross et al., 2012, Hyett et al., 2010). The $TiCl_4$ bubbler was heated to 68°C, whilst the ethyl acetate was heated to 40°C, with all gas lines heated to above 150°C. Around 30 CoCrMo discs were placed inside the deposition chamber which was heated to a temperature of 500°C. Discs were positioned near the gas inlet of the chamber to ensure complete coverage of the substrate surface. The deposition was carried out for 60 seconds with flow rates of 1.32 litres/min for $TiCl_4$, 0.3 litres/min for ethyl acetate, 3 litres/min for plain 1 and 1.85 litres/min for plain 2.

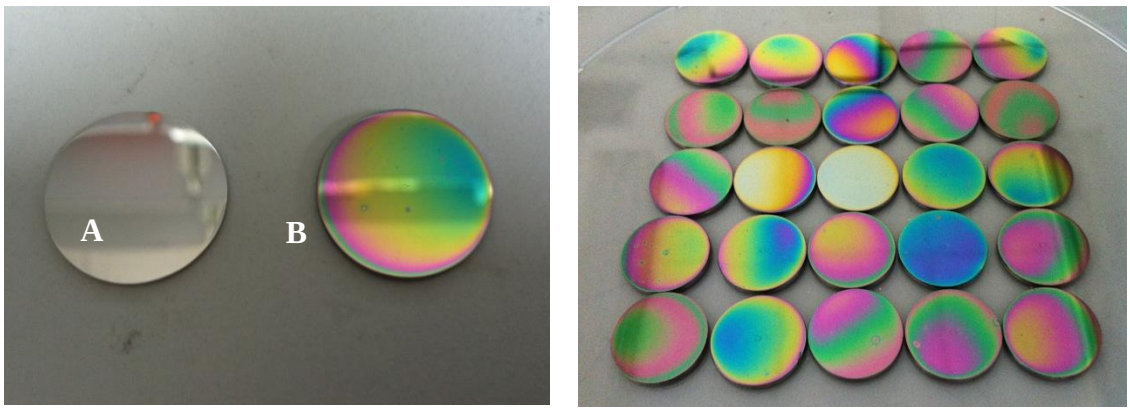

Figure 11 A polished CoCrMo disc before (A) and after (B) coating with TiO_2. (C) shows the variation in the appearance of the TiO_2 coating on 25 CoCrMo discs coated together in the same batch.

2.1.4. SUBSTRATE CHARACTERISATION

***Raman & XRD performed by Alison J Cross, Department of Chemistry, UCL.**

The presence of anatase TiO_2 on the surface of coated CoCrMo discs was examined by Raman spectroscopy and x-ray diffraction (XRD) methods. Surface topography of the substrates was analysed by obtaining R_a values through laser profilometry scans (Scantron, Proscan 1000). R_a is the arithmetic average of the absolute values of a roughness profile. Substrates were loaded onto the testing rig, fixed in place and brought into focus of the laser. An area of 6.25 mm^2 was then examined (n = 5) and R_a values obtained using Proscan software. Scanning electron microscopy (SEM) of the substrate surface was also performed. CoCrMo, CCMT and Ti discs were fixed onto mounts (G301, Agar Scientific) overnight using araldite ultra. Images of both low and high magnification were taken by SEM (Philips, XL30 FEGSEM) using a beam energy of 5 keV and spot size of 3. The wettability of the substrates was analysed by static contact angle measurements, using an optical contact angle meter (KSV Instruments LTD, CAM 200) with 2 µl drops of $_{dd}H_2O$ (n = 6). The thickness of the TiO_2 coating on each disc of each batch was analysed using filmetrics (F20) using FILMeasure software.

2.1.5. MSC ISOLATION

***Performed by the Tulane Center for Gene Therapy, US.**

Bone marrow aspirate was drawn from the iliac crest of three individuals; two male aged 22 and 24, and a female aged 37. Using density centrifugation, the mononuclear cells were first separated and then plated onto tissue culture plastic (TCP) to obtain the adherent MSCs. The culture media consisted of minimum essential media – α (MEM-α) containing 16.5% foetal bovine serum (FBS). When the MSCs reached 60-80% confluence they were harvested as passage 0, re-expanded and harvested again, and then either frozen or re-expanded for characterisation testing as passage 1. Freezing media consisted of MEM-α containing 30% FBS and 5% dimethyl sulfoxide (DMSO).

Characterisation of the MSCs was performed on cells ranging from passage 2 up to passage 4. Using flow cytometry, MSCs of passage 2 were tested for markers known to be expressed by MSCs, and were positive (> 95 %) for CD147, CD166, CD90, CD49c, CD29, CD105, CD73a, CD59, CD146. MSCs were also negative (< 2 %) for blood cell markers CD14, CD79a, CD45, CD11b, CD19 and CD34. To determine cell growth and differentiation, MSCS were analysed over three passages (2-4), and shown to have sufficient fold increase in cell numbers and were capable of differentiating into bone, cartilage and fat.

Vials containing the MSCs at a concentration of 1 x 10^6 cells/ml/vial, were delivered to the Eastman Dental Institute in liquid nitrogen, where they were then transferred to a permanent liquid nitrogen storage container, until required.

Table 2 Summary of the surface markers analysed for expression in MSCs. Information supplied by Tulane Centrer for Gene Therapy, US.

SURFACE MARKER	ROLE/FUNCTION	EXPRESSION
CD11b	Mediates adhesion to substrates	Negative
CD14	Monocyte differentiation antigen	Negative
CD19	Regulates B cells development, activation and differentiation	Negative
CD29	Fibronectin receptor	Positive

CD34	Cell-cell adhesion molecule and cell surface glycoprotein	Negative
CD45	Leucocyte common antigen	Negative
CD49c	Receptor for laminin, collagen, fibronectin, thrombospondin	Positive
CD59	Regulates complement mediated cell lysis by inhibiting formation of membrane attack complex	Positive
CD73a	Catalyses dephosphorylation of ribo- and deoxyribonucleotides. Protect against vascular inflammation	Positive
CD79a	Encodes Ig-alpha protein on the B cell antigen receptor	Negative
CD90	Thy-1	Positive
CD105	Mediates cellular response to TGF-β 1	Positive
CD146	Cell surface glycoprotein	Positive
CD147	ECM metalloproteinase inducer	Positive
CD166	Cell adhesion molecule	Positive

2.1.6. CELL CULTURE

MSCs were resuscitated by half submerging the passage 1 cryovials in a water bath set to 37˚C (Grant, Y28 GD100) until thawed. Cells were defrosted as quickly as possible to prevent damage to the cells from DMSO. The vials were then transferred to a sterile laminar flow hood to minimise the risk of contamination. All further cell culture protocols were performed in a laminar flood hood, unless otherwise stated. The MSCs

were seeded on TCP at a density of 833 cells cm^{-2} and expanded in complete growth medium (GM) that comprised of MEM-α (Gibco, 22571-020) containing 10% FBS (Gibco, 10270-106) and 1% penicillin-streptomycin (Sigma-Aldrich, P0781). Both FBS and penicillin-streptomycin were filter sterilised before being added to the media bottle (Millipore, SLGPM33RS). All media was pre-warmed for a minimum time of 30 minutes in a 37°C water bath. MSCs were incubated at standard culture conditions of 37 °C/5% CO_2 in a humidified atmosphere with media changed every 3 or 4 days. MSCs were then harvested by treatment of trypsin (0.025%)/elthylenediaminetetraactic acid (EDTA) (0.01%) (Gibco, R-001-100) when they reached 80% confluence. To help ensure the integrity of the results in the study, only cells of low passage (<5) were used for experiments. Osteogenic media consisted of Dulbecco's Modified Eagle's Medium (DMEM) low glucose pyruvate (Gibco, 31885-023), containing 10% FBS, 1% penicillin-streptomycin, with the addition of osteogenic supplements in the following concentrations; 10mM β-glycerol phosphate (Sigma-Aldrich, G9891), 50μg/ml L-ascorbic acid 2-phosphate (Sigma-Aldrich, A8960) and 10nM dexamethasone (Sigma-Aldrich, D9402).

2.1.6.1. SUB-CULTURE

As previously mentioned dissociation of the cells was performed using trypsin/EDTA. Firstly, MSCs were washed twice using Dulbecco's phosphate buffer saline (PBS) and then incubated at 37 °C for 5 minutes with pre-warmed trypsin/EDTA at a volume of 1 mL per 25 cm^2. Following this, cell dissociation was confirmed using an inverted optical microscope (Olympus, CXK31) and trypsin/EDTA was deactivated by added a 1 : 1 ratio of GM. The suspension was then pelleted by centrifugation at 5000 rpm for 5 minutes (Sorvall, Legend RT). The media containing trypsin was then aspirated off and replaced with fresh GM. Cells were then resuspended, counted and sub-cultured at known densities.

2.1.6.2. CRYOPRESERVATION

Following culture, MSCs were pelleted, re-suspended and counted in freezing media which consisted of 70% GM, 20% FBS and 10% DMSO (Sigma-Aldrich, D2650). 1 millilitre (mL) of MSCs was then aliquoted into individual cryovials at a density between 0.5 – 1 x 10^6 cells per mL. Vials were then brought down to -80 °C at a rate of 1 °C per minute using a freezing container in a -80 °C freezer. After 24 hours, vials were transferred to cryogenic storage tanks containing liquid nitrogen (Taylor Wharton, LS3000).

2.1.7. PROLIFERATION

AlamarBlue (AbD Serotec, BUF012A) was used to assess the cellular proliferation of the human MSCs. AlamarBlue is an indicator of the metabolic activity of cells, working as an oxidation reduction reagent. The indicator dye both fluoresces and changes colour in response to the chemical reduction of growth media resulting from cell growth and can be used to quantitatively measure the proliferation of cells.

MSCs were seeded onto CoCrMo, CCMT and Ti using a 24 well plate at a density of $2x10^3$ cells per well (n = 3) and were incubated at 37˚C, 5% CO_2 in a humidified atmosphere. Individual plates were setup for both GM and OM, and the media was changed on each day of analysis. 100 µl of dye was added to each well containing 1 ml of either GM or OM, and incubated at standard culture conditions for 4 hours. Thereafter, two 100 µl aliquots of supernatant were taken from each well and transferred to a 96 well plate for analysis. The level of oxidation reduction was then assessed using a fluorescence plate reader (Biotek, FLX800) with an excitation wavelength of 530 nm and emission wavelength of 590 nm. The amounts of cells was calculated via interpolating from a standard curve.

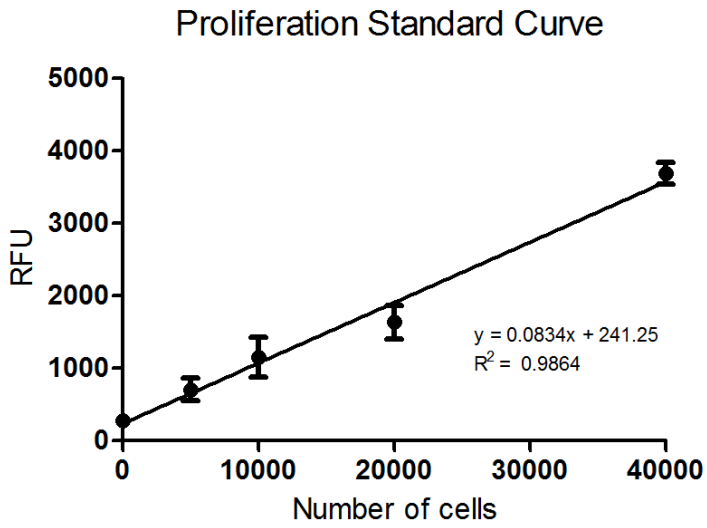

Figure 12 Standard curve data for the proliferation study. Each point represents the mean ± 1SD (n = 6).

2.1.8. CELL MORPHOLOGY - INTERNAL

Confocal laser microscopy was used to analyse the morphology of MSCs on the three substrates. Specifically, fluorescent markers for both cell nuclei and f-actin were used. Labelling the cell nuclei allows for easy cell identification, whilst f-actin is one of the abundant proteins expressed in the cytoskeletal structure of the MSCs, hence allowing for the visualisation of the internal cellular structure.

A total of 12.5 x 10^3 MSCs were seeded on each CoCrMo and CCMT disc (n = 3) using OM. Cultures were incubated at standard culture conditions of 37°C, 5% CO2 in a humidified atmosphere and had the media replaced after 3 days. Following 24 hours and 7 days incubation, the MSCs were washed twice using 1 ml of PBS (Lonza, 17-512F). 500 µl of 4% paraformaldehyde (PFA, Sigma-Aldrich, P6148) was used as a fixative for 15 minutes at RT. Following 3 washes with 1 ml PBS, the MSCs were treated with 500 µl 0.15% Triton X-100 (BDH, 30632 4N) in PBS for 4 minutes to permeabilise the cellular membrane. After three further washes in 1 ml of PBS, the f-actin was labelled using 200 µl Alexa fluor 488 phalloidin in PBS (Life Technologies, A12379, 2.5:100) for 20 minutes at room temperature in the dark. After 3 washes with 1ml PBS, whilst protected from light, the cultures were then counterstained to label the nuclei using 200 µl propidium iodide (PI) in PBS for 10 minutes (Life Technologies, P3566, 4 µg/ml). Cells were then washed three times in 1ml of PBS and suspended in 3 ml of PBS in for

viewing. MSCs were analysed using a X40 wet lens connected to a Radiance 2100 Laser Scanning System.

2.1.9. CALCIUM ASSAY

The amount of calcium produced by cells can be used to monitor different bone diseases or calcium related disorders. As MSCs differentiate into osteoblasts and form new bone tissue, one of the stages of this process is the deposition of an ECM rich in calcium. Therefore the same practice used to monitor bone diseases, can be applied to measure the rate of osteogenic differentiation occurring in cell culture. The QuantiChrom Calcium Assay kit (Bio Assay Systems, DICA-900) was used to measure the amount of calcium produced. The kit is designed to measure calcium directly in biological samples without the need for pre-treatment, through the use of a phenolsulphonephthalein dye which forms a stable blue coloured complex with free calcium. The intensity of the colour is directly related to the calcium concentration of the sample and is measured at 612 nm.

MSCs from three donors were seeded at a density of 12.5 x 10^3 cells per well in OM, incubated at 37˚C, 5% CO_2 in a humidified atmosphere with media changes every 3-4 days. After 7, 14 and 21 days the cultures were examined. Prior to performing the QuantiChrom calcium assay, to normalise the data, the amounts of cells were assessed using AlamarBlue, as previously described in 2.1.7 PROLIFERATION – (Page 62). Following 2 washes with 1 ml of PBS, calcium content was measured as per the manufacturer's instructions. The cell monolayer was homogenised by incubation with 500 µl 1M hydrochloric acid (HCl, Sigma-Aldrich, 258148) for 60 minutes at room temperature on a rocking plate. 5 µl aliquots were then taken from each sample and transferred to a clear 96 well plate and combined with 200 µl assay reagent. Calcium levels were then measured (λ = 620 nm, Tecan M200) and concentrations calculated with use of known concentration standards.

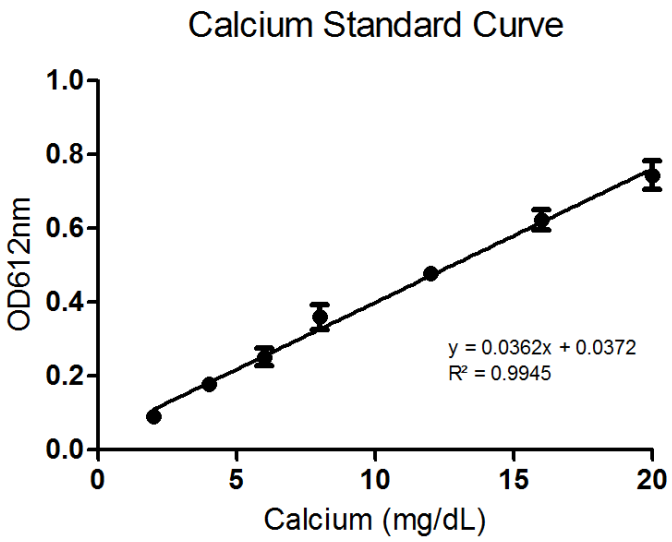

Figure 13 Standard curve data for calcium assay. Each point represents the mean ± 1SD (n = 3).

2.1.10.HYDROXYAPATITE NODULE FORMATION

In addition to calcium ion content, the osteogenic differentiation of MSCs can also be shown by the formation of mineralised nodules of hydroxyapatite. Inorganic hydroxyapatite ($Ca_{10}(PO_4)_6(OH)_2$) and type I collagen make up the matrix of bone tissue, with more mineralised bone tissue having abundant hydroxyapatite throughout. The OsteoImage Mineralisation Assay (Lonza, PA-1503) was used to assess the hydroxyapatite content. Unlike better established *in vitro* mineralisation techniques such as von Kossa and alizarin red, OsteoImage binds specifically to the hydroxyapatite portion of bone nodules formed by MSCs, allowing for them to be visualised under a fluorescent microscope fitted with the correct filters (Excitation = 492nm, emission = 520nm).

MSCs were seeded on CoCrMo, CCMT and Ti at 12.5 x 10^3 cells per well in OM (n = 3), incubated at 37˚C, 5% CO_2 in a humidified atmosphere and underwent media changes every 3-4 days. Hydroxyapatite staining was performed using the OsteoImage kit as per the manufacturer's instructions after 7, 14 and 21 days. MSCs were washed twice with 1 ml of PBS and fixed for 15 minutes using 500 µl of 4% PFA. Using 1 ml of OsteoImage diluted wash buffer, cultures were washed twice and then incubated with 500 µl of staining reagent (1:100 Staining reagent in staining reagent dilution buffer) for 30 minutes at room temperature, protected from light. After incubation, the staining reagent was

removed and the cultures were washed a further 3 times with wash buffer (5 minutes per wash), before having images taken using a fluorescent microscope fitted with the appropriate filters (Leica DMIRB). Image analysis was performed using a pixel based method as described in section 2.1.11 IMAGE QUANTITATION – (Page 66).

2.1.11. IMAGE QUANTITATION

To obtain semi-quantitative data from qualitative images, a protocol was employed to calculate the total area of the subject of interest, by way of converting raw images to binary images and computing the total amount of pixels. Firstly, using freeware ImageJ software (Windows version 1.49), raw images were converted to 8-bit binary using the threshold tool, only highlighting the areas of interest. The measurements to be analysed were redirected to the chosen image and selected using the set measurements tool, which included area, perimeter and Feret's diameter. The analyse particles tool was then used to quantify the selected measurements of all objects highlighted using the threshold tool. This action created a duplicate image that labelled all objects that were analysed and opened a complimentary worksheet that summarised the previously selected set measurements for all objects. When conversion of pixels to micrometres was used, this was calculated using the Leica DMIRB pixel-micrometre conversion sheet.

2.1.12. TYPE I COLLAGEN DEPOSITION

The formation of healthy bone tissue is not solely reliant on having abundant amounts of mineral but is subject to a careful balance of inorganic mineral and collagenous material (Viguet Carrin et al., 2006). Achieving the correct balance of mineral-collagen in the bone tissue deposited by MSCs is vital, hence the inclusion of type I collagen formation in the present study. A fluorescent microscopy protocol was developed to allow for external type I collagen to be visualised and imaged, and from this data, quantitative analysis could be performed by converting the images into binary data.

MSCs were seeded on CoCrMo, CCMT and Ti at 12.5 x 10^3 cells per well in OM (n = 3), incubated at 37˚C, 5% CO_2 in a humidified atmosphere and underwent media changes every 3-4 days. After 7 and 14 days the MSCs were prepared for analysis. MSCs were

washed twice with 1 ml of PBS and fixed using 500 µl of 4% PFA for 15 minutes. Following 3 further washes with PBS, the cells were incubated with 500 µl of 10% goat serum (Sigma-Aldrich, G9023) in PBS for 30 minutes at room temperature to prevent any unspecific antibody binding. Primary antibody incubation was then performed overnight a 4˚C using anti-type I collagen antibody (Sigma-Aldrich, C2456, 1:1000) diluted in 300 µl of 1.5% skim milk in PBS. Following 3 washes with PBS, the MSCs were incubated for 60 minutes at room temperature in the dark with alexa fluor 488 goat anti-mouse (Life Technologies, A11001, 2.5:100), diluted in 250 µl of 1.5% skim milk in PBS. The MSCs were then washed in PBS and counterstained with 400µl of 4′,6-Diamidino-2-phenylindole dihydrochloride (DAPI: Sigma-Aldrich, D9542, 10 µg/ml) in PBS for 40 minutes at room temperature protected from light. Lastly after one final wash in PBS the samples were mounted on microscope slides and viewed using a fluorescent microscope fitted with the appropriate filters (Leica DMIRB). Images were taken and quantifiable analysis was performed via a pixel based method using ImageJ software as described in section 2.1.11 IMAGE QUANTIFICATION – (Page 66).

2.1.13. VINCULIN EXPRESSION

Following implant surgery the ability for the implant surface to promote the differentiation of MSCs into osteoblasts capable of forming new healthy bone tissue is extremely important, although for this to take place, the successful attachment and colonisation of the MSC population must first occur (Anselme, 2000). The attachment of MSCs to the surface of such implants involves the combination of a number of adhesion and structural molecules found on the exterior and interior of the cells (Humphries et al., 2007). One such molecule is the focal adhesion protein vinculin, which congregates at complexes known as focal adhesions. Vinculin was studied using the established fluorescent microscopy protocol, and quantitative analysis was performed on a randomised group of single cells of similar size on each substrate.

MSCs were seeded on CoCrMo, CCMT and Ti at 5 x 10^3 cells per well (n = 3) in OM at standard culture conditions for 24 hours and 7 days. The media was changed after 3 days. The MSCs were washed twice with 1 ml of PBS then fixed for 15 minutes at room temperature with 500 µl of 4% PFA. Following three further washes with PBS, to permeabilise the cellular membrane, the substrates were incubated with 500 µl of 0.15%

Triton X-100 in PBS for 4 minutes, then washed an additional 3 times with PBS. The substrates were then incubated overnight at 4˚C with 300 µl of the primary antibody solution composed of the mouse anti-vinculin antibody (Abcam, ab18058, 1:200) diluted in 1.5% skim milk in PBS. After three additional washes in PBS the substrates were then incubated for 60 minutes at room temperature in the dark with the alexa fluor 568 goat anti-mouse secondary antibody (Life Technologies, A11031, 2.5:100) diluted in 1.5% skim milk in PBS. After a final wash in PBS the substrates were then suspended in 3 ml of PBS and viewed under a x40 wet lens connected to a Radiance 2100 Laser Scanning System. Images of individual cells were taken and vinculin expression was quantified as a pixel based method using ImageJ software as described in section 2.1.11 IMAGE QUANTIFICATION – (Page 66).

2.1.14. SINGLE CELL ADHESION

***Performed by Anas Sherif, Eastman Dental Institute, UCL.**

Whereas vinculin fluorescent microscopy analysis can give a qualitative indication of the adhesion strength a single cell possesses, recent novel advances in how atomic force microscopy (AFM) is utilised can now allow for real time quantitative adhesion measurements to be taken on live single cells.

A total of 1 $x10^3$ MSCs were transferred to a 35 mm petri dish containing CGM with one disc of CoCrMo, CCMT and Ti. The substrates were then transferred into the heated chamber located on the NanoWizard AFM stage (JPK-Berlin) to maintain the MSCs at 37˚C. The CGM was replaced with long lasting CO_2 serum free media (Sigma Aldrich, 14571C). AFM non-conductive silicon nitride tip-less cantilevers (Bruker, NP-010) were modified with glass beads (10-30 microns, Polysciences, 07666) which had been coated with concanavalin A (Con A) biomolecules as previously described (Weder et al., 2009). The modified AFM cantilever was then approached to a single free moving MSC, with a maximum load varying between 400 and 900 pN, to ensure contact adhesion between the cell and the con A coated glass bead. This load was also low enough to prevent any compressive damage to the cell. The cantilever was then retracted and left undisturbed for 15 minutes to ensure that the cell had adhered strongly to the con A coated glass bead. Following completion of these preparation steps, adhesion measurements were then taken between the modified cantilever/bead/cell and the substrates by performing force-distance curves using the AFM. An initial load of 4.5 nN, a dwell time of 1 second and

a retraction loading rate of 0.5 μm/sec were the experimental parameters. At all times the sample and cell were kept in physiologically relevant conditions and confirmation of the MSC attachment to the con A coated glass bead was performed by SEM and the AFM camera.

2.1.15. STATISTICAL ANALYSIS

For each experiment, samples were performed in triplicate ($n = 3$) except for surface characterisation analysis which used a sample size of $n = 6$ for contact angle and $n = 5$ for roughness. Quantification of vinculin expression was performed using 10 cells ($n = 10$). GraphPad Prism software was used to examine the statistical significance between groups with $p < 0.05$ to be considered significant. A one-way ANOVA followed by Bonferroni's multiple comparison test was used to analyse characterisation and AFM data, whereas the two-way ANOVA followed by the Bonferroni post-test was used to analyse calcium, collagen, hydroxyapatite and vinculin data sets. A post-hoc power calculator was used to confirm the statistical power of significant results observed in the study.

2.2. RESULTS

2.2.1. SUBSTRATE CHARACTERISATION

2.2.1.1. RAMAN SPECTROSCOPY

***Performed by Alison J Cross, Department of Chemistry, UCL.**

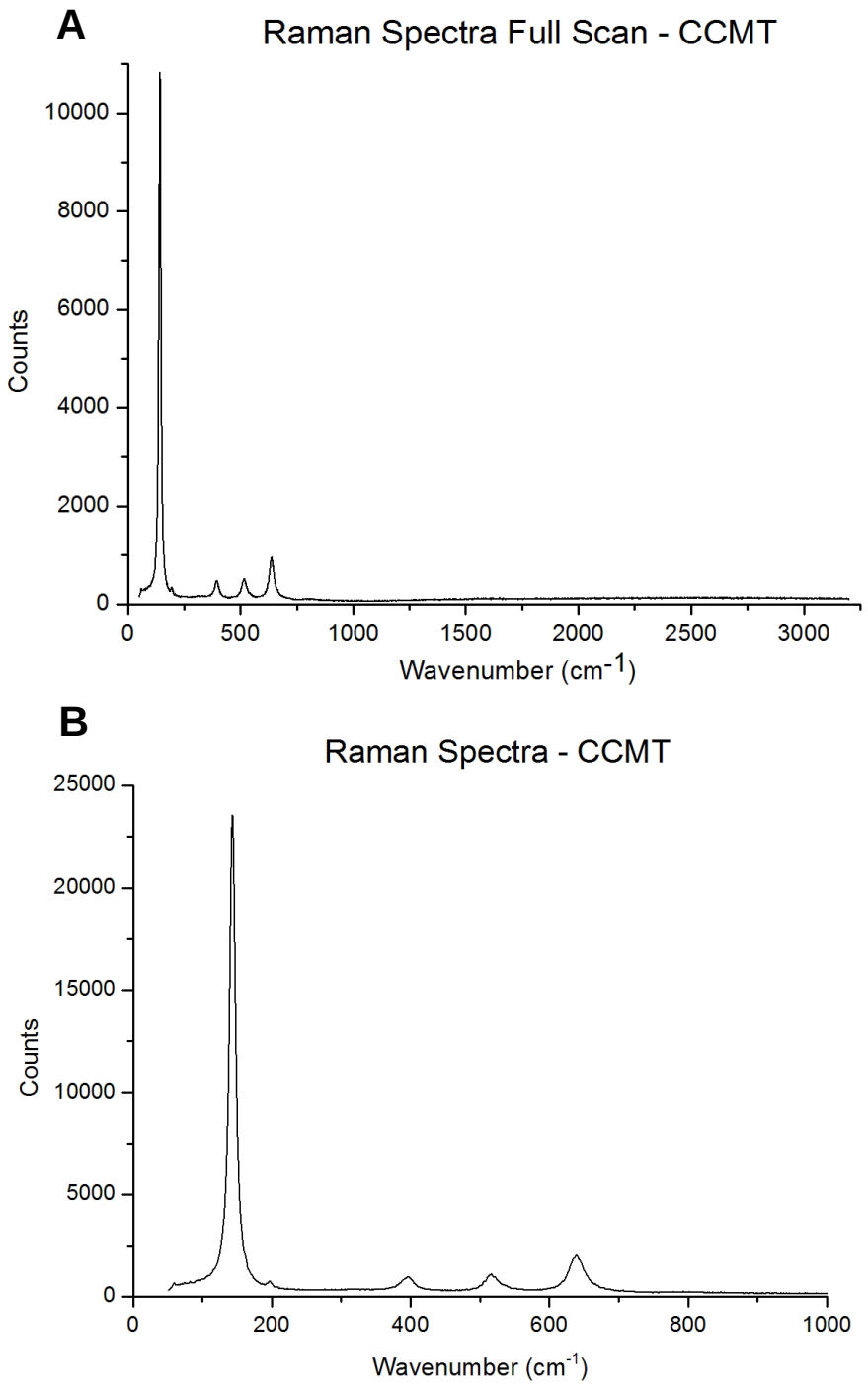

Figure 14 A Raman spectra of CCMT. A shows a full scan, whereas for B the scan stops at 1000cm^{-1} allowing for more clear identification of the TiO_2 anatase peaks.

Raman spectroscopy of the CCMT substrate confirmed the presence of TiO_2 in its anatase form by the strong peaks present at 143, 392, 515, 625 cm^{-1} (Turkovic et al., 1991). Each coated disc underwent Raman analysis to confirm that the deposition of the coating was successful. A small proportion of the samples were shown to have a minute trace of rutile TiO_2.

2.2.1.2. XRD

***Performed by Alison J Cross, Department of Chemistry, UCL**.

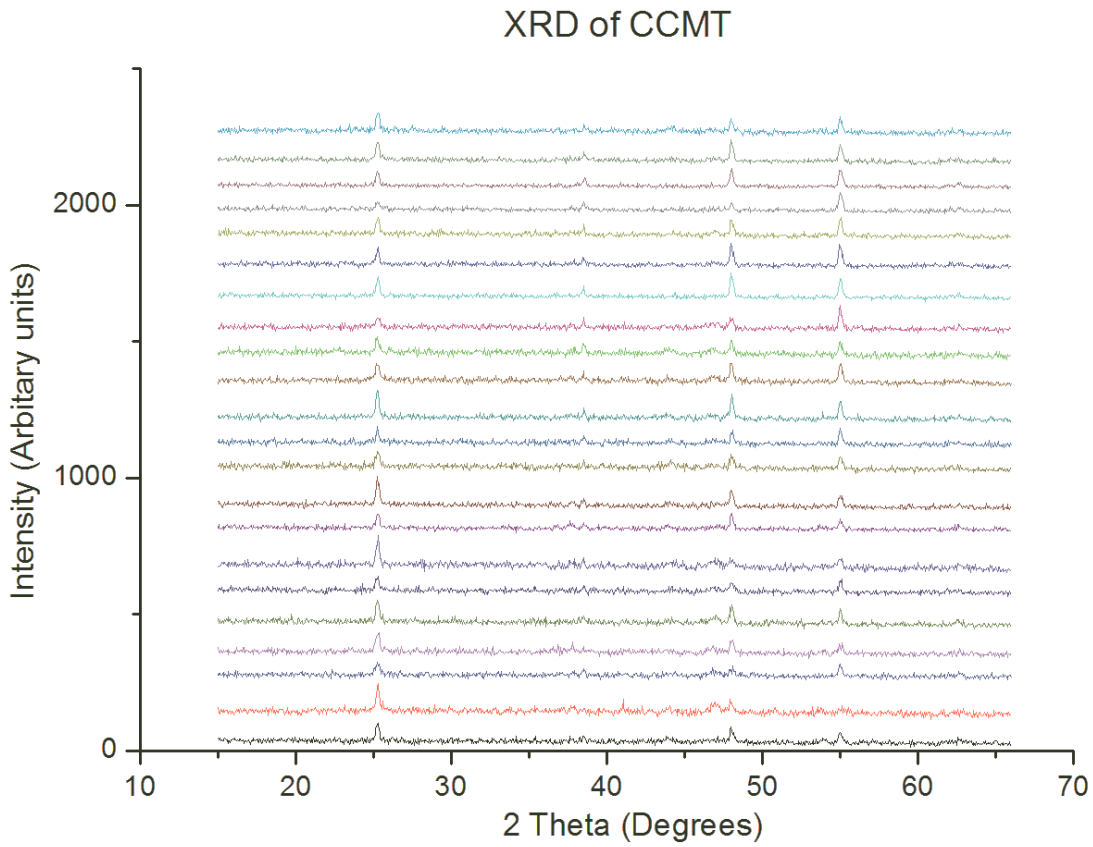

Figure 15 XRD data for CCMT discs 1-22 of batch AJC248.

XRD analysis was performed to confirm the presence of anatase TiO_2 on the substrate surface. Shown above in figure 15, is an example of the data, with each coloured spectra representing an individual disc of batch AJC248. The data supports that found during Raman analysis, confirming the presence of anatase TiO_2 with peaks at theoretical anatase points.

2.2.1.3. CONTACT ANGLE

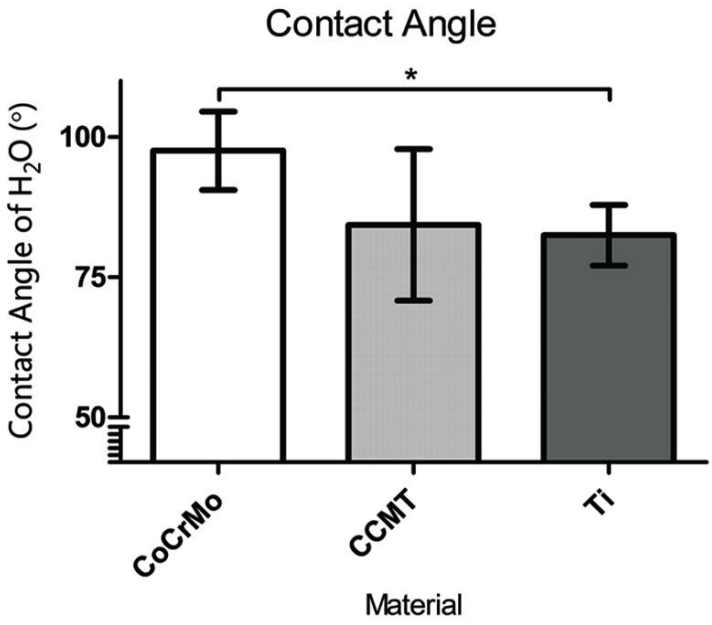

Figure 16 Contact angle results; CoCrMo surface is significantly more hydrophobic than Ti, with the CCMT surface ranging in the middle of the two. Each bar represents the mean ± 1SD (n = 6), *=p<0.05 material vs. one surface, #=p<0.05 material vs. both surfaces.

Contact angle data can give a measure of the wettability of a surface, with most materials commonly referred to as either hydrophobic (>65˚) or hydrophilic (<65˚). Using $_{dd}H_2O$, the contact angle on all three materials fell into the hydrophobic range, with CoCrMo shown to be the most hydrophobic (97 ± 7˚), followed by CCMT (84.3˚ ± 13.5˚) and lastly Ti (82.5 ± 5.4˚).

2.2.1.4. SURFACE ROUGHNESS

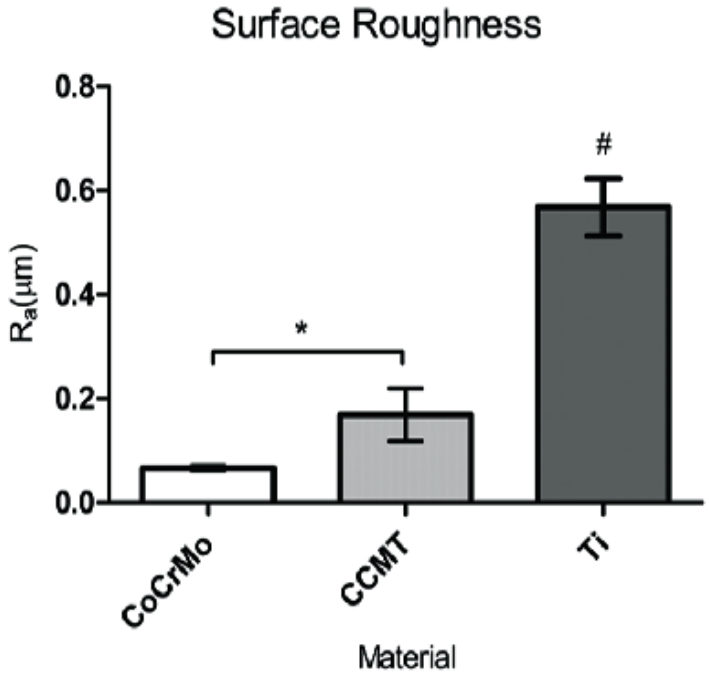

Figure 17 Surface roughness results; a significantly greater level of roughness was observed on the Ti surface, compared to both CoCrMo and CCMT. In addition, the CCMT surface was significantly rougher compared to CoCrMo. Each bar represents the mean ± 1SD (n = 5), *=$p<0.05$ material vs. one surface, #=$p<0.05$ material vs. both surfaces.

Laser profilometry of the substrate surface showed that Ti (0.56 µm) was significantly rougher ($p<0.0001$) than both CoCrMo (0.07 µm) and CCMT (0.17 µm). Despite this increase in surface roughness on Ti, all three substrates can still be referred to as smooth as they fall within the range listed as smooth in a recent review (Wennerberg and Albrektsson, 2009). A slight increase in surface roughness was also observed on the CCMT substrate compared to CoCrMo ($p<0.05$).

2.2.1.5. TIO_2 COATING THICKNESS

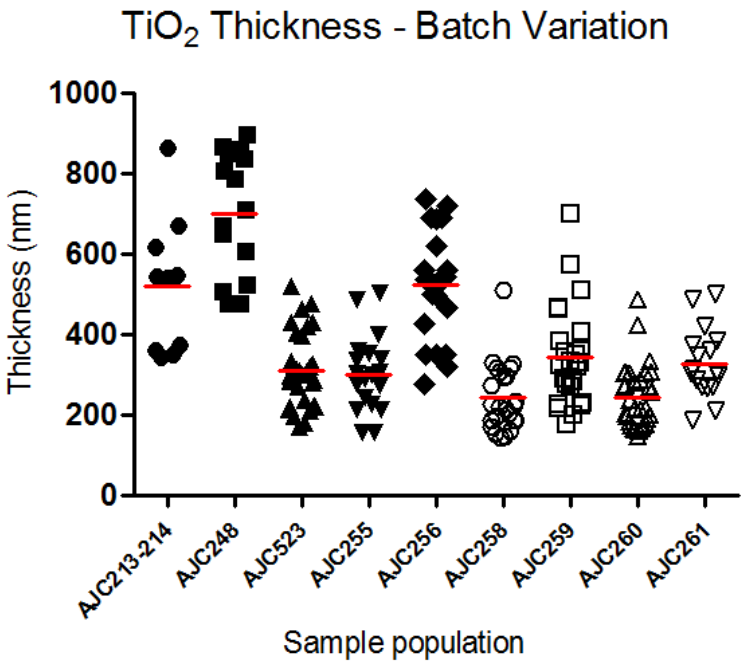

Figure 18 Filmetrics data displaying the thickness of the TiO_2 coating on CCMT discs within individual groups and between all batches. The red line shows the mean of each group.

To ascertain a measure of the thickness of the TiO_2 coating, filmetrics measurements were performed on each disc of every batch of coated discs. As shown in figure 18, the first couple of batches of TiO_2 were moderately thicker than more recent batches such as AJC260 and AJC261, with the exception of AJC256 which was slightly thicker than anticipated.

2.2.1.6. SEM

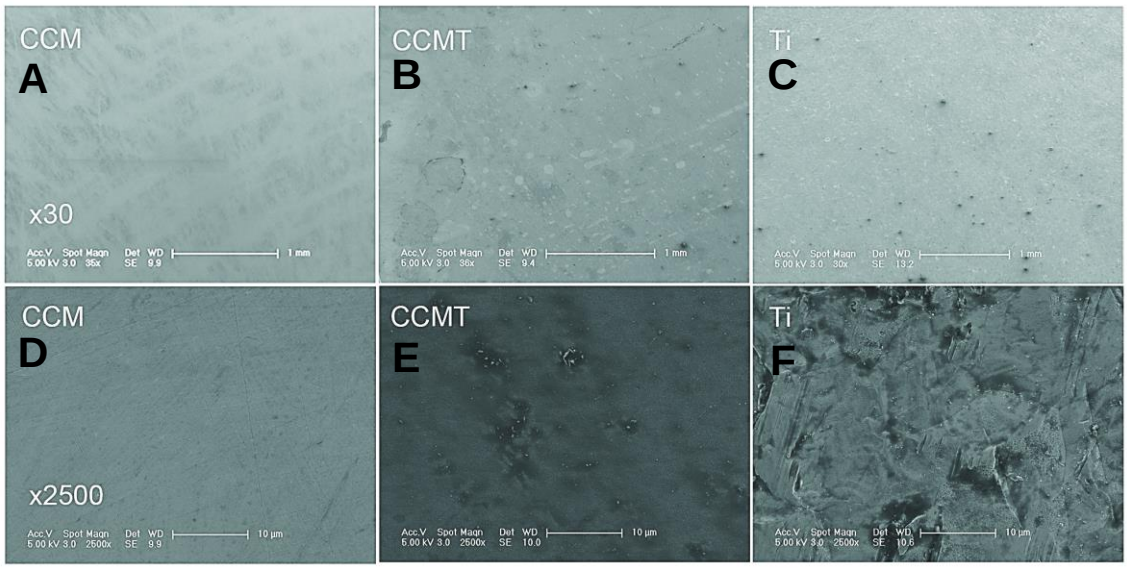

Figure 19 SEM images of surface topography on CCM, CCMT and Ti taken at low (A-C) and high magnification (D-F). A-C scale bar = 1 mm, E-F scale bar = 10 μm.

SEM analysis at low magnification (Figure 20 A-C) showed a similar, featureless, smooth topography on all three substrates. Under higher magnification (Figure 20 – D-F) the differences between the surfaces became evident, where an increase in surface roughness on CCMT and Ti compared to CoCrMo was observed, in the form of indentations on the material surface. As previously mentioned, despite this variation in topography, all three substrates can still be described as smooth.

2.2.2. PROLIFERAION

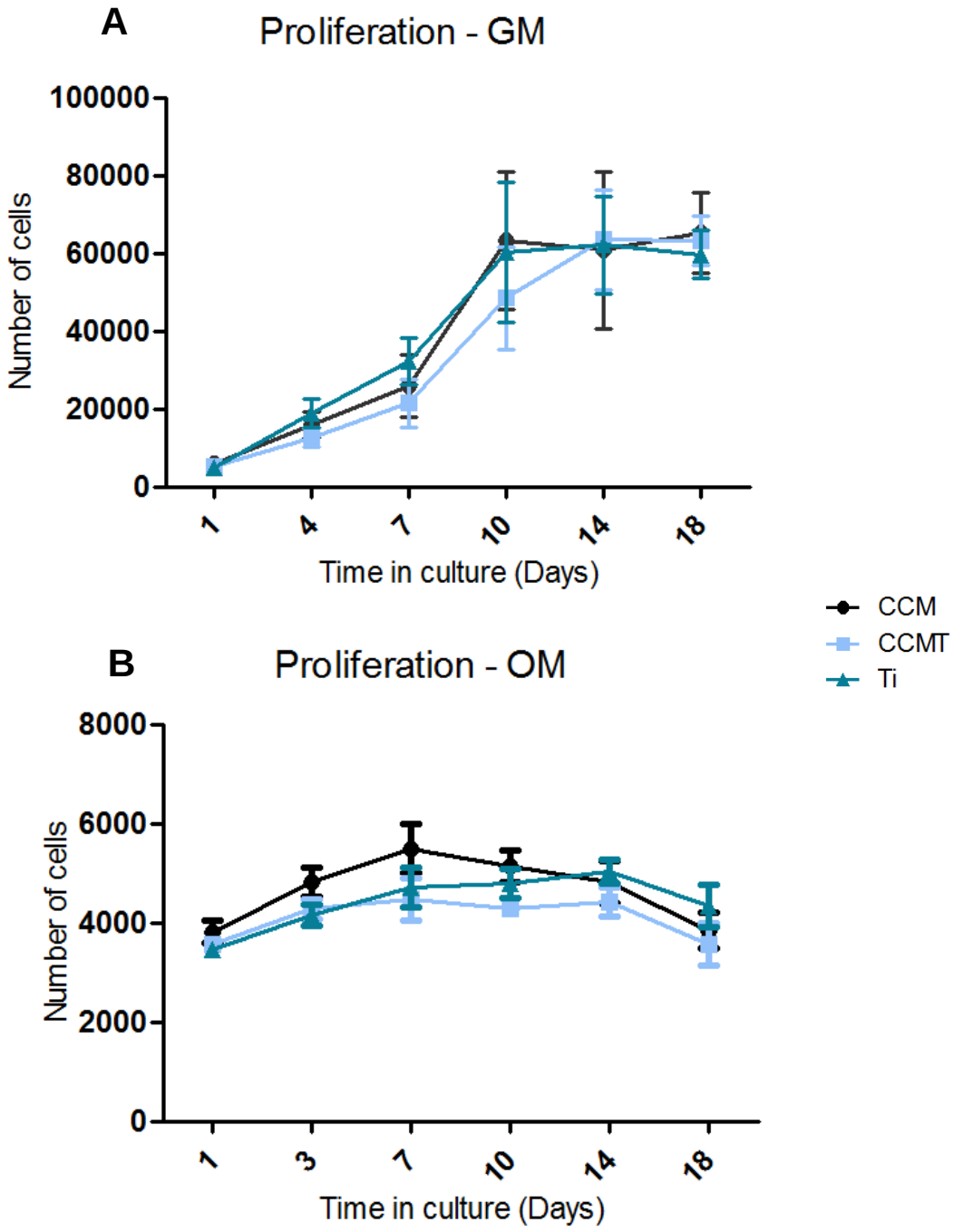

Figure 20 Proliferation data for all three substrates in both growth media (A) and osteogenic media (B). Cultures were allowed to proliferate for 18 days. Each bar represents the mean ± 1SD (n = 3) (N = 3).

The proliferation of human MSCs on the three substrates was studied using both GM and OM. The trend of proliferation was similar between all three substrates in GM although MSCs reached confluence on CoCrMo and Ti after 10 days, whilst CCMT took 14 days. The numbers of cells on each surface was similar after 14 days in culture. The

proliferation of MSCs in OM showed a minor increase in cell proliferation up to day 7, which after this point either levelled out or began to decrease. CoCrMo was shown to have increased cell numbers up to day 10 compared to CCMT and Ti.

2.2.3. CELL MORPHOLOGY - INTERNAL

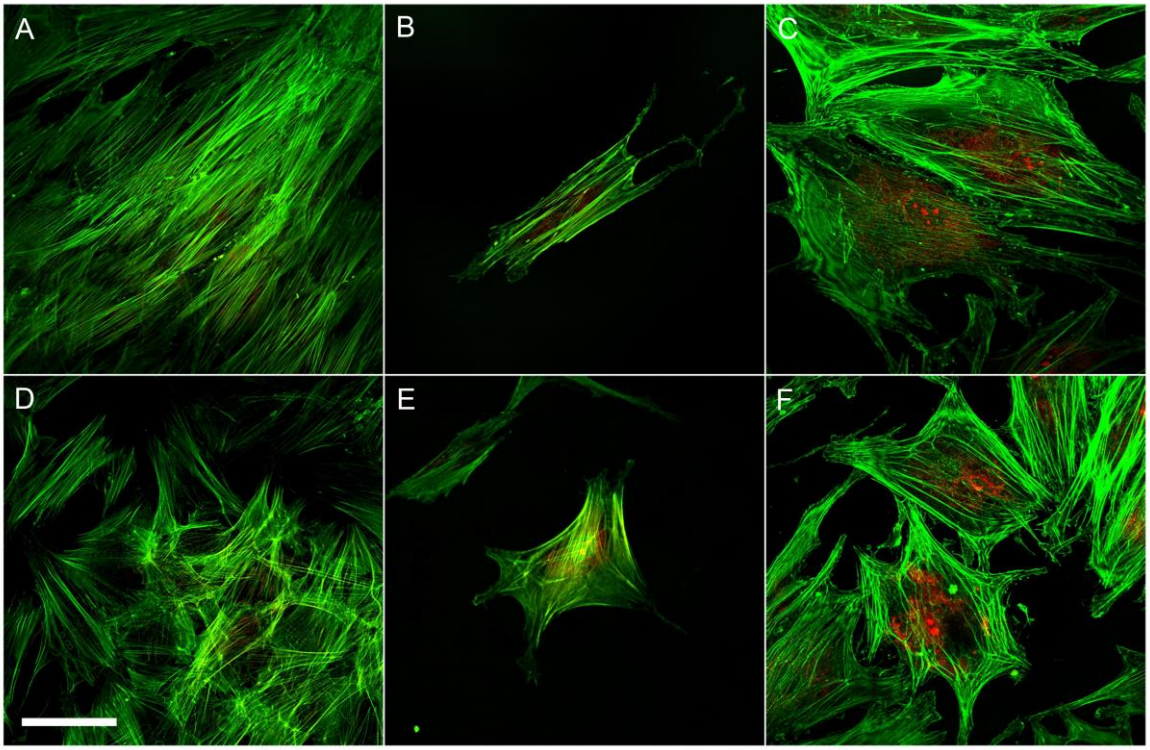

Figure 21 Confocal images showing f-actin (Green) counterstained with PI (Red). Images A-C show MSCs culture in OM on CoCrMo, with cell aggregates at day 1 (A), single cells at day 1 (B) and single cells at day 7 (C). MSCs on CCMT (D-F), cell aggregates (D), single cell at day 1(E) and lastly single cell at day 7 (F). Cell morphology at day 1 is noticeably different in both aggregates and on the single cell level. Aggregates on CoCrMo appear to be have ordered, elongated, parallel stress fibres, in comparison to the more robust criss-cross fibres found on the CCMT surface. Scale bar = 50 µm.

The morphology of human MSCs was analysed on CoCrMo and CCMT after 24 hours and 7 days in OM, by fluorescent microscopy. MSCs were labelled with phalloidin to visualise the f-actin and counterstained with PI which allows the cell nucleus to be observed. As shown above, the morphology of the MSC was clearly different on each surface after 24 hours in culture, as cell aggregates found on the CoCrMo substrate were shown to have cells with elongated actin fibres, ordered in parallel to one another (Figure 21 A), which when compared to aggregates found on CCMT, the cells were disorganised with robust actin fibres in a criss-cross pattern (Figure 22 D). This variation between to

the two substrates was also present on a single cell level with MSCs on CoCrMo being fibroblastic in appearance (Figure 22 B), compared to the more spread cells found on CCMT which had protrusions in the form of lamellipodia (Figure 22 E). By 7 days in culture variation between the two substrates was not clear, as MSCs had differentiated along their osteogenic linage, shown by the formation of thick bundles of f-actin around the periphery of the cells, which is a marker of this process.

2.2.4. CALCIUM ASSAY

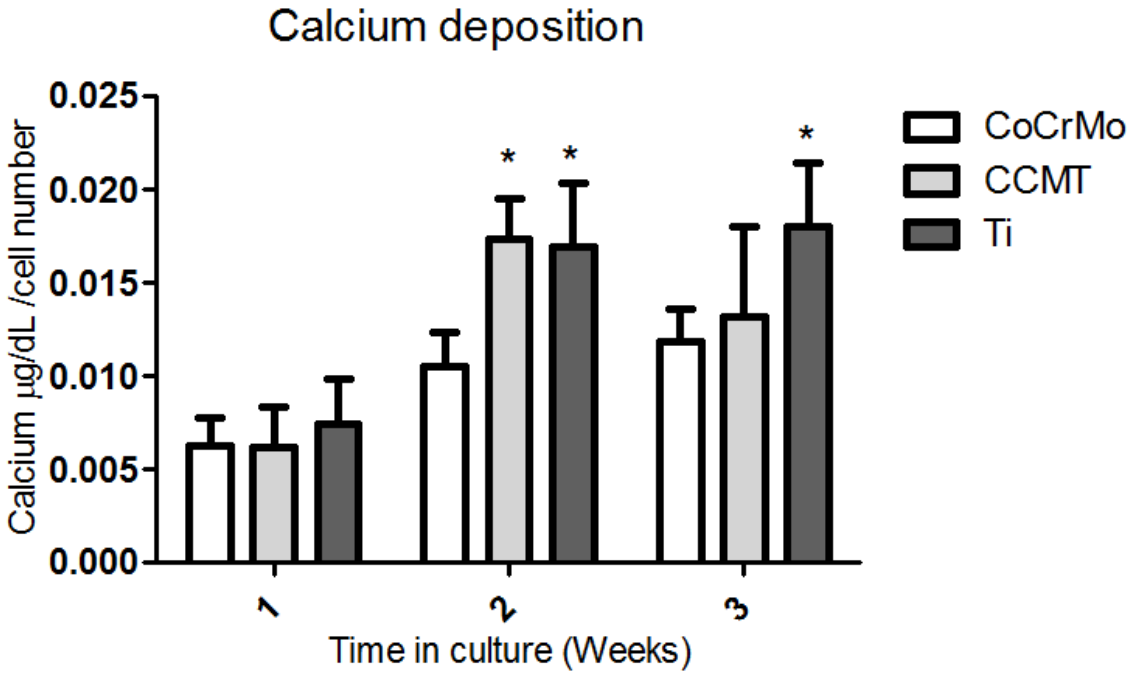

Figure 22 Calcium deposition per cell over a three week time course. At two weeks there is a significant increase in the amount of calcium present on CCMT compared to CoCrMo, suggesting a greater level of osteogenesis is occurring at this time point on the CCMT surface, to a similar level as that found on Ti. At three weeks there is still greater calcium content on CCMT although this is not statistically significant. Each bar represents the mean ± 1SD (n = 3) (N = 3), *=$p<0.05$ material vs. CoCrMo.

The amounts of calcium in cultures can be a measure of the extent of osteogenic differentiation occurring as MSCs undergo osteogenesis and form mineralised tissue. It was found that significantly more calcium per cell was present on the CCMT surface compared to CoCrMo after 2 weeks in osteogenic culture ($p<0.05$). There was a slight drop in calcium content on CCMT after 3 weeks although this is a consequence of an increase in cell proliferation at this time point. In addition, Ti was shown to have significantly more calcium per cell compared to CoCrMo after 2 and 3 weeks ($p<0.05$).

2.2.5. HYDROXYAPATITE NODULE FORMATION

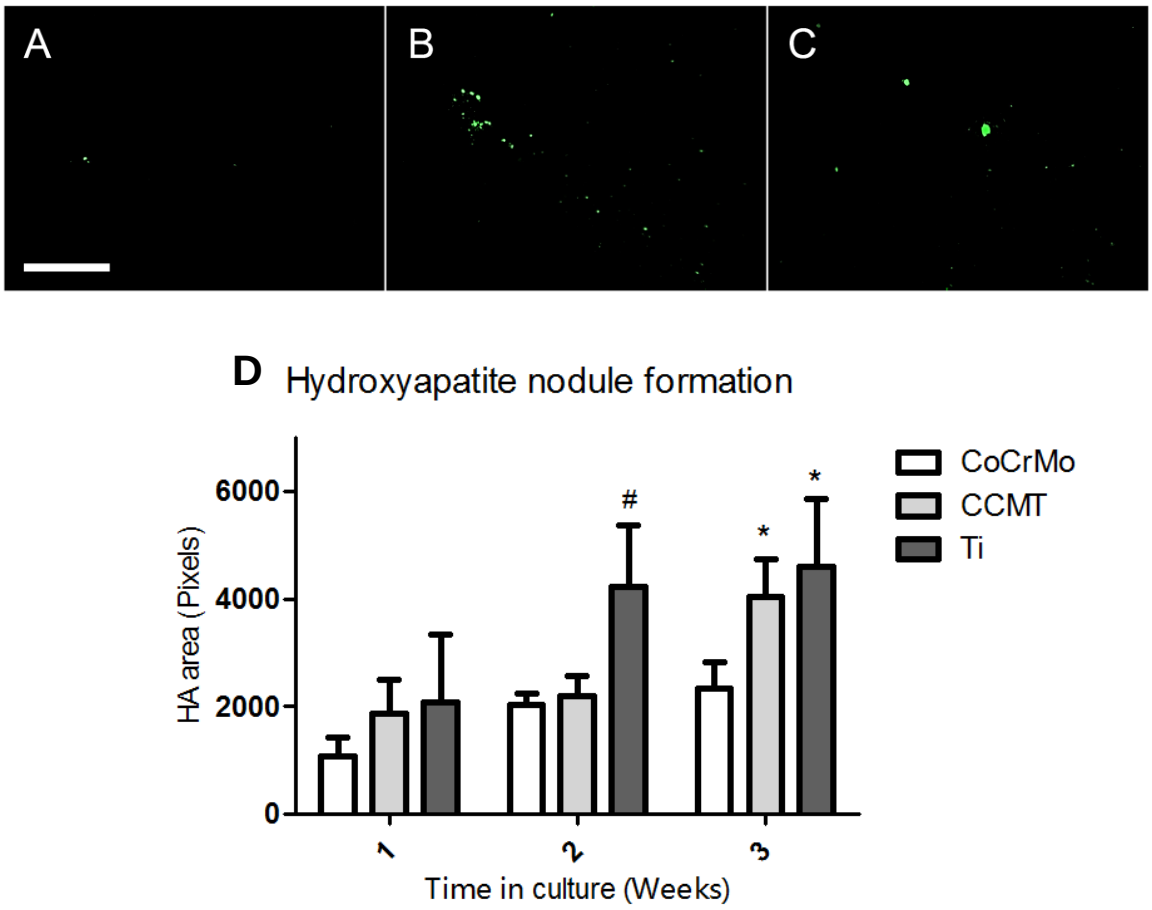

Figure 23 Data showing hydroxyapatite nodule formation. Greater hydroxyapatite content was found on CCMT (B) and Ti (C) in comparison to CoCrMo (A) after 21 days in culture. Quantification analysis was performed using ImageJ software (D). HA shown as green (A-C), scale bar = 200µm. Each bar represents the mean ± 1SD (n = 10), *=$p<0.05$ material vs. CoCrMo, #=$p<0.05$ material vs. both surfaces.

In addition to calcium content, the level of ostegenic differentiation was also analysed by hydroxyapatite formation. Following fluorescent micrscopy analysis, images were converted into quantitative data and plotted above in figure 23 D. Ti was shown to promote the greatest amount of hydroxyapatite at all three time points. After three weeks in osteogenic culture it was found that CCMT had significantly more hydroxyapatite nodule formation compared to CoCrMo ($p<0.05$) implying that there was superior mineralisation occuring on CCMT.

2.2.6. TYPE I COLLAGEN DEPOSITION

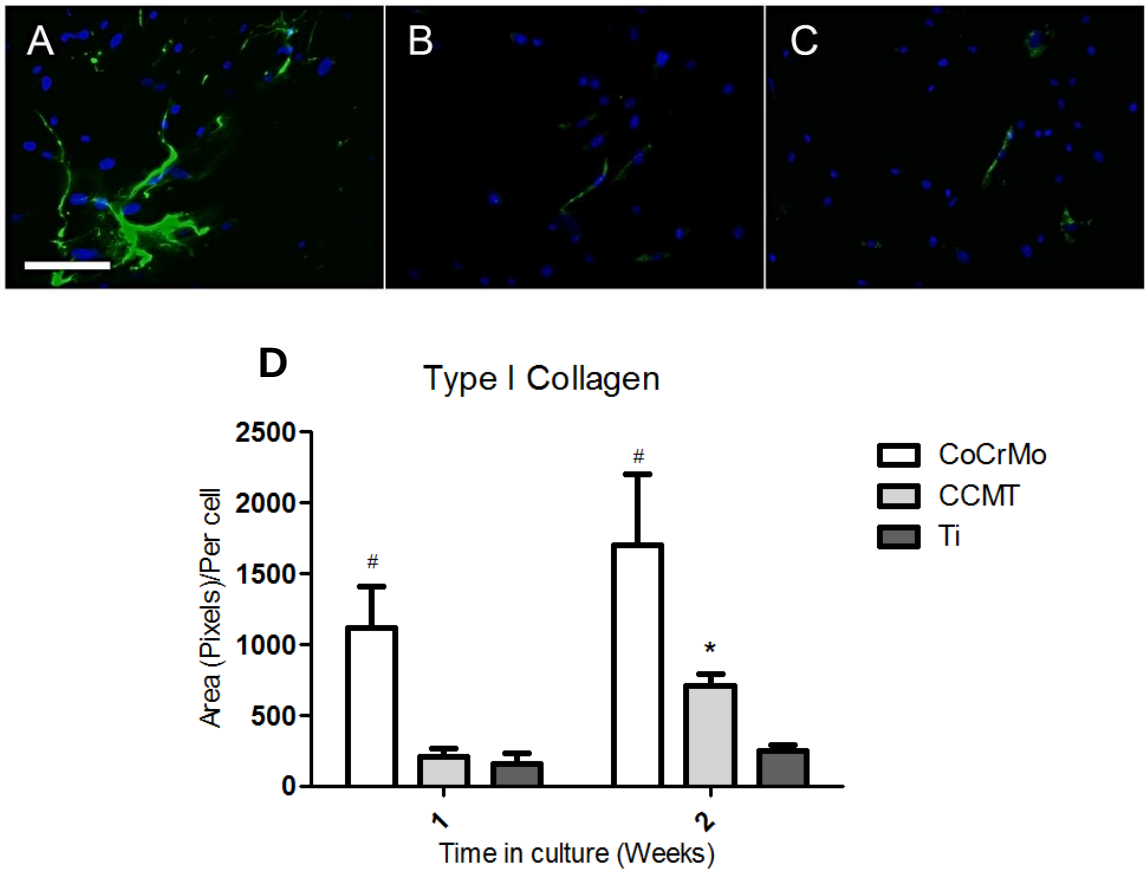

Figure 24 Fluorescent images and quantification analysis for type I collagen after 7 days in culture (A-D). Type I collagen deposition was enhanced on the CoCrMo surface (A), shown by the formation of dense collagen fibrils (Green), which were not present on either CCMT (B) or Ti (C). Cultures were counterstained with the nucleic acid stain DAPI (Blue). Scale bar = 100 µm. Image quantification analysis was performed using ImageJ software (D). Each bar represents the mean ± 1SD (n = 8), *=$p<0.05$ material vs. one surface, #=$p<0.05$ material vs. both surfaces.

Type I collagen plays an important role in bone formation as it acts as a scaffold for calcium nucleation sites (Davies, 1998). In addition, the ratio of collagen to mineral is an important factor in the properties of new bone. Using fluorescent microscopy the amounts of type I collagen was ascertained on all three substrates after 1 and 2 weeks in culture. It was found that significantly more collagen was present on the CoCrMo over both CCMT and Ti at both time points ($p<0.05$). This is due to the presence of thick bundles of type I collagen (Figure 25 A) which were not present on Ti or CCMT. After two weeks there was significantly more collagen on CCMT compared to Ti ($p<0.05$).

2.2.7. VINCULIN EXPRESSION

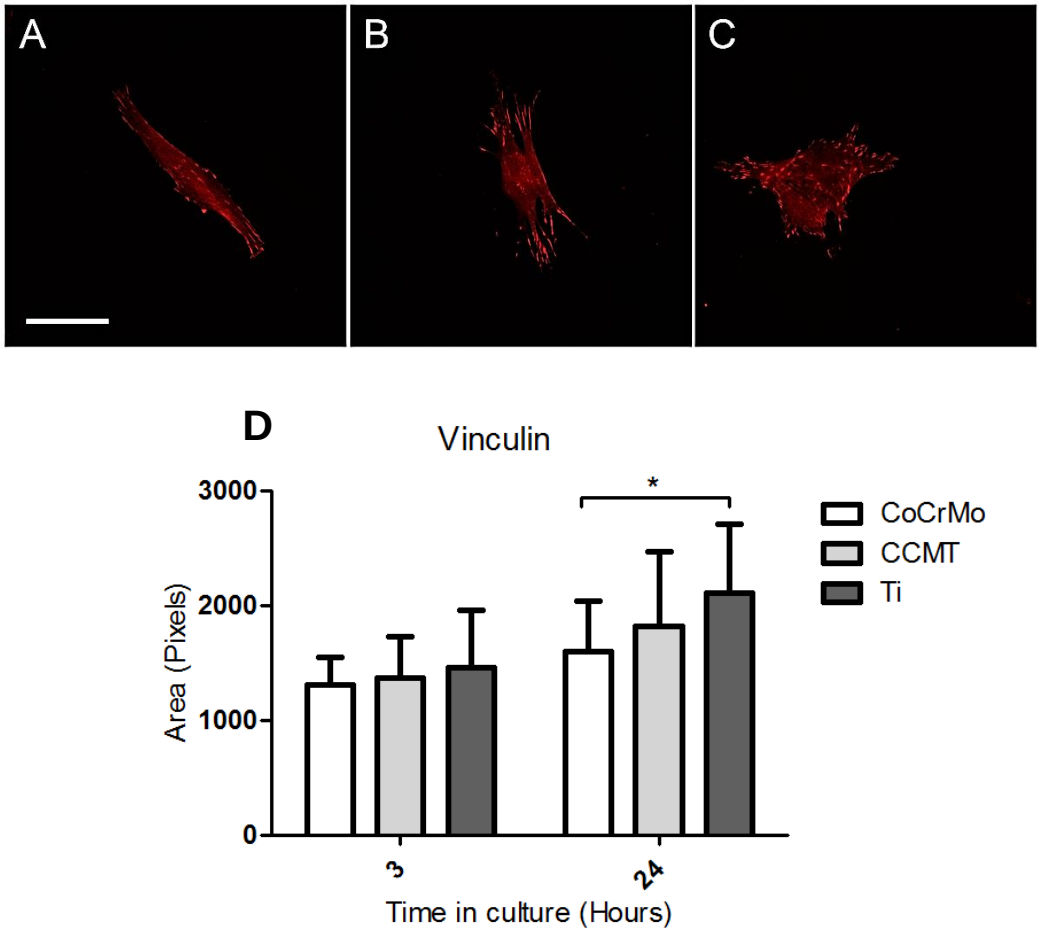

Figure 25 Vinculin expression in MSCs on CoCrMo (A), CCMT (B) and Ti (C) after 24 hours in culture. Fluorescent images show vinculin expression throughout the cell with concentrated regions thought to represent focal adhesions. Quantification of vinculin expression in individual cells (D) was performed using ImageJ software where it was found Ti had greater vinculin present in comparison to CoCrMo, with CCMT ranging in the middle. Each bar represents the mean ± 1SD n=10, *=$p<0.05$ material vs. CoCrMo. Scale bar = 50 μm

The expression of the focal adhesion protein vinculin was analysed by fluorescent microscopy after 3 and 24 hours in osteogenic culture. For both time points it was found that MSCs on the CoCrMo substrate had the least vinculin, Ti had the greatest and CCMT fell in the middle. Ti had significantly more vinculin expression per cell compared to CoCrMo after 24 hours in culture ($p<0.05$).

2.2.8. SINGLE CELL ADHESION

***Performed by Anas Sherif, Eastman Dental Institute, UCL.**

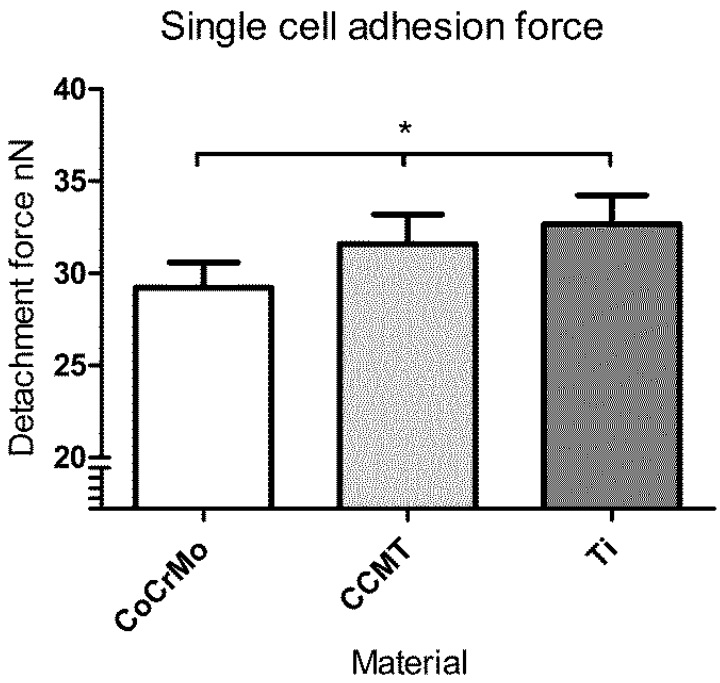

Figure 26 Graphical representation of the adhesion forces required to detach a single MSC from CoCrMo, CCMT and Ti, after a one second dwell time on the surface of each material. The single MSC had been attached the AFM cantilever prior to the measurement via a Con-A coated glass bead. CoCrMo had the lowest detachment force of the three materials with Ti promoting the greatest force. Each bar represents the mean ± 1SD n=75, *=$p<0.0001$ material vs. all other materials.

The adhesive forces of a single cell following a 1 second dwell time on the substrate surface agreed with the vinculin data. The greatest force to remove the cell from the substrate surface was found using Ti. CoCrMo required the least force to remove the MSC, with CCMT requiring significantly more force than CoCrMo ($p<0.0001$), although not to the same level as found on Ti.

2.3. DISCUSSION

In this section of the thesis, a study was performed to find out if the biocompatibility of CoCrMo could be increased by coating the material in a thin layer of TiO_2, the same naturally occurring oxide layer as found on titanium and its alloys (Textor, 2001). When a device is implanted into the body, the cells that colonise onto the surface of the implant do not interact with the bulk of the material, but instead are mediated by the surface, or in this case the surface oxide layer. Therefore by coating the surface of CoCrMo in a layer of TiO_2, the cells should recognise the material as titanium and as a consequence, increase their osteogenic activity and improve bone formation.

Firstly, characterisation of the TiO_2 layer was performed before undergoing any cell culture experiments. After coatings were completed on CoCrMo discs using atmospheric pressure CVD, the phase of the TiO_2 was assessed via Raman spectroscopy (Figure 15) and XRD (Figure 16). The majority of the samples were pure anatase TiO_2 although some discs had some traces of rutile. This was probably due to temperature fluctuations that may have arisen in different locations of the reaction chamber during the deposition. In addition to traces of rutile, a small number of discs had minute traces of the brookite phase which is fairly uncommon. A proliferation experiment was performed to check if the brookite phase of the TiO_2 had any effect on cell behaviour and it was found that cells were able to proliferate on both phases of TiO_2. Despite this, only anatase TiO_2 discs were used for the experiments to help make the study more reproducible.

Cell behaviour can be influenced by many factors including the wettability (Zhao et al., 2005, Khan et al., 2012) and topography of the surface (Dalby et al., 2007). In the present study, wettability was tested via measuring static water contact angle of $_{dd}H_2O$, where it was found that CoCrMo was the most hydrophobic surface and Ti the most hydrophilic (Figure 17). Interestingly, the CCMT surface fell in the middle of the two controls, implying that the TiO_2 coating is having some effect on the wettability of the substrate, but may not completely be blocking out the bulk properties of the underlying CoCrMo. It should also be pointed out that the standard deviation was greatest for the CCMT group, suggesting that the coating technique does not deposit an entirely uniform layer of TiO_2 on the surface of the disc.

The topography of the substrates was studied by laser profilometry (Figure 18) and SEM. Low magnification SEM images showed a similar smooth topography on all substrates

with no evident surface features. Under higher magnification the variation between the substrates was more apparent with small pits being observed on CCMT and Ti (Figure 19). It was found that the control Ti substrate had a significantly greater R_a value than both CoCrMo and CCMT. Despite this, all three substrates were referred to as smooth when taken into account *Wennerberg et al's* review, which studied the influence of surface topography on bone integration and concluded that substrates with a S_a of less than 0.5 μm could be described as smooth (Wennerberg and Albrektsson, 2009). Ti was found to have a R_a value of 0.56μm which was on the extreme limit of this range and because of this, may have been a contributing factor to the increased calcium and hydroxyapatite deposition observed on the Ti substrate. In addition, the CCMT substrate was found to have a R_a value 0.1 μm greater than that found on CoCrMo. This is likely to be a result of fluctuations in the thickness of the coating that occurred during the deposition process. Despite attempts to create a TiO_2 coating as uniform as possible, variation in the thickness of the coating in different regions on the surface of the disc is likely and this may have affected the topography. The thickness of the coating on each of the discs was analysed by filmetrics. As shown in figure 19, the first three batches were thicker than those that followed. It was found that a slightly thinner deposition was less prone to adherence issues and more uniform in appearance. From batches AJC523 through to AJC621 the TiO_2 thickness was approximately 300 nm. Variation in the thickness of TiO_2 coatings may be influential in how the cells respond to the coating, but at this stage of the project the complete coverage and reproducibility of the coating on the CoCrMo surface was priority.

In regards to cell culture data, the level of cellular proliferation in both GM and OM was similar between all substrates. After 14 days culture in GM, all substrates had reached confluence, which showed good levels of cytocompatibility. The first difference in how the MSCs behaved on CoCrMo compared to CCMT, was evident whilst analysing cell morphology and shape via confocal microscopy. MSCs were labelled to display f-actin and it was found that those on CoCrMo were fibroblastic in appearance after 24 hours in OM, compared to the more spread cells found on CCMT, which had developed protrusions in the form of lamellipodia (Figure 22 E). Cell shape is thought to play an important role in the differentiation process (Kilian et al., 2010, McBeath et al., 2004). This observation suggests that the MSCs on CCMT are differentiating at a faster rate than those on CoCrMo, as cytoskeletal changes occur during the differentiation process (Yourek et al., 2007), in the form of changing from fibroblastic to a more spherical-star

shape (Rodriguez et al., 2004). This effect was again present in cell aggregates (figure 22 D). MSC aggregates on CoCrMo appeared to have actin fibres that were elongated and ordered, compared to the more robust, criss-crossed fibres seen on the CCMT surface, which has been previously observed in MSCs undergoing osteogenesis (Yourek et al., 2007). This data suggests that the CCMT surface is promoting an accelerated early osteogenic response. By day 7 no noticeable difference was observed between the two substrates, with both showing MSCs in the later stages of the osteogenic differentiation process, indicated by thick bundles of f-actin around the edges of the cells (Rodriguez et al., 2004).

As MSCs differentiate along their osteogenic linage, they deposit an extracellular matrix (ECM) rich in calcium and collagen as well as changing shape. The rate of osteogenic differentiation occurring in MSCs on CoCrMo, CCMT and Ti was analysed by a number of techniques, which included calcium content, hydroxyapatite nodule formation and type I collagen deposition. An increased amount of mineral was deposited on CCMT and Ti substrates when compared to CoCrMo, as shown by enhanced calcium deposition per cell after 14 days (Figure 23) and superior hydroxyapatite nodule formation at 14 and 21 days (Figure 24 D). In addition to the amounts of mineral deposited, type I collagen was shown to be significantly different between CoCrMo, and CCMT and Ti. The formation of dense fibrils of type I collagen was observed on CoCrMo at both 7 and 14 days (Figure 25) which was not evident on either CCMT or Ti. There was a slight increase in the amount of collagen present on CCMT by day 14, but not to the same extent as found on CoCrMo. When combined with the calcium and hydroxyapatite data, this implies that the deposited matrix on the CoCrMo substrate may be over collagenous and mechanically weak compared to that found on CCMT and Ti (Khan et al., 2012). Whilst fluorescent microscopy and calcium assays are valid approaches of identifying mineralisation, there are other methods of assessing the rate of osteogenic differentiation that were not explored in this thesis, such as gene expression. One particular gene of interest which would've interesting to study is Runx2, also known as Cbfa1, as it is widely accepted that Runx2 is master switch for osteogenesis. The importance of the gene to the osteogenesis process was highlighted in a study analysing Runx2 knockout mice. It was found that in the Runx2 knockout mice, ossification was completed absent due to the maturational arrest of osteoblasts (Komori et al., 1997). Despite the importance of Runx2, it is not the only gene crucial to the osteogenic differentiation process. Runx2 plays an important role in differentiating MSCs into preosteoblasts, although Osterix is required to push these cells

into becoming mature osteoblasts. Markers of a mature osteoblast can include osteocalcin, osteonectin, osteopontin and bone sialoprotein (Cohen, 2006), all of which were not expressed in Osterix knockout mice, highlighting the importance of this gene in the osteogenesis process. The level of expression of Runx2 and Osterix in human MSCs can be assessed by quantitative polymerase chain reaction (qPCR). If test samples were not so limited throughout this study, it would've been advantageous to analyse the expression of Runx2 and Osterix in human MSCs seeded on the three substrates at different time points. This data would've eluded if there was any early or late up regulation in these osteogenic associated genes occurring on the CCMT or Ti surface compared to CoCrMo, which would ultimately support the increased hydroxyapatite and calcium deposition observed after 14-21 days in culture. Another option of assessing osteogenic differentiation, rather than looking at the master switch genes, would've been to analyse the different signalling pathways known to be involved in osteogenesis. One of the central signalling pathways involved in osteogenesis is BMP signalling. BMPs are extracellular cytokines that are members of the transforming growth factor-β (TGF-β) superfamily, that induce osteogenic differentiation by working in combination with Osterix, using both autocrine and paracrine pathways. BMPs bind to surface BMP ligands, initiating downstream signalling elements including MAP kinase, c-Jun N-terminal kinase and Smad1/5/8 (James, 2013). BMP-2,-4,-6,-7 and 9 have been shown to promote osteogenesis (Kang et al., 2009) and therefore would be ideal markers to use in this study if sample limitations were not an issue. Another signalling pathway important to osteogenesis is wingless-type MMTV integration site (Wnt) signalling. Extracellular Wnt ligands bind to frizzled receptors found on the cell surface and initiate a β-catenin dependent pathway, inducing a complex formation with low density lipoprotein receptor 5/6, as well as proteins of the dishevelled family. Through additional downstream signalling, glycogen synthase kinase 3, which promotes β-catenin degradation, is inhibited, resulting in the accumulation of β-catenin in the cell nucleus (James, 2013). Once there, β-catenin plays an important role in MSC osteogenic differentiation, with inhibitors of the Wnt/β-catenin pathway shown to disrupt osteogenesis (Holmen et al., 2005). Enzyme linked immunosorbent assays (ELISA) are a potential method of measuring the amounts of these osteogenic proteins found in cell culture media. As previously stated, if the limitations regarding the number of CoCrMo test samples available were not a factor, it would've been extremely beneficial to perform ELISAs, assessing the quantities of osteogenic proteins, such as BMPs, in the culture media, following 7, 14 and 21 days in culture.

As important as the osteogenic differentiation process is to bone formation, for this to occur successfully, the substrate must first promote a sufficient level of cell adhesion to allow for the colonisation and attachment of cells capable of participating in bone healing. Numerous proteins from both the ECM and internal structure of the cells are altered by the cell-material interactions that occur during the adhesion process (Anselme, 2000). Vinculin is a protein that plays a role in the adhesion process by forming complexes known as focal adhesions and interacting with the cytoskeletal proteins actin and talin (Humphries et al., 2007). Focal adhesions are ordinarily found around the periphery of the cell and are assemblies of proteins that connect f-actin to the substrate and convey mechanical signals and forces. An increase in vinculin was observed on both CCMT and Ti compared to CoCrMo (Figure 25). This data suggests that there are more focal adhesions formed on CCMT and Ti which has been highlighted as an important factor for osteogenesis, in comparison to adipogenesis and chondrogenesis that prefer fewer focal adhesions (Mathieu and Loboa, 2012). In addition to the visual analysis of vinculin, quantitative data of cell adhesion was performed using AFM. The technique is commonly used for imaging surfaces and objects on the nanoscale, but was recently highlighted as a possible tool to measure various force interactions between objects, such as between cells and biomolecules (Francis et al., 2010). Following a one second dwell time, it was found that MSCs on both CCMT and Ti required significantly more force to be removed from the substrate compared to CoCrMo (Figure 26). This data supports the vinculin observations and implies that the CCMT and Ti surfaces would promote stronger cell adhesion compared to CoCrMo.

In this section of the thesis it has been shown that coating the surface of CoCrMo in a thin layer of TiO_2 by atmospheric pressure CVD can enhance various markers of cell adhesion and osteogenic differentiation in human MSCs *in vitro*. The use of TiO_2 as a means of improving the biocompatibility of a material has not been extensively researched but may hold great potential. TiO_2 sol-gel dip coatings on CoCrMo were recently shown to improve cell cytocompatibility by reducing the expression of genes involved in inflammation and oxidative stress response in human endothelial cells (Tsaryk et al., 2013). The effect was attributed to the coatings ability to reduce the leaching of metallic ions such as Co^{2+} (Hoffmann et al., 2007). Despite the potential to transfer the biocompatibility of TiO_2 onto other less bioactive materials, the majority of studies have focused on coating titanium substrates in an additional layer of TiO_2 using a variety of techniques, such as deposition of molten TiO_2 particles (Sugita et al., 2011, Ishizaki et

al., 2011), sputter coating (Kubo et al., 2009, Tsukimura et al., 2008), micro arc oxidation (Chen et al., 2010a, Ma et al., 2008) and sol-gel dip coating (Singh, 2011, Rossi et al., 2008, Areva et al., 2004). TiO_2 coated titanium has been shown to be superior to uncoated controls by enhancing osteogenic response (Sugita et al., 2011, Ishizaki et al., 2011, Kubo et al., 2009, Tsukimura et al., 2008, Singh, 2011, Chen et al., 2010a, Ma et al., 2008). In addition, soft tissue attachment for dental applications have been shown to be improved on TiO_2 coated samples (Rossi et al., 2008, Areva et al., 2004). Despite the numerous positive conclusions drawn from these studies the focus has been on improving titanium rather than applying TiO_2 to materials that lack biocompatibility. Furthermore, coating CoCrMo in a layer of TiO_2 is relatively simple surface modification, compared to other attempts which have included the formation of nanophase topographies and BMP peptide immobilisation (Webster and Ejiofor, 2004, Poh et al., 2011). These techniques may be difficult to upscale effectively, in comparison to TiO_2 coatings which is already industrialised.

2.4. CONCLUSION

This section of the thesis analysed cellular markers of human MSCs on CoCrMo, CCMT and Ti to ascertain whether coating CoCrMo in a layer of TiO_2 by atmospheric pressure CVD enhanced the bioactivity of the material to a comparable level as found on titanium. The results indicated that both markers of adhesion and osteogenic differentiation were enhanced on CCMT compared to CoCrMo, implying that TiO_2 coatings may have the potential in the future to improve the efficacy of orthopaedic implants formed of non-bioactive materials such as CoCrMo.

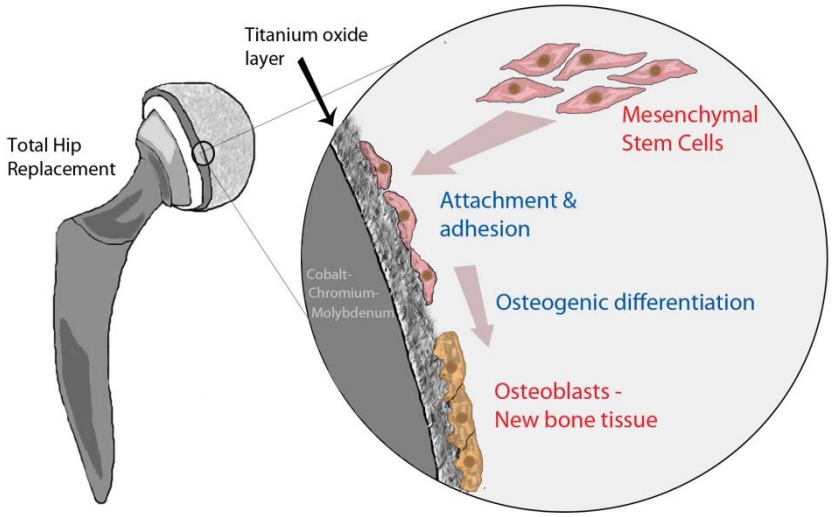

Figure 27 Graphical conclusion – chapter two.

CHAPTER THREE:

THE EFFECT OF UV-PHOTOFUNCTIONALIZATION ON TiO_2 COATED COBALT CHROMIUM MOLYBDENUM

3. INTRODUCTION

It has been shown that coating the surface of CoCrMo in a layer of TiO_2 can improve the osteogenic differentiation and adhesion of MSCs *in vitro* (Logan et al., 2014b). Despite these improvements to cellular behaviour, it may be possible to further enhance this response by utilising the photo reactivity of the TiO_2 layer.

TiO_2 is highly photoreactive and upon irradiation with UV light transitions from a hydrophobic state to super-hydrophilic (Contact angle < 5°) (Wang et al., 1997). It is proposed that the mechanism behind this phenomenon is the creation of surface oxygen vacancies at bridging sites, where Ti^{4+} sites are converted to Ti^{3+} sites which are more favourable for dissociative water adsorption (Carp et al., 2004). This unique property of TiO_2 allows for its application in self-cleaning windows, as the UV irradiation from sunlight is sufficient enough that hydrophilic or oleophilic contaminants are removed by rain (Wang et al., 1997).

In addition, the photo reactivity of TiO_2 has been investigated as a potential tool for functionalising the surface of titanium and TiO_2 surfaces for biomedical application. Known as 'UV photofunctionalization', preliminary studies have reported an enhancement in osteogenic response (Aita et al., 2009b, Ueno et al., 2010, Sawase et al., 2008, Yamada et al., 2010, Iwasa et al., 2010, Lan et al., 2015, Yamazaki et al., 2015). Using human MSCs, markers of cell differentiation, adhesion, proliferation, attachment and migration have been shown to be enhanced on UV photofunctionalized titanium surfaces compared to their non UV exposed counterparts (Aita et al., 2009a). In addition to improving the bioactivity of titanium and TiO_2 substrates, UV photofunctionalization has been shown to be capable of restoring materials from the recently discovered time dependant degradation of biomaterial osteoconductivity (Att et al., 2009, Hori et al., 2010b).

This part of the project aimed to investigate if UV photofunctionalization could be applied to CCMT as a means of improving the bioactivity of the material. Markers of cell attachment, proliferation, adhesion, differentiation and migration were studied using human MSCs on UV treated CCMT and substrates which had not undergone UV photofunctionalization. Characterisation of the substrates was also performed including a wettability study and Fourier transform infrared spectroscopy (FTIR).

The hypothesis explored in this chapter is:

1. UV photofunctionalization of the CCMT surface would generate increased cell proliferation, migration, attachment, retention and osteogenic differentiation in human MSCs, when compared to the control CCMT surface, which had not undergone the UV functionalization protocol.

3.1. MATERIALS AND METHODS

3.1.1. SAMPLE PREPARATION

***CVD, Raman spectroscopy and XRD was performed by Alison J Cross, Department of Chemistry, UCL.**

Discs of CoCrMo were prepared to a smooth finish as previously described in section 2.1.1 SAMPLE PREPARATION – (Page 59). Following this, a layer of anatase TiO_2 was deposited onto the surface of all the samples by atmospheric pressure CVD, as previous described in section 2.1.3 CHEMICAL VAPOUR DEPOSITION – (Page 60). All coated samples underwent Raman Spectroscopy, XRD and filmetrics analysis to confirm the presence of anatase TiO_2 as previously described in section 2.1.4 SURFACE CHARACTERISATION – (Page 61). All CCMT samples were then split into two groups known as non-UV and UV treated. UV treated CCMT discs were irradiated for 24 hours using UVC light (BONMAY, BR-506), whereas non-UV discs were only irradiated for 20 minutes, then left for 48 hours in a sterile environment to allow recovery of the surface to a hydrophobic state. UV treated substrates were used for cell culture experiments immediately after the 24 hour irradiation period.

3.1.2. CELL CULTURE

Human MSCs were prepared and cultured as previously described in section 2.1.6 CELL CULTURE – (Page 63).

3.1.3. WATER CONTACT ANGLE

The wettability of non UV and UV treated substrates was studied via measuring water contact angle over a time course. Contact angle measurements were performed (n = 5) using an optical contact angle meter (KSV Instruments LTD, CAM 200) with 2 µl drops of $_{dd}H_2O$. Measurements were taken over a time course up to 24 hours UV irradiation and 48 hours immediately post irradiation. Following irradiation all samples remained in the dark. Images were also recorded.

3.1.4. FOURIER TRANSFORM INFRARED SPECTROSCOPY

FTIR is an analytical technique used to measure infrared data in a wide spectral range. One such application is to measure hydrocarbon content in samples, which result in a change in the degree of absorbance in relation to the concentration of hydrocarbon (Perston, 2011).

To ascertain if any reduction in hydrocarbon content had occurred due to UV photofunctionalization, FTIR analysis was performed on substrates both before and after UV irradiation. CCMT substrates were loaded onto the FTIR (Perkin Elmar, System 2000) and spectra were taken in the range of 3100 – 2700 cm^{-1} using an average of 16 scans per sample. CCMT substrates were then transferred to the UVC cabinet and irradiation for 24 hours, then immediately scanned again using the same parameters.

3.1.5. PROLIFERATION

MSCs from three donors (N = 3) were seeded on non UV and UV treated CCMT substrates at a density of 2 x 10^3 cells per well (n = 3) in a 24 well plate. Plates for both GM and OM were setup individually and cultured at 37˚C, 5% CO_2 in a humidified atmosphere with media changes performed on each day of analysis. Cellular proliferation was then analysed as previously described in section 2.1.7 PROLIFERATION – (Page 65).

3.1.6. ATTACHMENT

A total of 3 x 10^4 MSCs from three donors were seeded on non UV and UV treated substrates (n = 3) in GM in 24 well plates. After 24 hours in culture conditions of 37˚C, 5% CO_2 in a humidified atmosphere, the media was replaced with fresh GM and cells were counted as previously described in section 2.1.7 PROLIFERATION – (Page 65) to gain a measure of cell attachment on each substrate.

3.1.7. RETENTION

To gain a measure of how well adhered each population of MSCs was to both UV treated and non UV CCMT substrates, cell retention to the surface following three mechanical washes was studied. A total of 3.5 x 10^4 MSCs from three donors were seeded on each substrate (n = 3) in GM and incubated at standard culture conditions of 37˚C, 5% CO_2 in a humidified atmosphere. After 3 and 24 hours in culture, MSCs were washed three times in 1 ml of PBS on an orbital shaker (60 seconds at 60 revolutions per minute) and then using the same method as described in section 2.1.6 PROLIFERATION – (Page 65), the remaining cells were quantified via AlamarBlue assay.

3.1.8. MIGRATION

How cells move and migrate is important in regards to bone healing, as implant surfaces must stimulate the colonisation of cells capable of facilitating bone formation. Chemotaxis is the movement of a cell in response to a stimuli usually in the form of a chemical or growth factor and is assessed through use of migration or invasion assays. The functionalisation of an implant surface may have the same potential to enhance the migration of cell populations. A cell migration assay (Cultrex, 3465-024-K) was used to determine if UV photofunctionalization had the capability to influence MSC migration. The cultrex assay consisted of a number of chambers, each fitted with a polyethylene terephthalate membrane that contained 8 μm pores to allow cell transition. Following the incubation period, the number of cells that migrated through the chamber could be measured via calcein acetomehtylester (AM). Calcein AM is internalised by MSCs and intercellular esterases dissociate the AM moiety. This leaves only free calcein which fluoresces at 485 nm excitation, 520 nm emission.

MSCs from three donors were serum starved for 24 hours prior to performing the assay to allow for a more robust migratory response. The MSCs were then seeded at 7.5 x 10^4 cells per well (n = 3) into the top chamber of the assay inserts which were placed over non UV and UV treated substrates in a 24 well plate. 500 μl of GM was transferred to the bottom chamber of the insert and the cells were incubated at standard culture

conditions for 4.5 hours. Following this, the inserts were then washed three times using wash buffer and incubated with cell dissociation solution containing calcein AM for a further 60 minutes at 37˚C, 5% CO_2. Two 100 µl aliquots were then taken from each well and the fluorescent intensity measured using a fluorescent plate reader (Biotek, FLX800). The remaining cells were then calculated via interpolation through use of a standard curve.

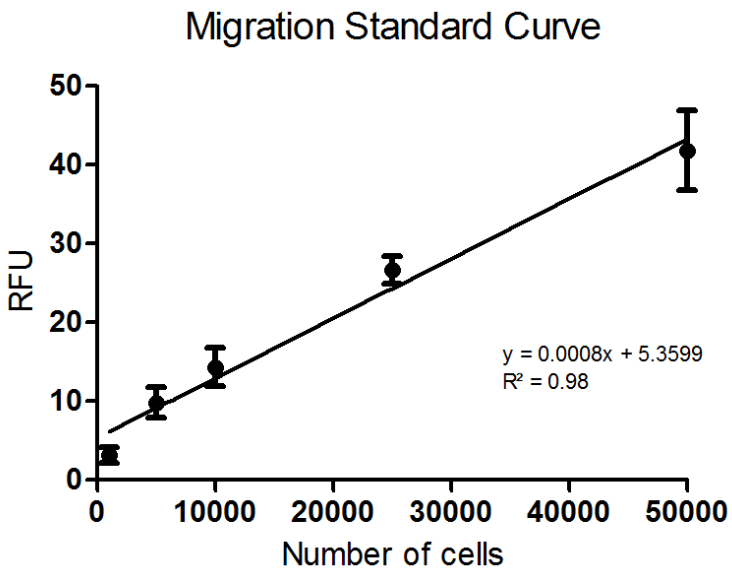

Figure 28 Standard curve data for the migration study. Each point represents the mean ± 1SD (n = 6).

3.1.9. CELL MORPHOLOGY - INTERNAL

The adhesion protein vinculin and cytoskeletal protein f-actin were studied by fluorescence microscopy. A total of 5 x 10^3 MSCs per well were seeded in OM on non UV and UV treated substrates (n = 3) in a 24 well plate. Following 24 hours in culture the MSCs were fixed using 4% PFA for 15 minutes at room temperature. Cultures were then washed three times with 1 ml of PBS before being incubated with 0.15% Triton-X-100 (BDH, 30632 4N) in PBS for 4 minutes at room temperature to permeabilise the cellular membranes. Following three additional washes in 1 ml of PBS, the MSCs were blocked using 10% goat serum in PBS for 30 minutes to prevent any unspecific binding. Primary antibody incubation was performed overnight at 4°C using anti-vinculin antibody (Abcam, ab18015, 1:200). The cultures were then washed three times using 1 ml of PBS then incubated with alexa fluor 568 goat anti-mouse antibody (Life Technologies, A11031, 2.5:100) for 60 minutes at room temperature in the dark. All

antibodies were diluted in 1.5% skim milk in PBS to further reduce potential unspecific binding. Cultures were then washed using PBS and counterstained with alexa fluor 488 phalloidin in PBS (Life Technologies, A12379, 2.5:100). Substrates were mounted and viewed using a fluorescence microscope (Leica, DMIRB) fitted with the appropriate filters. Image analysis was performed via a pixel based method using ImageJ software as described in section 2.1.11 IMAGE QUANTIFICATION – (Page 69).

3.1.10. MINERALISATION

To determine whether UV photofunctionalization had any effect on the osteogenic differentiation of human MSCs, markers of both early and late stages of the differentiation process were studied. Alkaline phosphatase (ALP) was analysed after 6 days in culture, whilst calcium content and hydroxyapatite formation was studied after 21 days. MSCs from three donors were seeded at 2 x 10^4 cells per well (n = 3) in OM on non UV and UV treated substrates in a 24 well plate.

The amount of ALP was normalised by counting the number of cells prior to performing the assay, as previously described in detail in section 2.1.7 PROLIFERATION – (Page 65). The activity of ALP was assessed through use of a colorimetric assay (Abcam, ab83369) following the manufacturer's instructions. Following 6 days in osteogenic culture, the MSCs were washed twice using PBS and dissociated from the substrate through use of 0.5ml of trypsin/EDTA. 0.5ml of GM was added to the wells after 5 minutes incubation at standard culture conditions to cancel the dissociative reagent. The suspension was then centrifuged at 13,000 rpm for 6 minutes to form a pellet, before being re-suspended in 200 µl of buffer by use of a vortex. The samples were then left for 15 minutes at room temperature to allow the buffer to effectively lyse the cells. 80 µl was then taken from each sample and combined with 50 µl of 5 mM p-nitrophenyl phosphate (pNPP) in a clear 96 well plate. Following 60 minutes incubation at room temperature in the dark, 20 µl of stop solution was added to all samples and the optical density was measured at 405 nm (Tecan, M200). Concentrations of ALP were calculated through use of a standard curve.

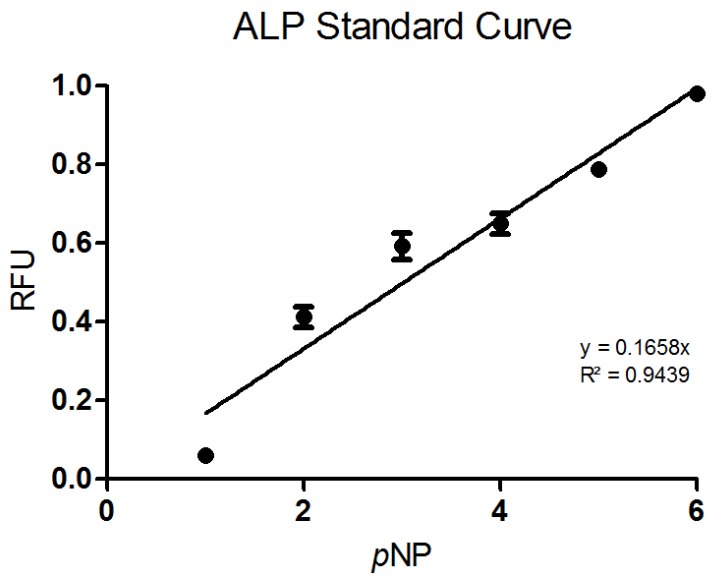

Figure 29 Standard curve data for ALP assay. Each point represents the mean ± 1SD (n = 3).

After 21 days in culture, calcium ion content was analysed using the QuantiChrom calcium assay using the same method that has been described in detail in section 2.1.9 CALCIUM ASSAY – (Page 67).

Hydroxyapatite formation was studied after 21 days in osteogenic culture and analysed by both fluorescence microscopy and fluorescence plate reader. The OsteoImage mineralisation kit (Lonza, PA-1503) was again used as previously described in section 2.1.10 HYDROXYAPATITE NODULE FORMATION – (Page 68). Before microscopy images were taken, the substrates were analysed using fluorescence plate reader (Biotek, FLX800, excitation = 492 nm, emission = 520 nm).

3.1.11. STATITICAL ANALYSIS

For this study human MSCs from three donors (N = 3) were used in triplicate (n = 3). Contact angle studies were performed at n = 5, and cytomorphometric analysis was performed at n = 13. Statistical analysis was carried out using the student's t test in GraphPad Prism software (v5.04), with $p < 0.05$ deemed to be statistically significant. A post-hoc power calculator was used to confirm the statistical power of significant results observed in the study. In addition, when no statistical significance was observed between two groups where a statistically significant result was expected, a sample size calculator was used to ascertain if the sample size was sufficient for the study.

3.2. RESULTS

3.2.1. WATER CONTACT ANGLE

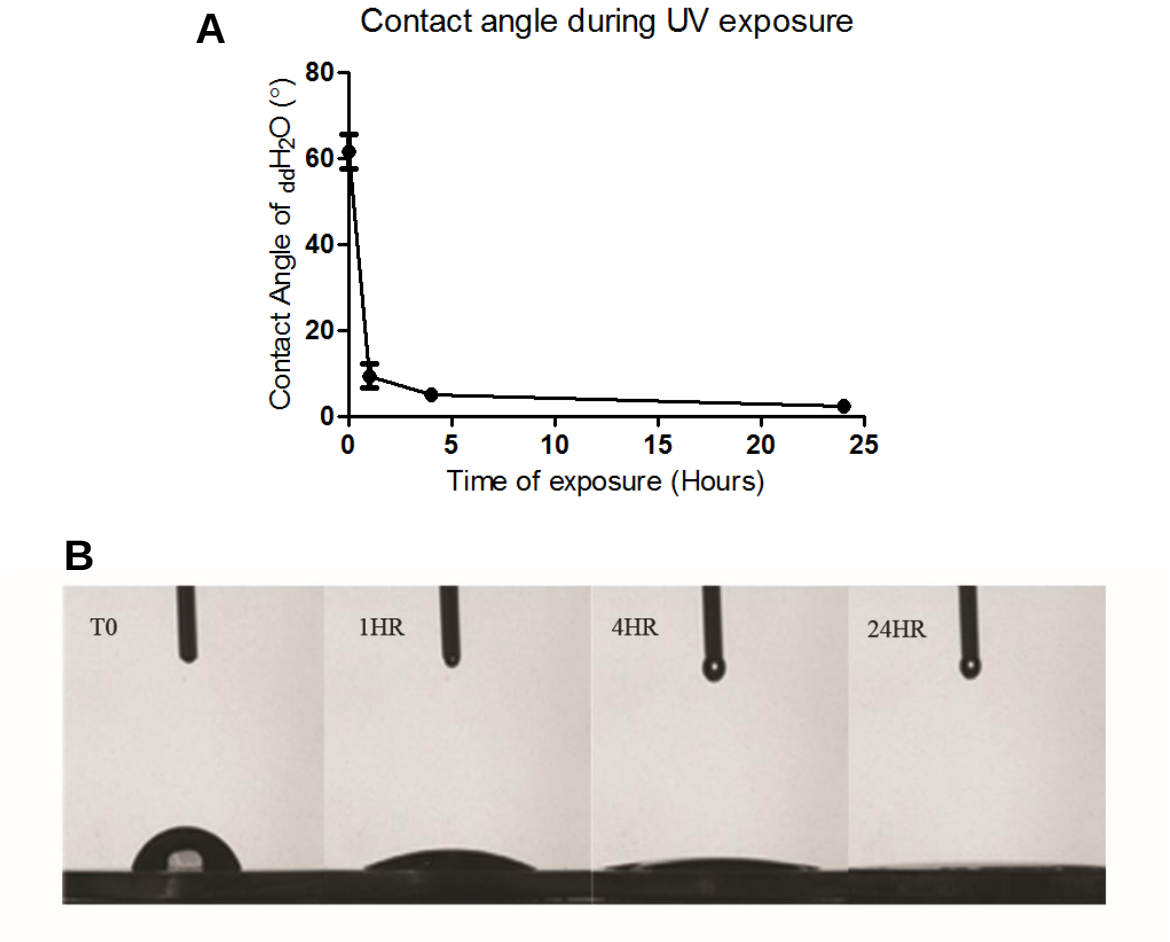

Figure 30 Time course displaying the reduction in contact angle of $_{dd}H_2O$ on CCMT irradiated with UV light (A). Images of water contact angle at time of analysis (B). Error bars represent ± 1 SD (n = 5).

The photo-reactivity of CCMT was studied by monitoring the contact angle of $_{dd}H_2O$ whilst the substrate was exposed to UV light over time. The wettability of the surface can be ascertained using this method, with the more hydrophobic materials having a greater contact angle. Time zero (T0) contact angle of CCMT substrates was 61.62˚ ± 8.70˚ which decreased to 9.44˚ ± 6.21˚ after 60 minutes of UV light exposure. This decreased further to 5.10˚ ± 0.98˚ and then ultimately became super-hydrophilic (< 5˚) after 24 hours which can be seen in figure 31.

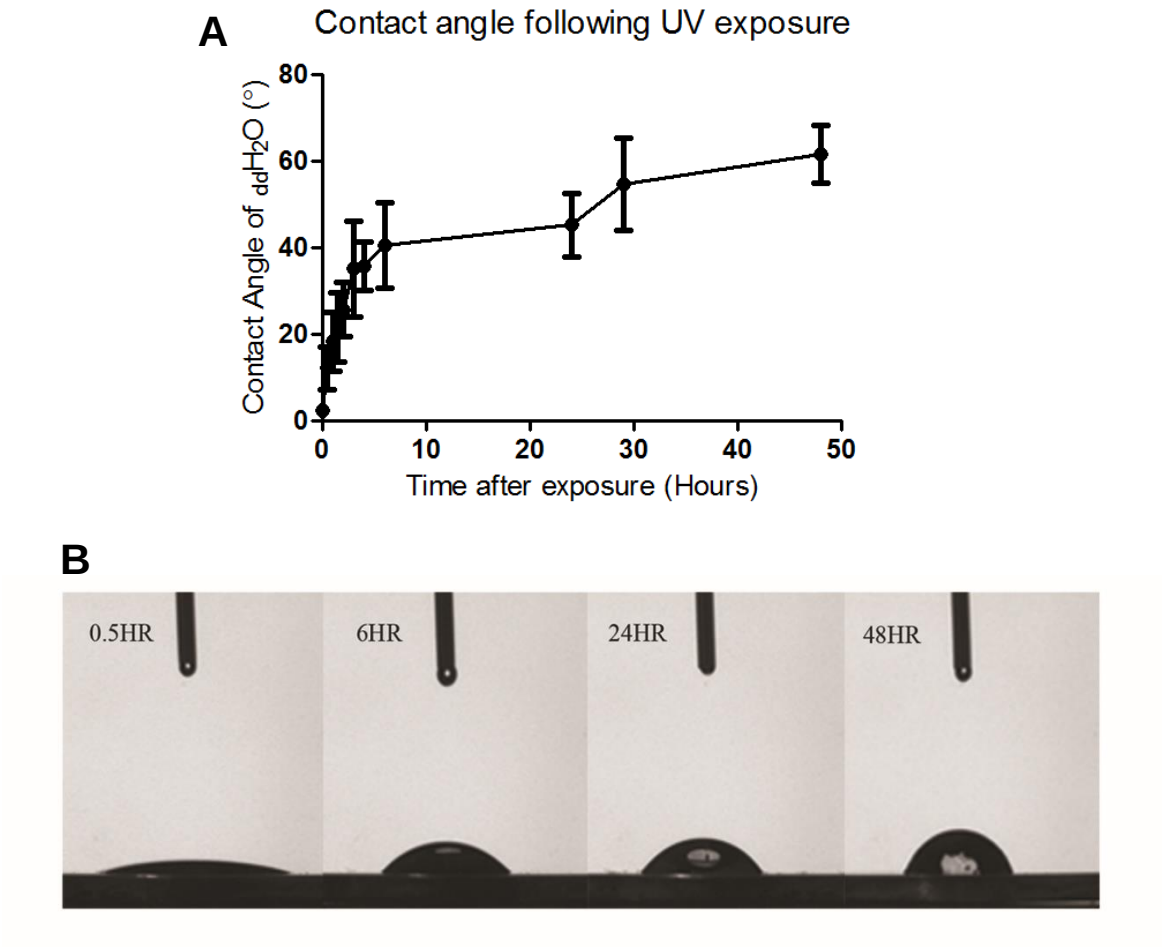

Figure 31 Time course representing contact angle recovery of $_{dd}H_2O$ following the immediate removal of the CCMT substrates from UV exposure (A). Images of water contact angle at time of analysis (B). Error bars represent ± 1 SD (n = 5).

The recovery of the CCMT substrate to its original T0 contact angle was ascertained using the same method. Once the CCMT substrates had been removed from the UV chamber the contact angle increased from~0˚ to 12.17˚ ± 4.85˚ after 30 minutes. The contact angle continued to rise, reaching 40.45˚ ± 9.82˚ by 4 hours. After 48 hours the original T0 value was recorded and the substrates had recovered to their original level of wettability as shown in figure 32.

3.2.2. FTIR

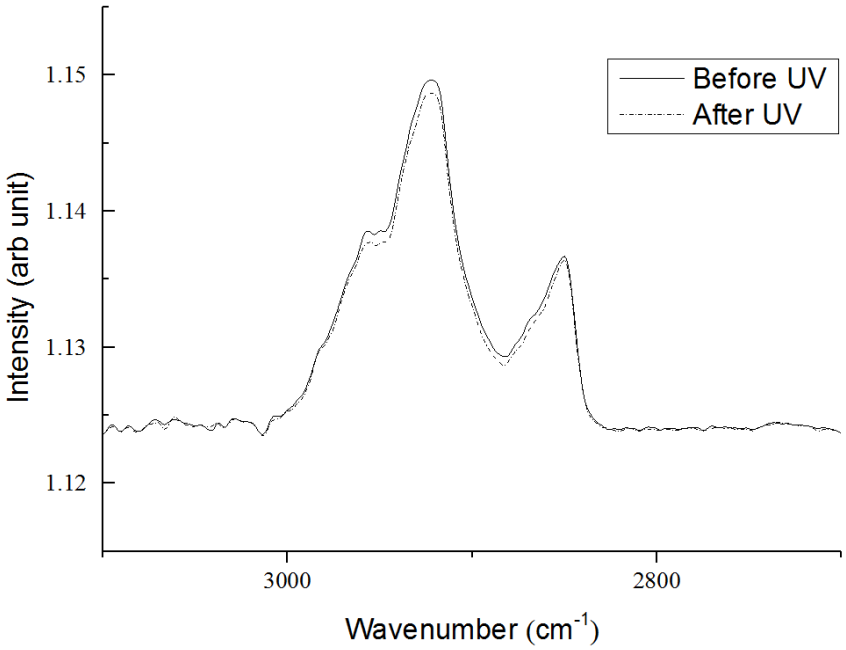

Figure 32 FTIR spectra of methylene hydrocarbon groups on CCMT before and after 24 hours UV exposure.

No significant reduction in hydrocarbon peaks was able to be observed following UV photofunctionalization of CCMT, as shown in figure 33.

3.2.3. PROLIFERATION

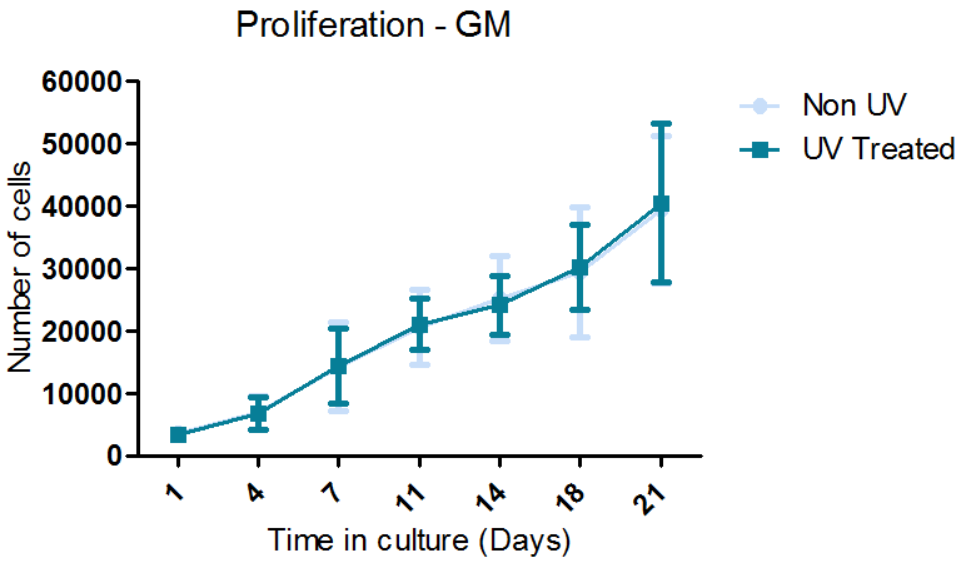

Figure 33 Proliferation of human MSCs in GM assessed by AlamarBlue until 21 days. UV treatment of CCMT prior to seeding the MSCs did not have an effect on the proliferative ability of the cells. Each line represents the mean ± 1 SD, N = 3, n = 3.

UV photofunctionalization of CCMT did not affect the proliferation of MSCs in GM. Both non UV and UV treated substrates successfully stimulated proliferation at a comparable rate over 21 days as shown in figure 34.

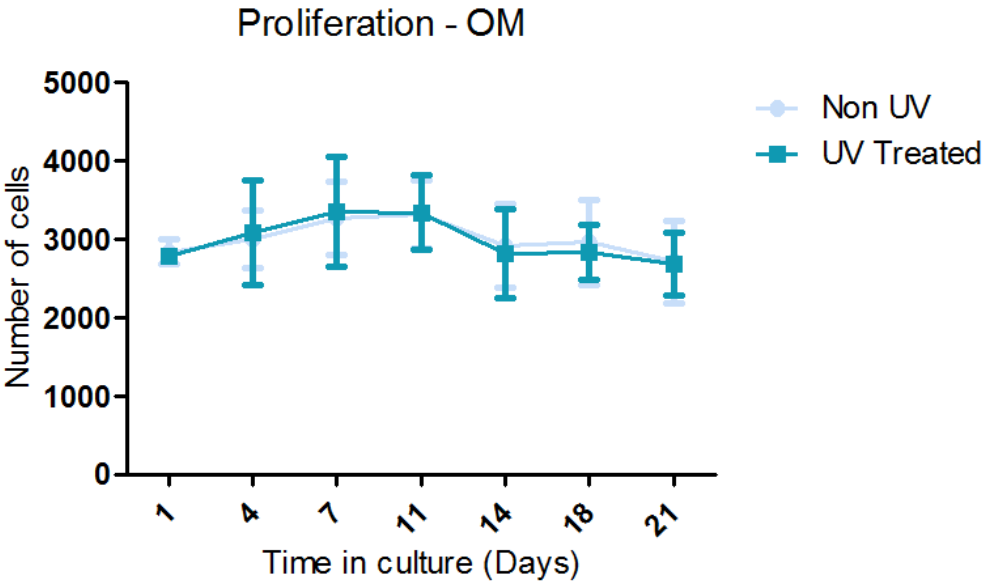

Figure 34 Proliferation of human MSCs in osteogenic media assessed by AlamarBlue over 21 days. No difference was observed between UV treated and non UV substrates. Each line represents the mean ± 1 SD, N = 3, n = 3.

Proliferation in OM was examined over 21 days as shown in figure 35. No significant difference was observed between non UV and UV treated CCMT. Both substrates stimulated a slow rate of proliferation for 7 days which was then followed by a minor decrease in cell numbers, which was possibly due to contact inhibition or apoptosis triggered during the differentiation process. An equivalent number of cells was found at day 21 compared to day 1.

3.2.4. ATTACHMENT

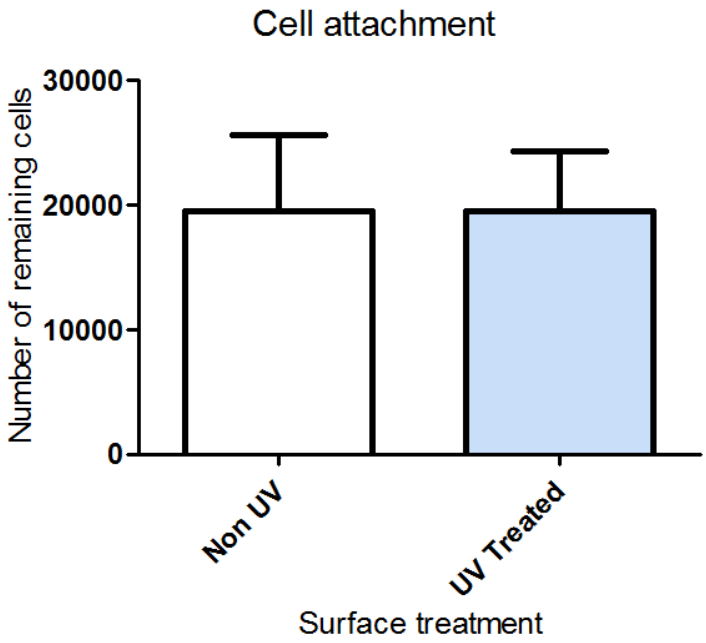

Figure 35 Evaluation of cell attachment after 24 hours in culture. No difference between UV treated and non-UV CCMT substrates was observed. Each column represents the mean ± 1 SD, N = 3, n = 3.

After 24 hours in culture there was no significant difference in the number of attached cells between non UV (19518 ± 6051) and UV treated (19460 ± 4802) CCMT.

3.2.5. RETENTION

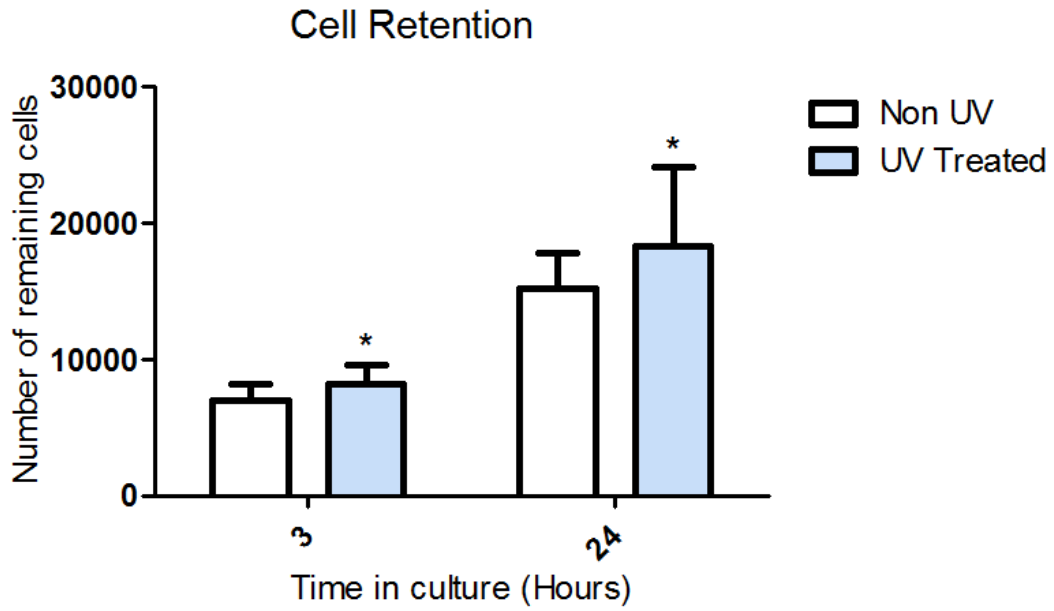

Figure 36 Evaluation of cell retention, displaying the remaining cell population following three washes in PBS after 3 and 24 hours incubation. The UV treated substrate was shown to have a greater remaining cell population. Each column represents the mean ± 1 SD, N = 3, n = 3. * = $p < 0.05$.

Cell retention was analysed to gain a measure of how well adhered each population of MSCs was to the substrate surface. Following 3 and 24 hours in culture, MSCs were mechanically washed three times and the remaining cells quantified. Significantly more cells remained on the UV treated substrate (8183 ± 1382) after 3 hours compared to non UV CCMT (7017 ± 1194). This effect was again present at 24 hours where significantly more cells were found on the UV treated substrate (18333 ± 5745) compared to non UV (15250 ± 2557), as shown in figure 37.

3.2.6. MIGRATION

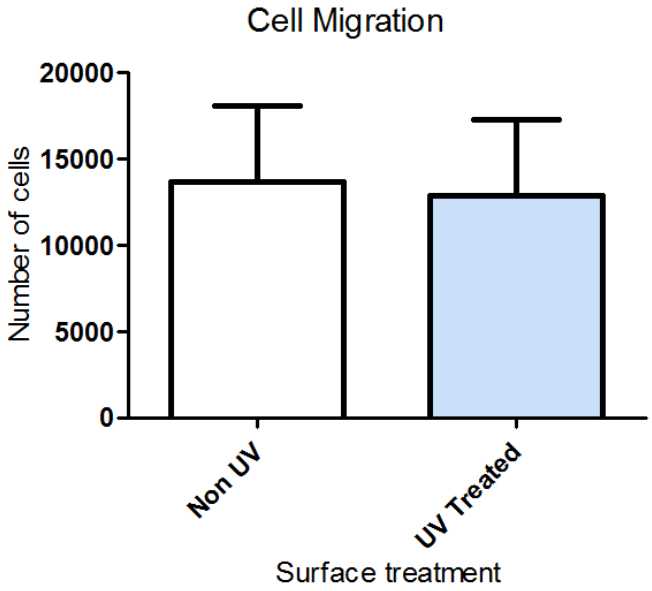

Figure 37 Evaluation of cell migration, displaying the migratory cell populations after a 4.5 hour incubation period. There was no difference between UV treated and non-UV CCMT substrates. Each column represents the mean ± 1 SD, N = 3, n = 3.

The use of UV photofunctionalization as a chemotactic factor that could influence cell invasion and migration was analysed through use of a migration assay. It was found that after 4.5 hours incubation, there was no significant difference in the number of cells that had colonised UV treated (12847 ± 4419) and non UV (13681 ± 4370) CCMT substrates (Figure 38).

3.2.7. CELL MORPHOLOGY - INTERNAL

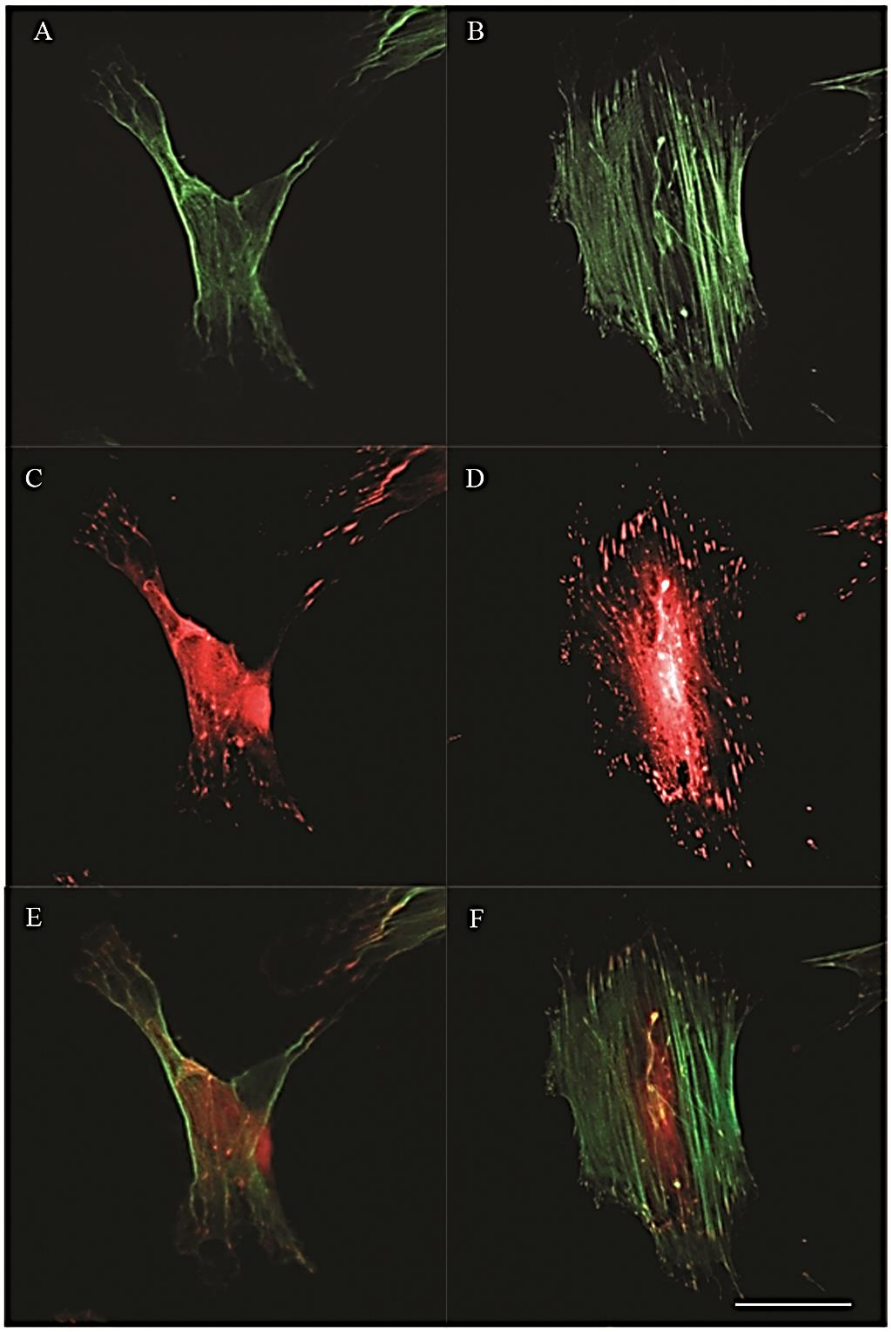

Figure 38 Fluorescent microscopy images displaying the cytoskeletal organisation of MSCs on non-UV (A, C, E) and UV-treated (B, D, F) CCMT substrates after incubation for 24 hours in OM. MSCs are noticeably larger on UV treated CCMT, with more developed actin fibres. Green depicts f-actin (A B), whilst red shows vinculin expression (C D). Images were taken at X 40. Scale bar = 50 μm.

After 24 hours in osteogenic culture there was some clearly discernible differences in the morphology of the MSCs found on the two substrates. MSCs found on the UV treated

CCMT substrate appeared larger and more spread than those on non UV CCMT (Figure 39). Non UV CCMT did promote some cytoskeletal restructuring in the form of protrusions in the form of lamellipodia although the cells were clearly smaller than those found on UV treated CCMT. F-actin fibres appeared to be more developed and robust in MSCs on UV treated CCMT compared to MSCs on non UV substrates (Figure 39 A & B). Furthermore, the increased size of MSCs on the UV treated substrate resulted in greater expression of vinculin throughout the cell and as a consequence the formation of a greater number of FAs (Figure 39 D).

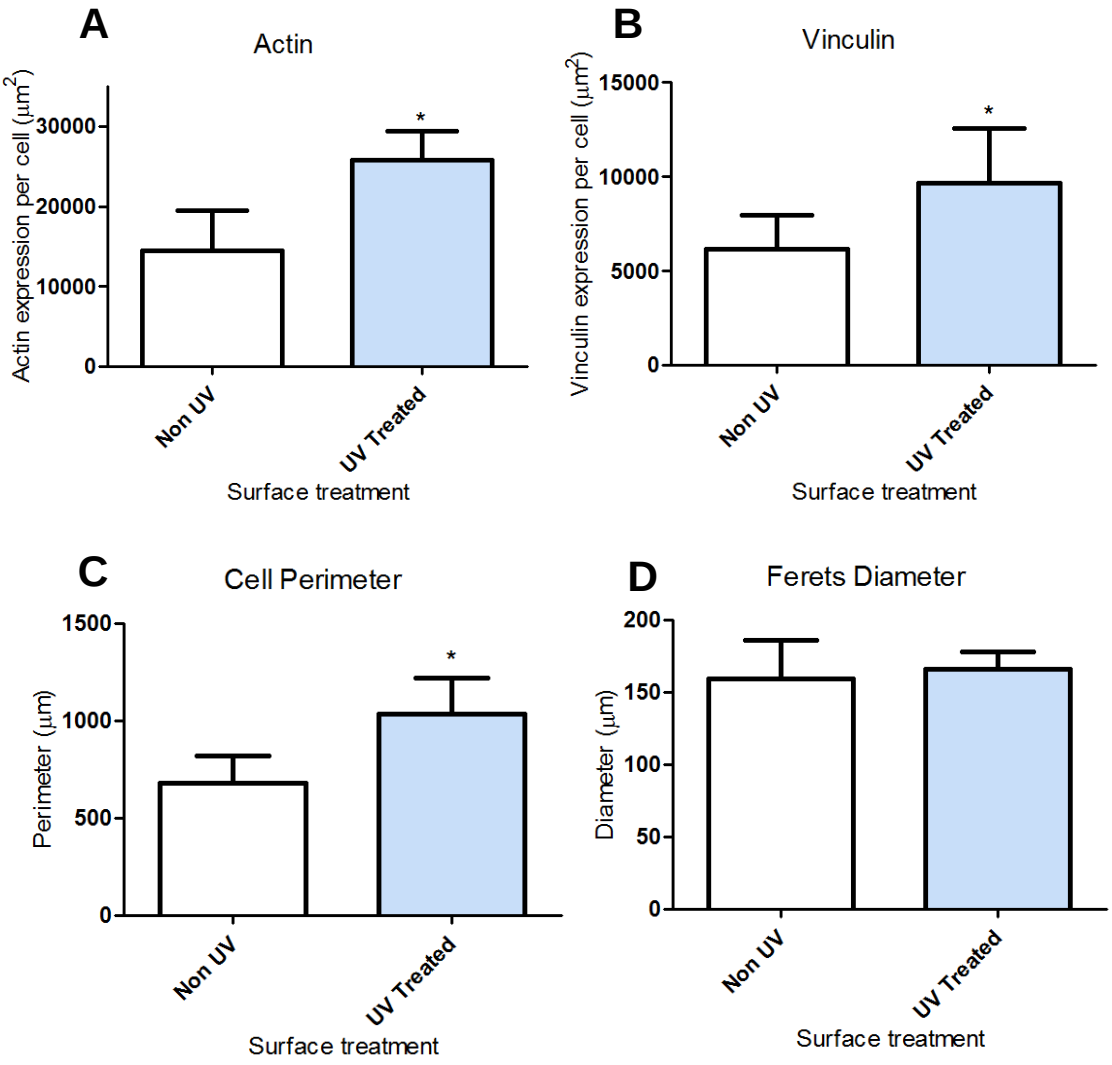

Figure 39 Cytomorphometric analysis of actin (A), vinculin (B), cell perimeter (C) and ferets diameter (D) of human MSCs after 24 hours culture in OM. Each column represents the mean ± 1SD, n = 13. * = $p < 0.05$.

Cytomorphology was carried out on MSCs on both substrates. MSCs on UV treated CCMT were larger and as a result, had significantly greater cell perimeter ($p < 0.05$) than those found on non UV CCMT (Figure 40 C). Interestingly, the ferets diameter, which can be described as the measure of an object along a specific direction, was similar in MSCs on both substrates and showed no significant difference (Figure 40 D). Both f-actin and vinculin were shown to be more widely expressed to a significant level in MSCs found on the UV treated CCMT substrate (Figure 40 A & B).

3.2.8. MINERALISATION

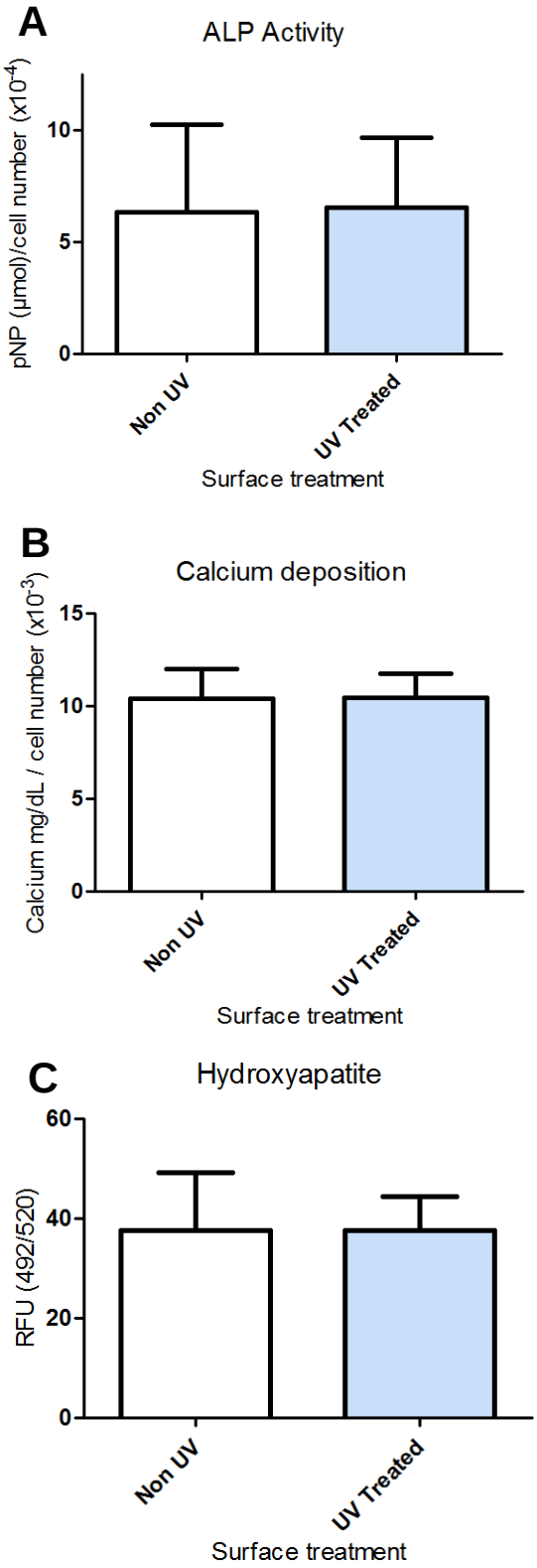

Figure 40 Markers of mineralisation were studied, showing ALP activity (A), calcium ion content (B) and hydroxyapatite formation (C). No significant difference was observed between UV treated and non-UV substrates for all markers. Each column represents the mean ± 1SD, N = 3, n = 3.

ALP plays a role in the early stage of osteogenesis (Golub and Boesze-Battaglia, 2007), whilst calcium and hydroxyapatite formation are widely recognised as late markers of the process. There was no significant difference between UV treated and non UV CCMT for amounts of ALP, calcium or hydroxyapatite (Figure 41 A-C).

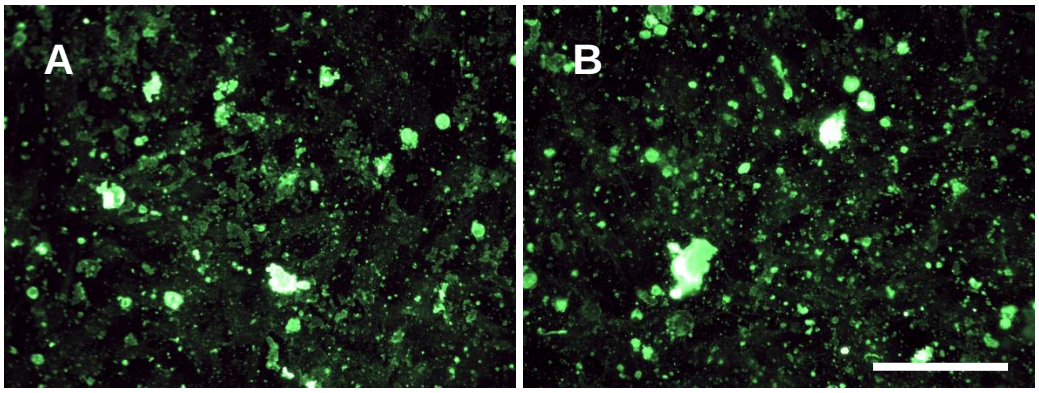

Figure 41 Fluorescent microscopy analysis of hydroxyapatite was also performed and showed no apparent difference in deposition between non UV (A) and UV treated CCMT (B). Scale bar = 200 μm.

In addition to the assays performed in the study, the amount of hydroxyapatite mineralisation was also assessed by fluorescence microscopy. Both substrates stimulated the formation of a mineral rich matrix. No clear and discernible difference could be observed between the two substrates as shown in figure 42.

3.2.9. SAMPLE SIZE

A previous publication where UV photofunctionalized titanium promoted significant improvements in cell migration, attachment, proliferation and differentiation in human MSCs was used as a reference for sample size (Aita et al., 2009a). In *Aita et al's* study experiments were performed in triplicate (n = 3) and statistically significant results were obtained using student's t test and two-way ANOVAs when appropriate. In this chapter of the thesis, the student's t test, the same as in *Aita et al's* study, was utilised to ascertain significance between UV treated and non-UV substrates. A sample size calculator was used to determine if the sample size used in the proliferation, migration and osteogenic

differentiation data sets was large enough to determine statistically significant results. When using *Aita et al's* data as a reference to estimate expected means and standard deviations, the result was a required total sample size of 8 (4 per group). As the sample size used per group was 9 per group, the data should therefore be sufficient to show significance and therefore it can be determined that the lack of any significant results in proliferation, migration and osteogenic differentiation datasets is not due to a small sample size.

3.3. DISCUSSION

Coating the surface of CoCrMo in a thin layer of TiO_2 has been shown to improve the osteogenic differentiation and adhesion of mesenchymal stem cells *in vitro* (Logan et al., 2014b, Logan et al., 2015). As the surface oxide layer found on titanium and its alloys, TiO_2 has a unique ability that makes it advantageous as a surface coating; TiO_2 is highly photoreactive and upon irradiation with UV light transitions from hydrophobic to superhydrophilic. This useful ability has resulted in the application of TiO_2 coated glass self-cleaning windows, as UV light from the sun is capable of generating this reaction and can remove surface contaminants (Wang et al., 1997). The photo reactivity of TiO_2 is not limited to industrial applications and is currently being investigated as a means of increasing the efficacy of orthopaedic devices and is known as UV photofunctionalization.

In this section of the thesis, a study was performed to assess UV photofunctionalization of CCMT. The photo reactivity of CCMT was investigated by obtaining water contact angle measurements during UVC exposure over a time course of up to 24 hours (Figure 31). The CCMT surface successfully converted from hydrophobic to superhydrophilic, confirming the photo reactivity of the anatase TiO_2 layer. This change in wettability has been reported numerous times and is one of the traits of UV photofunctionalization on bulk titanium and TiO_2 films (Aita et al., 2009b, Att et al., 2009, Miyauchi et al., 2010, Aita et al., 2009a, Hori et al., 2010b, Ueno et al., 2010, Yamada et al., 2010, Minamikawa et al., 2013, Terriza et al., 2013). The recovery of the UV treated CCMT substrate to its original hydrophobic state was assessed using the same method. It was found that CCMT substrates returned to their original levels of wettability after 48 hours storage in the dark (Figure 31). Interestingly, recovery following UV photofunctionalization has not been widely reported. *Aita et al* reported a recovery time of between 16 days for one titanium surface and another failed to return to its original level of surface energy after 32 days analysis (Aita et al., 2009b). This is significantly different to the recovery times observed in the present study, which only took a total of 48 hours. This difference may be due to variation in how UV photofunctionalization affects bulk titanium substrates and TiO_2 coated materials such as CCMT. Dissimilarities between bulk titanium and sputter coated titanium on glass has previously been reported using MC3T3-E1 cells, where it was found that bulk titanium was superior to the titanium coating (Oya et al., 2010).

Following confirmation of the change in surface wettability on CCMT by UV photofunctionalization, FTIR was used to try and gain an understanding of the mechanism behind this phenomenon. In particular, wavenumbers of specific hydrocarbons were studied both before and after UV irradiation, as hydrocarbon removal or decomposition is thought to be one of the main mechanisms behind UV photofunctionalization (Aita et al., 2009b, Att et al., 2009, Miyauchi et al., 2010, Ueno et al., 2010, Yamada et al., 2010). Vibration bands of C-H bonds at 2853, 2923 and 2957 cm^{-1}, which account to stretching modes of CH_2 and CH_3 were measured (Charpentier et al., 2012). No significant reduction in hydrocarbon content was observed on CCMT substrates following UV photofunctionalization (Figure 33). This result did not coincide with a previous publication where a reduction in hydrocarbon content was observed on UV irradiated TiO_2 coated silicon (Takeuchi et al., 2005). It may be that the UVC light source used in the present study was not powerful enough to generate the decomposition of surface hydrocarbons, although a secondary UVC light source was tested and also failed to generate any hydrocarbon reduction, which makes the UVC light source unlikely to be the cause of the variation, but it should not be ruled out entirely. In addition, it may be that the FTIR equipment did not have a suitable degree of sensitivity to detect these minute changes in hydrocarbon content. A lack of significant hydrocarbon removal following UV photofunctionalization has also been reported on TiO_2 thin films deposited by plasma enhanced CVD (Terriza et al., 2013). When compared to the results of the present study, it may be that UV photofunctionalization of CVD TiO_2 coatings is not an effective way of reducing hydrocarbon content. In addition, *Gao et al* studied cellular response on substrates treated with UVC and UVA light. The amount of hydrocarbon removal was comparable between the two light sources although UVC was superior in various cell markers, which implies that hydrocarbon decomposition may not be the main mechanism behind UV photofunctionalization (Gao et al., 2013).

To test the effectiveness of UV photofunctionalization as means of increasing the efficacy and osteoconductivity of CCMT, numerous markers of cell behaviour were studied using a variety of cell culture techniques. Cellular proliferation in both GM and OM was studied using Alamar blue assay. No difference in cell proliferation was observed between UV treated and non UV substrates in both GM (Figure 34) and OM (Figure 35). This data did not concur with a number of other publications where proliferation has been shown to be enhanced on UV photofunctionalized titanium (Att et al., 2009, Aita et al., 2009a, Ueno et al., 2010) and TiO_2 coated materials (Miyauchi et al., 2010, Sawase et

al., 2008). This difference in cell response may be due to dissimilarities between the present study and those that observed enhanced proliferation, including cell type (Att et al., 2009, Sawase et al., 2008, Miyauchi et al., 2010, Ueno et al., 2010), surface topography (Att et al., 2009, Sawase et al., 2008, Aita et al., 2009a, Ueno et al., 2010) and the bulk material tested (Miyauchi et al., 2010, Aita et al., 2009a, Sawase et al., 2008, Att et al., 2009, Ueno et al., 2010).

Cellular proliferation was not the only marker to be unaffected by UV photofunctionalization. Cell attachment (Figure 36), migration (Figure 38) and various markers of osteogenic differentiation (Figure 41) were shown to be similar on UV treated and non UV CCMT substrates. This data doesn't coincide with many publications where cell attachment has been reported to be enhanced on UV treated substrates (Att et al., 2009, Miyauchi et al., 2010, Sawase et al., 2008, Hori et al., 2010b, Aita et al., 2009a, Yamada et al., 2010). Cell migration (Aita et al., 2009a, Hori et al., 2011), osteogenic differentiation (Att et al., 2009, Miyauchi et al., 2010, Hori et al., 2010b, Aita et al., 2009a) and *in vivo* osteogenic response (Sawase et al., 2008, Ueno et al., 2010) have also all been reported to be improved on UV photofunctionalized substrates. As with the difference observed for cell proliferation, the lack of an enhanced cell response for these factors may be due to differences in the experimental parameters used between studies, although the number of factors which were not affected suggests that this may not be the case and that UV photofunctionalization may not be as effective on CVD TiO_2 coatings on CoCrMo compared to Ti.

Whilst numerous factors were not affected by UV photofunctionalization, a significant difference was observed for cell retention to the substrate surface. After both 3 and 24 hours in culture, a larger population of MSCs remained on UV treated CCMT following three mechanical washes with PBS (Figure 37). This data indicates that cells found on the UV treated substrate were better adhered to the surface and less likely to be dislodged from external forces. Increased cell adhesion strength on UV photofunctionalization substrates has been reported in the literature (Miyauchi et al., 2010, Yamada et al., 2010, Iwasa et al., 2010). *Miyauchi et al* and *Yamada et al* both used a more sophisticated technique to study the adhesion strength of individual cells using AFM and found that cells on UV treated substrates had both a significantly greater shear strength value and total detachment energy (Miyauchi et al., 2010, Yamada et al., 2010). *Iwasa et al* studied the adhesion strength of a population of cells as a whole, using a similar mechanical detachment method to that in the present study, and found that significantly more cells

remained on the UV treated substrates following the process (Iwasa et al., 2010). An enzymatic detachment method was also studied and UV photofunctionalized substrates were again shown to have a significantly larger remaining cell population to non UV substrates (Iwasa et al., 2010). The observed enhancement in cell adhesion strength following UV photofunctionalization does not seem to be affected by whether the substrate is bulk titanium or a TiO_2 photoreactive coating. *Iwasa et al* (Iwasa et al., 2010) and *Yamada et al* (Yamada et al., 2010) used bulk titanium as there experimental substrate, whereas *Miyauchi et al* used TiO_2 coated glass plate (Miyauchi et al., 2010), which is comparable to the CCMT used in the present study. This data suggests that whilst the UV photofunctionalization process seems to be considerably less effective on CCMT compared to bulk titanium (Att et al., 2009, Aita et al., 2009a, Hori et al., 2010b, Sawase et al., 2008, Yamada et al., 2010) or sputter coated TiO_2 (Miyauchi et al., 2010), the functionalisation process is still have an effect on the cells to a certain degree.

To gain an understanding of what may be behind the increased cell retention observed on UV treated CCMT, fluorescent microscopy was used to assess the cellular morphology of the MSCs after 24 hours in culture. During the cell-substrate adhesion process the structure of the cell can change and various proteins have their expression changed (Anselme, 2000). In particular, the adhesion protein vinculin was studied as it is known to play a role in forming focal adhesion complexes which integrate with the cytoskeletal structure of the cell through talin and actin (Humphries et al., 2007). Focal adhesions can be influential to the differential process with osteogenesis requiring a large number of focal adhesions compared to chondrogenesis and adipogenesis which discourage focal adhesion attachment (Mathieu and Loboa, 2012). The expression of vinculin within the cells was noticeably different between MSCs on UV treated and non UV CCMT. MSCs on UV treated CCMT were more spread and had more focal adhesions than those found on the non UV substrate (Figure 39 C & D). This observation was confirmed by quantitative image analysis which showed that there was significantly more vinculin per cell on UV treated CCMT (Figure 40 B). In addition to vinculin, the cytoskeletal protein, f-actin was assessed simultaneously and it was found that MSCs on the UV treated substrate had superior actin fibre development to those found on non UV substrates (Figure 39 A & B). More robust f-actin fibres has been shown to increase cellular stiffness which may be mechanically advantageous for attached cells (Yamada et al., 2010). As with vinculin expression, quantitative image analysis was performed and significantly more actin was present per cell in MSCs found on UV treated CCMT

compared to non UV substrates (Figure 40 A). Superior vinculin and actin expression in cells on UV photofunctionalized substrates has been widely reported in other studies (Att et al., 2009, Miyauchi et al., 2010, Aita et al., 2009a, Hori et al., 2010b, Yamada et al., 2010, Iwasa et al., 2010, Minamikawa et al., 2013). The combination of more widespread focal adhesion complexes and superior cytoskeletal f-actin development should result in stiffer, better adhered cells.

3.4. CONCLUSION

The process of UV photofunctionalization has been shown to have little or no effect on cell proliferation, attachment, migration or osteogenic differentiation, although the significant enhancement to cell adhesion markers may prove highly advantageous for orthopaedic applications (Logan et al., 2014a). Following surgery, the surface of an orthopaedic device is exposed to multiple forces capable of dislodging attached cells, such as blood flow, micro motion and fluid forces (Cross, 2008a). UV photofunctionalized CCMT was shown to stimulate significantly superior cell retention to the substrate surface by enhancing vinculin and actin development. By enhancing these adhesion molecules, a larger population of cells with osteogenic potential should be able to colonise and remain on the surface of an implantable device, therefore accelerating the healing time post-surgery.

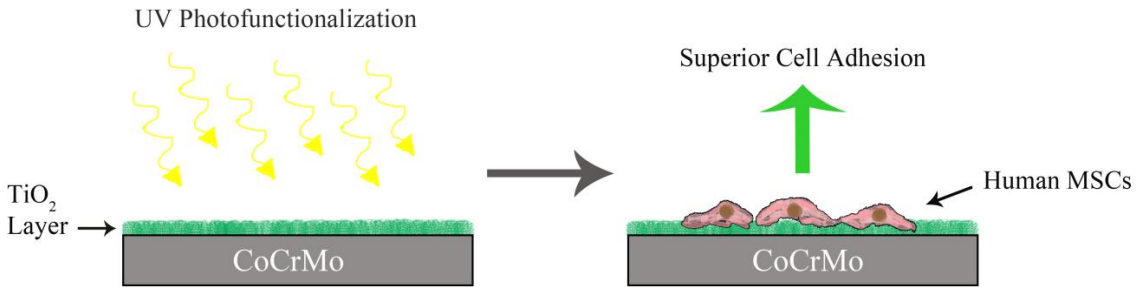

Figure 42 Graphical conclusion – chapter three.

CHAPTER FOUR:

MESENCHYMAL STEM CELL RESPONSE TO TOPOGRAPHICALLY MODIFIED COBALT CHROMIUM MOLYBDENUM

4. INTRODUCTION

An effective and widely used method of improving implant performance is topographical modification of the implant surface. Such methods have been shown to enhance cell response, promoting superior levels of bone to implant contact and bone formation around the implant (Shalabi et al., 2006).

One of the most widely used surface modification techniques for titanium dental implants is the sand blasted acid etched surface. Referred to as SLA, the process involves sand blasting the material surface with 250 µm aluminium oxide (Al_2O_3) particles, and then hot acid etching using a combination of chemicals. The two step procedure results in the formation of both a micro and nano topography on the implant surface. Both the *in vitro* and *in vivo* performance of implants modified with the SLA surface have shown an improved osteogenic response compared to smooth and machined surfaces (Cochran et al., 2011, Mendonca et al., 2010, Khan et al., 2012, Wall et al., 2009).

Despite the excellent performance of the SLA surface in dental implants, studies looking into whether the same surface modification procedure can be applied to other materials for orthopaedic application have not been fully investigated.

This part of the project aimed to investigate whether the SLA surface, used widely on titanium dental implants, could be replicated onto CoCrMo in an effort to enhance the biological performance of the material for orthopaedic application. Four topographies were created on CoCrMo with the aim of generating a variety of different surfaces, ranging from smooth to moderately rough. These included two SLA surfaces; one blasted using 50µm Al_2O_3 and the other using 250µm Al_2O_3 particles. In addition to studying SLA surfaces, CoCrMo that had only undergone the acid etching process was also included to study the effect of acid etching alone. Lastly, a CoCrMo surface polished to a mirror finish was included as a smooth control. Cellular markers for proliferation, attachment, viability, adhesion and differentiation were studied using human MSCs, which are known to be highly sensitive to topographical features present on a material surface (Dalby et al., 2007, Logan and Brett, 2013). Surface characterisation of all substrates was also performed, including profilometry, wettability, scanning electron microscopy and elemental analysis.

The hypothesis explored in the chapter is:

1. The addition of an SLA topography onto the surface of CoCrMo would generate increased cellular retention and osteogenic differentiation in human MSCs when compared to the smooth CoCrMo control.

4.1. MATERIALS AND METHODS

4.1.1. SAMPLE PREPARATION

Discs of CoCrMo were prepared to a smooth finish as previously described in section 2.1.1 SAMPLE PREPARATION – (Page 59) and throughout this chapter are referred to as SMO. Three additional topographies were created from SMO discs; acid etched (AE), sand blasted acid etched using 50µm Al_2O_3 grit (SLA50), and sand blasted acid etched using 250µm Al_2O_3 grit (SLA250). Acid etching to create AE substrates and etch sand blasted substrates was performed based on a previously reported protocol (Durual et al., 2013). To create AE substrates, SMO discs were immersed in HCl 7.4% and H_2SO_4 76% for 6 minutes at 100°C, rinsed under H_2O and then immersed in HNO_3 30% for 5 minutes at 60°C. Substrates were again rinsed under H_2O and then sonicated in isopropanol for 15 minutes at 30°C (Sigma-Aldrich, 190764), followed by $_{dd}H_2O$ for 10 minutes at RT. To create sandblasted substrates, SMO discs were secured on a mount and subsequently blasted with either 50µm or 250µm Al_2O_3 grit at a pressure of 95 Psi, approximately 5 centimetres from the blasting tip (Vaniman, Sandstorm 2, 80301). 250µm Al_2O_3 was used as the blasting media for SLA250 substrates (Renfert, Cobra, 15851005), whilst 50µm Al_2O_3 media was used for SLA50 (Renfert, Cobra, 15941205). SLA substrates were then removed from the mount and sonicated in isopropanol for 15 minutes at 30°C, followed by $_{dd}H_2O$ for 10 minutes at RT. Following this, SLA substrates underwent the same acid etching process as AE. Before discs were used for cell culture experiments all discs were washed in $_{dd}H_2O$, air dried and sterilised using UV light irradiation for 20 minutes on each side (BONMAY, BR-506).

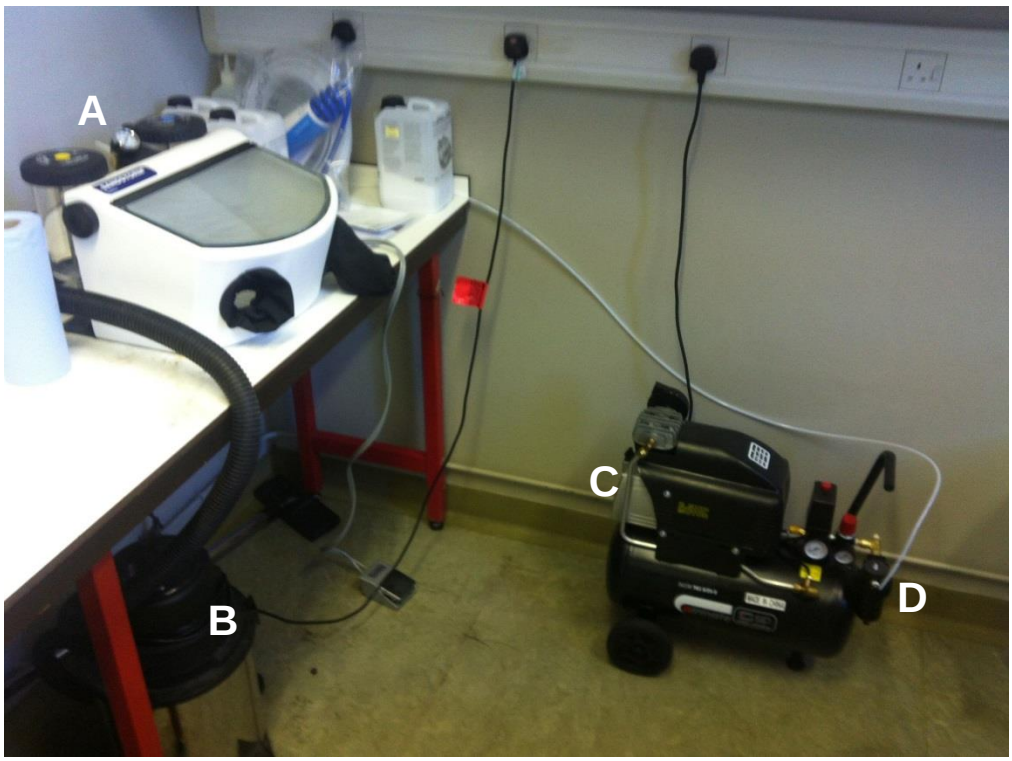

Figure 43 Photograph of sand blasting equipment setup showing Sandstorm 2 sandblaster (A), dust extraction (B), air compressor (C) and air filter (D).

4.1.2. CELL CULTURE

Human MSCs were prepared and cultured as previously described in section 2.1.6 CELL CULTURE – (Page 63).

4.1.3. SUBSTRATE CHARACTERISATION

The wettability of each substrate was studied by measuring the water contact angle (n = 10) as previously described in section 2.1.4 SUBSTRATE CHARACTERISATION – (Page 61). In addition to wettability, the surface features of the substrates were profiled using laser profilometry (n = 3). R_a values were then calculated as previously described in section 2.1.4 SUBSTRATE CHARACTERISATION – (Page 61). SEM was performed simultaneously with energy dispersive x-ray analysis (EDX) to visually assess the surface topography and quantify its elemental composition. Substrates were mounted on stubs using araldite ultra and had images taken at low and high magnifications using a beam energy of 5 keV and spot size of 3. For EDX measurements the SEM was setup

to X500 magnification, with a beam energy of 20 keV and a spot size of 5. Acquisitions were performed at five locations for 30 seconds on each substrate to obtain quantitative elemental data. Elemental maps were also obtained to observe the distribution of each element on the substrate surface. Acquisition time for each map was 300 seconds.

4.1.4. VIABILITY

MSCs are highly sensitive to topographical features found on a materials surface (Dalby et al., 2007). This considering, it is important to test cell viability to ensure that there is no cytotoxic affect induced on the cells due to the surface topography. The Live/Dead Cell Imaging kit (Life technologies, R37601) was used to determine viability and cytotoxicity. The principle of the assay works by exposing the cells to two components. Live cells are distinguished by enzymatically converting the first component of non-fluorescent calcein AM to the highly fluorescent calcein which is retained within live cells and fluoresces green. The second component is impermeant to cells and will only enter cells with damaged membranes where the component actively binds to DNA and fluoresces red.

MSCs were seeded at 3.5 x 10^4 cells per well onto SMO, AE, SLA50 and SLA250 substrates in a 24 well plate (n = 3) in GM. Following 24 hours incubation at standard culture conditions of 37°C, 5% CO_2 in a humidified atmosphere, MSCs were washed twice using 1 ml of PBS. The MSCs were then incubated in the dark for a period of 15 minutes at RT with 300 µl of Live/Dead reagent which was prepared as a 1 : 1 ratio of kit components A and B. Substrates were then viewed using a fluorescence microscope fitted with the appropriate filters (Leica, DMIRB).

4.1.5. PROLIFERATION

MSCs from three donors (N = 3) were seeded on SMO, AE, SLA50 and SLA250 substrates at a density of 2 x 10^3 cells per well (n = 3) in a 24 well plate. Plates for both GM and OM were setup individually and cultured at 37˚C, 5% CO_2 in a humidified atmosphere with media changes performed on each day of analysis. Cellular proliferation was then analysed as previously described in section 2.1.7 PROLIFEATION – (Page 65).

4.1.6. ATTACHMENT

MSCs from three donors (N = 3) were seeded on SMO, AE, SLA50 and SLA250 at a density of 4 x 10^4 cells per substrate in 24 well plates in GM (n = 3). After 24 hours in culture at conditions of 37˚C, 5% CO_2 in a humidified atmosphere, the attachment on each substrate was analysed as previously described in section 3.1.6 ATTACHMENT – (Page 97).

4.1.7. CELL MORPHOLOGY - EXTERNAL

The morphology of MSCs on the substrate surface was analysed using SEM to study the cell integration into the topographical features present on the material surface.

MSCs were seeded at a density of 7 x 10^3 cells onto SMO, AE, SLA50 and SLA250 substrates in GM in a 24 well plate. Following 24 hours incubation at standard culture conditions of 37°C, 5% CO_2 in a humidified atmosphere, the cells were washed using 1 ml of $_{dd}H_2O$ and fixed with 300 µl of 4% PFA in PBS for 15 minutes at RT. MSCs were then dehydrated sequentially using alcohol at concentrations of 50%, 70%, 90% and 100% x 2 for 10 minutes each. Substrates were then immersed in hexamethyldisilazane (Sigma-Aldrich, 379212) for 2 minutes, air dried and mounted on aluminium stubs using conductive carbon tape. Lastly, substrates were sputter coated in gold using a deposition chamber (Polaron, E5000) for a period of 90 seconds before being transferred to the SEM for analysis. Images were taken at high and low magnifications using a beam energy of 5 keV and spot size of 3.

4.1.8. RETENTION

A total of 3.5 x 10^4 MSCs from three donors were seeded on SMO, AE, SLA50 and SLA250 (n = 3) in GM and incubated at standard culture conditions of 37˚C, 5% CO_2 in a humidified atmosphere. After 24 hours in culture, cell retention to the substrate surface was analysed as previously described in section 3.1.7 RETENTION – (Page 98).

4.1.9. CELL MORPHOLOGY – INTERNAL

A total of 5 x 10^3 cells per substrate were seeded on SMO, AE, SLA50 and SLA250 in a 24 well plate using OM (n = 3). After 24 hours at standard culture conditions, analysis of both the cytoskeletal protein f-actin and adhesion protein vinculin were studied as previously described in section 3.1.9 CELL MORPHOLOGY – INTERNAL – (Page 99) although quantitative image analysis was omitted. In addition, MSCs were counterstained with 400 µl of DAPI (10 µg/ml) in PBS for 20 minutes at RT in the dark to allow for cell identification.

4.1.10. OSTEOGENIC MARKERS

Markers of the early and late stages of the osteogenic differentiation process were studied. ALP was analysed after 5 days in culture, whilst hydroxyapatite and calcium content were tested after 21 days (N = 3)(n = 3). For ALP, 2 x 10^4 cells were seeded on SMO, AE, SLA50 and SLA250 substrates in OM, whilst 12.5 x 10^3 cells were used for hydroxyapatite and calcium assays. The level of each osteogenic marker was collected as previously described in section 3.1.10 MINERALISATION – (Page 100).

4.1.11. STATISTICAL ANALYSIS

Human MSCs from three donors (N = 3) were used in triplicate (n = 3). SEM EDX scans were performed at n = 8, contact angle analysis was performed at n = 10 and profilometry scans were completed at n = 3. Statistical analysis was primarily carried out using a one-way ANOVA followed by the Bonferroni post-test in GraphPad Prism software (v5.04) with $p < 0.05$ deemed to be statistically significant. The student's t test was used to analyse total Al area data. A post-hoc power calculator was used to confirm the statistical power of significant results observed in the study

4.2. RESULTS

4.2.1. ROUGHNESS

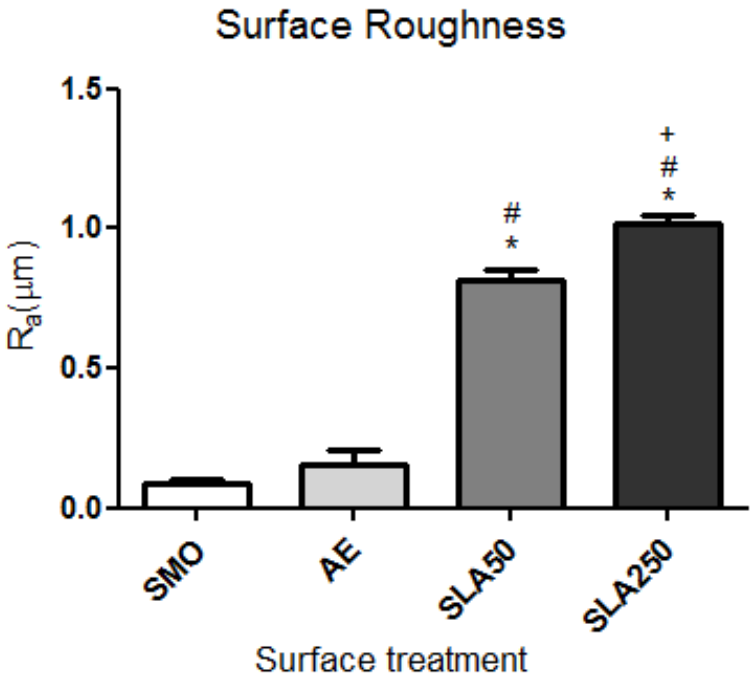

Figure 44 Surface roughness results displaying R_a values; SMO had the lowest R_a which was followed by AE. Both SLA surfaces were significantly rougher, with SLA250 having the largest R_a value of the four. Each bar represents the mean ± 1SD, n = 3, * = $p < 0.05$ substrate verse SMO, # = $p < 0.05$ substrate verses AE, + = $p < 0.05$ substrate verses SLA50.

Laser profilometry was used to ascertain the surface roughness of each substrate by obtaining R_a values. The SMO surface, which had a R_a of 0.09 ± 0.01 µm was the smoothest of the four surfaces. AE was rougher than SMO, with an R_a of 0.15 ± 0.05 µm, whilst both SLA surfaces were significantly rougher than SMO and AE. Additionally, SLA250 (1.02 ± 0.03 µm) was found to have a significantly higher R_a value compared to SLA50 (0.82 ± 0.03 µm), and was established to be the most rough of the four surfaces.

4.2.2. CONTACT ANGLE

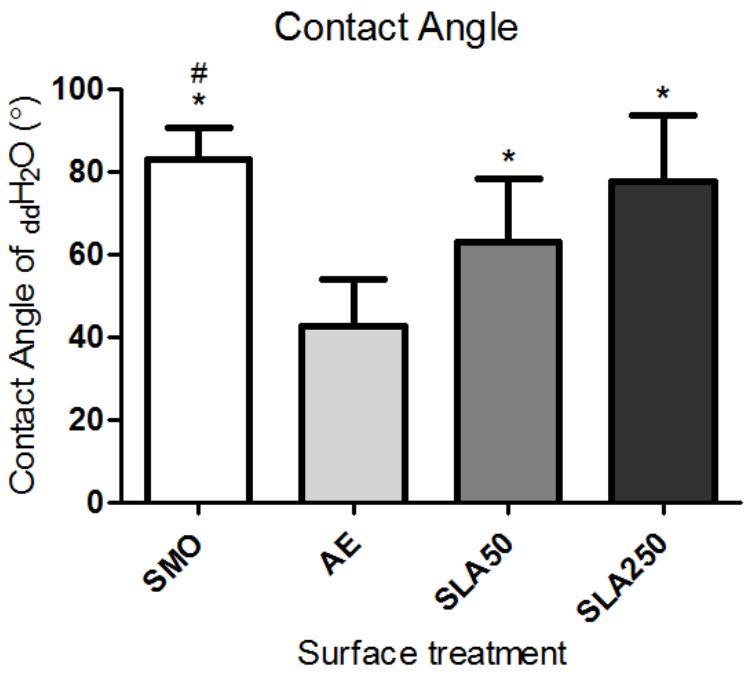

Figure 45 Contact angle results using $_{dd}H_2O$; SMO was the most hydrophobic of the four surfaces. AE, SLA50 & SLA250 appeared to show a linear trend of increasing hydrophobicity in relation to roughness values. Each bar represents the mean ±1 SD, n = 10. * = $p < 0.05$ substrate verses AE, # = $p < 0.05$ substrate verses SLA50.

Contact angle measurements were performed to gain a measure of wettability on each surface. As shown in figure 45, SMO was the most hydrophobic of the four surfaces which a contact angle of 83.11 ± 7.41°. AE (42.70 ± 11.45°) was observed to have the lowest contact angle of all the surfaces which was followed by SLA50 (63.09 ± 15.26°) and lastly SLA250 (77.60 ± 16.05°). The change in wettability of AE, SLA50 and SLA250 appeared to correlate with the increasing roughness parameters of each surface shown in figure 46.

4.2.3. SURFACE MORPHOLOGY

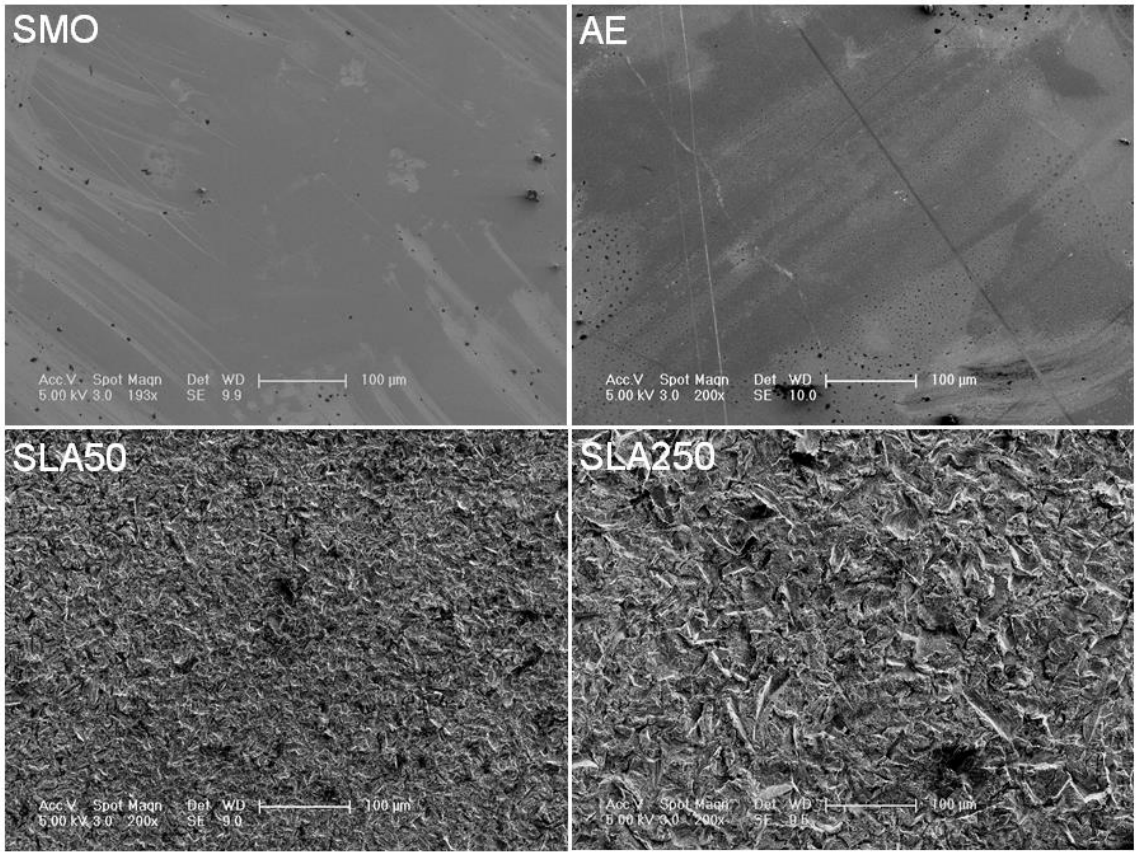

Figure 46 SEM images showing the topographical features present on each surface under X200 magnification. SMO and AE surfaces appear to have a smooth featureless topography whilst SLA surfaces are noticeably rougher. Scale bar = 100 μm.

SEM images taken at X200 are shown in figure 47. Under low magnification, both SMO and AE surfaces were similar in appearance without the presence of distinct topographical features, although markings in the form of scratches did appear to be present on both surfaces. SLA50 and SLA250 had an undoubtedly roughened topography with what appeared to be larger and more distinct features present on the SLA250 surface.

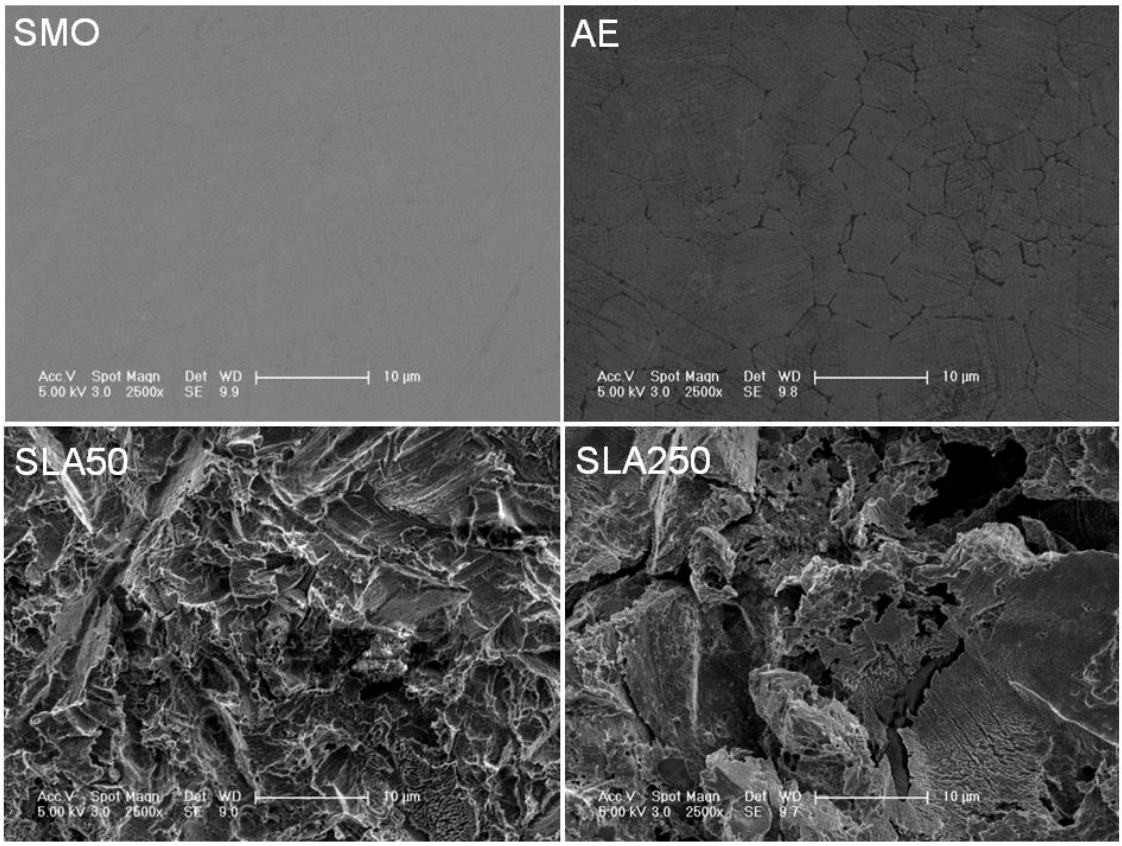

Figure 47 SEM images showing the four surface topographies under X2500 magnification. SMO still appears to have a featureless topography whilst on AE, lines are now present on the surface. Both SLA surfaces show a rough surface with peaks and valleys, which appear to be more prominent on SLA250. Scale bar = 10 µm.

SEM images taken under higher magnification (X2500) are shown in figure 48 and begin to show the differences in the topographical morphology of each surface. As with low magnification SEM images, no clear features were present on SMO. In contrast, a pattern in the form of a web of lines and ridges was now visible on the surface of AE. The SLA50 surface displayed a variety of sharp and wavy peaks and valleys, whilst features on the SLA250 appeared to be more pronounced and have more height distribution due to the occurrence of pits.

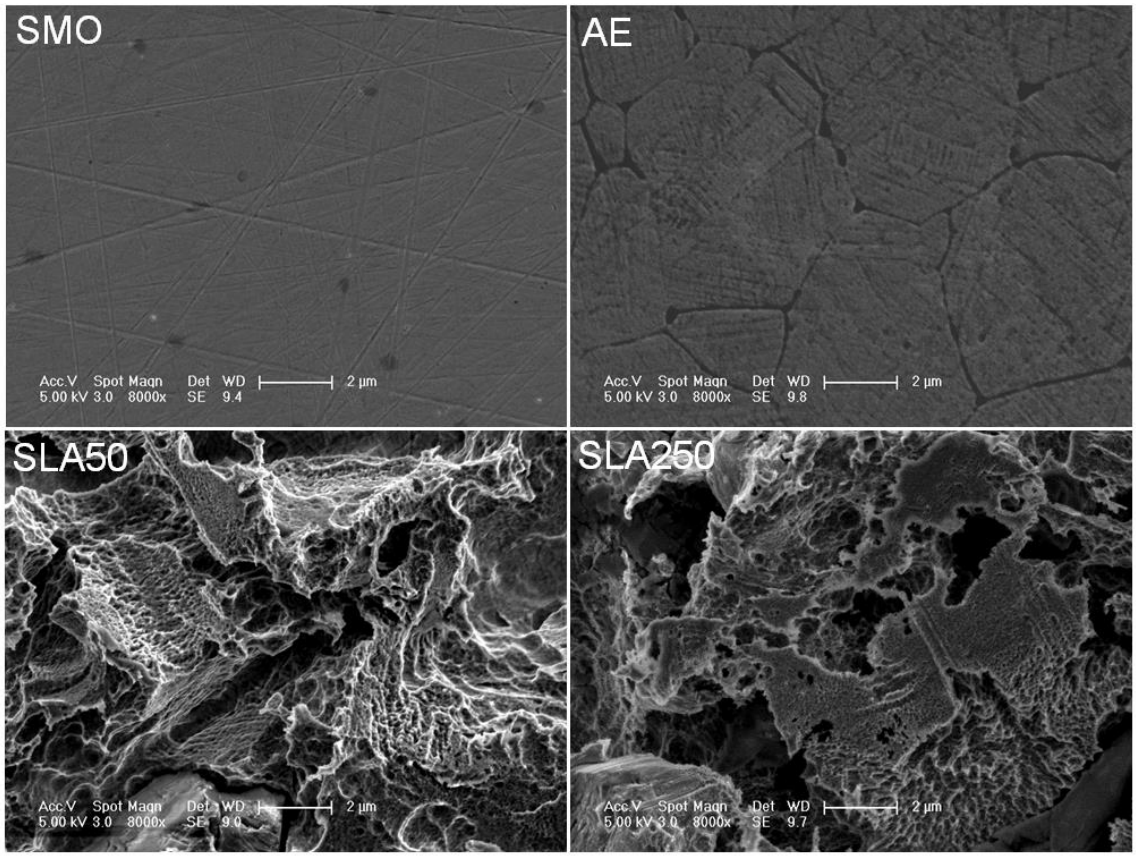

Figure 48 SEM images of the four surface topographies under X8000 magnification. Lines are now visible on SMO and AE although these appear to be deeper and without order on AE. The effect of the acid etching process is now visible on both SLA surfaces which show wavy, disordered features. Scale bar = 2 µm.

As shown in figure 49, the occurrence of scratch marks on SMO was visible under X8000 magnification although they appeared to be shallow in depth. Contrarily, the boundaries observed on AE appear to be dark, suggesting they might have some depth. In addition, the presence of an array of lines and grooves was existent across the entirety of the surface of AE, which supports the profilometry data shown in figure 44, were AE was significantly rougher than SMO. Both SLA surfaces clearly had a wavy/spikey topography formed on top of the larger surface features created from the blasting process.

4.2.4. SURFACE ELEMENTAL COMPOSITION

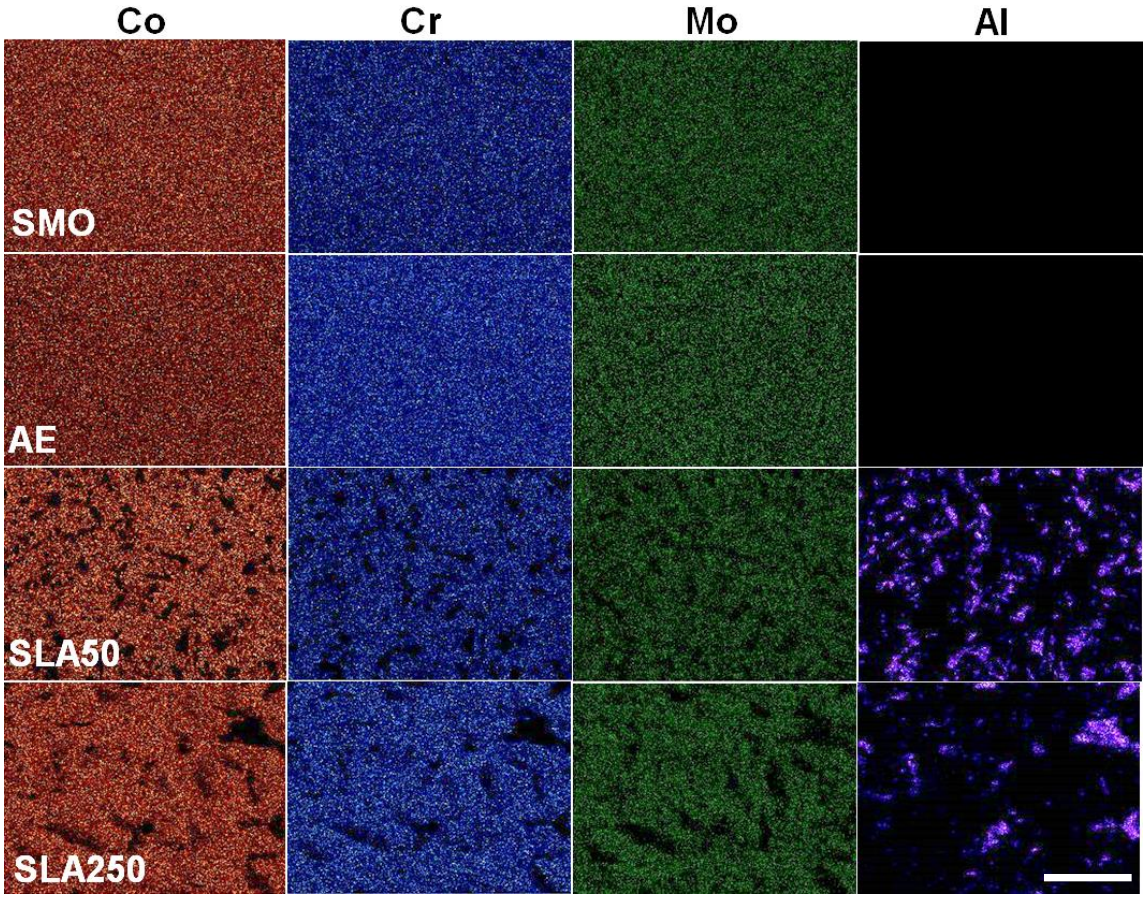

Figure 49 Grid showing the elemental maps of each substrate surface detected by EDX analysis. Red = cobalt, blue = chromium, green = molybdenum & purple/violet = aluminium. Scale bar = 100 μm.

Elemental maps were created using SEM EDX to determine the spread and location of specific elements across the surface of each substrate. Specifically Co, Cr, Mo and Al were studied with the results shown in figure 50. An even distribution of Co, Cr and Mo was found on SMO and AE substrates. In comparison, holes in the maps of Co, Cr and Mo were observed in SLA50 and SLA250 substrates which were found to correlate with the detection of Al, confirming the presence of aluminium contamination. Interestingly the distribution of Al on SLA50 and SLA250 was evidently different. SLA50 had a large number of Al particles that were small in size, but were widespread across the surface. In comparison SLA250 had clearly larger particles of Al, but as a consequence, had large sections of the surface that were not affected by residual Al. Both quantitative data taken from SEM EDX scans (Table 3) and image pixel analysis (Figure 51), showed SLA50 to have a larger amount of residual Al, although not to a statistically significant level.

Table 3 Quantitative data showing elemental composition from multiple EDX scans (n = 8)

	Co	Cr	Mo	Al	Si
SMO	63.5 ± 0.3	29.5 ± 0.3	6.2 ± 0.3	0	0.7 ± 0.1
AE	63.6 ± 0.3	29.5 ± 0.3	6.2 ± 0.4	0	0.7 ± 0.1
SLA50	58.0 ± 3.7	27.8 ± 1.9	4.9 ± 0.3	8.6 ± 5.7	0.7 ± 0.1
SLA250	59.0 ± 0.6	28.0 ±0.5	4.9 ± 0.3	7.4 ± 0.9	0.7 ± 0.1

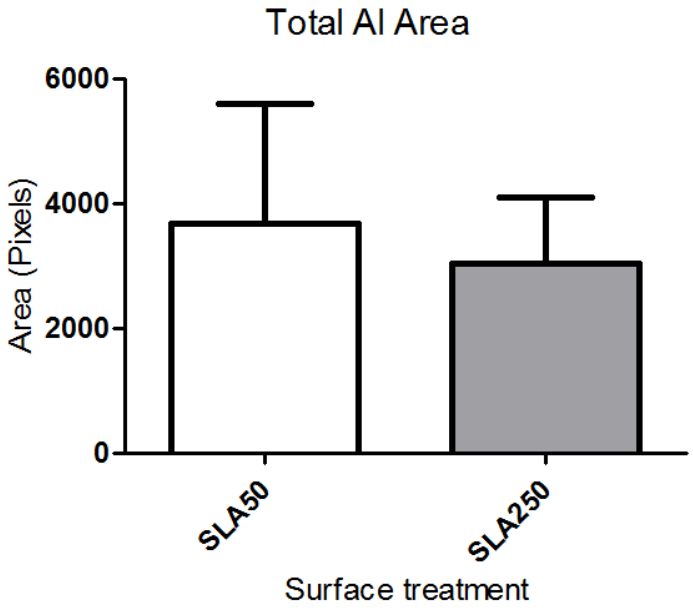

Figure 50 Image analysis data comparing total area of Al coverage. A larger area of Al was present on SLA50 although this was not significant. Each bar represents the mean ± 1 SD, n = 8.

Whilst more Al was found on the SLA50 surface in comparison to SLA250, this difference was not significant.

4.2.5. VIABILITY

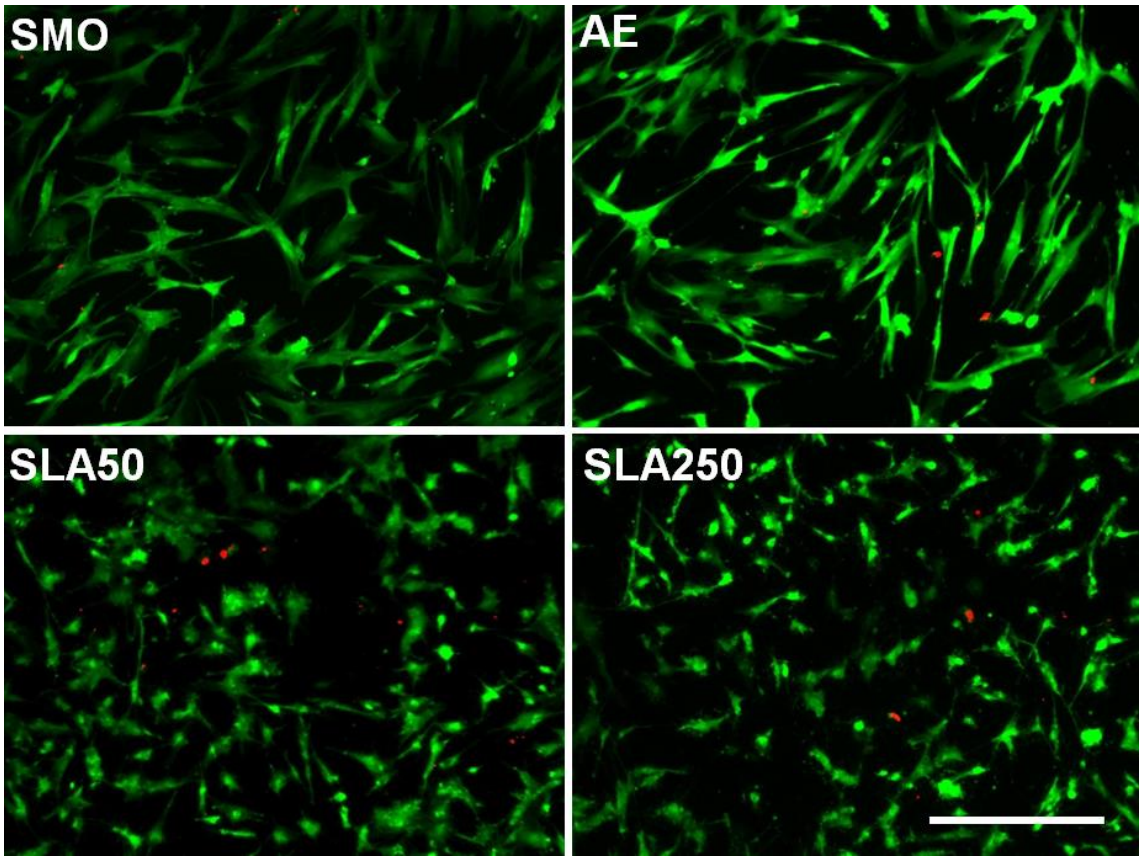

Figure 51 Live/Dead images showing cell viability after 24 hours in culture. Green shows live cells stained with calcein AM, whilst red nucleic staining indicates dead or dying cells. Scale bar = 130 μm.

A fluorescent live/dead staining kit was used to ascertain if any of the surfaces stimulated a cytotoxic response in the human MSCs. It was found that after 24 hours in culture, all four substrates promoted acceptable cytocompatibility, shown by rapid uptake of the green component. Dead cells, that stained red, were present on each substrate in low numbers, although appeared to be most frequent on the SLA50 as shown in figure 52.

4.2.6. PROLIFERATION

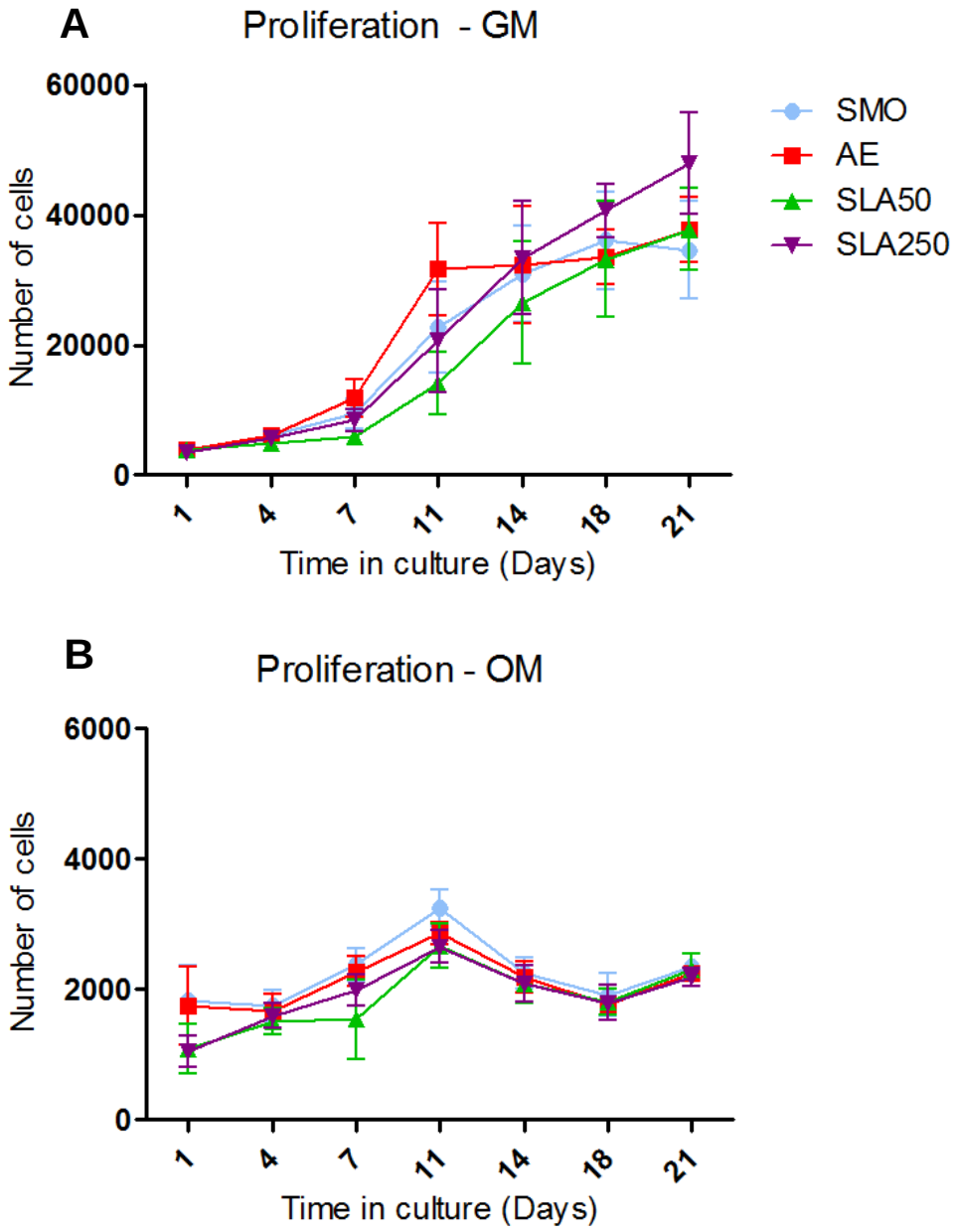

Figure 52 Proliferation data on all four topographies in both GM (A) and OM (B). All subjects were allowed to proliferate up to 21 days. Each line represents the mean ± 1 SD, N = 3, n = 3.

Cellular proliferation was studied in both GM and OM over a period of 21 days as shown in figure 53. In GM, AE stimulated an enhanced rate of proliferation at 7 and 11 days. In comparison, SLA50 appeared to show slowed proliferation resulting in the lowest number of cells at day 7, 11 and 14. By day 14, cell numbers were comparable on SMO, AE and SLA250, although whilst SMO and AE appeared to level out, SLA250 promoted further proliferation and as a result ended up with the largest cell population by day 21.

The rate of proliferation in OM was similar across all substrates. Interestingly, a lower number of cells was observed on SLA substrates compared to SMO and AE after 1 day in both GM and OM.

4.2.7. ATTACHMENT

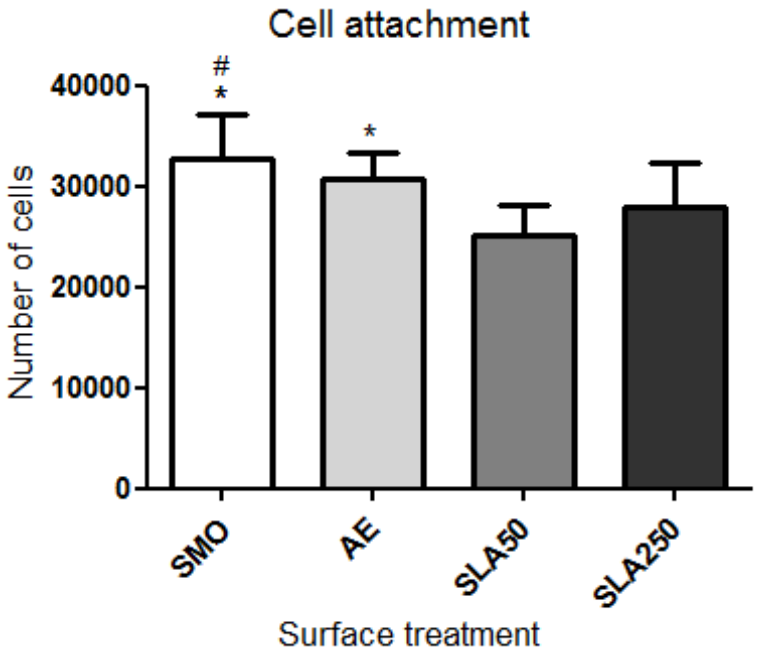

Figure 53 Cell attachment data after 24 hours incubation. SLA surfaces appeared to have a lower amount of attached cells compared to SMO and AE. Each bar represents the mean ± 1 SD, N = 3, n = 3. * = $p < 0.05$ substrate verses SLA50. # = $p < 0.05$ substrate verses SLA250.

Cell attachment was studied on each surface after 24 hours in culture. As shown in figure 54, the largest cell population was found on SMO with a total of 32815 ± 4380, which was closely followed by AE (30635 ± 2650). Both SLA surfaces had a significantly lower amount of attached cells compared to SMO, whilst SLA250 (28017 ± 4305) was also found to have more remaining cells than SLA50 (25123 ± 3015).

4.2.8. CELLULAR EXTERNAL MORPHOLOGY

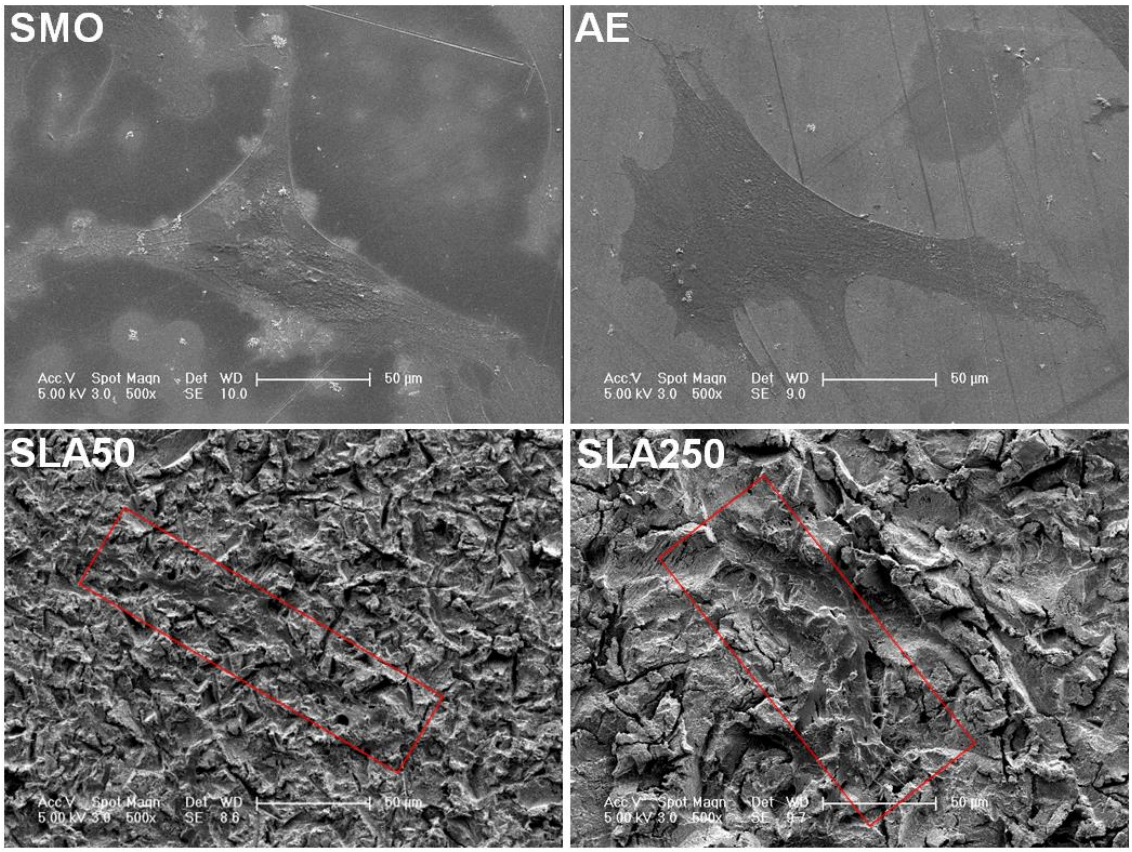

Figure 54 SEM images showing cell morphology on the four substrates under X500 magnification. Cells are noticeably larger and more spread on SMO and AE compared to the SLA substrates. Scale bar = 50 µm.

The morphology of MSCs and their interaction with the surface topography on each substrate was analysed by SEM. As can be seen in figure 55, MSCs were highly spread on the smooth SMO and AE surfaces largely due to the lack of distinct surface features. MSCs on both SLA50 and SLA250 were difficult to identify due to their integration within the features of each surface. The cell shape of MSCs on the SLA surfaces appeared to be mediated by the topographical features, as cells appeared to be elongating and found along channels and grooves in the surface. As a result, the majority of MSCs observed on SLA surfaces were not as spread as those found on SMO and AE. The presence of smaller, spherical cells was also observed on SLA50.

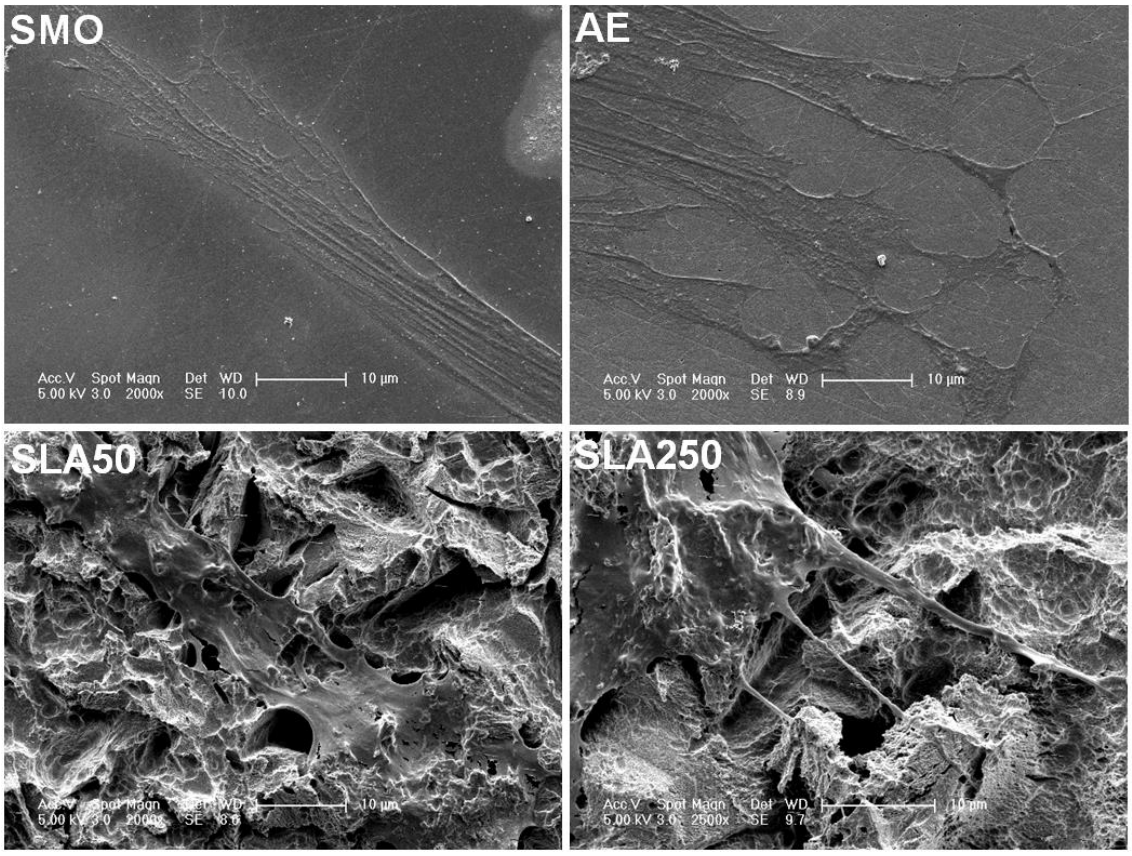

Figure 55 SEM images taken at X2000 magnification showing cellular extensions over the topographical features of each substrate. Scale bar = 10 μm.

Under high magnification, cellular extensions in the form of lamellipodia and filopodia can be observed. On the smoother surfaces, extensive protrusions in the form of filopodia are present in MSCs on the AE substrate, which are not found to the same extent on SMO. This same observation is also evident on SLA250, where highly pronounced, long filopodia extensions can be observed bridging a large gap on the surface, in comparison to SLA50 where filopodia are not clearly observed.

4.2.9. RETENTION

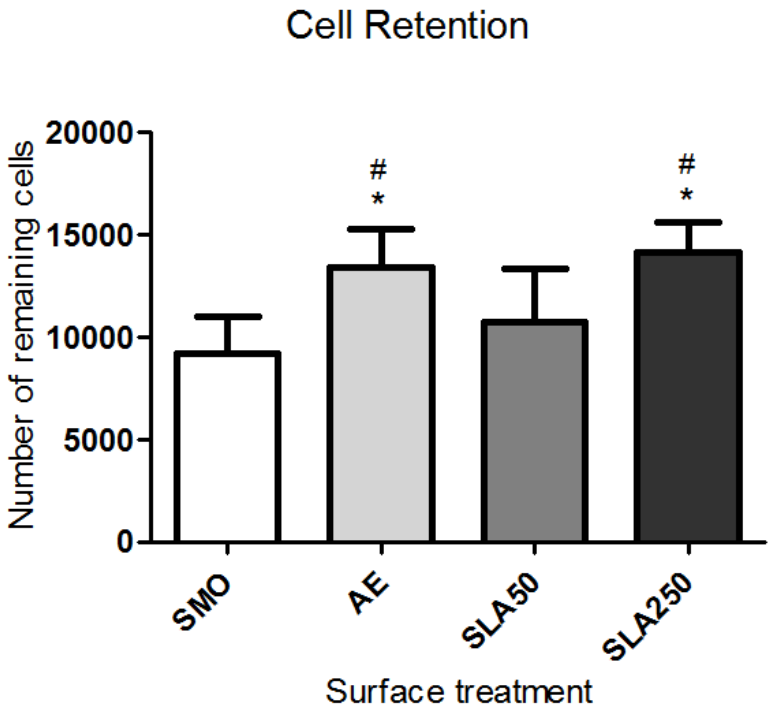

Figure 56 Cell retention data displaying the remaining cell population following three mechanical washes. Each bar represents the mean ± 1 SD, N = 3, n = 3. * $p < 0.05$ substrate verses SMO. # $p < 0.05$ substrate verses SLA50.

To gain a measure of how well adhered each MSC was to the substrate surface, cells were exposed to a mechanical dissociation test using PBS washes after 24 hours in culture. The remaining cells were counted and the results shown in figure 57. It was found that significantly more cells remained on AE (13431 ± 1827) and SLA250 (14105 ± 1479), compared to SMO (9221 ± 1765) and SLA50 (10709 ± 2652).

4.2.10. CELL MORPHOLOGY – INTERNAL

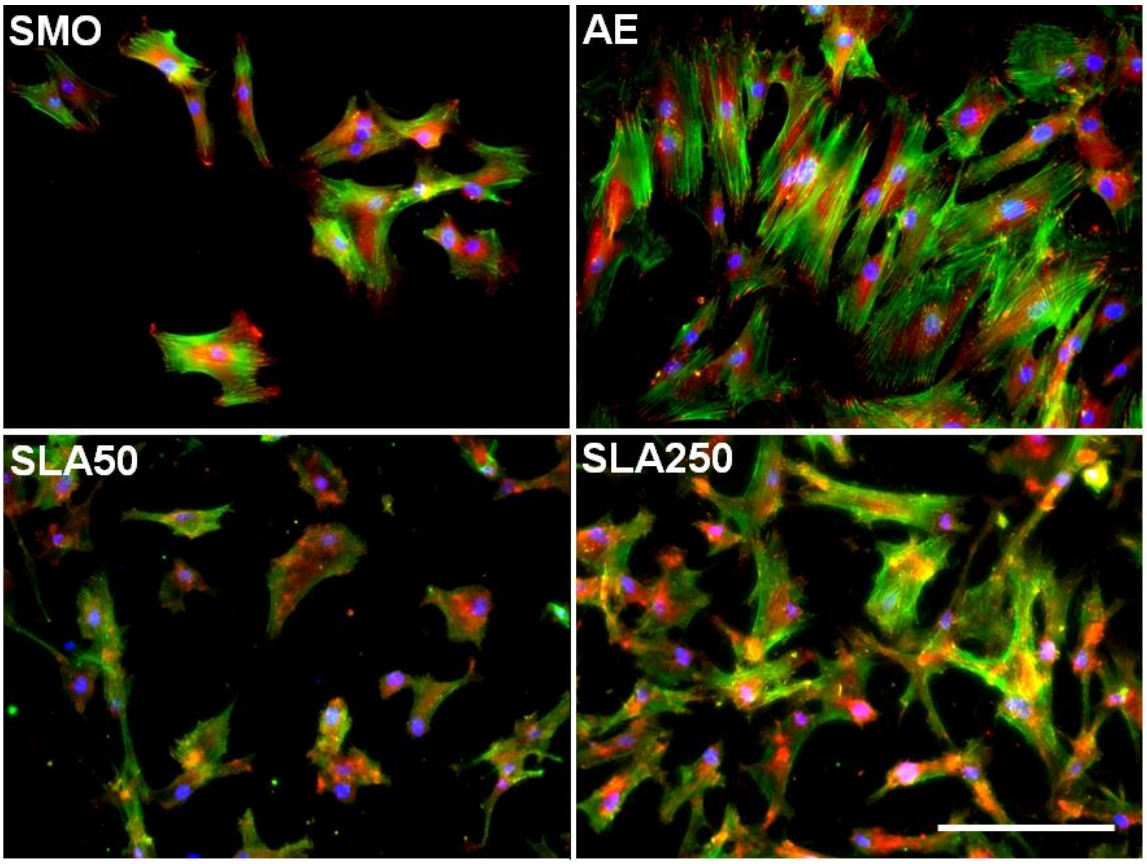

Figure 57 Fluorescent microscopy images showing f-actin (Green), vinculin (red) and DAPI (blue) in MSCs on all four substrates. MSCs on the SLA50 substrate appeared to have poor actin fibre formation and no clear presence of focal adhesions. Scale bar = 130 μm.

The internal cellular proteins f-actin and vinculin were assessed using fluorescent microscopy after 24 hours culture in OM, with representative images shown in figure 58. The cytoskeletal protein f-actin appeared to be more widely expressed in the smoother substrates, in particular AE which promoted MSCs with clear robust internal actin fibres. Interestingly, actin distribution within MSCs found on SLA50 appeared to be somewhat inhibited as fibres were not clearly observed, implying cells on SLA50 were not undergoing cytoskeletal reorganisation successfully. Actin was more clearly observed on the SLA250 surface compared to SLA50. Vinculin was expressed in MSCs on all substrates although the formation of focal adhesions was more evident in cells on SMO and in particular, AE. Focal adhesions were not clearly observed in cells on SLA50 although some were present on SLA250 implying cells had better adhesion to the substrate.

4.2.11. OSTEOGENIC MARKERS

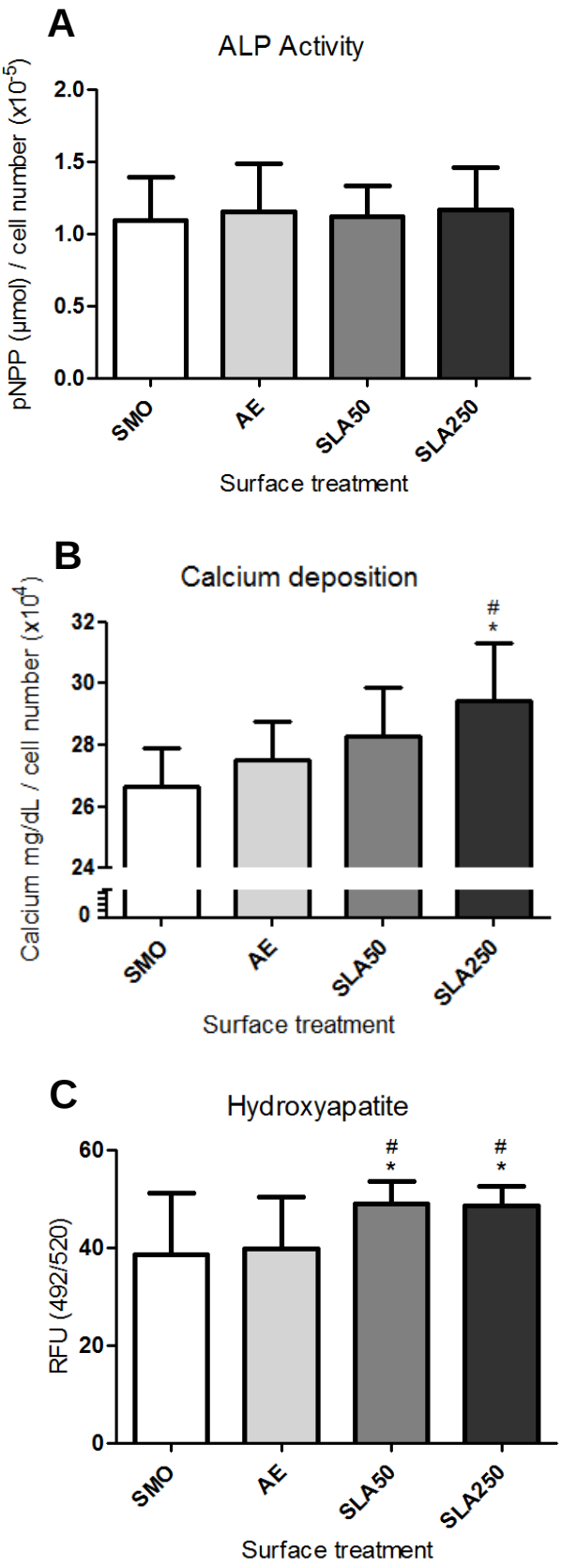

Figure 58 Osteogenic differentiation markers, showing ALP activity (A), calcium deposition (B) and hydroxyapatite formation (C). Each column represents the mean ± 1 SD, N = 3, n = 3. * $p < 0.05$ substrate verses SMO, # $p < 0.05$ substrate verses AE.

A number of osteogenic markers were studied to assess the rate of osteogenic differentiation occurring in MSCs on each substrate, with the results shown in figure 59. ALP, an early marker of the differentiation process was studied after 5 days in culture although no difference was observed in the activity across all substrates. Late markers of osteogenic differentiation included calcium deposition and hydroxyapatite formation. Hydroxyapatite formation was found to be significantly greater on both SLA50 and SLA250 compared to SMO and AE ($p < 0.05$). Furthermore, calcium deposition was significantly greater on SLA250 compared to SMO and AE ($p < 0.05$). This data implies that whilst early stage differentiation did not seem to be affect, later stage mineralisation was significantly greater on SLA250.

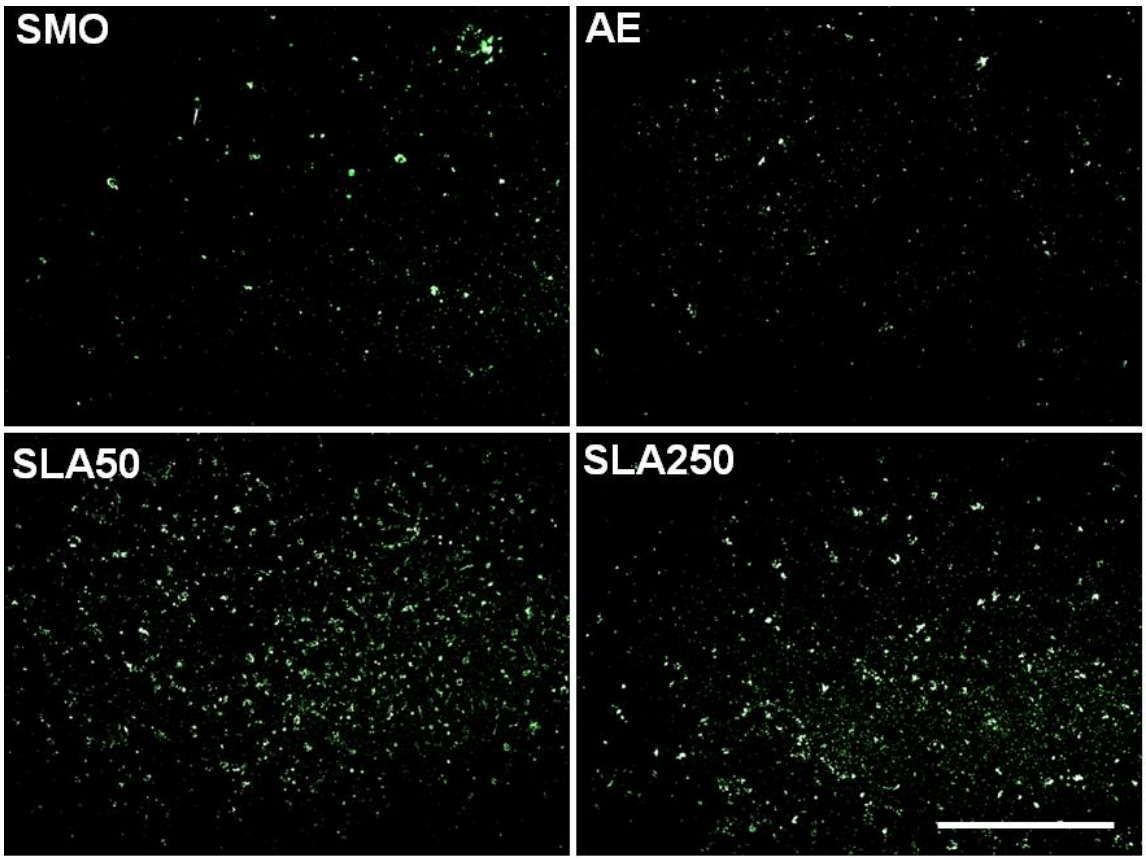

Figure 59 Hydroxyapatite fluorescent microscopy images showing nodules of hydroxyapatite (Green) on the substrate surface. Both SLA surfaces show the formation of widespread hydroxyapatite nodule formation. Scale bar = 800 µm.

In addition to assessing hydroxyapatite quantitatively via a fluorescent plate reader, the presence of nodules were also assessed qualitatively using fluorescent microscopy as shown in figure 60. Hydroxyapatite nodules were found in greater numbers on both SLA surfaces compared to SMO and AE, a greater amount of mineralised tissue was present on the SLA surfaces.

4.3. DISCUSSION

The performance of implants can be influenced by multiple factors, such as the mechanical properties of the material the implant is formed of (Simon et al., 2003) and the surface features of the implant (Sykaras et al., 2000, Shalabi et al., 2006). Orthopaedic materials, such as stainless steel and CoCrMo, which have the mechanical strength required to form orthopaedic devices, are combined with a low degree of bioactivity, resulting in an implant that is mechanically strong but has poor osseointegration ability (Stiehler et al., 2008). Whilst efforts are ongoing to create biomaterials with increased mechanical and bioactive properties, modification to the surface of existing implant materials is a viable option to improve the current generation of implants which lack bioactivity.

The performance of an implant can be improved by influencing the biological reactions that occur at the bone implant interface to produce a desirable response (Puleo and Nanci, 1999). This can be achieved by modifying the implant surface to manipulate and partially control cell behaviour (Logan and Brett, 2013). In regards to orthopaedic implants, a surface that stimulates osteogenic cells to form new bone tissue whilst preventing fibrous encapsulation is ideal. Methods of surface modification are varied and can range from topographical (Brett et al., 2004), surface chemistry (Khan et al., 2012), functionalisation (Aita et al., 2009a), coatings (Zhang et al., 2014) and nanotopographies (Dalby et al., 2008).

One of the most influential factors that can stimulate a desired response in bone cells is topographical modification. Implants can be topographically modified on the micron scale to produce, smooth, machined, acid etched and blasted surfaces (Balloni et al., 2009). In addition, substrates can be created with surface features on the nanoscale that are capable of directing stem cell fate, which can vary from grooves (Zhang et al., 2012), tubes (Oh et al., 2009), pores (Lavenus et al., 2012) and pillars (Sjöström et al., 2009). One of the most widely used and successful surface topographies for titanium dental implants, utilises features on both the micron and nanoscale. Referred to as sand blasted acid etched or SLA, the topography is produced by a 2-stage procedure of sandblasting the surface with Al_2O_3 grit particles, followed by hot acid etching using a combination of HCl and H_2SO_4. In both *in vitro* and *in vivo* studies, the SLA surface has been shown to promote an increased osteogenic reponse compared to smooth and machined

topographies (Cochran et al., 2011, Mendonca et al., 2010, Khan et al., 2012, Wall et al., 2009).

This section of the thesis investigated whether SLA could be replicated onto the orthopaedic alloy CoCrMo, in an effort to improve the bioactivity of the material. Laser profilometry was performed on all four substrates to gain a measure of surface roughness. Specifically, the arithmetic average roughness of the surface, referred to as R_a, was measured. For implants formed of titanium, it is thought moderately rough surfaces with an R_a between 1 – 2 µm can stimulate an increase osteogenesis, compared against smooth (R_a 0-0.5 µm), minimally rough (R_a 0.5-1 µm) and rough surfaces (R_a > 2 µm) (Wennerberg and Albrektsson, 2009). The SLA250 surface had an R_a of 1.02 ± 0.03 µm which fell within the moderately rough range, implying that it may be best suited at enhancing mineralisation compared to SMO, AE and SLA50, which were smooth and minimally rough, respectively. Whilst the review that concluded that moderately rough surfaces were preferable focused primarily on titanium (Wennerberg and Albrektsson, 2009), it is widely accepted that titanium and its alloys are the gold standard orthopaedic material (Geetha et al., 2009), and surface properties that are ideal on titanium should try to be applied to other materials of similar properties, such as CoCrMo.

Following laser profilometry testing, the wettability of each surface was assessed by measuring the contact angle of $_{dd}H_2O$. Interestingly, AE, SLA50 and SLA250 appeared to have a different response compared to SMO. Those samples that had undergone the acid etching process were evidently more hydrophilic than the SMO surface. AE had the lowest contact angle of the four, whilst both SLA50 and SLA250 showed an increase in contact angle that correlated to surface roughness. Conversely, SMO did not follow this trend, as it was the smoothest surface, yet was observed to be the most hydrophobic. Treatment of CoCrMo with NHO_3 has been reported to be a method of activating the surface of the material (Paredes et al., 2014). NHO_3 was shown to affect the wettability of CoCrMo causing the surface to become more hydrophilic, due to the removal of surface contaminants, such as hydrocarbons. It has been reported that the exposure of hydrocarbons to osteoblasts can reduce their activity in the form of lowering ALP expression and calcium mineralisation (Hayashi et al., 2014). This wettability data therefore indicates that acid etching may not only be advantageous by way of modifying the substrate topographically, but also chemically through cleansing of the surface.

In addition to laser profilometry, the surface topography of each substrate was studied using SEM. Low magnification images showed that both SMO and AE were similar in appearance without the presence of distinct surface features, but under increased magnification clear differences in the morphology of each surface became apparent. The presence of parallel grooves was evident on SMO (Figure 49), which has been previously reported on smooth titanium surfaces and is the result of mechanical polishing using silicon carbide paper (Le Guehennec et al., 2008, Singh, 2011). In comparison, grooves were also observed on AE, which was expected since AE also underwent silicon carbide polishing, but in addition, the presence of what appeared to be grain boundaries were observed. The surface morphology of SLA50 and SLA250 were clearly more roughened in comparison to SMO and AE. Whilst both SLA substrates had irregular rough morphologies, SLA250 appeared to have larger, more pronounced individual features which are likely due to the use of larger Al_2O_3 grit. A similar effect was reported on the morphologies of sandblasted titanium using small (100 µm) and large grit (300 µm), where the small grit surface still had roughened features, but had noticeably less verticality on its surface. (Hakki et al., 2012). Under high magnification the effect of the acid etching procedure was clear on SLA surfaces, as the formation of small pores was observed on top of the larger features created from the sandblasting step (Figure 49). Sandblasted acid etched surfaces have been reported as superior compared to sandblasted surfaces (Sader et al., 2005, Rosales-Leal et al., 2010, Le Guehennec et al., 2008). It may be that acid etching procedure facilitates in smoothening out any overly sharp peaks on the surface and in its place creates a network of nanopores. As native bone tissue has surface features that range from the macro (Osteoids), micro (Mineralised structures, 0.8 – 1.4 µm (Bozec et al., 2005)) and nanoscale (Collagen fibre bundles, 5 – 10 nm with 67 nm striation and hydroxyapatite crystals 225 nm (Bozec and Horton, 2006)), the combination of micron and nano features found on the SLA surfaces may be more suited to stimulating an enhanced osteogenic response in MSCs by replicating an *in vivo* environment.

Elemental analysis was performed on each surface and it was found that SMO and AE had an even distribution of Co, Cr and Mo across the entirety of the map (Figure 50). In contrast, gaps/holes were present on SLA maps for the alloying elements, which correlated with positive signalling for Al. This data confirmed the presence of residual aluminium on the surface of both SLA substrates, which has been reported on other engineered SLA surfaces, despite the implementation of cleaning steps (Durual et al.,

2011). SLA50 was shown to have a larger amount of aluminium compared to SLA250 although this was not significant ($p = 0.4748$). Interestingly, the distribution of aluminium on the surface of SLA50 and SLA250 was clearly different. As shown in figure 50, SLA50 appeared to have a larger amount of aluminium particles that were small in size but widely distributed over the entirety of the surface. In contrast, SLA250 had noticeably larger particles, but were in fewer numbers and as a consequence, had large portions of the surface that were not contaminated with aluminium. It has been reported that high concentrations of aluminium can negatively interfere with matrix mineralisation in osteoblasts (Canabarro et al., 2008, Hayashi et al., 2014), implying that the widespread residual aluminium found on SLA50 may not be ideal.

The cytotoxicity of each substrate was analysed using a live/dead kit after 24 hours in culture. All of the substrates were largely non-toxic as shown in figure 52, although of the four, SLA50 appeared to have a greatest amount of dead cells. An increase in the amount of apoptotic cells on SLA titanium surfaces compared against smooth has been previously reported (Wall et al., 2009), implying that there may be a topographical property of the SLA surface that can trigger a degree of apoptosis in some human MSCs.

As well as cytocompatibility, the ability of a biomaterial to promote cellular proliferation is an important factor in regards to implant performance. In GM, AE promoted an accelerated rate of proliferation compared to the other three substrates (Figure 52 A), which has also been reported using the osteoblast like MG63 cell line (Rosales-Leal et al., 2010). AE was shown to be the most hydrophilic substrate which may have been a contributing factor to this observation, as hydrophilic surfaces have been reported to stimulate superior rates of proliferation compared to their identical hydrophobic counterparts (Att et al., 2009, Aita et al., 2009a). SLA50 appeared to slow down and inhibit proliferation in GM. This may be a result of the widespread residual aluminium which can reduce osteoblast proliferation (Sader et al., 2005) or an effect of the SLA topography (Khan et al., 2012). Interestingly, SLA250 did not inhibit proliferation in GM despite having a similar amount of aluminium residue (Table 3). SLA250 stimulated a consistent rate of proliferation and obtained the largest amount of cells by day 21, which may be due to the increased surface area of the substrate. It is likely that the difference in the distribution of aluminium between the two SLA substrates is the cause of the variation in proliferative ability. Proliferation was low in cells on all surfaces cultured in OM, which is similar to previous publications (Khan et al., 2012). It is believed that cells focus on differentiating into osteoblasts when exposed to OM, and as a consequence they

do not proliferate to the same extent observed in GM. Interestingly, after 24 hours in OM and GM, a lower amount of cells was present on both SLA surfaces compared to SMO and AE although this recovered by day 4 (Figure 53 B).

Cell attachment was studied after 24 hours in GM with the data shown in figure 54. Both SMO and AE appeared to promote a higher rate of attachment compared to the SLA surfaces. In addition, SLA250 was found to have more attached cells than SLA50. When combining this data with the cytotoxicity and proliferation data, where lower cell numbers were observed at 24 hours on SLA, it is likely that the lower number of cells found on SLA250 and specifically SLA50 are due to a relatively mild cytotoxic effect from the SLA surface, which has also been observed on roughened titanium (Wall et al., 2009). The higher number of dead cells observed in figure 52 supports this data.

How strongly adhered the cell populations were to the substrate surface was analysed using a mechanical dissociation protocol. It was found that both AE and SLA250 had significantly more remaining cells compared to SMO and SLA50 (Figure 56). Increased hydrophilicity has been shown to enhance actin and vinculin formation in osteoblasts (Yamada et al., 2010), which implies that the increased wettability found on the AE may have contributed to its superior performance. The expression of these proteins were studied in MSCs on all substrates and it was found that more robust actin fibres and increased focal adhesion formation were present on AE (Figure 57). In contrast, SLA50 appeared to have no clear actin fibre development and the presence of focal adhesion complexes could not be easily observed, implying that the surface was inhibiting factors important to cell adhesion (Humphries et al., 2007). This was evident in the cell retention study where significantly fewer cells were found on SLA50 compared to AE and SLA250. In contrast to SLA50, SMO appeared to have adequate actin and vinculin expression in MSCs located on its surface. The poor performance of SMO in the retention study could be a result of the combination of the extremely low roughness profile and hydrophobicity of the surface (Yamada et al., 2010). In addition to wettability, cell adhesion has been reported to be increased on roughened sand blasted titanium (Rosales-Leal et al., 2010). This would therefore imply that the blasted acid etched topography formed on SLA250 may be suitable at improving cellular adhesion in MSCs. Whilst SLA50 was also a roughened surface, the aluminium contamination found throughout the substrate surface may have contributed to its poor adhesive properties (Canabarro et al., 2008, Hayashi et al., 2014). The external morphology of the MSCs was also assessed using SEM and it was found that MSCs on both AE and SLA250 had more pronounced

cellular extensions in the form of filopodia (Figure 55). Filopodia are thin membrane extensions comprised of bundles of cross linked actin fibres and can be described as the pioneers of the leading edge of the cells which act as probes to test the environment for cues (Wood and Martin, 2002). In keratinocytes it has been shown that there is a dependence on filopodia for the formation of lamellipodia adhesion sites. In filopodia complexes small adhesions which stained positive for adhesion markers were present (Schäfer et al., 2009). Whilst there is little data focusing on the adhesive properties of filopodia in MSCs, it is possible that they play some supportive role in the adhesive process.

One of the most important factors for implant performance is the ability of the implant surface to facilitate in the osteogenic differentiation of MSCs. Following implantation, MSCs are believed to be the first cells recruited to such sites were they colonise and differentiate into osteoblasts capable of forming new bone tissue (Davies, 1998, Davies, 2003). If an implant can be modified to enhance this process it should result in an improved rate of osseointegration and ultimately a more stable device (Le Guehennec et al., 2007). It was found that both SLA surfaces stimulated a higher rate of differentiation in MSCs compared to SMO and AE, through the deposition of calcium (Figure 58 B) and hydroxyapatite nodule formation (Figure 59 C). Whilst the amount of hydroxyapatite was similar on both SLA surfaces, SLA250 had the greatest amount of mineralisation (Figure 59). It has been reported that high amounts of aluminium residue inhibits matrix mineralisation in osteoblasts (Canabarro et al., 2008, Hayashi et al., 2014), although this was not observed in this study. ALP is recognised as an early marker for the differentiation process (Golub and Boesze-Battaglia, 2007), although no difference was observed in ALP activity between the four substrates (Figure 59 A).

The results of this section of the thesis are an early indication that modification of CoCrMo by way of sand blasting and acid etching with 250 µm Al_2O_3 grit, may prove to be advantageous for orthopaedic implants by improving markers of proliferation, adhesion and differentiation in human MSCs. The combination of surface features on both the micro and nanoscale are a possible reason behind the improved performance of the SLA250 surface (Mendonca et al., 2010), as CoCrMo substrates with either nano or micro scale features have been shown to be superior compared to conventional CoCrMo (Webster and Ejiofor, 2004, Jaeger et al., 2008). Topographical modification is highly sensitive. In a study that looked at CoCrMo porous bead coated implants that had been acid etched, it was found that there was no significant improvement over controls in a

canine model (Jakobsen et al., 2010). This high degree of sensitivity was observed in the present study where only a slight alteration in surface roughness of 0.2 µm R_a was recorded between SLA50 and SLA250, although this resulted in significant changes in how the MSCs responded to the substrates. It is likely that the increased surface roughness found on SLA250, combined with the reduced aluminium residue contamination resulted in its improved performance compared to SLA50 (Wennerberg and Albrektsson, 2009, Sader et al., 2005, Canabarro et al., 2008, Hayashi et al., 2014).

4.4. CONCLUSION

This section of the thesis focused on assessing the response of human MSCs to four surface topographies engineered on CoCrMo. The results indicate that SLA250 promoted increased bioactivity as determined by the enhanced expression in markers of proliferation, adhesion and mineralisation in human MSCs, despite the presence of low levels of aluminium residue. The application of this surface topography onto implants formed of CoCrMo may prove to be advantageous by enhancing bone formation, which could result in reduced healing times and increased implant stability.

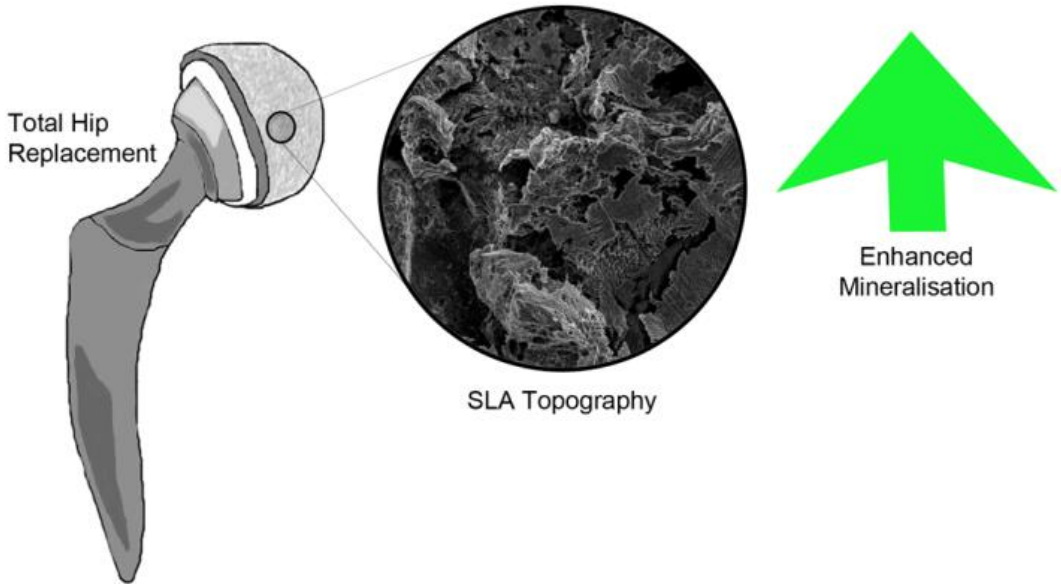

Figure 60 Graphical conclusion - chapter four.

CHAPTER FIVE:

TIO_2 COATED SLA COBALT CHROMIUM MOLYBDENUM: AN *IN VITRO* CELL STUDY

5. INTRODUCTION

It has been shown that the bioactivity of CoCrMo can be improved by coating the substrate with anatase TiO_2 by way of atmospheric pressure CVD or by topographically modifying the surface using a sandblasting acid etching technique (Logan et al., 2015). A combination of the two techniques may prove to be an even more beneficial method of improving the bioactivity of the material.

This part of the project aimed to investigate if the application of a TiO_2 coating by CVD onto SLA250 topographically modified CoCrMo could stimulate an enhanced osteogenic response in human MSCs compared to SLA250 CoCrMo. In addition to studying these two surfaces, a third SLA substrate formed of pure titanium was created to replicate the SLA surface widely used on titanium implants by Institut Straumann AG (Walderberg, Switzerland).

Cellular markers of proliferation, viability, morphology, adhesion and osteogenic differentiation were studied. Characterisation of the substrates included wettability, roughness, morphology, elemental analysis and Raman spectroscopy.

The hypothesis explored in this chapter is:

1. The addition of an anatase TiO_2 layer created by CVD onto the surface of SLA250 CoCrMo, would generate increased osteogenic differentiation in human MSCs to a comparable level as that observed on the titanium SLA control surface.

5.1. MATERIALS AND METHODS

5.1.1. SAMPLE PREPARATION

CoCrMo discs (Cr 26-30, Mo 5-7) supplied by Corin Ltd (Cirencester, UK) were engineered to achieve the SLA250 topography as previously described in section 4.1.1 SAMPLE PREPARATION – (Page 122). These discs were referred to as CoCrMo. CoCrMo discs were then coated in TiO_2 as described below in section 5.1.2 CHEMICAL VAPOUR DEPOSITION – (Page 154) and referred to as CCMT. Before the CVD protocol was finalised, a preliminary test which assessed the effect of chamber position on the thickness/phase of the TiO_2 coating was performed using Raman spectroscopy with the results shown in section 7 Appendix A – TiO2 Coating Chamber Position Testing (Page 210). Discs formed of SLA titanium were used as a control and referred to as Ti. Firstly, Ti discs were ground using SiC paper decreasing in roughness from #220, #500 to #1000. Following this, discs were removed from their resin bases and sonicated in isopropanol for 15 minutes at 30°C, followed by $_{dd}$H2O for 10 minutes at RT. Ti discs were then mounted on a block and underwent sand blasting using 250 μm Al_2O_3 grit (Renfert, Cobra, 15851005), at a distance of approximately 5 centimetres, at a pressure of 72.5 Psi (Vaniman, Sandstorm 2, 80301). Ti discs were then removed from the mount and subsequently sonicated in isopropanol for 15 minutes at 30°C, followed by $_{dd}$H2O for 10 minutes at RT. Once the discs had air dried they were etched in a combination of HCl 7.4% and H_2SO_4 76% for 8 minutes at 100°C. Lastly, the Ti samples were rinsed under H_2O before being sonicated in isopropanol for 15 minutes at 30°C, followed by $_{dd}H_2O$ for 10 minutes. Before being used for cell culture experiments all samples were sterilised and passivated as described in section 2.1.2 SAMPLE PASSIVATION AND STERILISATION – (Page 59).

5.1.2. CHEMICAL VAPOUR DEPOSITION

***Performed by Carlos Sotelo-Vasquez, Department of Chemistry, UCL.**

The substrate CoCrMo discs were placed on top of the graphite block with separating glass sheet to avoid carbon contamination from the graphite block. Titanium tetrachloride (99%) and ethyl acetate (99.8%), both from Sigma-Aldrich, were used as metal and oxygen sources, respectively. All the components of the CVD apparatus were kept at

high temperature (200 ºC). The precursors were heated independently in stainless steel bubblers and carried under controlled flows using pre-heated nitrogen gas (Supplied by BOC). The precursors were mixed in a stainless steel chamber (250 ºC) before accessing the CVD reactor and then plain nitrogen flow dragged the gas precursor mixture through a triple baffel manifold to generate a wide laminar flow. The deposition of TiO_2 was controlled by heating up the stainless steel bubblers of titanium tetrachloride and ethyl acetate to 70 °C and 40 °C, respectively. The mass flow conditions for metal and oxygen precursors were 6.7×10^{-3} and 3.1×10^{-3} g min^{-1}, respectively. The deposition time used to coat the CoCrMo discs was 30 seconds, whilst the reaction chamber was at a temperature of 500 ºC. This deposition time was found optimum in order to achieved discs coated with a uniform TiO_2 layer without compromising the morphology of the discs. All coated discs were chemical stable in air. The coated materials showed no pin-hole defects and no particulates were observed in the exhaust gas.

5.1.3. CELL CULTURE

Human MSCs were prepared and cultured as previously described in section 2.1.6 CELL CULTURE – (Page 63).

5.1.4. SUBSTRATE CHARACTERISATION

The wettability of CoCrMo, CCMT and Ti was assessed by water contact angle as previously described in section 2.1.4 SUBSTRATE CHARACTERISATION – (Page 61). Further, the roughness of each substrate was analysed by laser profilometry as previously described in section 2.1.4 SUBSTRATE CHARACTERISATION – (Page 61). SEM and EDX were also performed on CoCrMo and CCMT to assess the coverage of the TiO_2 layer on the substrate surface. This microscopy analysis was performed as previously stated in section 4.1.3 SUBSTRATE CHARACTERISATION – (Page 123). In addition, SEM was performed on engineered Ti created in the laboratory and SLA discs obtained from Institut Straumann AG (Walderberg, Switzerland) to compare the morphology of each surface with the results shown in section 7 APPENDIX B – TI SLA MORPHOLOGY – (Page 213). Raman spectroscopy was used to assess the phase of the

TiO_2 layer on CoCrMo using a LabRam Micro-Raman Spectrometer (Horiba Jobin-Yvon HR300) fitted with an optical microscope and 50x objective lens for a total magnification of 500x. Excitation of the Raman signal was achieved using a 632.8 nm helium/neon ion laser. The spectral array comprised of a 4 x 4 grid with an accumulation number of 16. This improved the quality of the spectra by allowing an average of the signals and by mapping multiple locations.

5.1.5. VIABILITY

Human MSCs were seeded in GM at a density of 3.3 x 10^4 cells per well on CoCrMo, CCMT and Ti using a 24 well plate (n = 3). They were incubated at standard culture conditions of 37°C, 5% CO_2 in a humidified atmosphere. After 24 hours in culture, cells were taken for LIVE/DEAD imaging analysis as previously described in section 4.1.4 VIABILITY – (Page 124).

5.1.6. PROLIFERATION

MSCs from three donors (N = 3) were seeded on CoCrMo, CCMT and Ti at a density of 2 x 10^3 cells per well (n = 3). A separate 24 well plate was used for GM and OM. Cells were then incubated at standard culture conditions and proliferation was studied as previously described in section 2.1.7 PROLIFEATION – (Page 65).

5.1.7. RETENTION

Human MSCs from three donors (N = 3) were seeded in GM at a density of 3.5 x 104 cells per well on CoCrMo, CCMT and Ti using a 24 well plate (n = 3). Following 24 hours incubation at standard culture conditions, cell retention was assessed as previously described in section 3.1.7 RETENTION – (Page 98).

5.1.8. CELL MORPHOLOGY – INTERNAL

A total of 7 x 103 cells were seeded on CoCrMo, CCMT and Ti in OM using a 24 well plate (n = 3). Following 24 hours incubation at standard culture conditions of 37°C, 5% CO_2 in a humidified atmosphere, MSCs were assessed by fluorescent microscopy for expression of f-actin as previously described in section 2.1.8 CELL MORPHOLOGY – INTERNAL – (Page 66), although the nucleic stain DAPI was used in place of PI. In addition, the adhesion protein vinculin was also studied as previously described in section 3.1.9 CELL MORPHOLOGY – INTERNAL – (Page 99).

5.1.9. TYPE I COLLAGEN DEPOSITION

MSCs were seeded at 5 x 10^4 cells per well on CoCrMo, CCMT & Ti in OM using a 24 well plate (n = 3). Following 17 days in culture at standard conditions of 37°C, 5% CO2 in a humid atmosphere, MSCs were taken for type I collagen analysis using fluorescent microscopy as previously described in section 2.1.12 TYPE I COLLAGEN DEPOSITION – (Page 69), although image quantitation was not performed.

5.1.10. OSTEOGENIC MARKERS

A total of 12.5 x 10^3 cells from three donors (N = 3) were seeded on CoCrMo, CCMT and Ti in OM using a 24 well plate (n = 3). After 21 days in osteogenic culture, MSCs were harvested to analyse the osteogenic markers of calcium ion content and hydroxyapatite nodule formation as previously described in section 2.1.9 CALCIUM ASSAY – (Page 647 and 3.2.10 MINERALISATION – (Page 100), respectively.

5.1.11. STATISTICAL ANALYSIS

Human MSCs from three donors (N = 3) were used in triplicate (n = 3). Contact angle analysis was performed at n = 12 and profilometry scans were completed at n = 6. Statistical analysis was primarily carried out using a one-way ANOVA followed by the Bonferroni post-test in GraphPad Prism software (v5.04) with $p < 0.05$ deemed to be statistically significant. A post-hoc power calculator was used to confirm the statistical power of significant results observed in the study

5.2. RESULTS

5.2.1. CONTACT ANGLE

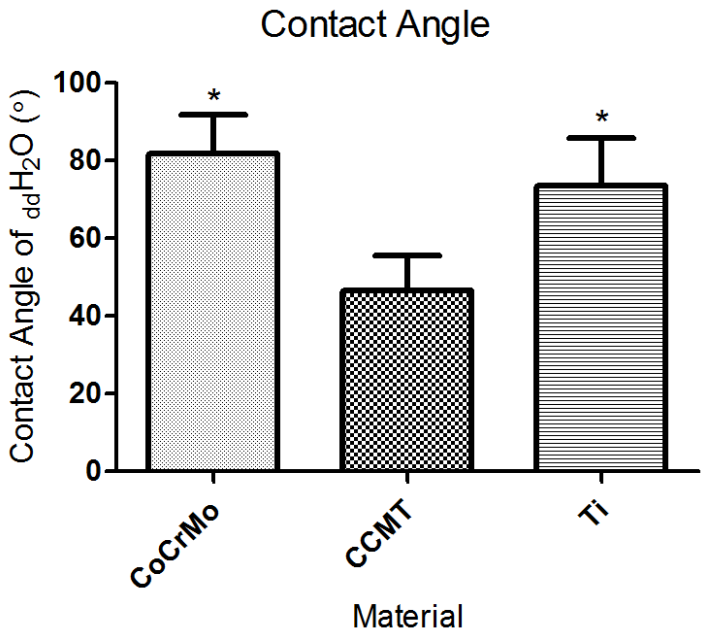

Figure 61 Wettability data showing contact angle of ddH2O on each substrate. CCMT appeared to be the most hydrophilic of the three. Each bar represents the mean ± 1 SD, n = 12. * = $p < 0.05$ substrate verses CCMT.

It was found that CCMT had the lowest contact angle of the three substrates (46.42 ± 9.12°). Both CoCrMo (81.78 ± 10.05°) and Ti (73.64 ± 12.16°) were significantly more hydrophobic compared to CCMT ($p < 0.05$).

5.2.2. ROUGHNESS

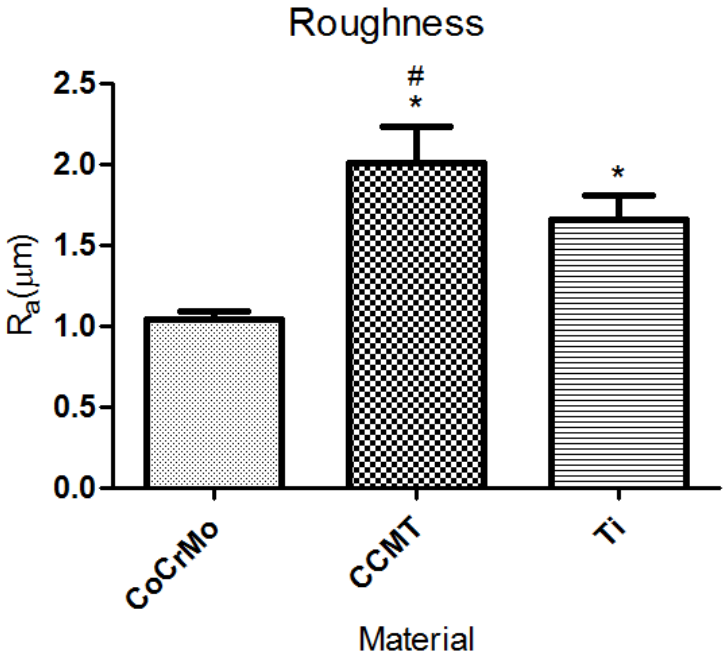

Figure 62 Laser profilometry data showing surface roughness on each substrate in the form of Ra. CCMT was found to have the greatest Ra value of the three whilst CoCrMo had the lowest. Each bar represents the mean ± 1 SD, n = 6. * = $p < 0.05$ substrate verses CoCrMo. # = $p < 0.05$ substrate verses Ti.

Of the three substrates CCMT (2.01 ± 0.27 µm) had the greatest R_a value which was significantly larger than both CoCrMo (1.04 ± 0.05 µm) and Ti (1.66 ± 0.15 µm) ($p < 0.05$). It was also found that Ti was significantly rougher compared to CoCrMo ($p < 0.05$).

5.2.3. SEM – EDX

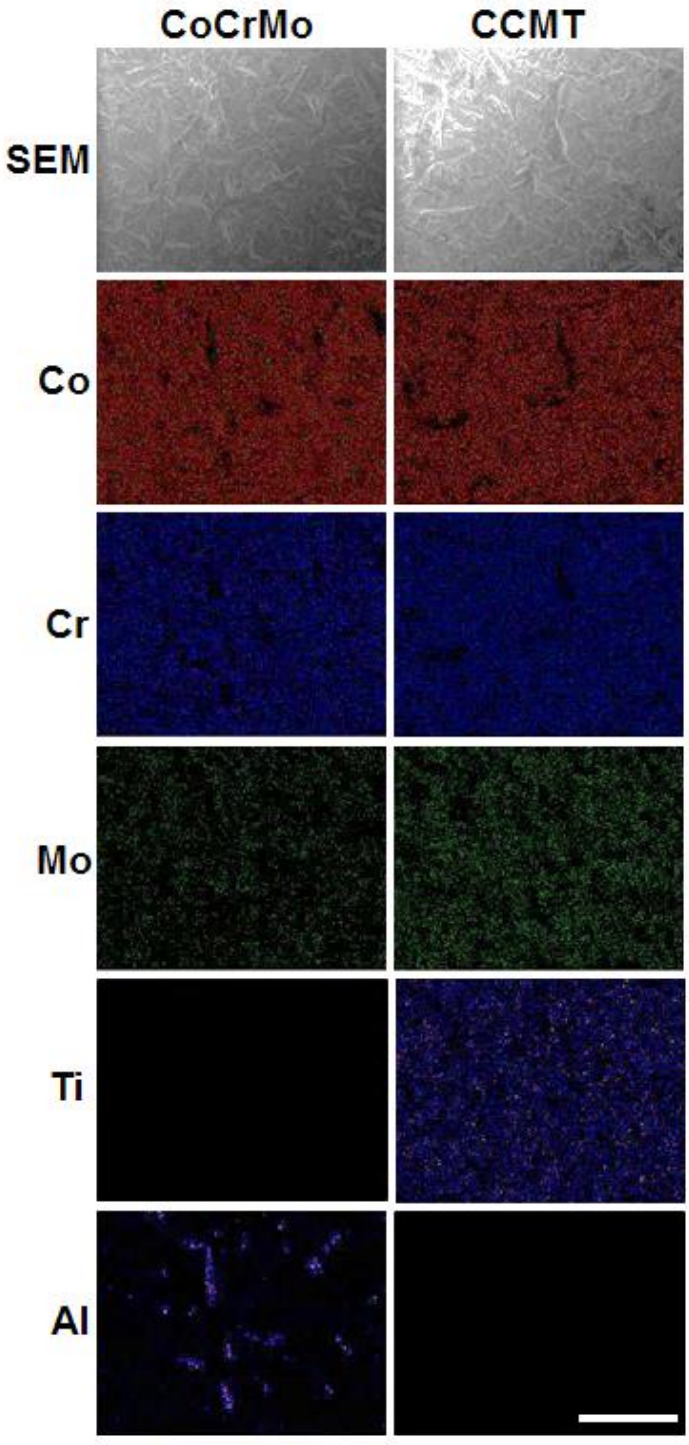

Figure 63 Low magnification SEM and elemental maps showing the presence of a titanium layer on CCMT. Scale bar = 100 μm.

SEM combined with EDX was used to assess the morphology of each surface as well as the elemental composition. Each surface was irregular and roughened although no

obvious difference could be observed between the surface features found on CoCrMo and CCMT despite the different R_a values obtained in profilometry scans. Both of the substrates showed abundant Co, Cr and Mo although CCMT also showed comprehensive coverage of Ti on the materials surface. Interestingly Al residue was observed on CoCrMo although not found on CCMT.

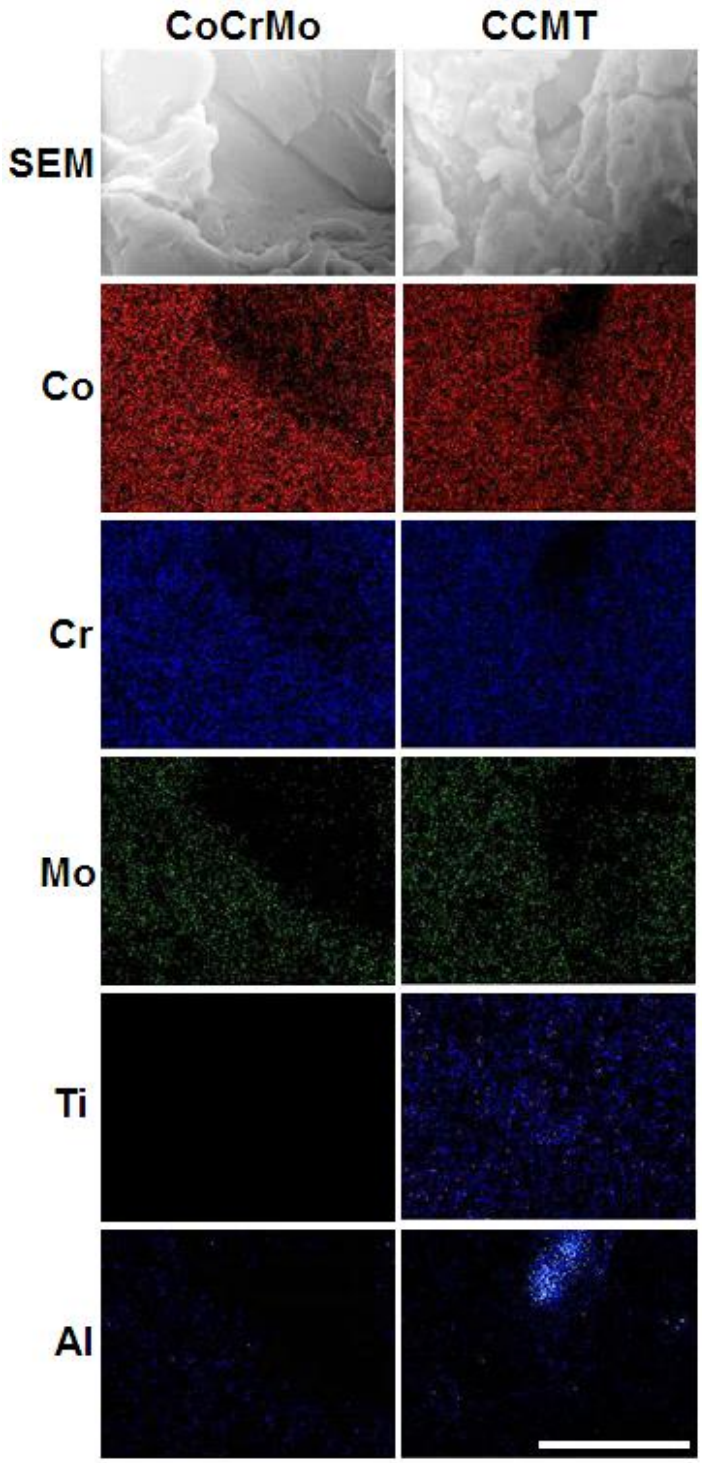

Figure 64 High magnification SEM and elemental maps of CoCrMo and CCMT. The presence of titanium is still found on CCMT although both substrates show some aluminium residue. Scale bar = 7 μm.

Under higher magnification CCMT did appear to have a somewhat rougher surface and Co, Cr and Mo were again widely expressed on each substrate. As with the low magnification images in figure 64, Ti was again found over the entirety of the scan. In

contrast to the low magnification images Al was found on the surface of CCMT under higher magnification (Figure 65).

5.2.4. RAMAN SPECTROSCOPY

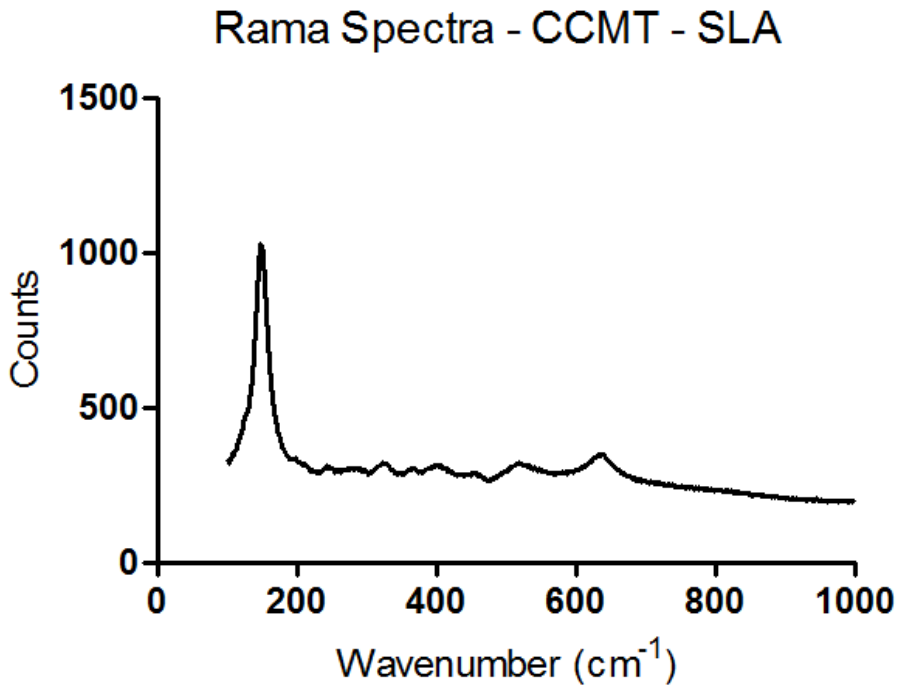

Figure 65 Raman spectra of CCMT showing predominantly anatase TiO_2.

Raman spectroscopy was used to confirm the presence of TiO_2 on the surface of CCMT. Peaks at 198, 394, 514 and 634, which correlate to the anatase phase of TiO_2 (Turkovic et al., 1991) were observed although additional peaks were also present. These additional peaks appeared to correlate with the uncoated CoCrMo control sample and possibly the rutile phase of TiO_2. The CoCrMo control spectra can be found in section 7 APPENDIX A – TIO2 CHAMBER POSITION TESTING – (Page 210).

5.2.5. VIABILITY

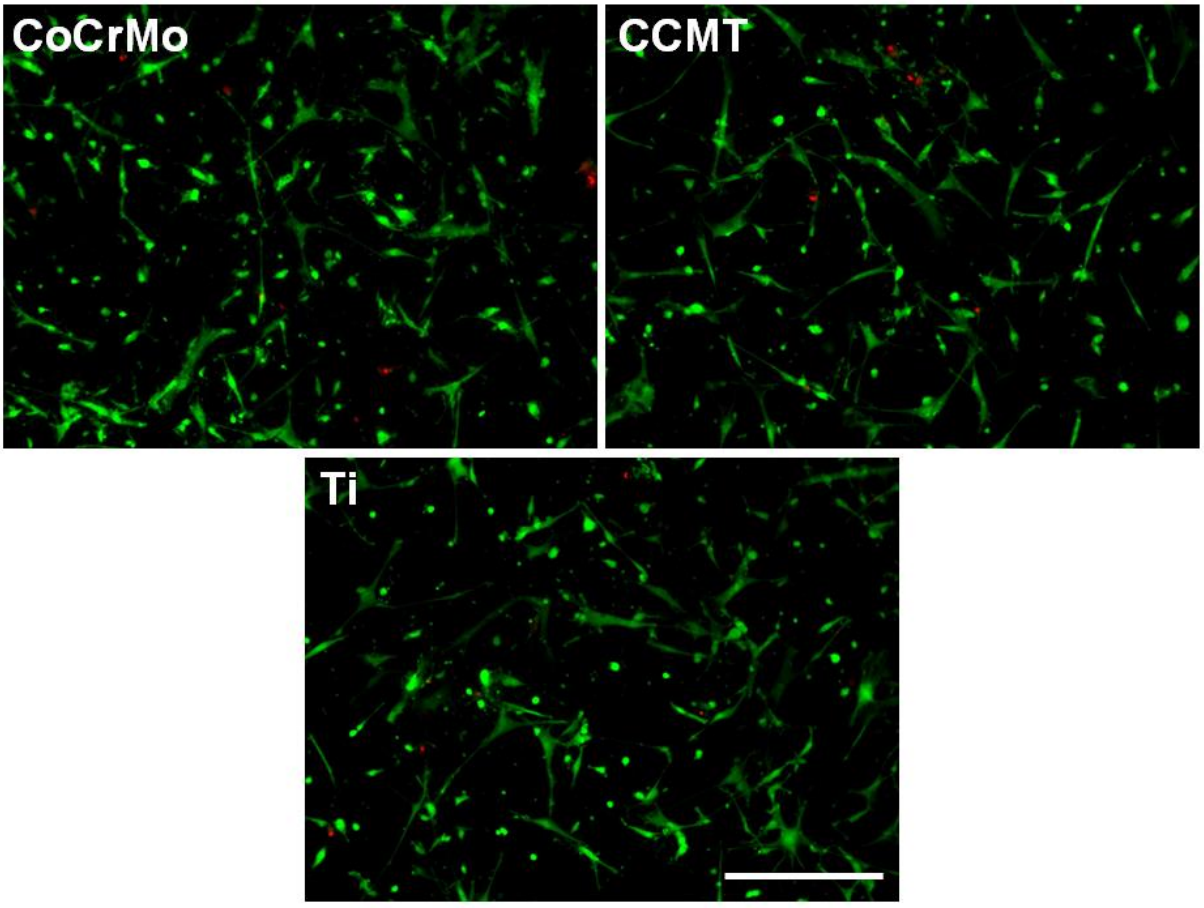

Figure 66 Live/dead fluorescent images showing cell viability on each substrate. Green shows live cells stained with calcein AM, whilst red shows dead cells that have a compromised cellular membrane. Scale bar = 100 µm.

Live/dead fluorescent staining was used to gain a measure of the toxicity of each substrate with results shown in figure 67. It was found that each substrate promoted an acceptable level of cytocompatibility as the majority of cells expressed the live green component of the kit. A small portion of dead cells that expressed the red component were found on each substrate although this was to be expected for SLA topographies.

5.2.6. PROLIFERATION

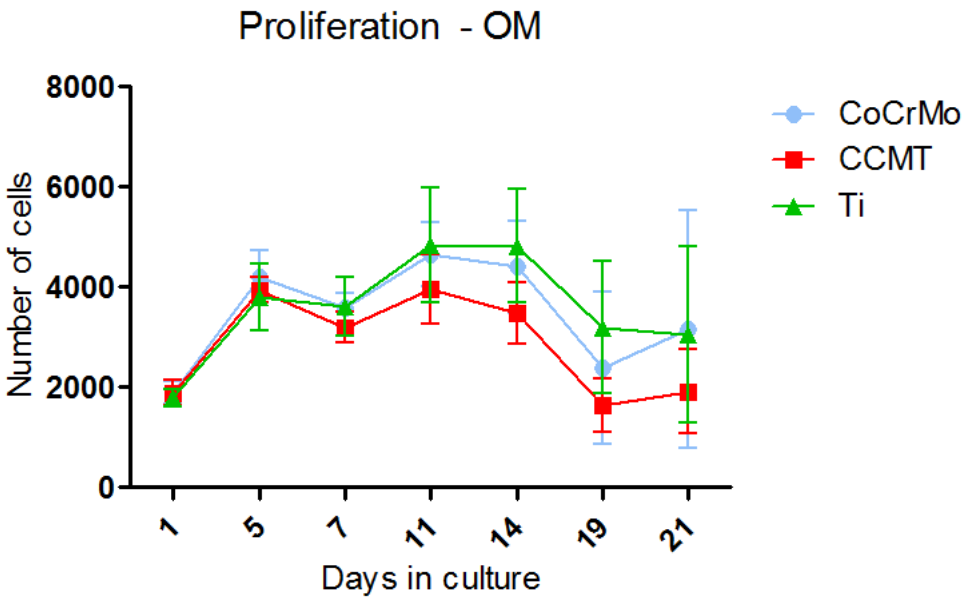

Figure 67 Proliferation data. Each point represents the mean ±1 SD, N = 3, n = 3.

The proliferation in OM was assessed using AlamarBlue and no clear difference was observed between the three substrates. Cell numbers appeared to be lower on CCMT compared to CoCrMo and Ti from day 11 onwards.

5.2.7. RETENTION

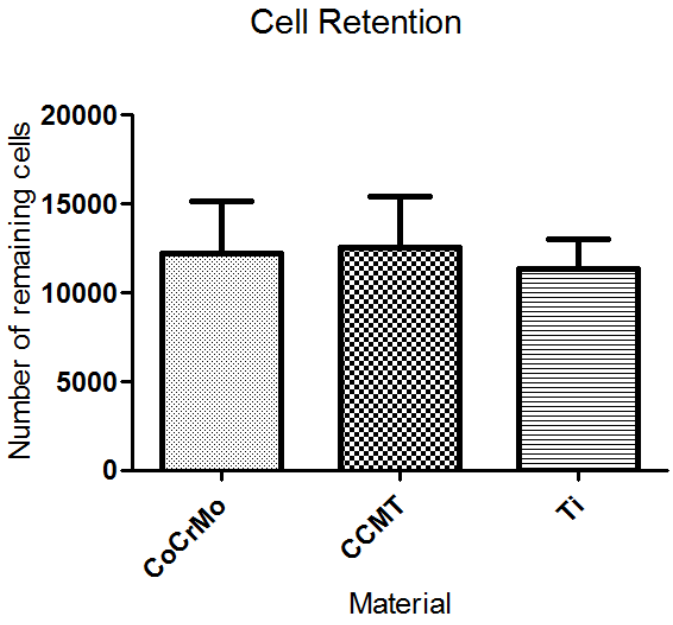

Figure 68 Cell retention data showing the remaining cell populations found on each substrate after three mechanical washes. No difference was observed between the three materials. Each bar represents the mean ± 1 SD, N = 3, n = 3.

The adhesion of MSCs to each substrate was studied by counting the remaining cells after 24 hours incubation and three mechanical washes. No significant difference was observed between CoCrMo (12208 ± 2912), CCMT (12533 ± 2870) and Ti (11316 ± 1716) as shown in figure 69.

5.2.8. CELL MORPHOLOGY – INTERNAL

5.2.8.1. ACTIN

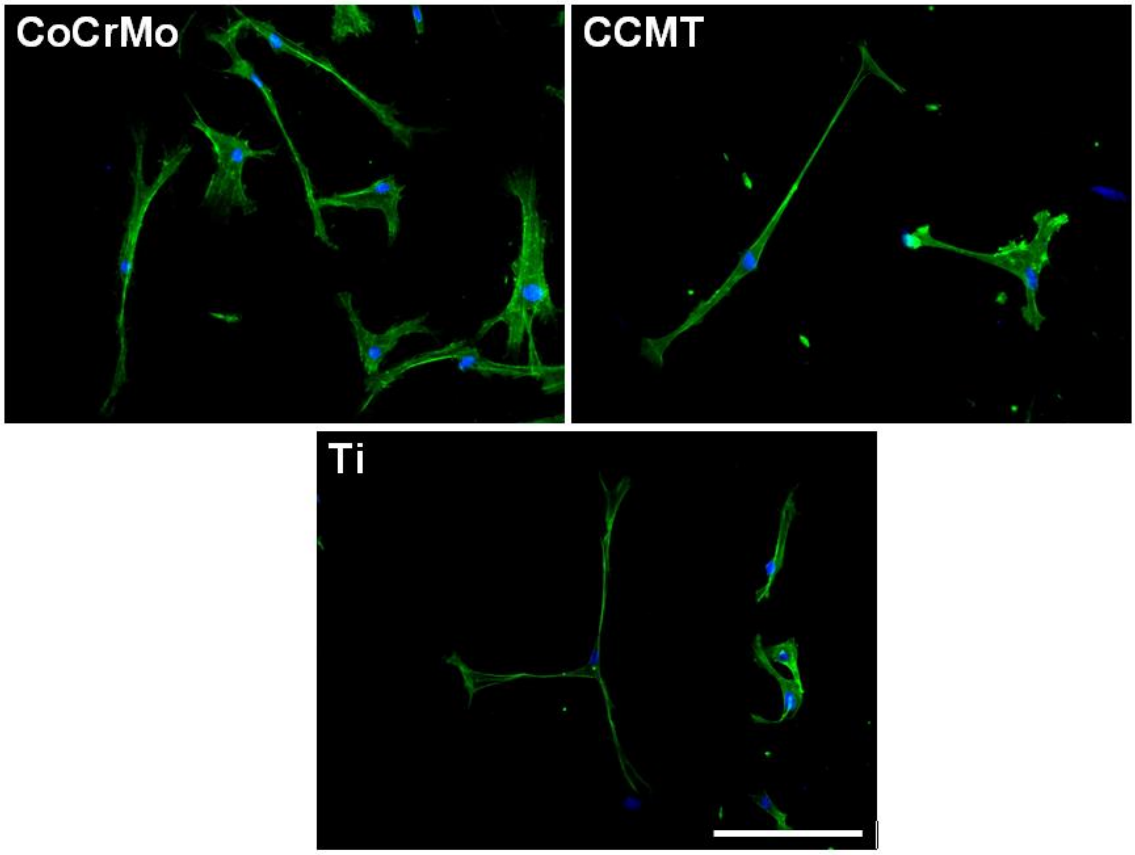

Figure 69 Fluorescent microscopy images showing the cytoskeletal protein f-actin in MSCs on each substrate. Green - f-actin. Blue – nucleic stain DAPI. Scale bar = 100 µm.

The cytoskeletal structure of MSCs on each substrate was analysed after 24 hours culture in OM with images shown in figure 70. The morphology of MSCs on each surface was similar, although it was clear that cells with different cytoskeletal structures were present on each surface. MSCs were either small in size and partly spread, or in contrast, highly elongated and narrow. It's likely that the roughened features of each surface are the cause of these differences in cell morphology. Narrow and elongated MSCs are likely being extended across peaks on the surface, whilst the smaller more spread cells may be located in the pits between peaks which would facilitate cell spreading.

5.2.8.2. VINCULIN

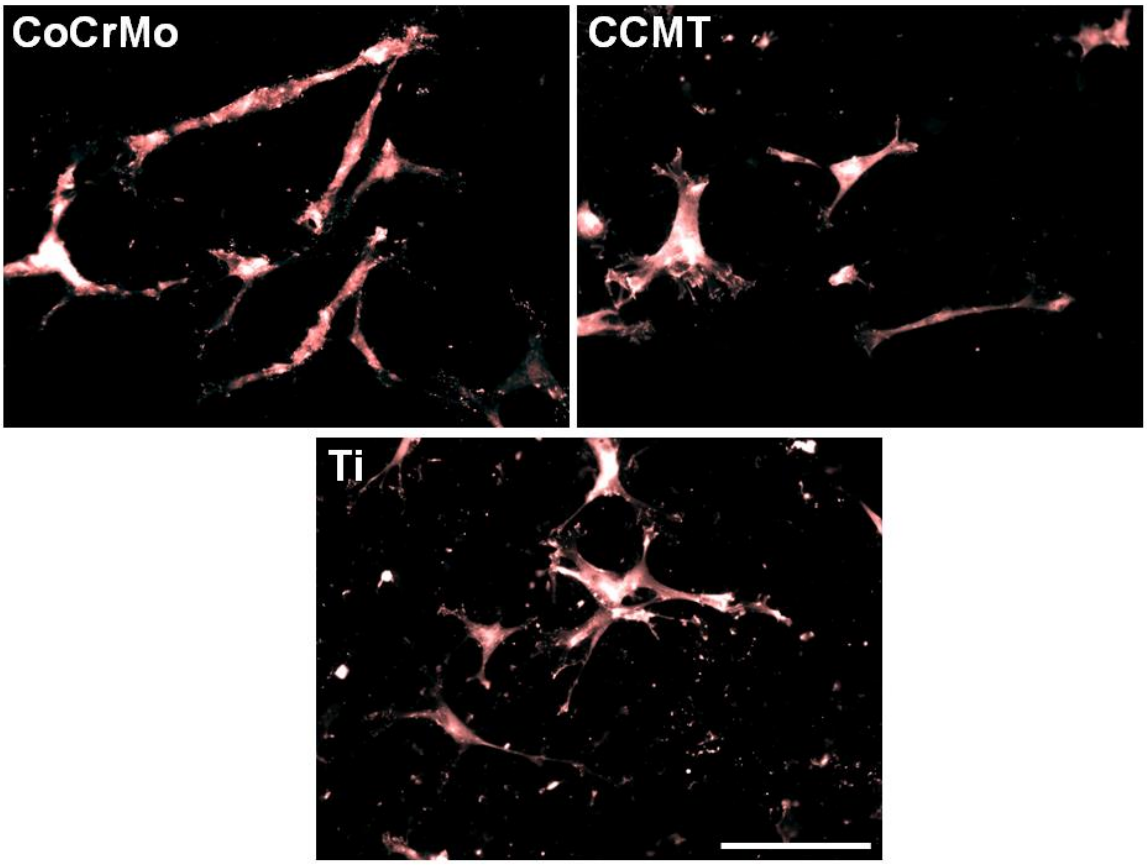

Figure 70 Fluorescent microscopy images showing the expression of the adhesion protein vinculin in MSCs on each substrate. Red - vinculin. Scale bar = 100 μm.

The adhesion protein vinculin was assessed using fluorescent microscopy after 24 hours culture in OM. As shown in figure 71, vinculin was expressed in MSCs on all three substrates although no clear difference between the surfaces was evident. This correlates with the retention data shown in section 5.2.7 RETENTION – (Page 166) which showed no significant difference in MSC adhesion between the substrates.

5.2.9. TYPE I COLLAGEN DEPOSITION

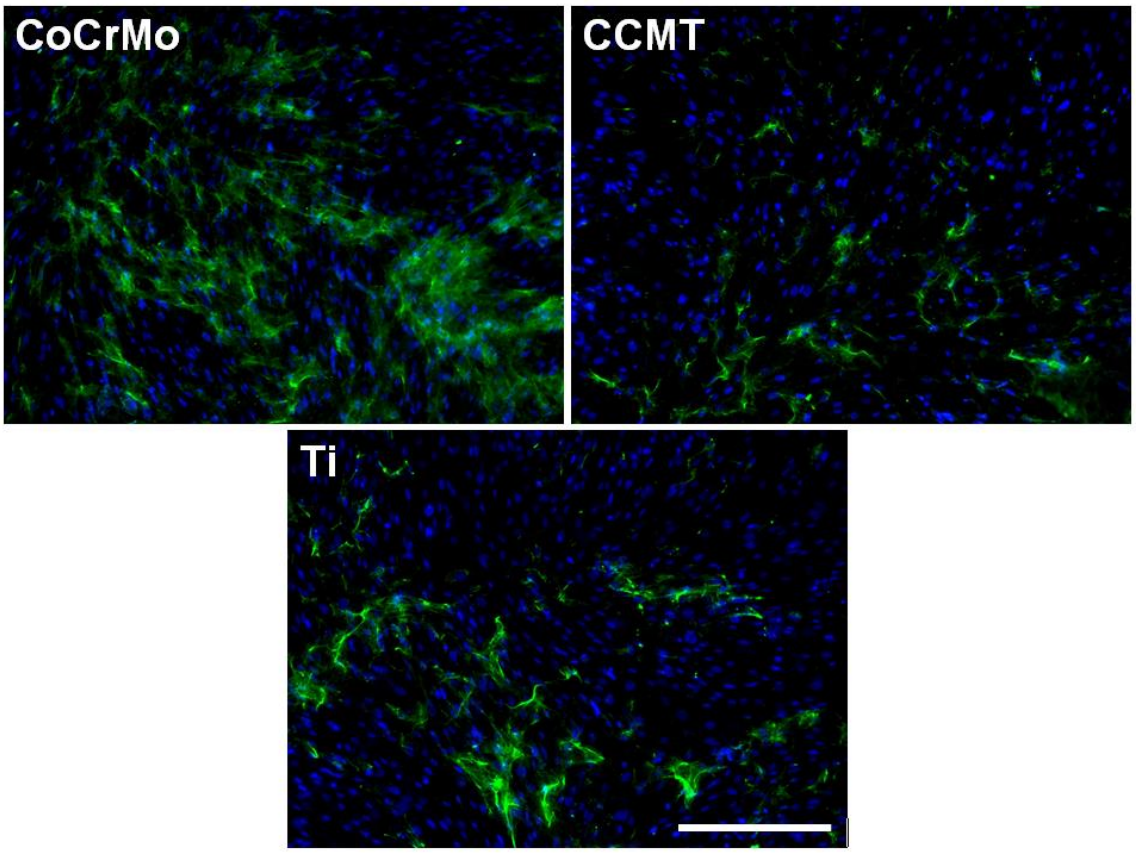

Figure 71 Fluorescent microscopy images showing type I collagen deposition on each substrate. CoCrMo appeared to show a greater amount of collagen deposition compared to CCMT and Ti. Green - type I collagen, blue - nucleic stain DAPI. Scale bar = 200 µm.

As MSCs differentiate into osteoblasts they deposit an ECM rich in mineral and collagen. Type I collagen plays an important role in bone formation as it acts as a scaffold for calcium nucleation sites (Davies, 1998). The deposition of type I collagen was assessed using fluorescent microscopy and it was observed that CoCrMo had a greater amount of collagen bundles/fibrils compared to Ti and CCMT (Figure 72). Type I collagen was observed on CCMT and Ti although to a lesser extent than that seen on CoCrMo.

5.2.10. OSTEOGENIC MARKERS

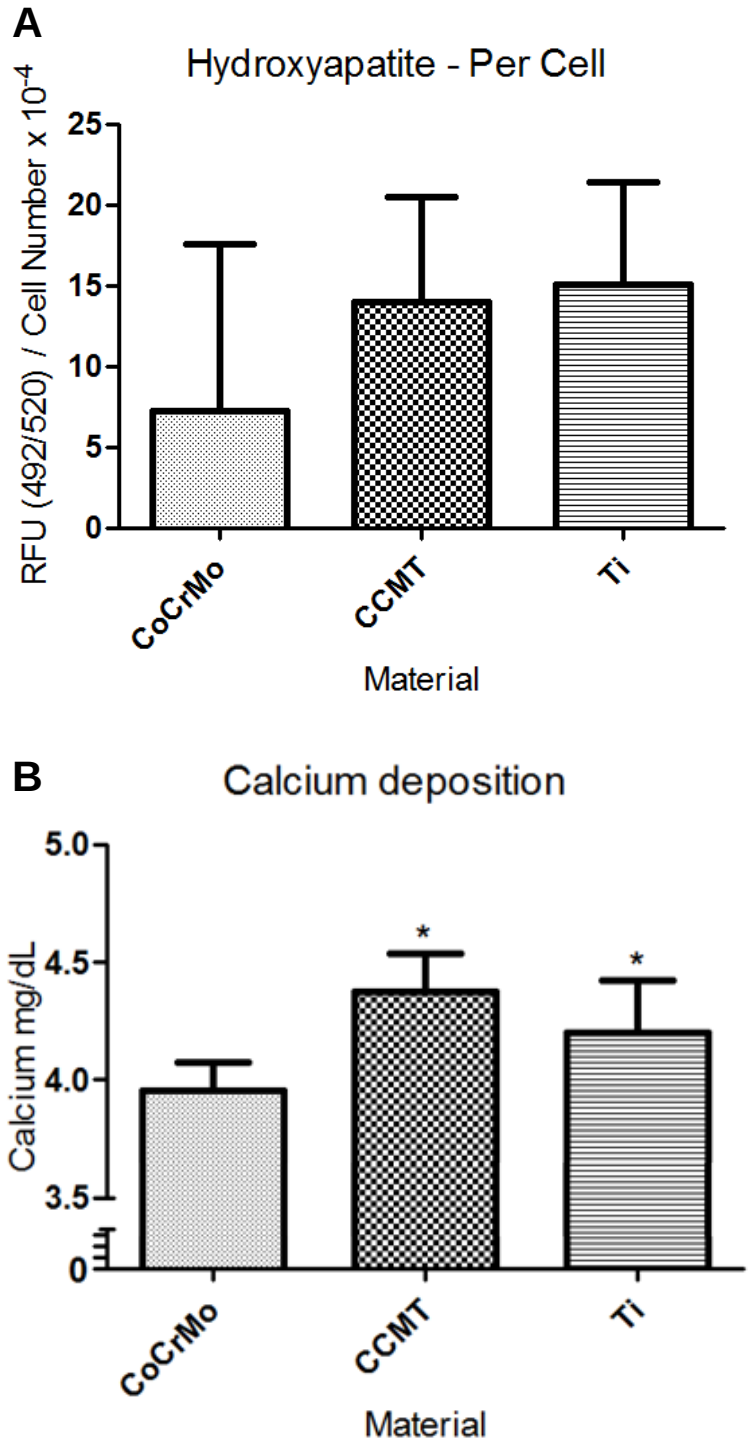

Figure 72 A- Hydroxyapatite formation. B - Calcium deposition. Each bar represents the mean ± 1 SD, N = 3, n = 3. * $p < 0.05$ substrate verses CoCrMo.

Late markers of osteogenic differentiation were studied in the form of hydroxyapatite formation and calcium content with the results shown in figure 73. Both osteogenic markers showed that CCMT and Ti had significantly greater amounts of mineralisation

occurring, with this change deemed significant for calcium content ($p < 0.05$) suggesting that there was a greater amount of osteogenic differentiation occurring on these surfaces compared to CoCrMo.

5.3. DISCUSSION

The surface of an orthopaedic implant is highly influential in whether a device can promote the formation of new healthy bone tissue or stimulate an inflammatory response that can lead to the failure of the device. The surface of the implant should ideally stimulate an environment that facilitates nearby osteoblasts to deposit ECM rich in mineral, whilst also promoting the colonisation and differentiation of cells with osteogenic potential to the implant, such a MSCs (Davies, 1998, Davies, 2003).

The material of choice for orthopaedic applications is titanium alloy based primarily due to its ability to stimulate osseointegration (Geetha et al., 2009). As discussed in previous sections of this thesis, titanium alloys cannot always be used for all orthopaedic applications and other materials that are mechanically superior, such as CoCrMo, are often preferred in devices in TKA. CoCrMo is accepted as having a lower degree of bioactivity compared to Ti and methods to improve its biological response have been investigated. These have included coating the material in TiO_2 (Logan et al., 2014b, Tsaryk et al., 2013), topographically modifying the surface (Jakobsen et al., 2010, Logan et al., 2015), functionalisation of surface coatings (Logan et al., 2014a, Miyauchi et al., 2010) and immobilisation of the surface with BMPs (Poh et al., 2011, Tan et al., 2013b, Tan et al., 2013a).

In this section of the thesis, a study was performed to investigate whether two of the previously reported methods of enhancing the bioactivity of CoCrMo could be combined to produce an implant surface that would further improve the bioactivity of the material. Specifically, topographical modification of the surface to form the SLA250 topography and coating the surface with TiO_2 by atmospheric CVD were chosen, both of which individually, were shown to enhance the mineralisation of MSCs (Logan et al., 2015, Logan et al., 2014b).

Characterisation of the three SLA surfaces was performed by assessing the surface wettability, roughness, morphology and elemental composition. Using water contact angle, it was found that CCMT was the most hydrophilic of the three substrates (Figure 62). It has been reported that materials with increased hydrophilicity promote a superior cell response over complimentary hydrophobic samples (Zhao et al., 2005, Khan et al., 2012). By significantly reducing the water contact angle on CCMT, it would imply that the surface would be more advantageous for cell-surface interaction compared to

CoCrMo. Interestingly, the water contact found on Ti was also significantly greater than that found on CCMT. Seeing as a layer of TiO_2 was present on the surface of both CCMT and Ti, the change in wettability between the substrates would imply that the properties of the oxide layer on each substrate were different. A study which looked at the osteogenic MC3T3-E1 cell line on bulk titanium and sputter coated titanium on glass, found that the cells behaved differently between the two materials (Oya et al., 2010). Bulk titanium samples promoted a superior level of mineralisation compared to sputter coated titanium, which suggested that despite the elemental composition being similar on each surface, the properties and cell response can be significantly different, possibly due to the crystal structure of the material.

The roughness of each substrate was analysed by laser profilometry (Figure 63). The hypothesis was that coating the surface of CoCrMo in a thin layer of TiO_2 would act as sheet, filling up any of the nano features on the surface, such as the pits created from the etching process. It was predicted that ultimately this sheet of TiO_2 would smoothen the surface. Conversely, it was found that CCMT had the largest R_a value of the three substrates (2.01 ± 0.27 μm), with a value significantly more than both CoCrMo (1.04 ± 0.05 μm) and Ti (1.66 ± 0.15 μm). On titanium alloy substrates it has been reported that a moderately rough surfaces with an R_a value between 1 – 2 μm are ideal (Wennerberg and Albrektsson, 2009). CCMT is arguably at the upper limit of this range. To ascertain why the deposition of TiO_2 onto the surface of CoCrMo significantly increased the R_a value and to check the distribution of TiO_2 over the substrate, SEM and EDX were performed. SEM analysis showed a rough, irregular morphology on the surface of both CCMT and CoCrMo, although it was challenging to confirm any clear dissimilarities between the two, despite CCMT appearing to have a slightly rougher appearance (Figure 64). The presence of titanium was confirmed on CCMT by EDX maps and was evenly distributed across the entirety of the surface. Under higher magnification, the presence of titanium on the jagged peaks and pits of the surface was assessed and comprehensive coverage was again observed (Figure 65). Whilst EDX scans confirmed titanium coverage, the technique is not entirely capable of distinguishing how much of the element is present at each point. Considering this, it is possible that the increased R_a value observed on CCMT may be due to a denser deposition of the TiO_2 coating on the peaks of the irregular surface morphology compared to the pits, and as a consequence, this may have amplified the roughness profile.

The phase and precursor chemistry of CVD TiO_2 has been reported to be influential to osteogenic cell behaviour (Altmayer et al., 2013). On TiO_2 films created by magnetron sputtering, it was found that the anatase phase stimulated a greater osteogeni response in osteoblasts compared against rutile and amorphous phase TiO_2 (He et al., 2008). Markers of proliferation, morphology and mineralisation were enhanced. The phase of TiO_2 on CCMT was assessed by Raman spectroscopy and strong peaks for anatase TiO_2 were observed (Figure 66). Additional peaks were observed in the spectra which were thought to be background from the CoCrMo sample largely due to the thin nature of the TiO_2 coating. This effect can occur due to penetration of the Raman laser through the TiO_2 into the sample.

To assess the bioactivity of the substrates human MSCs were used a model. Firstly, cell viability was studied by fluorescence microscopy using a live/dead kit and all three substrates were found to be relatively non cytotoxic as shown in figure 67. The presence of dead cells, which were detected by the uptake of the red component of the kit due to the compromised cellular membrane of dead or apoptotic cells, was observed on all three materials. It has been previously reported on titanium, that an increase in cell death can occur on SLA substrates compared to smooth (Wall et al., 2009), although this effect has been largely overlooked due to the excellent mineralising properties of the surface (Cochran et al., 2011, Khan et al., 2012).

Following cell viability, a number of cellular processes were studied, which included proliferation, retention and morphology. It was found that there was no significant difference in cell proliferation (Figure 68) or retention (Figure 69) between the three substrates. In addition, the internal morphology of the MSCs was assessed, specifically for the cytoskeletal protein f-actin and the adhesion protein vinculin. As before, no clear difference in the morphology of the MSCs and their distribution of the internal proteins was evident. Vinculin plays an active role in cell adhesion by forming focal adhesions that link the cell to the substrate surface. These focal adhesion complexes can mediate signals directly to the structural components of the cells such as f-actin and talin (Humphries et al., 2007). The expression of vinculin within MSCs on the three surfaces was similar, supporting the cell retention data which showed no significant difference in cell adhesion between the three materials (Figure 71). Interestingly, despite the morphology of cells remaining similar on all materials, there appeared to be two populations of cells on each surface, which are most clearly seen in the f-actin microscopy images (Figure 70). MSCs were both highly elongated and narrow, or in contrast, smaller

in size but more spread. It's possible that cell attachment and distribution over the irregular morphology of the SLA surfaces is stimulating this change in cell shape. MSCs that colonise in the pits are likely to spread over that immediate surface area, whilst those that are elongated and narrow, may be extended across different peaks, or be stretched along narrow channels on the surface. Cell shape and f-actin distribution are known to play a role in the regulation of MSC fate (Mathieu and Loboa, 2012), which implies that the MSCs found in different areas on the surface may have different biological properties and activities.

One of the most important properties of an orthopaedic implant surface is the materials ability to promote an environment that stimulates the formation of new bone tissue. Surfaces with rough microtopographies have been reported to generate osteogenic microenvironments comprised of ECM rich in mineral and collagen (Boyan et al., 2003). Significantly more calcium was present on CCMT compared to CoCrMo, signifying that MSCs were differentiating a faster rate and ultimately deposited a greater amount of mineral on CCMT (Figure 73). In addition to the level of mineral content, type I collagen, which acts a scaffold for calcium nucleation sites (Davies, 1998), was assessed using fluorescence microscopy. It was found that CoCrMo promoted a greater rate of collagen fibril formation compared to CCMT and Ti (Figure 72). Therefore, in comparison to CCMT and Ti, CoCrMo stimulated a lower concentration of total mineral whilst simultaneously promoting a higher rate of collagen deposition. This data would suggest that bone tissue formed on the CoCrMo surface may be over collagenous and not have the mechanical strength of tissue found on CCMT, which owns a significantly higher mineral content.

The use of TiO_2 as a coating on a roughened SLA surface formed of CoCrMo was shown to improve the osteogenic differentiation ability of human MSCs, compared to uncoated CoCrMo. This same effect was observed on smooth CoCrMo (Logan et al., 2014b). In a comparable SLA study, the use of titanium nitride oxide (TiNO) as a coating on roughened CoCrMo substrates was investigated as a means of improving the biocompatibility of the material (Durual et al., 2013). Similarly to the present investigation, CoCrMo was engineered to create an SLA topography. Following this, a TiNO coating was applied to the SLA CoCrMo by means of plasma vapour deposition, implants were implanted into the jawbone of miniature pigs and BIC was measured. After two weeks, a greater BIC was observed on TiNO CoCrMo compared to Ti SLA control. A similar enhancement in osteoconduction was observed on TiO_2 coated substrates in the

present study, highlighting the potential of titanium oxide based coatings for implant applications. In a related study, a TiNO coating on titanium enhanced proliferation in human osteoblasts (Durual et al., 2011). A separate study that also utilised both a titanium coating and roughening of the surface was performed by *Han et al.* In contrast to the present study and previously cited TiNO SLA projects (Durual et al., 2011, Durual et al., 2013), *Han et al* enhanced the biocompatibility of Co-Cr by firstly placing a titanium layer on the substrate surface by electron beam deposition and then subsequently roughening the surface using micro arc oxidation (Han et al., 2009). The process thickened and roughened the surface TiO_2 layer and consequently resulted in improvements in cell viability and ALP activity in MC3T3-E1 cells.

5.4. CONCLUSION

In this section of the thesis it was shown that coating the surface of roughened SLA CoCrMo with TiO_2 can enhance cellular markers related to mineralisation in human MSCs *in vitro*. When compared to CoCrMo SLA, CCMT SLA was shown to have greater bioactivity by demonstrating comparable levels of mineralisation as found on SLA titanium. By altering the response of these markers, such as calcium deposition and type I collagen formation, it would suggest that implants that have been modified using the SLA topography and TiO_2 CVD coating, may promote a higher rate of osteoinduction and osteoconduction in cells with osteogenic capacity. This in turn may ultimately lead to increased implant stability and reduced healing times following surgery.

CHAPTER SIX:

GENERAL DISCUSSION

6. GENERAL DISCUSSION

The average life expectancy in the UK has risen 4.2 years in the past two decades largely due to improvements in diagnostic and therapeutic techniques (Murray et al., 2013). One consequence of this situation is a growing demand on healthcare services. Included in this situation is TJA, as UK databases have seen a 7.5% and 7.3% increase in the total amount of procedures performed between 2011 and 2012 for THA and TKA, respectively. This amounts to an increase of 6,174 THA procedures and 6,189 TKA procedures over a 12 month period (Borroff et al., 2014). Considering the cost of TJA procedures can range from £7,137 - £14,444 (Jenkins et al., 2013), this puts significant pressure on the healthcare industry in an economic climate where budget cuts are prevalent. Whilst the national joint registry database does not cover the entire UK, the trend of an increasing demand for TJA is evident. A similar situation has been reported in the USA, which expect to see an increase of 363,000 for THA and 3,031,000 for TKA procedures between 2005 and 2030 (Kurtz et al., 2007a). Furthermore, in an international study assessing the procedure rate for both primary and revision TKA surgeries, there was a global trend showing an increase in the demand for TKA (Kurtz et al., 2011). Whilst there is no immediate solution to the increasing demand for TJA, the current situation highlights the importance of improving current generation implants so that they have increased longevity and reduced healing times. The current material of choice for creating orthopaedic implants is titanium and its alloys, primarily due to its ability to stimulate osseointegration (Geetha et al., 2009, Branemark, 1983). Despite the popularity of titanium alloys, they cannot always be used and other materials, such as the cobalt alloy CoCrMo, are often preferred due to their greater mechanical strength and resistance to wear. CoCrMo is widely used in TKA devices as its mechanical strength can withstand the immense load of the joint whilst its wear resistance allows for its application as a bearing surface. Despite these advantages CoCrMo does not have the biocompatibility of titanium alloys, and as a consequence, is less effective at stimulating bone healing following implantation.

The aim of this project was to develop and assess several strategies aimed at improving the bioactivity of CoCrMo in an attempt to improve its performance when used in orthopaedic applications. The main application of this approach would be in THR and TKRs where CoCrMo, used primarily as the bulk material of components, could have the

surface modified to promote a more beneficial environment for new bone formation and ultimately lead to improved levels of osseointegration.

Chapter 2 describes the investigation of the use of TiO_2 coatings as a method of enhancing the bioactivity of CoCrMo. The basis of this initial study revolved around the understanding that the TiO_2 layer would act as a mask and in doing so, would block out the underling CoCrMo surface. In theory, cells that colonise the surface of the material would not "see" the CoCrMo, but would interact with the TiO_2 layer, the same oxide layer as found on native titanium (Textor, 2001). Therefore, this first surface modification technique was assessed by comparing the TiO_2 coated sample with uncoated CoCrMo, and titanium as a positive control. To study the bioactivity of the surface, an appropriate cell type had to be chosen for *in vitro* cell analysis. Osteoblasts were the obvious choice, but relatively low numbers are yielded after the dissociation of tissue and their expansion rate *in vitro* is low (Salgado et al., 2004). The ideal cell candidate was human MSCs, which are undifferentiated, multipotent cells capable of self-renewal. Specifically, human MSCs isolated from bone marrow of the iliac crest were used, which have the potential to differentiate into osteoblasts, as well as other mesenchymal linages, such as adipocytes and chondrocytes (Pittenger et al., 1999).

Before the study could begin, the development of a mechanical polishing protocol was required to remove the machined topography present on CoCrMo discs supplied by Corin Ltd. MSCs are highly sensitive to topographical cues on material surfaces (Dalby et al., 2007, Logan and Brett, 2013, Wennerberg and Albrektsson, 2009, Sykaras et al., 2000), and due to the primary aim of this chapter being the investigation of the oxide coating, topographical influence on the results was not desired. A polishing protocol for cobalt was supplied by Struers, although in its initial form the process was unrefined, time consuming and had poor reproducibility in samples. Over an extensive period of time, the polishing protocol was refined by changing variables such as SiC papers, polishing force, sample fixation method and manual rotation in place of automatic. The final protocol was able to produce a high number of CoCrMo samples with a reproducible mirror finish. Whilst still fairly time consuming, the protocol was much more efficient than the original.

Once the topographical finish of the CoCrMo had been finalised, substrates were coated with anatase TiO_2 using atmospheric pressure CVD. The anatase phase of TiO_2 was chosen due to its photo-reactivity and it had been reported to promote a better response

in osteogenic cells compared to rutile and amorphous phases of TiO_2 (He et al., 2008). The coating was characterised using Raman spectroscopy and XRD. One of the variables of surface coatings is the thickness, which for CVD is correlated to the deposition time. Considering the CoCrMo discs were coated in batches of approximately 30, a 60 second deposition time was selected to ensure coverage of all the discs in the chamber, therefore some variation between the thicknesses of the coating was observed. As the project progressed, the oxide thickness became fairly consistent, averaging at around 300 – 400 nm per batch. Deposition of a uniform coating on each disc of every batch would have been ideal, but the complete coverage of the discs in TiO_2 was the priority.

When *in vitro* cell culture studies were completed, an enhancement in the rate of mineralisation was observed on CCMT compared to CoCrMo. This observation was in the form of a larger amount of calcium and hydroxyapatite deposition, whilst concurrently promoting less type I collagen formation in the form of dense fibrils. The calcium to collagen ratio was a concept proposed by *Khan et al,* where it was stated that biomaterial surfaces that promote greater mineral content, whilst simultaneously stimulating lower amounts of collagen deposition, would result in bone tissue that had greater mechanical properties (Khan et al., 2012). *Khan et* al studied titanium in both smooth and roughened forms, specifically SLA and SLActive topographies and concluded that the roughened surfaces were preferable against smooth. They were able to draw conclusions from their *in vitro* study, by comparing it to *in vivo* results in the literature, where SLA and SLActive implants were superior compared to polished/machined (Cochran et al., 2011, Abron et al., 2001, Buser et al., 1991). By observing a greater amount of mineral deposition coupled with lower collagen formation, they concluded that this result may be related to the SLA *in vivo* performance in the literature. Although it's difficult to compare *in vitro* and *in vivo* studies, the data in chapter 2 would suggest that there is a similar effect occurring and considering the calcium/collagen ratio, the properties of bone tissue deposited on the CCMT surface was concluded to be preferable compared to that found on CoCrMo.

The potential applications of TiO_2 coatings generated by atmospheric pressure CVD go beyond improving the osteogenic performance of CoCrMo orthopaedic implants, as such oxide based coatings can be doped with additional elements. This system can be used to enhance the osteogenic performance of coatings, demonstrated by the inclusion of silicon in a TiO_2 coating which improved the response of osteoblasts (Wang et al., 2012a, Wang et al., 2012b, Wang et al., 2014b). Furthermore, inclusion of other elements, such as

calcium, in TiO_2 coatings may help facilitate bone formation by transporting calcium to the direct location of osseointegration. Conversely, inclusion of other elements, such as silver, could support alternative applications for the coating; Silver nanoparticles applied as a monolayer on material surfaces have gained significant interest as an anti-infective strategy due to its antimicrobial properties. Monolayers of silver nanoparticles have been shown to inhibit biofilm formation in strains of bacteria, such as *Pseudomonas aeruginosa* and *Staphylococcus epidermidis* (Taglietti et al., 2014, Ansari et al., 2014), whilst application of silver can restrict the adhesion of *Streptococcus mutans* and marine bacteria (Espinosa-Cristóbal et al., 2013, Liu et al., 2012). The potential application of silver doped TiO_2 coatings could include dental implants, which are prone to bacterial infection due to bacteria colonising in gaps located in the implant. Peri-implantitis is a result of such bacterial infection and is a destructive inflammatory process that affects hard and soft tissues around the implant, ultimately resulting in bone loss (Mombelli, 2002). Therefore, silver doped TiO_2 coatings applied onto dental implants may prove to be an advantageous strategy for inhibiting peri-implantitis. Interestingly, studies which have examined the addition of TiO_2 onto titanium substrates via a number of techniques, have reported positive responses (Ma et al., 2008, Chiang et al., 2009, Drnovsek et al., 2012, Tsukimura et al., 2008), indicating that dental implants which are formed primarily of titanium, may also benefit from an improvement in their osteogenic ability as well the antimicrobial effect. In a very recent publication, titanium-silver coatings created by a one-step magnetron sputtering process have shown favourable antimicrobial and osseointegration ability (Bai et al., 2015).

To follow on from chapter 2, the second results chapter investigated a method of functionalising the surface TiO_2 layer on CoCrMo by utilising the unique photo-reactive properties of TiO_2. In its anatase form, TiO_2 is highly photoreactive and transitions from hydrophobic to super-hydrophilic upon irradiation with UV light (Wang et al., 1997). Exposure to sunlight can activate this effect, causing the removal of hydrophilic or oleophilic contaminants by rainfall, allowing for TiO_2 to be applied in self-cleaning windows (Wang et al., 1997). The photo-reactivity of anatase TiO_2 is not limited to self-cleaning window applications, but has also been investigated as a method of enhancing the performance of metallic implants. Used specifically on titanium and TiO_2 coated materials; the method is referred to as 'UV photofunctionalization'. Numerous studies have reported enhancements both *in vitro* and *in vivo* on UV photofunctionalized materials compared to untreated substrates (Sawase et al., 2008, Aita et al., 2009b, Ueno

et al., 2010, Yamada et al., 2010, Iwasa et al., 2010, Yamazaki et al., 2015). Furthermore, the application of UV light on biomaterials has been shown to be capable of restoring materials from the recently discovered time dependant degradation of material osteoconductivity (Att et al., 2009, Hori et al., 2010b). These advantageous results in the literature justified the assessment of UV photofunctionalization on CCMT as a means of further enhancing the bioactivity of the material.

The wettability of CCMT was measured using water contact angle and it was found that the surface successfully transitioned from hydrophobic to superhydrophilic after 24 hours exposure to UV light. This reduction in water contact angle is one of the main traits of UV photofunctionalization and has been reported widely in the literature (Sawase et al., 2008, Iwasa et al., 2011, Tsukimura et al., 2011, Hori et al., 2010b, Hori et al., 2011, Ueno et al., 2010, Yamada et al., 2010, Minamikawa et al., 2013). Following this, the carbon content of the surface was assessed using FTIR, as a reduction in surface contaminants is thought to be one of the main mechanisms of UV photofunctionalization. Surprisingly there was no reduction in the peaks that correlate with C-H bonds. This result was attributed to the equipment not having the sensitivity to detect these minute changes in carbon. Ideally, analysis of this concept would have been tested using X-ray photoelectron spectroscopy (XPS) if it had been available, as the technique would be more suited to detecting the small changes in the surface hydrocarbon content. Conversely, it may have been that reduction in carbon content was not occurring, as the mechanisms behind UV photofunctionalization is a topic which is continuously debated in the literature. The reduction of surface hydrocarbons has been widely proposed (Att et al., 2009, Yamada et al., 2010, Miyauchi et al., 2010, Ueno et al., 2010, Aita et al., 2009b) although another study found no significant hydrocarbon reduction following UV photofunctionalization (Terriza et al., 2013). Furthermore, in a study which assessed different wavelengths of UV light, it was found that whilst both UVA and UVC promoted a similar amount of carbon decomposition, UVC stimulated a superior cell response, calling into question hydrocarbon removal as the main mechanism of UV photofunctionalization (Gao et al., 2013). It has also been proposed that there is an electrostatic effect occurring on the substrate surface following UV photofunctionalization, that results in enhanced protein adsorption and eventually improved osteoblast adhesion (Hori et al., 2010a, Iwasa et al., 2010). Whilst the mechanisms behind UV photofunctionalization is an interesting topic and needs to be further investigated, a considerable amount of time and resources would need to be used

to determine the exact mechanism. Considering that super-hydrophilicity was achieved on CCMT following UV irradiation, it was decided that a cell culture study should be completed to ascertain its effect on cell behaviour.

Consulting the literature found that UV photofunctionalization had a significant effect on the behaviour of osteogenic cells. Specifically for human MSCs, *Aita et al* found that UV photofunctionalized titanium enhanced markers of proliferation, adhesion, migration, retention and osteogenic differentiation (Aita et al., 2009a). In addition, *Lan et al* found that markers of cell adhesion, morphology and osteogenic differentiation were enhanced on UV treated titanium substrates (Lan et al., 2015). Considering this, it was surprising that the majority of cellular markers studied in chapter 3 were not affected by CCMT UV photofunctionalization. Only cell adhesion was enhanced by the procedure, which resulted in greater cell retention to the material surface following mechanical dissociation. This effect was attributed to the MSCs on UV treated CCMT having greater spread, with increased actin and vinculin expression, which has been reported in the literature in several studies (Iwasa et al., 2011, Tsukimura et al., 2011, Hori et al., 2011, Hori et al., 2010b, Yamada et al., 2010, Minamikawa et al., 2013, Iwasa et al., 2010). It may be that the difference in cell behaviour is again related to how cells behave differently on bulk titanium substrates compared to titanium coated materials (Oya et al., 2010). Despite the aim of chapter 3 being to significantly build upon the improvements shown in chapter 2, the enhancement to cell adhesion alone is still an important step forward in enhancing the bioactivity of CoCrMo. Although improving osseointegration is a priority for orthopaedic implants, the surface must also stimulate the colonisation of osteogenic cells and promote an environment that allows them to remain on the surface. UV photofunctionalization is an effective means of achieving this and builds upon early improvements shown in chapter 2.

Whilst the first half of the thesis focused on TiO_2 coating and its functionalisation using UV irradiation, the aim of chapter 4 was to assess a different surface modification technique in the form of topographical modification. The surface topographies used in chapter 2 and 3 could be described as smooth surfaces, with an R_a within the range of 0.07 – 0.17 μm, which are not ideal for bone formation, but were chosen to remove any topographical influence from the results (Wennerberg and Albrektsson, 2009). It has been reported that moderately rough surfaces with an R_a between 1 – 2 μm show stronger bone responses than rough surfaces (R_a > 2 μm) (Wennerberg and Albrektsson, 2009). Therefore the aim of chapter 3 was to develop a unique surface topography on CoCrMo

within the moderately rough range, which was capable of creating a microenvironment that would be advantageous for bone growth and osseointegration (Boyan et al., 2003). Several methods are widely used to roughen implant materials (Wennerberg and Albrektsson, 2010). Plasma spraying is a method of roughening an implant surface and is commonly used to apply titanium or hydroxyapatite (Sykaras et al., 2000). Although this is popular technique, the roughened topography is formed by the addition of a bioactive layer, which when considering that the future work for the project would involve coating the topography with the TiO_2 layer studied in chapters 2 and 3, the application of an additional layer to create the topography would not be ideal, as this would result in another interface, which could lead to possible mechanical and delamination issues. Considering this, the creation of the surface topography via removal of surface constituents was preferable. One of the most popular surface finishes created in this manner and used extensively on titanium dental implants is the SLA topography. SLA has been shown to be superior both *in vitro* and *in vivo* when compared to smooth or machined surfaces (Khan et al., 2012, Wall et al., 2009, Mendonca et al., 2010, Cochran et al., 2011). It is not commonly used in orthopaedic applications, therefore the development of a primarily dental associated topography onto an orthopaedic biomaterial was an interesting project considering the similarities between the two fields.

To create SLA required a two-step process of firstly sand blasting using Al_2O_3 particles following by acid etching. A comprehensive literature search found only one article that created SLA on CoCrMo and this was used a reference (Durual et al., 2013). Numerous variables were altered to try and obtain a surface roughness within the 1 – 2 μm moderately rough range, although the majority of early attempts resulted in surfaces that were minimally rough (0.5 – 1 μm). The roughness was found to increase when the blasting pressure was set to its maximum and a surface with a R_a of 1.02 μm was produced using 250 μm Al_2O_3 grit (SLA250). To broaden the study, a number of other surface topographies were created, which included SLA using small Al_2O_3 grit (50 μm, SLA50), a surface that only underwent acid etching (AE) and lastly, a mirror finish smooth control (SMO).

During wettability analysis, it was found that those samples that had undergone acid etching, appeared to be more hydrophilic compared to the smooth control, which was hydrophobic. It was found that treatment with NHO_3 can activate the surface of CoCrMo by removing surface hydrocarbons (Paredes et al., 2014). High concentrations of hydrocarbons have been reported reduce mineralisation activity in osteoblasts (Hayashi

et al., 2014), suggesting that the acid etching process may be advantageous not only by modifying surface topography, but also by removing surface contaminants.

When cell culture experiments were performed it was found that the hypothesis, that stated that the SLA250 topography would promote increased osteogenic differentiation in human MSCs, was mostly correct. Cellular markers related to osteogenesis were found to be enhanced on the SLA250 surface, which included calcium concentration and hydroxyapatite formation. The other SLA surface, created using 50 μm Al_2O_3, promoted adequate levels of mineralisation, although interestingly inhibited other important cellular activities such as proliferation and adhesion. Elemental analysis found the presence of residual aluminium contamination spread throughout the surface which was not present to the same extent on SLA250. Aluminium in high concentrations has been reported to have inhibitory effects on cell performance, indicating that the residual particles found on SLA50 may have been accountable for its poor performance compared to SLA250 (Sader et al., 2005, Le Guehennec et al., 2008). A number of other cellular processes were investigated such as proliferation, adhesion, attachment, morphology and viability. Proliferation and cell attachment were found to be slightly enhanced on the smooth topographies which has been previously reported in the literature (Khan et al., 2012), as the absence of pronounced surface features on smooth topographies promotes an advantageous environment for proliferation. In contrast, a topography with features on the micron scale is preferred for mineralisation which is what was observed in this chapter (Boyan et al., 2003). The enhanced mineralisation observed on roughened topographies has been investigated by *Harle et al*, who found differences in the genetic expression in alveolar bone cells cultured on smooth and rough titanium substrates (Harle et al., 2004). A number of genes were up regulated on roughened titanium, including neurotrophin 4, which is associated with increased expression of ALP and osteopontin. Therefore, the surface roughness has a profound effect on the genetic expression of osteogenic cells by modulating specific genes referred to as "Roughness response genes" (Brett et al., 2004). These cell-material interactions are influential in why roughened titanium implants are superior *in vivo* compared to those with a smooth or machined finish (Buser et al., 1991, Cochran et al., 2011, Abron et al., 2001). These studies are comparable to the results recorded in this chapter of the thesis, where roughened CoCrMo surfaces promoted superior levels of mineralisation in human MSCs compared to those found on smooth substrates. It was concluded that the SLA250 surface was the most advantageous surface for orthopaedic applications due to its ability to enhance osteogenic differentiation

markers, stimulate a consistent rate of cell proliferation and promote better levels of cell retention.

In the final results chapter of the thesis, the aim was to connect the previous research chapters by applying two of the methods together to produce a CoCrMo surface that would stimulate the largest enhancement in performance. The aim was to coat the SLA250 surface developed in chapter 4 with the TiO_2 coating from chapter 2. Whilst it would've been ideal to also assess UV photofunctionalization in this final chapter, limitations to the resources and time available prevented this option. In theory, by creating the SLA topography on CoCrMo and coating the surface with TiO_2, the same oxide layer as found on the surface of titanium (Textor, 2001), the coated surface on CoCrMo should be extremely similar to SLA titanium used in dental implants (Cochran et al., 2011).

The CVD technique for TiO_2 used in chapter 2 was altered to a shorter deposition time. The reason behind this was due to the micro and nano features found on the SLA topography, the 60 second deposition as used in chapter 2 produced a relatively thick coating and this may have possibly filled in some of these surface features. Surfaces with features on both the nano and micro scale are thought to be ideal for orthopaedic applications (Mendonca et al., 2010, Rosales-Leal et al., 2010) therefore a thinner TiO_2 was preferable to help preserve these features. As CoCrMo discs were coated in batches of around 30, the shorter deposition had to be tested to determine if the location of the discs within the chamber had an effect on the oxide layer. It was found that discs placed at the front of the chamber were adequately coated, although those at the middle and rear of the chamber had a coating that was too thin, as a clear TiO_2 anatase spectrum could not be obtained using Raman spectroscopy. Following this, all discs to be coated had to do so at the front position of the chamber. Further testing of the TiO_2 coating was performed using EDX analysis and comprehensive coverage was confirmed by the presence of titanium over the entirety of the surface at both low and high magnifications.

Profilometry data showed that rather than the TiO_2 layer reducing the R_a of the surface, it significantly increased the value, making CCMT the roughest surface of the three SLA topographies. This was unexpected and was attributed to a greater amount of the coating being deposited on the peaks of the irregular surface. This would result in a larger roughness profile and an increased R_a. In addition to increasing the surface roughness, the coating also promoted an increase in hydrophilicity compared to CoCrMo and Ti

SLA. The combination of a rougher topography with increased wettability is advantageous for an orthopaedic implant surface (Wennerberg and Albrektsson, 2009, Zhao et al., 2005, Vlacic-Zischke et al., 2011).

Cell culture experiments found that the TiO_2 coating did have a positive effect on cell behaviour. As seen earlier in chapter 2 on the smooth topography, the TiO_2 coating on SLA stimulated an enhancement in mineralisation in the form of greater calcium and hydroxyapatite formation. Furthermore, CoCrMo was again observed to stimulate a greater amount of type I collagen deposition compared to CCMT and Ti, implying that the same effect is occurring on the SLA topographies that was observed on smooth. This is in regards to the calcium to collagen ratio proposed by *Khan et al* where an increase in mineralisation and decrease in collagen formation was determined to be preferable compared to an over collagenous matrix (Khan et al., 2012). Conversely, *Mendonca et al* assessed the extra cellular matrix produced by human MSCs on smooth and rough titanium substrates and found that the rough surface stimulated the highest collagen content (Mendonça et al., 2011). This data did not conform with the present study as CCMT had the greatest roughness although produced to lowest collagen content. *Mendonca et al* only assessed titanium substrates, suggesting that surface chemistry may be highly influential and precede the role of topography in the process of collagen deposition. Other cellular markers that were affected on the smooth coatings in chapter 2, such as cell retention and morphology, were not altered on SLA. This may have occurred due to the SLA topography being the primary mechanism driving cell behaviour by modulating roughness response genes (Brett et al., 2004). As the SLA topography was similar on all three substrates this may have taken a primary role in how the cells responded to the surfaces, which may have resulted in the similar responses observed in morphology and retention. By not having this additional factor in chapter 2, the cells would have been able to respond more directly to the chemical changes present on the surfaces and as a result, altered their behaviour accordingly.

In comparison to other coatings created for orthopaedic applications, such as those that use hydroxyapatite, atmospheric pressure CVD TiO_2 has a number of potential benefits. Firstly as shown in chapter two of the thesis, the thickness of the TiO_2 coating is relatively thin at around 300 nm. This is favourable, as when orthopaedic implants undergo cyclic loading, the bond strength of the coating to the material is highly important, as delamination can occur when the adhesion strength at this interface is inadequate. The thickness of surface coatings has been shown to be highly influential in this mechanism,

as shown by *Lynn et al,* who reported that an increase in thickness of hydroxyapatite resulted in substrate fatigue and delamination (Lynn and DuQuesnay, 2002). The substrates used by *Lynn et als* were in the micron range, whilst coatings created by atmospheric CVD can be nanometres thick, potentially reducing the risk of delamination. The trend of increasing thickness reducing the adhesive strength and delamination resistance was highlighted in a recent review (Mohseni et al., 2014). Interestingly, the review stated that the best adhesion of hydroxyapatite to a substrate was through use of an interfacial TiO_2 layer (Nie et al., 2000). Testing of the mechanical properties of atmospheric pressure CVD TiO2 coatings were unfortunately delayed multiple times throughout this project and are now to be addressed in the future work.

An additional benefit of the TiO2 coatings investigated in this project is the process can be easily scaled up for orthopaedic industrial application. At present, TiO_2 is widely used in the construction industry for self-cleaning glass (Paz et al., 1995). Pilkington glass are a manufacturer of a product known as 'Activ' which utilises the photo-reactivity of anatase TiO_2 coatings to breakdown dirt (Pilkington, 2015). This is the same process studied in chapter three of this thesis. Considering the production of TiO2 coatings via CVD are currently in place on an industrial scale, this reduces the complexity and cost of scaling up these technologies for use in orthopaedic sector.

Overall the combination of the SLA topography with TiO_2 coating stimulated an enhanced response in human MSCs to a comparable level as that found on titanium SLA. Considering titanium and its alloys are accepted as the material of choice for orthopaedic applications (Geetha et al., 2009), use of the surface modification techniques studied in this thesis may prove to be advantageous for improving the performance and bioactivity of implants formed of CoCrMo. Furthermore, in addition to improving the response of orthopaedic CoCrMo implants, there is evidence in the literature that TiO_2 coatings may prove advantageous in other fields such as dentistry, where titanium implants are most commonly used. This is due to studies reporting an improved response in titanium implants that have been modified with additional TiO_2 when compared against pure titanium (Ma et al., 2008, Chiang et al., 2009, Drnovsek et al., 2012, Tsukimura et al., 2008).

6.1. GENERAL CONCLUSIONS

- The use of anatase TiO_2 coatings created by atmospheric pressure CVD on smooth CoCrMo can enhance markers of cell adhesion and osteogenic differentiation in human MSCs *in vitro*.

- UV photofunctionalization of anatase TiO_2 layers on CoCrMo created by atmospheric pressure CVD have no effect on the attachment, osteogenic differentiation, migration and proliferation of human MSCs, although can significantly enhance cell retention.

- Enhancements to cell retention in human MSCs on UV photofunctionalized TiO_2 coated CoCrMo are thought to be caused by increased expression of the cytoskeletal protein f-actin and the adhesion protein vinculin.

- The sandblasted acid-etched topography used widely on titanium can be partially replicated onto CoCrMo. Specifically, the SLA250 topography can support an environment that stimulates a superior response in human MSCs in the form of enhanced osteogenic differentiation, proliferation and retention.

- Coating the SLA250 topography on CoCrMo with anatase TiO_2 can enhance markers of mineralisation in human MSCs to a comparable level as those found on titanium SLA.

- Application of some of the surface modification techniques studied in this thesis may prove to be advantageous at increasing the efficacy of implants formed of CoCrMo for orthopaedic applications.

6.2. FUTURE WORK

Further investigations into modifying the TiO_2 coating to promote an environment tailored to enhancing the osteogenic differentiation of human MSCs would be an interesting project that would follow on easily from the initial work completed in this thesis. Doping of TiO_2 coatings with silicon using the cathodic arc technique has shown to be beneficial to osteoblasts in the form of enhanced mineralisation rates and upregulating the expression of osteogenic genes, such as osteocalcin, Runx2 and ALP (Wang et al., 2012b, Wang et al., 2012a, Wang et al., 2013a). In addition to improving the osteogenic activity of the cells, markers of cell adhesion and proliferation were also observed to be significantly enhanced on silicon doped TiO_2 (Wang et al., 2012b). Therefore, inclusion of silicon or other elements such as calcium, would be a clear next step for investigating methods of enhancing the efficacy of TiO_2 coatings for use in orthopaedic applications.

The process of doping TiO_2 coatings with the additional elements could also increase the range of potential applications for the coating. Silver has developed significant interest due to its antimicrobial properties, including that when it is applied in a monolayer, it can inhibit and restrict biofilm formation (Taglietti et al., 2014, Ansari et al., 2014). Inclusion of silver into TiO_2 based CVD coatings would allow for the coating to be applied where an antimicrobial agent is also desired. For example, silver doped coatings could be applied to dental implants to prevent peri-implantitis (Mombelli, 2002). The advantage of this method would be the direct application of silver to the area in which it is required.

Investigating the mechanical properties of coating, for example, wear resistance and fatigue strength, would be a useful topic to address in future work, as this is an important factor if the coating is to be used in orthopaedic applications. The future work could include wear testing to elude the exact mechanical properties of the coating. This is a major factor in regards to surface coatings, as the bond strength between the material substrate and the applied film has to be adequate to prevent delamination and other potential failure mechanisms. This area of the project could be addressed by completing wear testing using pin on plate techniques to replicate cyclic loading. Analysis of ion release in lubricating solutions and high resolution surface analysis, could elucidate any potential issues that may arise from continuous loading. Other experiments that could address this aspect of testing could include scratch analysis.

Lastly, another area of interest that could be examined in future work, is a comparative study using the TiO_2 SLA CCMT topography created in this thesis, against other industrial surface modification techniques currently used on CoCrMo implants. The industrial sponsor of this project, Corin Ltd (Cirencester), current apply a hydroxyapatite coating using a plasma spraying technique to their CoCrMo devices. A direct comparison of the current surface modification used by Corin, against the TiO_2 coated SLA250 topography created in this project would be highly interesting to ascertain the efficacy of each substrate.

To summarise, from this project there is a lot of potential for future work, ranging from direct comparative studies against commercial products, mechanical testing and the potential for antimicrobial applications.

CHAPTER SEVEN:

BIBLIOGRAPHY

7. BIBLIOGRAPHY

ABDULKARIM, A., ELLANTI, P., MOTTERLINI, N., FAHEY, T. & O'BYRNE, J. M. 2013. Cemented versus uncemented fixation in total hip replacement: a systematic review and meta-analysis of randomized controlled trials. *Orthopedic Reviews,* 5**,** e8.

ABRON, A., HOPFENSPERGER, M., THOMPSON, J. & COOPER, L. F. 2001. Evaluation of a predictive model for implant surface topography effects on early osseointegration in the rat tibia model. *Journal of Prosthetic Dentistry,* 85**,** 40-46.

ADVINCULA, M., RAHEMTULLA, F., ADVINCULA, R., ADA, E., LEMONS, J. & BELLIS, S. 2006. Osteoblast adhesion and matrix mineralization on solgel-derived titanium oxide. *Biomaterials,* 27**,** 2201-2212.

AIELLO, L. & DEAN, C. 1990. *An introduction to human evolutionary anatomy,* Academic Press.

AITA, H., ATT, W., UENO, T., YAMADA, M., HORI, N., IWASA, F., TSUKIMURA, N. & OGAWA, T. 2009a. Ultraviolet light-mediated photofunctionalization of titanium to promote human mesenchymal stem cell migration, attachment, proliferation and differentiation. *Acta Biomaterialia,* 5**,** 3247-57.

AITA, H., HORI, N., TAKEUCHI, M., SUZUKI, T., YAMADA, M., ANPO, M. & OGAWA, T. 2009b. The effect of ultraviolet functionalization of titanium on integration with bone. *Biomaterials,* 30**,** 1015-1025.

ALTMAYER, J., BARTH, S. & MATHUR, S. 2013. Influence of precursor chemistry on CVD grown TiO2 coatings: differential cell growth and biocompatibility. *RSC Advances,* 3**,** 11234-11239.

ANSARI, M. A., KHAN, H. M., KHAN, A. A., CAMEOTRA, S. S., SAQUIB, Q. & MUSARRAT, J. 2014. Gum arabic capped-silver nanoparticles inhibit biofilm formation by multi-drug resistant strains of Pseudomonas aeruginosa. *J Basic Microbiol,* 54**,** 688-99.

ANSELME, K. 2000. Osteoblast adhesion on biomaterials. *Biomaterials,* 21**,** 667-681.

AREVA, S., NARHI, T., PALDAN, H., PELTOLA, T., NÃ¤RHI, T., JOKINEN, M. & LINDÃ©N, M. 2004. Use of sol-gel-derived titania coating for direct soft tissue attachment. *Journal of biomedical materials research. Part A,* 70**,** 169-78.

ATT, W., HORI, N., IWASA, F., YAMADA, M., UENO, T. & OGAWA, T. 2009. The effect of UV-photofunctionalization on the time-related bioactivity of titanium and chromium-cobalt alloys. *Biomaterials,* 30**,** 4268-4276.

BAI, L., HANG, R., GAO, A., ZHANG, X., HUANG, X., WANG, Y., TANG, B., ZHAO, L. & CHU, P. K. 2015. Nanostructured titanium–silver coatings with good antibacterial activity and cytocompatibility fabricated by one-step magnetron sputtering. *Applied Surface Science,* 355**,** 32-44.

BALDINI, N., ET AL 2009. Bone repair and regeneration. *In:* PLANELL, J. (ed.) *Bone repair biomaterials.* Cambridge: Woodhead Publishing Limited.

BALLONI, S., CALVI, E., DAMIANI, F., BISTONI, G., CALVITTI, M., LOCCI, P., BECCHETTI, E. & MARINUCCI, L. 2009. Effects of titanium surface roughness on mesenchymal stem cell commitment and differentiation signaling. *The International journal of oral & maxillofacial implants,* 24**,** 627-35.

BONEWALD, L. F. 2007. Osteocytes as dynamic multifunctional cells. *Skeletal Biology and Medicine, Pt A,* 1116**,** 281-290.

BORNSTEIN, M. M., SCHMID, B., LUSSI, A., BUSER, D. & BELSER, U. C. 2005. Early loading of non-submerged titanium implants with a sandblasted and acid-etched surface. *Clinical oral implants research,* 16**,** 631-638.

BORROFF, M., GREEN, M., GREGG, P., MACGREGOR, A., PORTER, M., TUCKER, K., WISHART, N., ESLER, C., HOWARD, P., JOHN, A., PORTEOUS, M., GOLDBERG, A., PALAN, J., BEAUMONT, R., THORNTON, J., YOUNG, E., MCCORMACK, V., MISTRY, A., NEWELL, C., PICKFORD, M., ROYALL, M., SAWNSON, M., SHLOMO, Y. B., BLOM, A., CLARK, E., DIEPPE, P., HUNT, L., KING, G., SMITH, M. & TOBIAS, J. 2014. The National Joint Registry Annual Report 2014. Pad Creative.

BOYAN, B. D., LOSSDÖRFER, S., WANG, L., ZHAO, G., LOHMANN, C. H., COCHRAN, D. L. & SCHWARTZ, Z. 2003. Osteoblasts generate an osteogenic microenvironment when grown on surfaces with rough microtopographies. *European cells & materials,* 6**,** 22-7.

BOYCE, B. F., YAO, Z., ZHANG, Q., GUO, R., LU, Y. A. N., SCHWARZ, E. M. & XING, L. 2007. New Roles for Osteoclasts in Bone. *Annals of the New York Academy of Sciences,* 1116**,** 245-254.

BOZEC, L., DE GROOT, J., ODLYHA, M., NICHOLLS, B. & HORTON, M. A. 2005. Mineralised tissues as nanomaterials: analysis by atomic force microscopy. *Nanobiotechnology, IEE Proceedings* -, 152**,** 183-186.

BOZEC, L. & HORTON, M. A. 2006. Skeletal tissues as nanomaterials. *Journal of Materials Science-Materials in Medicine,* 17**,** 1043-1048.

BRAMMER, K. S., FRANDSEN, C. J. & JIN, S. 2012. TiO2 nanotubes for bone regeneration. *Trends in Biotechnology,* 30**,** 315-322.

BRANEMARK, P. I. 1983. OSSEOINTEGRATION AND ITS EXPERIMENTAL BACKGROUND. *Journal of Prosthetic Dentistry,* 50**,** 399-410.

BRETT, P. M., HARLE, J., SALIH, V., MIHOC, R., OLSEN, I., JONES, F. H. & TONETTI, M. 2004. Roughness response genes in osteoblasts. *Bone,* 35**,** 124-133.

BROHEDE, U., ZHAO, S. X., LINDBERG, F., MIHRANYAN, A., FORSGREN, J., STROMME, M. & ENGQVIST, H. 2009. A novel graded bioactive high adhesion implant coating. *Applied Surface Science,* 255**,** 7723-7728.

BRUNE, D., HULTQUIST, G. & LEYGRAF, C. 1984. Corrosion resistance of a passivated and non-passivated cobalt-chromium alloy. *Scandinavian journal of dental research,* 92**,** 262-7.

BURKE, M. 2008. Failure mechanisms in joint replacement. *In:* REVEL, P. A. (ed.) *Joint replacement technology.* Cambridge: Woodhead Publishing Limited.

BUSER, D., SCHENK, R. K., STEINEMANN, S., FIORELLINI, J. P., FOX, C. H. & STICH, H. 1991. INFLUENCE OF SURFACE CHARACTERISTICS ON BONE INTEGRATION OF TITANIUM IMPLANTS - A HISTOMORPHOMETRIC STUDY IN MINIATURE PIGS. *Journal of Biomedical Materials Research,* 25**,** 889-902.

BUSER, D., WITTNEBEN, J.-G., BRÄGGER, U., JANNER, S. F. M., RAMSEIER, C. A. & SALVI, G. E. 2012. 10-Year Survival and Success Rates of 511 Titanium Implants with a Sandblasted and Acid-Etched Surface: A Retrospective Study in 303 Partially Edentulous Patients. *Clinical implant dentistry and related research,* 14**,** 839-851.

CAMAZZOLA, D., HAMMOND, T., GANDHI, R. & DAVEY, J. R. 2009. A Randomized Trial of Hydroxyapatite-Coated Femoral Stems in Total Hip Arthroplasty: A 13-Year Follow-Up. *The Journal of Arthroplasty,* 24**,** 33-37.

CANABARRO, A., DINIZ, M. G., PACIORNIK, S., CARVALHO, L., SAMPAIO, E. M., BELOTI, M. M., ROSA, A. L. & FISCHER, R. G. 2008. High concentration of residual aluminum oxide on titanium surface inhibits extracellular matrix mineralization. *Journal of biomedical materials research. Part A,* 87**,** 588-597.

CARP, O., HUISMAN, C. L. & RELLER, A. 2004. Photoinduced reactivity of titanium dioxide. *Progress in solid state chemistry,* 32**,** 33-177.
CHARNLEY, J. 1961. Arthroplasty of the hip. A new operation. *Lancet (London, England),* 1**,** 1129-32.
CHARPENTIER, P. A., BURGESS, K., WANG, L., CHOWDHURY, R. R., LOTUS, A. F. & MOULA, G. 2012. Nano-TiO2/polyurethane composites for antibacterial and self-cleaning coatings. *Nanotechnology,* 23**,** 425606.
CHEN, D., ZHAO, M. & MUNDY, G. 2004. Bone morphogenetic proteins. *Growth factors,* 22**,** 233-41.
CHEN, H.-T., CHUNG, C.-J., YANG, T.-C., TANG, C.-H., CHEN, K.-C. & HE, J.-L. 2010a. Osteoblast growth behavior on micro-arc oxidized β-titanium alloy. *Surface & coatings technology,* 205**,** 1624-1629.
CHEN, J.-H., LIU, C., YOU, L. & SIMMONS, C. 2010b. Boning up on Wolff's Law: mechanical regulation of the cells that make and maintain bone. *Journal of Biomechanics,* 43**,** 108-18.
CHEN, Y. & ALMAN, B. A. 2009. Wnt Pathway, an Essential Role in Bone Regeneration. *Journal of Cellular Biochemistry,* 106**,** 353-362.
CHIANG, C.-Y., CHIOU, S.-H., YANG, W.-E., HSU, M.-L., YUNG, M.-C., TSAI, M.-L., CHEN, L.-K. & HUANG, H.-H. 2009. Formation of TiO2 nano-network on titanium surface increases the human cell growth. *Dental materials,* 25**,** 1022-1029.
CHOI, J.-M., KIM, H.-E. & LEE, I.-S. 2000. Ion-beam-assisted deposition (IBAD) of hydroxyapatite coating layer on Ti-based metal substrate. *Biomaterials,* 21**,** 469-473.
COCHRAN, D., JACKSON, J., BERNARD, J.-P., TEN BRUGGENKATE, C., BUSER, D., TAYLOR, T., WEINGART, D., SCHOOLFIELD, J., JONES, A. & OATES, T. 2011. A 5-year prospective multicenter study of early loaded titanium implants with a sandblasted and acid-etched surface. *The International journal of oral & maxillofacial implants,* 26**,** 1324-32.
COCHRAN, D., OATES, T., MORTON, D., JONES, A., BUSER, D. & PETERS, F. 2007. Clinical Field Trial Examining an Implant With a Sand-Blasted, Acid-Etched Surface. *Journal of periodontology,* 78**,** 974-982.
COGLE, C. R., GUTHRIE, S. M., SANDERS, R. C., ALLEN, W. L., SCOTT, E. W. & PETERSEN, B. E. 2003. An overview of stem cell research and regulatory issues. *Mayo Clinic Proceedings,* 78**,** 993-1003.
COHEN, M. M., JR. 2006. The new bone biology: pathologic, molecular, and clinical correlates. *Am J Med Genet A,* 140**,** 2646-706.
CROSS, A. J., DUNNILL, C. W. & PARKIN, I. P. 2012. Production of Predominantly Anatase Thin Films on Various Grades of Steel and Other Metallic Substrates From TiCl4 and Ethyl Acetate by Atmospheric Pressure CVD. *Chemical Vapor Deposition,* 18**,** 133-139.
CROSS, M. J. 2008a. Cementless fixation techniques in joint replacement. *In:* REVEL, P. A. (ed.) *Joint replacement technology.* Cambridge: Woodhead Publishing Limited.
CROSS, M. J., ET AL. 2008b. Cementless fixation techniques in joint replacement. *In:* REVELL, P. (ed.) *Joint replacement technology.* Woodhead Publishing Limited.
CUI, F. Z., LUO, Z. S. & FENG, Q. L. 1997. Highly adhesive hydroxyapatite coatings on titanium alloy formed by ion beam assisted deposition. *Journal of Materials Science-Materials in Medicine,* 8**,** 403-405.
CULLIFORD, D. J., MASKELL, J., BEARD, D. J., MURRAY, D. W., PRICE, A. J. & ARDEN, N. K. 2010. Temporal trends in hip and knee replacement in the United

Kingdom: 1991 TO 2006. *The Journal of Bone and Joint Surgery. British Volume,* 92**,** 130-135.

DALBY, M. J., ANDAR, A., NAG, A., AFFROSSMAN, S., TARE, R., MCFARLANE, S. & OREFFO, R. O. C. 2008. Genomic expression of mesenchymal stem cells to altered nanoscale topographies. *Journal of the Royal Society Interface,* 5**,** 1055-1065.

DALBY, M. J., GADEGAARD, N., TARE, R., ANDAR, A., RIEHLE, M. O., HERZYK, P., WILKINSON, C. D. W. & OREFFO, R. O. C. 2007. The control of human mesenchymal cell differentiation using nanoscale symmetry and disorder. *Nature Materials,* 6**,** 997-1003.

DAVIES, J. E. 1998. Mechanisms of endosseous integration. *Int J Prosthodont,* 11**,** 391-401.

DAVIES, J. E. 2003. Understanding peri-implant endosseous healing. *J Dent Educ,* 67**,** 932-49.

DE GROOT, K., GEESINK, R., KLEIN, C. P. A. T. & SEREKIAN, P. 1987. Plasma sprayed coatings of hydroxylapatite. *Journal of Biomedical Materials Research,* 21**,** 1375-1381.

DESCHASEAUX, F. D. R., SENSÃ©BÃ©, L. & HEYMANN, D. 2009. Mechanisms of bone repair and regeneration. *Trends in molecular medicine,* 15**,** 417-429.

DHAYAL, M., KAPOOR, R., SISTLA, P., KANT, C., PANDEY, R., GOVIND, K., SAINI, G., PANDE, M., DHAYAL, R., KAPOOR, P., SISTLA, C., KANT, R., PANDEY, K. & GOVIND, G. 2012. Growth, differentiation, and migration of osteoblasts on transparent Ni doped TiO2 thin films deposited on borosilicate glass. *Journal of biomedical materials research. Part A,* 100**,** 1168-1178.

DIMITRIEVSKA, S., BUREAU, M. N., ANTONIOU, J., MWALE, F., PETIT, A., LIMA, R. S. & MARPLE, B. R. 2011. Titania–hydroxyapatite nanocomposite coatings support human mesenchymal stem cells osteogenic differentiation. *Journal of Biomedical Materials Research Part A,* 98A**,** 576-588.

DOS SANTOS, A., ARAUJO, J. R., LANDI, S. M., KUZNETSOV, A., GRANJEIRO, J. M., DE SENA, L. A. & ACHETE, C. A. 2014. A study of the physical, chemical and biological properties of TiO2 coatings produced by micro-arc oxidation in a Ca-P-based electrolyte. *Journal of Materials Science-Materials in Medicine,* 25**,** 1769-1780.

DRNOVSEK, N., RADE, K., MILACIC, R., STRANCAR, J., NOVAK, S., DRNOVŠEK, N., MILAČIČ, R. & ŠTRANCAR, J. 2012. The properties of bioactive TiO2 coatings on Ti-based implants. *Surface & coatings technology,* 209**,** 177-183.

DURUAL, S., PERNET, F., RIEDER, P., MEKKI, M. & CATTANI LORENTE, M. 2011. Titanium nitride oxide coating on rough titanium stimulates the proliferation of human primary osteoblasts. *Clinical oral implants research,* 22**,** 552-9.

DURUAL, S. P., RIEDER, P., GARAVAGLIA, G., FILIERI, A., CATTANI LORENTE, M. & SCHERRER, S. 2013. TiNOx coatings on roughened titanium and CoCr alloy accelerate early osseointegration of dental implants in minipigs. *Bone,* 52**,** 230-7.

ENDO, M. M., BARBOUR, P. S. M., BARTON, D. C., FISHER, J., TIPPER, J. L., INGHAM, E. & STONE, M. H. 2001. Comparative wear and wear debris under three different counterface conditions of crosslinked and non-crosslinked ultra high molecular weight polyethylene. *Bio-Medical Materials and Engineering,* 11**,** 23-35.

ESPINOSA-CRISTÓBAL, L. F., MARTÍNEZ-CASTAÑÓN, G. A., TÉLLEZ-DÉCTOR, E. J., NIÑO-MARTÍNEZ, N., ZAVALA-ALONSO, N. V. &

LOYOLA-RODRÍGUEZ, J. P. 2013. Adherence inhibition of Streptococcus mutans on dental enamel surface using silver nanoparticles. *Materials Science and Engineering: C,* 33**,** 2197-2202.

FANDRIDIS, J. & PAPADOPOULOS, T. 2008. Surface characterization of three titanium dental implants. *Implant dentistry,* 17**,** 91-9.

FENG, J. Q., WARD, L. M., LIU, S., LU, Y., XIE, Y., YUAN, B., YU, X., RAUCH, F., DAVIS, S. I., ZHANG, S., RIOS, H., DREZNER, M. K., QUARLES, L. D., BONEWALD, L. F. & WHITE, K. E. 2006. Loss of DMP1 causes rickets and osteomalacia and identifies a role for osteocytes in mineral metabolism. *Nat Genet,* 38**,** 1310-1315.

FISCHER, K. & STENBERG, T. 2012. Prospective 10-Year Cohort Study Based on a Randomized Controlled Trial (RCT) on Implant-Supported Full-Arch Maxillary Prostheses. Part 1: Sandblasted and Acid-Etched Implants and Mucosal Tissue. *Clinical implant dentistry and related research,* 14**,** 808-815.

FRANCIS, L. W., LEWIS, P. D., WRIGHT, C. J. & CONLAN, R. S. 2010. Atomic force microscopy comes of age. *Biology of the Cell,* 102**,** 133-143.

FUCHS, R. K., ET AL. 2009. Bone anatomy, physiology and adaptation to mechanical loading. *In:* PLANELL, J. (ed.) *Bone repair biomaterials.* Cambridge: Woodhead Publishing.

GALLINI, G., SALVI, G. E. & LANG, N. P. 2004. Early loading (2 or 6 weeks) of sandblasted and acid-etched (SLA) ITI® implants in the posterior mandible. *Clinical oral implants research,* 15**,** 142-149.

GANDHI, R., DAVEY, J. R. & MAHOMED, N. N. 2009. Hydroxyapatite Coated Femoral Stems in Primary Total Hip Arthroplasty: A Meta-Analysis. *The Journal of Arthroplasty,* 24**,** 38-42.

GAO, Y., LIU, Y., ZHOU, L., GUO, Z., RONG, M., LIU, X., LAI, C. & DING, X. 2013. The effects of different wavelength UV photofunctionalization on micro-arc oxidized titanium. *PLoS ONE,* 8**,** e68086.

GEESINK, R. G. T. 2002. Osteoconductive coatings for total joint arthroplasty. *Clinical Orthopaedics and Related Research***,** 53-65.

GEETHA, M., SINGH, A. K., ASOKAMANI, R. & GOGIA, A. K. 2009. Ti based biomaterials, the ultimate choice for orthopaedic implants - A review. *Progress in Materials Science,* 54**,** 397-425.

GIANNONI, P., MURAGLIA, A., GIORDANO, C., NARCISI, R., CANCEDDA, R., QUARTO, R. & CHIESA, R. 2009. Osteogenic differentiation of human mesenchymal stromal cells on surface-modified titanium alloys for orthopedic and dental implants. *International Journal of Artificial Organs,* 32**,** 811-820.

GOLUB, E. E. 2009. Role of matrix vesicles in biomineralization. *Biochimica Et Biophysica Acta-General Subjects,* 1790**,** 1592-1598.

GOLUB, E. E. & BOESZE-BATTAGLIA, K. 2007. The role of alkaline phosphatase in mineralization. *Current Opinion in Orthopaedics,* 18**,** 444-448 10.1097/BCO.0b013e3282630851.

GONZALEZ-CARRASCO, J. 2009. Metals as bone repair materials. *In:* PLANELL, J. (ed.) *Bone repair biomaterials.* Cambridge: Woodhead Publishing Limited.

GOTMAN, I. 1997. Characteristics of Metals Used in Implants. *Journal of Endourology,* 11**,** 383-389.

GUO, Y.-P., TANG, H.-X., ZHOU, Y., JIA, D.-C. & NING, C.-Q. 2010. Effects of mesoporous structure and UV irradiation on in vitro bioactivity of titania coatings. *Applied surface science,* 256**,** 4945-4952.

GUTIERREZ-ARANDA, I., RAMOS-MEJIA, V., BUENO, C., MUNOZ-LOPEZ, M., REAL, P. J., MÁCIA, A., SANCHEZ, L., LIGERO, G., GARCIA-PAREZ, J. L. & MENENDEZ, P. 2010. Human Induced Pluripotent Stem Cells Develop

Teratoma More Efficiently and Faster Than Human Embryonic Stem Cells Regardless the Site of Injection. *STEM CELLS,* 28**,** 1568-1570.

HAKKI, S. S., BOZKURT, S. B., HAKKI, E. E., KORKUSUZ, P., PURALI, N., KOC, N., TIMUCIN, M., OZTURK, A. & KORKUSUZ, F. 2012. Osteogenic differentiation of MC3T3-E1 cells on different titanium surfaces. *Biomed Mater,* 7**,** 045006.

HAMILTON, D., CLEMENT, N., BURNETT, R., PATTON, J., MORAN, M., HOWIE, C., PATTON, J. T. & GASTON, P. 2013. Do modern total knee replacements offer better value for money? A health economic analysis. *International orthopaedics,* 37**,** 2147-2152.

HAN, C.-M., KIM, H.-E., KIM, Y.-S. & HAN, S.-K. 2009. Enhanced biocompatibility of Co-Cr implant material by Ti coating and micro-arc oxidation. *Journal of biomedical materials research. Part B, Applied biomaterials,* 90**,** 165-170.

HARLE, J., SALIH, V., OLSEN, I., BRETT, P., JONES, F. & TONETTI, M. 2004. Gene expression profiling of bone cells on smooth and rough titanium surfaces. *Journal of Materials Science-Materials in Medicine,* 15**,** 1255-1258.

HAYASHI, R., UENO, T., MIGITA, S., TSUTSUMI, Y., DOI, H., OGAWA, T., HANAWA, T. & WAKABAYASHI, N. 2014. Hydrocarbon Deposition Attenuates Osteoblast Activity on Titanium. *Journal of Dental Research,* 93**,** 698-703.

HE, J., ZHOU, W., ZHOU, X., ZHONG, X., ZHANG, X., WAN, P., ZHU, B. & CHEN, W. 2008. The anatase phase of nanotopography titania plays an important role on osteoblast cell morphology and proliferation. *Journal of materials science. Materials in medicine,* 19**,** 3465-3472.

HOFFMAN, A. 2004. Classes of materials used in medicine. *In:* RATNER, B. (ed.) *Biomaterials Science, an introduction to mateials in medicine.* Second ed.: Elsevier.

HOFFMANN, B., FELDMANN, M. & ZIEGLER, G. 2007. Sol–gel and precursor-derived coatings with cover function on medical alloys. *Journal of materials chemistry,* 17**,** 4034-4040.

HOLMEN, S. L., ZYLSTRA, C. R., MUKHERJEE, A., SIGLER, R. E., FAUGERE, M.-C., BOUXSEIN, M. L., DENG, L., CLEMENS, T. L. & WILLIAMS, B. O. 2005. Essential Role of β-Catenin in Postnatal Bone Acquisition. *Journal of Biological Chemistry,* 280**,** 21162-21168.

HONG, Z. D., MELLO, A., YOSHIDA, T., LUAN, L., STERN, P. H., ROSSI, A., ELLIS, D. E. & KETTERSON, J. B. 2010. Osteoblast proliferation on hydroxyapatite coated substrates prepared by right angle magnetron sputtering. *Journal of Biomedical Materials Research Part A,* 93A**,** 878-885.

HORI, N., IWASA, F., TSUKIMURA, N., SUGITA, Y., UENO, T., KOJIMA, N. & OGAWA, T. 2011. Effects of UV photofunctionalization on the nanotopography enhanced initial bioactivity of titanium. *Acta Biomater,* 7**,** 3679-91.

HORI, N., UENO, T., MINAMIKAWA, H., IWASA, F., YOSHINO, F., KIMOTO, K., LEE, M. & OGAWA, T. 2010a. Electrostatic control of protein adsorption on UV-photofunctionalized titanium. *Acta Biomaterialia,* 6**,** 4175-80.

HORI, N., UENO, T., SUZUKI, T., IWASA, F., YAMADA, M., ATT, W., OKADA, S., OHNO, A., AITA, H., KIMOTO, K. & OGAWA, T. 2010b. Ultraviolet light treatment for the restoration of age-related degradation of titanium bioactivity. *The International journal of oral & maxillofacial implants,* 25**,** 49-62.

HUMPHRIES, J. D., WANG, P., STREULI, C., GEIGER, B., HUMPHRIES, M. J. & BALLESTREM, C. 2007. Vinculin controls focal adhesion formation by direct interactions with talin and actin. *Journal of Cell Biology,* 179**,** 1043-1057.

HYETT, G., DARR, J. A., MILLS, A. & PARKIN, I. P. 2010. An Investigation into the Optimum Thickness of Titanium Dioxide Thin Films Synthesized by Using Atmospheric Pressure Chemical Vapour Deposition for Use in Photocatalytic Water Oxidation. *Chemistry – A European Journal,* 16**,** 10546-10552.

ISHIZAKI, K., SUGITA, Y., IWASA, F., MINAMIKAWA, H., UENO, T., YAMADA, M., SUZUKI, T. & OGAWA, T. 2011. Nanometer-thin TiO2,, enhances skeletal muscle cell phenotype and behavior. *International journal of nanomedicine,* 6**,** 2191-203.

ISHIZAWA, H. & OGINO, M. 1995. Formation and characterization of anodic titanium oxide films containing Ca and P. *Journal of biomedical materials research,* 29**,** 65-72.

IWASA, F., HORI, N., UENO, T., MINAMIKAWA, H., YAMADA, M. & OGAWA, T. 2010. Enhancement of osteoblast adhesion to UV-photofunctionalized titanium via an electrostatic mechanism. *Biomaterials,* 31**,** 2717-27.

IWASA, F., TSUKIMURA, N., SUGITA, Y., KANURU, R., KUBO, K., HASNAIN, H., ATT, W. & OGAWA, T. 2011. TiO2 micro-nano-hybrid surface to alleviate biological aging of UV-photofunctionalized titanium. *International journal of nanomedicine,* 6**,** 1327-41.

JACOBS, J. J., GILBERT, J. L. & URBAN, R. M. 1998. Corrosion of metal orthopaedic implants. *Journal of Bone and Joint Surgery-American Volume,* 80A**,** 268-282.

JAEGER, M., URSELMANN, F., WITTE, F., ZANGER, K., LI, X., JÄGER, M., AYERS, D. C. & KRAUSPE, R. 2008. Osteoblast differentiation onto different biometals with an endoprosthetic surface topographyin vitro. *Journal of biomedical materials research. Part A,* 86**,** 61-75.

JAKOBSEN, S. S., BAAS, J., JAKOBSEN, T. & SOBALLE, K. 2010. Acid etching does not improve CoCrMo implant osseointegration in a canine implant model. *Hip Int,* 20**,** 171-8.

JAMES, A. W. 2013. Review of Signaling Pathways Governing MSC Osteogenic and Adipogenic Differentiation. *Scientifica,* 2013**,** 684736.

JAYAKUMAR, P. & DI SILVIO, L. 2010. Osteoblasts in bone tissue engineering. *Proceedings of the Institution of Mechanical Engineers; Part H; Journal of Engineering in Medicine,* 224**,** 1415-1440.

JENKINS, P. J., CLEMENT, N. D., HAMILTON, D. F., GASTON, P., PATTON, J. T. & HOWIE, C. R. 2013. Predicting the cost-effectiveness of total hip and knee replacement: A health economic analysis. *The Bone & Joint Journal,* 95-B**,** 115-121.

JUNKER, R., DIMAKIS, A., THONEICK, M. & JANSEN, J. A. 2009. Effects of implant surface coatings and composition on bone integration: a systematic review. *Clinical Oral Implants Research,* 20**,** 185-206.

KAMACHIMUDALI, U., SRIDHAR, T. & RAJ, B. 2003. Corrosion of bio implants. *Sadhana,* 28**,** 601-637.

KANG, Q., SONG, W.-X., LUO, Q., TANG, N., LUO, J., LUO, X., CHEN, J., BI, Y., HE, B.-C., PARK, J. K., JIANG, W., TANG, Y., HUANG, J., SU, Y., ZHU, G.-H., HE, Y., YIN, H., HU, Z., WANG, Y., CHEN, L., ZUO, G.-W., PAN, X., SHEN, J., VOKES, T., REID, R. R., HAYDON, R. C., LUU, H. H. & HE, T.-C. 2009. A Comprehensive Analysis of the Dual Roles of BMPs in Regulating Adipogenic and Osteogenic Differentiation of Mesenchymal Progenitor Cells. *Stem Cells and Development,* 18**,** 545-558.

KASEMANANKUL, P., WITIT ANAN, N., CHAIYAKUN, S., LIMSUWAN, P. & BOONAMNUAYVITAYA, V. 2009. Low-temperature deposition of (110) and (101) rutile TiO2 thin films using dual cathode DC unbalanced magnetron

sputtering for inducing hydroxyapatite. *Materials chemistry and physics,* 117**,** 288-293.

KATTI, K. 2008. Materials for joint replacement. *In:* REVELL, P. (ed.) *Joint replacement technology.* Wooh Publishing.

KATZ, J. L. 1980. Anisotropy of Young's modulus of bone. *Nature,* 283**,** 106-107.

KEEGAN, G. M., LEARMONTH, I. D. & CASE, C. P. 2008. A systematic comparison of the actual, potential, and theoretical health effects of cobalt and chromium exposures from industry and surgical implants. *Critical Reviews in Toxicology,* 38**,** 645-674.

KHAN, M. R., DONOS, N., SALIH, V. & BRETT, P. M. 2012. The enhanced modulation of key bone matrix components by modified Titanium implant surfaces. *Bone,* 50**,** 1-8.

KILIAN, K. A., BUGARIJA, B., LAHN, B. T. & MRKSICH, M. 2010. Geometric cues for directing the differentiation of mesenchymal stem cells. *Proceedings of the National Academy of Sciences of the United States of America,* 107**,** 4872-4877.

KLUESS, D. 2008. Ceramics for joint replacement. *In:* REVELL, P. (ed.) *Joint replacement technology.* Woodhead Publishing.

KOCH, C. F., JOHNSON, S., KUMAR, D., JELINEK, M., CHRISEY, D. B., DORAISWAMY, A., JIN, C., NARAYAN, R. J. & MIHAILESCU, I. N. 2007. Pulsed laser deposition of hydroxyapatite thin films. *Materials Science and Engineering: C,* 27**,** 484-494.

KOMATH, M., VARMA, H., RAJESH, P. & MURALEEDHARAN, C. V. 2011. Pulsed laser deposition of hydroxyapatite on titanium substrate with titania interlayer. *Journal of materials science. Materials in medicine,* 22**,** 497-505.

KOMORI, T., YAGI, H., NOMURA, S., YAMAGUCHI, A., SASAKI, K., DEGUCHI, K., SHIMIZU, Y., BRONSON, R. T., GAO, Y. H., INADA, M., SATO, M., OKAMOTO, R., KITAMURA, Y., YOSHIKI, S. & KISHIMOTO, T. 1997. Targeted disruption of Cbfa1 results in a complete lack of bone formation owing to maturational arrest of osteoblasts. *Cell,* 89**,** 755-764.

KUBO, K., TSUKIMURA, N., IWASA, F., UENO, T., SARUWATARI, L., AITA, H., CHIOU, W.-A. & OGAWA, T. 2009. Cellular behavior on TiO2 nanonodular structures in a micro-to-nanoscale hierarchy model. *Biomaterials,* 30**,** 5319-29.

KURTZ, S., LAU, E., ONG, K., ZHAO, K., KELLY, M. & BOZIC, K. 2009. Future Young Patient Demand for Primary and Revision Joint Replacement: National Projections from 2010 to 2030. *Clinical orthopaedics and related research,* 467**,** 2606-2612.

KURTZ, S., ONG, K., LAU, E., MOWAT, F. & HALPERN, M. 2007a. Projections of primary and revision hip and knee arthroplasty in the United States from 2005 to 2030. *Journal of Bone and Joint Surgery; American volume,* 89**,** 780-5.

KURTZ, S., ONG, K., LAU, E., WIDMER, M., MARAVIC, M., GÃ³MEZ BARRENA, E., MANNO, V., TORRE, M., WALTER, W., DE STEIGER, R., PELTOLA, M., RÃ¶DER, C. & GEESINK, R. G. T. 2011. International survey of primary and revision total knee replacement. *International orthopaedics,* 35**,** 1783-1789.

KURTZ, S. M., ONG, K. L., SCHMIER, J., MOWAT, F., SALEH, K., DYBVIK, E., KARRHOLM, J., GARELLICK, G., HAVELIN, L. I., FURNES, O., MALCHAU, H. & LAU, E. 2007b. Future clinical and economic impact of revision total hip and knee arthroplasty. *Journal of Bone and Joint Surgery-American Volume,* 89A**,** 144-151.

LAI, M., CAI, K. Y., ZHAO, L., CHEN, X. Y., HOU, Y. H. & YANG, Z. X. 2011. Surface Functionalization of TiO2 Nanotubes with Bone Morphogenetic Protein 2 and Its Synergistic Effect on the Differentiation of Mesenchymal Stem Cells. *Biomacromolecules,* 12**,** 1097-1105.

LAN, G., LI, M., TAN, Y., LI, L., YANG, X., MA, L., YIN, Q., XIA, H., ZHANG, Y., TAN, G. & NING, C. 2015. Promoting Bone Mesenchymal Stem Cells and Inhibiting Bacterial Adhesion of Acid-Etched Nanostructured Titanium by Ultraviolet Functionalization. *Journal of Materials Science & Technology,* 31**,** 182-190.

LANEY, W. R., TOLMAN, D. E., KELLER, E. E., DESJARDINS, R. P., VANROEKEL, N. B. & BRANEMARK, P. I. 1986. DENTAL IMPLANTS - TISSUE-INTEGRATED PROSTHESIS UTILIZING THE OSSEOINTEGRATION CONCEPT. *Mayo Clinic Proceedings,* 61**,** 91-97.

LAVENUS, S., TRICHET, V., LE CHEVALIER, S., HOORNAERT, A., LOUARN, G. & LAYROLLE, P. 2012. Cell differentiation and osseointegration influenced by nanoscale anodized titanium surfaces. *Nanomedicine,* 7**,** 967-980.

LAZARINIS, S., KARRHOLM, J. & HAILER, N. P. 2010. Increased risk of revision of acetabular cups coated with hydroxyapatite A Swedish Hip Arthroplasty Register study involving 8,043 total hip replacements. *Acta Orthopaedica,* 81**,** 53-59.

LAZARINIS, S., KARRHOLM, J. & HAILER, N. P. 2011. Effects of hydroxyapatite coating on survival of an uncemented femoral stem A Swedish Hip Arthroplasty Register study on 4,772 hips. *Acta Orthopaedica,* 82**,** 399-404.

LE GUEHENNEC, L., LOPEZ HEREDIA, M.-A., ENKEL, B., WEISS, P., AMOURIQ, Y. & LAYROLLE, P. 2008. Osteoblastic cell behaviour on different titanium implant surfaces. *Acta Biomaterialia,* 4**,** 535-543.

LE GUEHENNEC, L., SOUEIDAN, A., LAYROLLE, P. & AMOURIQ, Y. 2007. Surface treatments of titanium dental implants for rapid osseointegration. *Dental Materials,* 23**,** 844-854.

LI, L.-H., KONG, Y.-M., KIM, Y.-W., KIM, H.-E., HEO, S.-J. & KOAK, J.-Y. 2004. Improved biological performance of Ti implants due to surface modification by micro-arc oxidation. *Biomaterials,* 25**,** 2867-2875.

LILJA, M., GENVAD, A., ASTRAND, M., STROMME, M., STRÃ¸MME, M., ENQVIST, H. K. & Ã…STRAND, M. 2011. Influence of microstructure and chemical composition of sputter deposited TiO2 thin films on in vitro bioactivity. *Journal of materials science. Materials in medicine,* 22**,** 2727-2734.

LIU, G., VIJAYAKUMAR, S., GRUMOLATO, L., ARROYAVE, R., QIAO, H., AKIRI, G. & AARONSON, S. 2009. Canonical Wnts function as potent regulators of osteogenesis by human mesenchymal stem cells. *The Journal of cell biology,* 185**,** 67-75.

LIU, T., YIN, B., HE, T., GUO, N., DONG, L. & YIN, Y. 2012. Complementary effects of nanosilver and superhydrophobic coatings on the prevention of marine bacterial adhesion. *ACS Appl Mater Interfaces,* 4**,** 4683-90.

LO, S. H. 2006. Focal adhesions: What's new inside. *Developmental Biology,* 294**,** 280-291.

LOGAN, N., BOZEC, L., TRAYNOR, A. & BRETT, P. 2015. Mesenchymal stem cell response to topographically modified CoCrMo. *Journal of Biomedical Materials Research Part A,* n/a-n/a.

LOGAN, N. & BRETT, P. 2013. The Control of Mesenchymal Stromal Cell Osteogenic Differentiation through Modified Surfaces. *Stem Cells Int,* 2013**,** 361637.

LOGAN, N., CROSS, A., TRAYNOR, A., BOZEC, L., PARKIN, I. & BRETT, P. 2014a. Mesenchymal stem cell response to UV-photofunctionalized TiO2coated CoCrMo. *RSC Advances,* 4**,** 59847-59857.

LOGAN, N., SHERIF, A., CROSS, A. J., COLLINS, S. N., TRAYNOR, A., BOZEC, L., PARKIN, I. P. & BRETT, P. 2014b. TiO2-coated CoCrMo: Improving the osteogenic differentiation and adhesion of mesenchymal stem cells in vitro. *Journal of Biomedical Materials Research Part A,* n/a-n/a.

LONG, P. H. 2008. Medical Devices in Orthopedic Applications. *Toxicologic Pathology,* 36**,** 85-91.

LUO, X., HE, S., LI, Z. & HUANG, D. 2011. Systematic review of cemented versus uncemented hemiarthroplasty for displaced femoral neck fractures in older patients. *Archives of Orthopaedic and Trauma Surgery,* 132**,** 455-463.

LYNN, A. K. & DUQUESNAY, D. L. 2002. Hydroxyapatite-coated Ti–6Al–4V: Part 1: the effect of coating thickness on mechanical fatigue behaviour. *Biomaterials,* 23**,** 1937-1946.

MA, W., WEI, J.-H., LI, Y.-Z., WANG, X.-M., SHI, H.-Y., TSUTSUMI, S. & LI, D.-H. 2008. Histological evaluation and surface componential analysis of modified micro-arc oxidation-treated titanium implants. *Journal of biomedical materials research. Part B, Applied biomaterials,* 86**,** 162-169.

MARYCZ, K., KRZAK, J., URBANSKI, W., PEZOWICZ, C. & URBAŃSKI, W. 2014. In Vitro and In Vivo Evaluation of Sol-Gel Derived TiO2 Coatings Based on a Variety of Precursors and Synthesis Conditions. *Journal of Nanomaterials,* 2014**,** 1-14.

MASHINCHIAN, O., TURNER, L. A., DALBY, M. J., LAURENT, S., SHOKRGOZAR, M. A., BONAKDAR, S., IMANI, M. & MAHMOUDI, M. 2015. Regulation of stem cell fate by nanomaterial substrates. *Nanomedicine,* 10**,** 829-847.

MATHIEU, P. S. & LOBOA, E. G. 2012. Cytoskeletal and Focal Adhesion Influences on Mesenchymal Stem Cell Shape, Mechanical Properties, and Differentiation Down Osteogenic, Adipogenic, and Chondrogenic Pathways. *Tissue Engineering Part B-Reviews,* 18**,** 436-444.

MCBEATH, R., PIRONE, D. M., NELSON, C. M., BHADRIRAJU, K. & CHEN, C. S. 2004. Cell shape, cytoskeletal tension, and RhoA regulate stem cell lineage commitment. *Developmental Cell,* 6**,** 483-495.

MCKEE, G. K. & WATSON FARRAR, J. 1966. Replacement of arthritic hips by the McKee-Farrar prosthesis. *The Journal of Bone and Joint Surgery. British Volume,* 48**,** 245-259.

MCKELLOP, H. A. 1995. *WEAR MODES, MECHANISMS, DAMAGE, AND DEBRIS - SEPARATING CAUSE FROM EFFECT IN THE WEAR OF TOTAL HIP REPLACEMENTS.*

MENDONÇA, D. B. S., MIGUEZ, P. A., MENDONÇA, G., YAMAUCHI, M., ARAGÃO, F. J. L. & COOPER, L. F. 2011. Titanium surface topography affects collagen biosynthesis of adherent cells. *Bone,* 49**,** 463-472.

MENDONCA, G., MENDONCA, D. B. S., ARAGAO, F. J. L. & COOPER, L. F. 2010. The combination of micron and nanotopography by H2SO4/H2O2 treatment and its effects on osteoblast-specific gene expression of hMSCs. *Journal of Biomedical Materials Research Part A,* 94A**,** 169-179.

MINAMIKAWA, H., IKEDA, T., ATT, W., HAGIWARA, Y., HIROTA, M., TABUCHI, M., AITA, H., PARK, W. & OGAWA, T. 2013. Photofunctionalization increases the bioactivity and osteoconductivity of the titanium alloy Ti6Al4V. *Journal of Biomedical Materials Research Part A***,** n/a-n/a.

MITRA, S. K., HANSON, D. A. & SCHLAEPFER, D. D. 2005. Focal adhesion kinase: in command and control of cell motility. *Nat Rev Mol Cell Biol,* 6**,** 56-68.

MIYAUCHI, T., YAMADA, M., YAMAMOTO, A., IWASA, F., SUZAWA, T., KAMIJO, R., BABA, K. & OGAWA, T. 2010. The enhanced characteristics of osteoblast adhesion to photofunctionalized nanoscale TiO2 layers on biomaterials surfaces. *Biomaterials,* 31**,** 3827-3839.

MOHSENI, E., ZALNEZHAD, E. & BUSHROA, A. R. 2014. Comparative investigation on the adhesion of hydroxyapatite coating on Ti–6Al–4V implant: A review paper. *International journal of adhesion and adhesives,* 48**,** 238-257.

MOMBELLI, A. 2002. Microbiology and antimicrobial therapy of peri-implantitis. *Periodontology 2000,* 28**,** 177-189.

MORSHED, S., BOZIC, K. J., RIES, M. D., MALCHAU, H. & COLFORD, J. M. 2007. Comparison of cemented and uncemented fixation in total hip replacement. *Acta Orthopaedica,* 78**,** 315-326.

MURRAY, C. J. L., RICHARDS, M., NEWTON, J., FENTON, K., ANDERSON, H. R., ATKINSON, C., BENNETT, D., BERNABÃ©, E., BLENCOWE, H., BOURNE, R., BRAITHWAITE, T., BRAYNE, C., BRUCE, N., BRUGHA, T., BURNEY, P., DHERANI, M., DOLK, H., EDMOND, K., EZZATI, M., FLAXMAN, A., FLEMING, T., FREEDMAN, G., GUNNELL, D., HAY, R., HUTCHINGS, S., OHNO, S., LOZANO, R., LYONS, R., MARCENES, W., NAGHAVI, M., NEWTON, C., PEARCE, N., POPE, D., RUSHTON, L., SALOMON, J., SHIBUYA, K., VOS, T., WANG, H., WILLIAMS, H., WOOLF, A., LOPEZ, A. & DAVIS, A. 2013. UK health performance: findings of the Global Burden of Disease Study 2010. *Lancet (London, England),* 381**,** 997-1020.

NAKASHIMA, K., ZHOU, X., KUNKEL, G., ZHANG, Z., DENG, J., BEHRINGER, R. & DE CROMBRUGGHE, B. 2002. The novel zinc finger-containing transcription factor osterix is required for osteoblast differentiation and bone formation. *Cell,* 108**,** 17-29.

NIE, X., LEYLAND, A., MATTHEWS, A., NIE, X. & NIE, A. 2000. Deposition of layered bioceramic hydroxyapatite/TiO2 coatings on titanium alloys using a hybrid technique of micro-arc oxidation and electrophoresis. *Surface & coatings technology,* 125**,** 407-414.

NIE, X., LEYLAND, A., MATTHEWS, A., YEROKHIN, A. L. & DOWEY, S. J. 1999. Plasma electrolysis for surface engineering. *Surface & coatings technology,* 122**,** 73-93.

OH, S., BRAMMER, K. S., LI, Y. S. J., TENG, D., ENGLER, A. J., CHIEN, S. & JIN, S. 2009. Stem cell fate dictated solely by altered nanotube dimension. *Proceedings of the National Academy of Sciences of the United States of America,* 106**,** 2130-2135.

OYA, K., TANAKA, Y., MORIYAMA, Y., YOSHIOKA, Y., KIMURA, T., TSUTSUMI, Y., DOI, H., NOMURA, N., NODA, K., KISHIDA, A. & HANAWA, T. 2010. Differences in the bone differentiation properties of MC3T3-E1 cells on polished bulk and sputter-deposited titanium specimens. *Journal of biomedical materials research. Part A,* 94**,** NA-NA.

PAREDES, V., SALVAGNI, E., RODRIGUEZ, E., GIL, F. J. & MANERO, J. M. 2014. Assessment and comparison of surface chemical composition and oxide layer modification upon two different activation methods on a cocrmo alloy. *Journal of Materials Science-Materials in Medicine,* 25**,** 311-320.

PARK, J., BAUER, S., PITTROF, A., KILLIAN, M. S., SCHMUKI, P. & VON DER MARK, K. 2012. Synergistic Control of Mesenchymal Stem Cell Differentiation by Nanoscale Surface Geometry and Immobilized Growth Factors on TiO2 Nanotubes. *Small,* 8**,** 98-107.

PARK, J., BAUER, S., SCHLEGEL, K. A., NEUKAM, F. W., VON DER MARK, K. & SCHMUKI, P. 2009. TiO2 Nanotube Surfaces: 15 nm - An Optimal Length Scale of Surface Topography for Cell Adhesion and Differentiation. *Small,* 5**,** 666-671.

PARK, J., BAUER, S., VON DER MARK, K. & SCHMUKI, P. 2007. Nanosize and vitality: TiO2 nanotube diameter directs cell fate. *Nano Letters,* 7**,** 1686-1691.

PAZ, Y., LUO, Z., RABENBERG, L. & HELLER, A. 1995. Photooxidative self-cleaning transparent titanium dioxide films on glass. *Journal of Materials Research,* 10**,** 2842-2848.

PERSTON, B., PISAL, A. 2011. *Determination of hydrocarbons in environmental samples with spectrum two* [Online]. Available: http://www.perkinelmer.co.uk/CMSResources/Images/44-130225APP_SpectrumTwoHydrocarbons.pdf [Accessed 05/11 2014].

PIERSON, H. O. 1999. *Handbook of chemical vapor deposition: principles, technology and applications*, William Andrew.

PILKINGTON. 2015. *Pilkington Activ™ Self-Cleaning Glass* [Online]. Available: http://www.pilkington.com/en-gb/uk/householders/types-of-glass/self-cleaning-glass [Accessed 10/10 2015].

PITTENGER, M. F., DOUGLAS, R., MACKAY, A. M., BECK, S. C., JAISWAL, R. K., MOSCA, J. D., MOORMAN, M. A., SIMONETTI, D. W., CRAIG, S. & MARSHAK, D. R. 1999. Multilineage potential of adult human mesenchymal stem cells. *Science,* 284**,** 143-7.

POH, C. K., SHI, Z. L., TAN, X. W., LIANG, Z. C., FOO, X. M., TAN, H. C., NEOH, K. G. & WANG, W. 2011. Cobalt Chromium Alloy with Immobilized BMP Peptide for Enhanced Bone Growth. *Journal of Orthopaedic Research,* 29**,** 1424-1430.

PULEO, D. A. & NANCI, A. 1999. Understanding and controlling the bone-implant interface. *Biomaterials,* 20**,** 2311-2321.

RAHBEK, O., OVERGAARD, S., JENSEN, T. B., BENDIX, K. & SOBALLE, K. 2000. Sealing effect of hydroxyapatite coating - A 12-month study in canines. *Acta Orthopaedica Scandinavica,* 71**,** 563-573.

REVELL, P. A. 2008. Biological causes of prosthetic joint failure. *In:* REVELL, P. A. (ed.) *Joint Replacement Technology*. Cambridge, England: Woodhead Publishing in Materials.

RIGGS, B. L., MELTON, L. J., ROBB, R. A., CAMP, J. J., ATKINSON, E. J., MCDANIEL, L., AMIN, S., ROULEAU, P. A. & KHOSLA, S. 2008. A population-based assessment of rates of bone loss at multiple skeletal sites: Evidence for substantial trabecular bone loss in young adult women and men. *Journal of Bone and Mineral Research,* 23**,** 205-214.

ROCCUZZO, M., AGLIETTA, M., BUNINO, M. & BONINO, L. 2008. Early loading of sandblasted and acid-etched implants: a randomized-controlled double-blind split-mouth study. Five-year results. *Clinical oral implants research,* 19**,** 148-152.

ROCCUZZO, M., BONINO, L., DALMASSO, P. & AGLIETTA, M. 2014. Long-term results of a three arms prospective cohort study on implants in periodontally compromised patients: 10-year data around sandblasted and acid-etched (SLA) surface. *Clinical oral implants research,* 25**,** 1105-1112.

RODRIGUEZ, J. P., GONZALEZ, M., RIOS, S. & CAMBIAZO, V. 2004. Cytoskeletal organization of human mesenchymal stem cells (MSC) changes during their osteogenic differentiation. *Journal of Cellular Biochemistry,* 93**,** 721-731.

ROSALES-LEAL, J. I., RODRIGUEZ-VALVERDE, M. A., MAZZAGLIA, G., RAMON-TORREGROSA, P. J., DIAZ RODRIGUEZ, L., ROSALES LEAL, J. I., RODRÍGUEZ VALVERDE, M. A., RAMÓN TORREGROSA, P. J., DÍAZ RODRÍGUEZ, L., GARCÍA MARTÍNEZ, O., VALLECILLO CAPILLA, M., RUIZ, C. & CABRERIZO VÍLCHEZ, M. A. 2010. Effect of roughness, wettability and morphology of engineered titanium surfaces on osteoblast-like cell adhesion. *Colloids and surfaces. A, Physicochemical and engineering aspects,* 365**,** 222-229.

ROSSI, S., TIRRI, T., PALDAN, H., KUNTSI VAATTOVAARA, H., TULAMO, R. & NÃ¤RHI, T. 2008. Peri-implant tissue response to TiO2 surface modified implants. *Clinical oral implants research,* 19**,** 348-55.

RUPP, F., SCHEIDELER, L., OLSHANSKA, N., DE WILD, M., WIELAND, M. & GEIS-GERSTORFER, J. 2006. Enhancing surface free energy and hydrophilicity through chemical modification of microstructured titanium implant surfaces. *Journal of Biomedical Materials Research Part A,* 76A**,** 323-334.

SADER, M. R., BALDUINO, A., SOARES, G. R. D. A. & BOROJEVIC, R. 2005. Effect of three distinct treatments of titanium surface on osteoblast attachment, proliferation, and differentiation. *Clinical oral implants research,* 16**,** 667-75.

SALGADO, A. J., COUTINHO, O. P. & REIS, R. L. 2004. Bone Tissue Engineering: State of the Art and Future Trends. *Macromolecular bioscience,* 4**,** 743-765.

SANGIORGIO, S., ET AL. 2013. Orthopaedic Implants. *In:* CULJAT, M. (ed.) *Medical devices: surgical and image-guided technologies.* John Wiley & Sons, Inc.

SATO, M., ASLANI, A., SAMBITO, M. A., KALKHORAN, N. M., SLAMOVICH, E. B. & WEBSTER, T. J. 2008. Nanocrystalline hydroxyapatite/titania coatings on titanium improves osteoblast adhesion. *Journal of Biomedical Materials Research Part A,* 84A**,** 265-272.

SAWASE, T., JIMBO, R., BABA, K., SHIBATA, Y., IKEDA, T. & ATSUTA, M. 2008. Photo-induced hydrophilicity enhances initial cell behavior and early bone apposition. *Clinical Oral Implants Research,* 19**,** 491-496.

SCHÄFER, C., BORM, B., BORN, S., MÖHL, C., EIBL, E.-M. & HOFFMANN, B. 2009. One step ahead: Role of filopodia in adhesion formation during cell migration of keratinocytes. *Experimental Cell Research,* 315**,** 1212-1224.

SHALABI, M. M., GORTEMAKER, A., VAN'T HOF, M. A., JANSEN, J. A. & CREUGERS, N. H. J. 2006. Implant surface roughness and bone healing: a systematic review. *Journal of Dental Research,* 85**,** 496-500.

SHI, P., NG, W. F., WONG, M. H. & CHENG, F. T. 2009. Improvement of corrosion resistance of pure magnesium in Hanks' solution by microarc oxidation with sol–gel TiO2 sealing. *Journal of alloys and compounds,* 469**,** 286-292.

SIMA, L. E., STAN, G. E., MOROSANU, C. O., MELINESCU, A., IANCULESCU, A., MELINTE, R., NEAMTU, J. & PETRESCU, S. M. 2010. Differentiation of mesenchymal stem cells onto highly adherent radio frequency-sputtered carbonated hydroxylapatite thin films. *Journal of Biomedical Materials Research Part A,* 95A**,** 1203-1214.

SIMON, U., AUGAT, P., IGNATIUS, A. & CLAES, L. 2003. Influence of the stiffness of bone defect implants on the mechanical conditions at the interface - a finite element analysis with contact. *Journal of Biomechanics,* 36**,** 1079-1086.

SINGH, R. 2011. Evaluation of the bioactivity of titanium after varied surface treatments using human osteosarcoma osteoblast cells: an in vitro study. *The International journal of oral & maxillofacial implants,* 26**,** 998-1003.

SINHA, R. K., MORRIS, F., SHAH, S. A. & TUAN, R. S. 1994. SURFACE-COMPOSITION OF ORTHOPEDIC IMPLANT METALS REGULATES CELL ATTACHMENT, SPREADING, AND CYTOSKELETAL ORGANIZATION OF PRIMARY HUMAN OSTEOBLASTS IN-VITRO. *Clinical Orthopaedics and Related Research***,** 258-272.

SJÖSTRÖM, T., DALBY, M. J., HART, A., TARE, R., OREFFO, R. O. C. & SU, B. 2009. Fabrication of pillar-like titania nanostructures on titanium and their interactions with human skeletal stem cells. *Acta Biomaterialia,* 5**,** 1433-1441.

STIEHLER, M., LIND, M., MYGIND, T., BAATRUP, A., DOLATSHAHI-PIROUZ, A., LI, H., FOSS, M., BESENBACHER, F., KASSEM, M. & BUNGER, C. 2008. Morphology, proliferation, and osteogenic differentiation of mesenchymal stem

cells cultured on titanium, tantalum, and chromium surfaces. *Journal of Biomedical Materials Research Part A,* 86A**,** 448-458.

STILLING, M., RAHBEK, O. & SØBALLE, K. 2009. Inferior Survival of Hydroxyapatite versus Titanium-coated Cups at 15 Years. *Clinical Orthopaedics and Related Research®,* 467**,** 2872-2879.

SUGITA, Y., ISHIZAKI, K., IWASA, F., UENO, T., MINAMIKAWA, H., YAMADA, M., SUZUKI, T. & OGAWA, T. 2011. Effects of pico-to-nanometer-thin TiO2 coating on the biological properties of microroughened titanium. *Biomaterials,* 32**,** 8374-84.

SURMENEV, R. A., SURMENEVA, M. A. & IVANOVA, A. A. 2014. Significance of calcium phosphate coatings for the enhancement of new bone osteogenesis – A review. *Acta Biomaterialia,* 10**,** 557-579.

SYKARAS, N., IACOPINO, A. M., MARKER, V. A., TRIPLETT, R. G. & WOODY, R. D. 2000. Implant materials, designs, and surface topographies: Their effect on osseointegration. A literature review. *International Journal of Oral & Maxillofacial Implants,* 15**,** 675-690.

SZESZ, E., DE SOUZA, G., DE LIMA, G., DA SILVA, B., KUROMOTO, N. & LEPIENSKI, C. 2014. Improved tribo-mechanical behavior of CaP-containing TiO2 layers produced on titanium by shot blasting and micro-arc oxidation. *Journal of materials science. Materials in medicine,* 25**,** 2265-2275.

TAGLIETTI, A., ARCIOLA, C. R., D'AGOSTINO, A., DACARRO, G., MONTANARO, L., CAMPOCCIA, D., CUCCA, L., VERCELLINO, M., POGGI, A., PALLAVICINI, P. & VISAI, L. 2014. Antibiofilm activity of a monolayer of silver nanoparticles anchored to an amino-silanized glass surface. *Biomaterials,* 35**,** 1779-88.

TAKAHASHI, K., TANABE, K., OHNUKI, M., NARITA, M., ICHISAKA, T., TOMODA, K. & YAMANAKA, S. 2007. Induction of pluripotent stem cells from adult human fibroblasts by defined factors. *Cell,* 131**,** 861-72.

TAKEUCHI, M., SAKAMOTO, K., MARTRA, G., COLUCCIA, S. & ANPO, M. 2005. Mechanism of photoinduced superhydrophilicity on the TiO2 photocatalyst surface. *The journal of physical chemistry. B,* 109**,** 15422-8.

TAN, H., POH, C., CAI, Y., SOE, M. & WANG, W. 2013a. Covalently grafted BMP-7 peptide to reduce macrophage/monocyte activity: An in vitro study on cobalt chromium alloy. *Biotechnology and bioengineering,* 110**,** 969-979.

TAN, H., POH, C., CAI, Y. & WANG, W. 2013b. Anti-fibrosis effect of BMP-7 peptide functionalization on cobalt chromium alloy. *Journal of Orthopaedic Research,* 31**,** 983-990.

TAYLOR, D. 2009. Long-term performance and failure of orthopaedic devices. *In:* PLANELL, J. (ed.) *Bone Repair Biomaterials.* Woodhead Publishing Limited.

TEITELBAUM, S. L. 2000. Bone resorption by osteoclasts. *Science,* 289**,** 1504-1508.

TERRIZA, A., DÍAZ-CUENCA, A., YUBERO, F., BARRANCO, A., GONZÁLEZ-ELIPE, A. R., GONZALEZ CABALLERO, J. L., VILCHES, J. & SALIDO, M. 2013. Light induced hydrophilicity and osteoblast adhesion promotion on amorphous TiO2. *Journal of Biomedical Materials Research Part A,* 101A**,** 1026-1035.

TEXTOR, M., . ET AL 2001. Properties and biological significance of natural oxide films on titanium and its alloys. *In:* TENGVALL, P., . ET AL (ed.) *Titanium in medicine.* New York: Springer.

TSARYK, R., PETERS, K., UNGER, R. E., FELDMANN, M., HOFFMANN, B., HEIDENAU, F. & KIRKPATRICK, C. J. 2013. Improving cytocompatibility of Co28Cr6Mo by TiO2 coating: gene expression study in human endothelial cells. *Journal of The Royal Society Interface,* 10**,** 20130428-20130428.

TSUKIMURA, N., KOJIMA, N., KUBO, K., ATT, W., TAKEUCHI, K., KAMEYAMA, Y., MAEDA, H. & OGAWA, T. 2008. The effect of superficial chemistry of titanium on osteoblastic function. *Journal of biomedical materials research. Part A,* 84**,** 108-16.

TSUKIMURA, N., YAMADA, M., IWASA, F., MINAMIKAWA, H., ATT, W., UENO, T., SARUWATARI, L., AITA, H., CHIOU, W.-A. & OGAWA, T. 2011. Synergistic effects of UV photofunctionalization and micro-nano hybrid topography on the biological properties of titanium. *Biomaterials,* 32**,** 4358-68.

TURKOVIC, A., IVANDA, M., DRASNER, A., VRANESA, V., PERSIN, M., TURKOVIĆ, A., DRAŠNER, A., VRANEŠA, V. & PERŠIN, M. 1991. Raman spectroscopy of thermally annealed TiO2 thin films. *Thin solid films,* 198**,** 199-205.

UENO, T., YAMADA, M., SUZUKI, T., MINAMIKAWA, H., SATO, N., HORI, N., TAKEUCHI, K., HATTORI, M. & OGAWA, T. 2010. Enhancement of bone-titanium integration profile with UV-photofunctionalized titanium in a gap healing model. *Biomaterials,* 31**,** 1546-57.

VIGUET CARRIN, S., GARNERO, P. & DELMAS, P. D. 2006. The role of collagen in bone strength. *Osteoporosis international,* 17**,** 319-336.

VLACIC-ZISCHKE, J., HAMLET, S. M., FRUS, T., TONETTI, M. S. & IVANOVSKI, S. 2011. The influence of surface microroughness and hydrophilicity of titanium on the up-regulation of TGF beta/BMP signalling in osteoblasts. *Biomaterials,* 32**,** 665-671.

WAIMANN, C., FERNANDEZ MAZARAMBROZ, R., CANTOR, S., LOPEZ OLIVO, M., ZHANG, H., LANDON, G., SIFF, S. & SUAREZ ALMAZOR, M. 2014. Cost-Effectiveness of Total Knee Replacement: A Prospective Cohort Study. *Arthritis Care & Research,* 66**,** 592-599.

WALL, I., DONOS, N., CARLQVIST, K., JONES, F. & BRETT, P. 2009. Modified titanium surfaces promote accelerated osteogenic differentiation of mesenchymal stromal cells in vitro. *Bone,* 45**,** 17-26.

WANG, B., SUN, J.-Y., QIAN, S., LIU, X.-Y., ZHANG, S.-L., DONG, S.-J. & ZHA, G.-C. 2013a. Adhesion of osteoblast-like cell on silicon-doped TiO2 film prepared by cathodic arc deposition. *Biotechnology letters,* 35**,** 975-982.

WANG, B., SUN, J., QIAN, S., LIU, X., ZHANG, S., LIU, F., DONG, S. & ZHA, G. 2012a. Proliferation and differentiation of osteoblastic cells on silicon-doped TiO(2) film deposited by cathodic arc. *Biomedicine & pharmacotherapy,* 66**,** 633-41.

WANG, H.-Y., ZHU, R.-F., LU, Y.-P., XIAO, G.-Y., ZHAO, X.-C., HE, K., YUAN, Y. F., LI, Y. & MA, X.-N. 2014a. Preparation and properties of plasma electrolytic oxidation coating on sandblasted pure titanium by a combination treatment. *Materials science & engineering. C, Biomimetic materials, sensors and systems,* 42**,** 657-664.

WANG, L., SHI, L., CHEN, J. J., SHI, Z. F., REN, L. & WANG, Y. J. 2014b. Biocompatibility of Si-incorporated TiO2 film prepared by micro-arc oxidation. *Materials Letters,* 116**,** 35-38.

WANG, Q., HU, H., QIAO, Y., ZHANG, Z. & SUN, J. 2012b. Enhanced Performance of Osteoblasts by Silicon Incorporated Porous TiO2 Coating. *Journal of materials science & technology,* 28**,** 109-117.

WANG, R., HASHIMOTO, K., FUJISHIMA, A., CHIKUNI, M., KOJIMA, E., KITAMURA, A., SHIMOHIGOSHI, M. & WATANABE, T. 1997. Light-induced amphiphilic surfaces. *Nature,* 388**,** 431-432.

WANG, X., WANG, Y., GOU, W., LU, Q., PENG, J. & LU, S. 2013b. Role of mesenchymal stem cells in bone regeneration and fracture repair: a review. *International orthopaedics,* 37**,** 2491-2498.

WEBB, J. C. J. & SPENCER, R. F. 2007. The role of polymethylmethacrylate bone cement in modern orthopaedic surgery. *The Journal of Bone and Joint Surgery. British Volume,* 89**,** 851-7.

WEBSTER, T. J. & EJIOFOR, J. U. 2004. Increased osteoblast adhesion on nanophase metals: Ti, Ti6Al4V, and CoCrMo. *Biomaterials,* 25**,** 4731-9.

WEDER, G., VOROS, J., GIAZZON, M., MATTHEY, N., HEINZELMANN, H. & LILEY, M. 2009. Measuring cell adhesion forces during the cell cycle by force spectroscopy. *Biointerphases,* 4**,** 27-34.

WENNERBERG, A. & ALBREKTSSON, T. 2009. Effects of titanium surface topography on bone integration: a systematic review. *Clinical Oral Implants Research,* 20**,** 172-184.

WENNERBERG, A. & ALBREKTSSON, T. 2010. On implant surfaces: a review of current knowledge and opinions. *The International journal of oral & maxillofacial implants,* 25**,** 63-74.

WHITE, A. 2009. Properties and characterisation of bone repair materials. *In:* PLANELL, J. (ed.) *Bone Repair Biomaterials.* Woodhead Publishing Limited.

WOLKE, J. G. C., VANDIJK, K., SCHAEKEN, H. G., DEGROOT, K. & JANSEN, J. A. 1994. Study of the Surface Characteristics of Magnetron-Sputter Calcium-Phosphate Coatings. *Journal of Biomedical Materials Research,* 28**,** 1477-1484.

WOOD, W. & MARTIN, P. 2002. Structures in focus—filopodia. *International journal of biochemistry & cell biology,* 34**,** 726-730.

WU, C. 2007. Focal Adhesion: A Focal Point in Current Cell Biology and Molecular Medicine. *Cell Adhesion & Migration,* 1**,** 13-18.

WU, K., SONG, W., ZHAO, L., LIU, M., YAN, J., KJEMS, J., GAO, S. & ZHANG, Y. 2013. MicroRNA functionalized microporous titanium oxide surface by lyophilization with enhanced osteogenic activity. *ACS applied materials & interfaces,* 5**,** 2733-44.

YAMADA, H., YOSHIHARA, Y., HENMI, O., MORITA, M., SHIROMOTO, Y., KAWANO, T., KANAJI, A., ANDO, K., NAKAGAWA, M., KOSAKI, N. & FUKAYA, E. 2009. Cementless total hip replacement: past, present, and future. *Journal of Orthopaedic Science,* 14**,** 228-241.

YAMADA, M., MIYAUCHI, T., YAMAMOTO, A., IWASA, F., TAKEUCHI, M., ANPO, M., SAKURAI, K., BABA, K. & OGAWA, T. 2010. Enhancement of adhesion strength and cellular stiffness of osteoblasts on mirror-polished titanium surface by UV-photofunctionalization. *Acta Biomaterialia,* 6**,** 4578-88.

YAMASHITA, K., ARASHI, T., KITAGAKI, K., YAMADA, S., UMEGAKI, T. & OGAWA, K. 1994. Preparation of Apatite Thin-Films through Rf-Sputtering from Calcium-Phosphate Glasses. *Journal of the American Ceramic Society,* 77**,** 2401-2407.

YAMAZAKI, M., YAMADA, M., ISHIZAKI, K. & SAKURAI, K. 2015. Ultraviolet-C irradiation to titanium implants increases peri-implant bone formation without impeding mineralization in a rabbit femur model. *Acta odontologica scandinavica,* 73**,** 302-11.

YOUREK, G., HUSSAIN, M. A. & MAO, J. J. 2007. Cytoskeletal changes of mesenchymal stem cells during differentiation. *Asaio Journal,* 53**,** 219-228.

ZHANG, B. G. X., MYERS, D., WALLACE, G., BRANDT, M., CHOONG, P. F. M., ZHANG, B. & CHOONG, P. 2014. Bioactive Coatings for Orthopaedic Implants Recent Trends in Development of Implant Coatings. *International journal of molecular sciences,* 15**,** 11878-11921.

ZHANG, W. J., LI, Z. H., LIU, Y., YE, D. X., LI, J. H., XU, L. Y., WEI, B., ZHANG, X. L., LIU, X. Y. & JIANG, X. Q. 2012. Biofunctionalization of a titanium surface with a nano-sawtooth structure regulates the behavior of rat bone marrow mesenchymal stem cells. *International Journal of Nanomedicine,* 7**,** 4459-4472.

ZHAO, G., SCHWARTZ, Z., WIELAND, M., RUPP, F., GEIS-GERSTORFER, J., COCHRAN, D. L. & BOYAN, B. D. 2005. High surface energy enhances cell response to titanium substrate microstructure. *Journal of Biomedical Materials Research Part A,* 74A**,** 49-58.

ZHOU, R., WEI, D. Q., YANG, H. Y., CHENG, S., FENG, W., LI, B. Q., WANG, Y. M., JIA, D. C. & ZHOU, Y. 2014. Osseointegration of bioactive microarc oxidized amorphous phase/TiO2 nanocrystals composited coatings on titanium after implantation into rabbit tibia. *Journal of Materials Science-Materials in Medicine,* 25**,** 1307-1318.

8. APPENDIX A – TIO2 CHAMBER POSITION TESTING

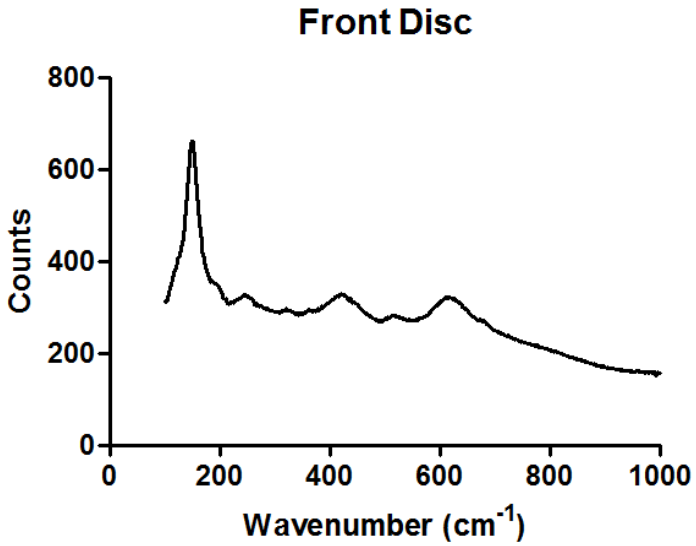

Figure 73 Raman spectra of TiO_2 on CoCrMo disc located at the front of the deposition chamber.

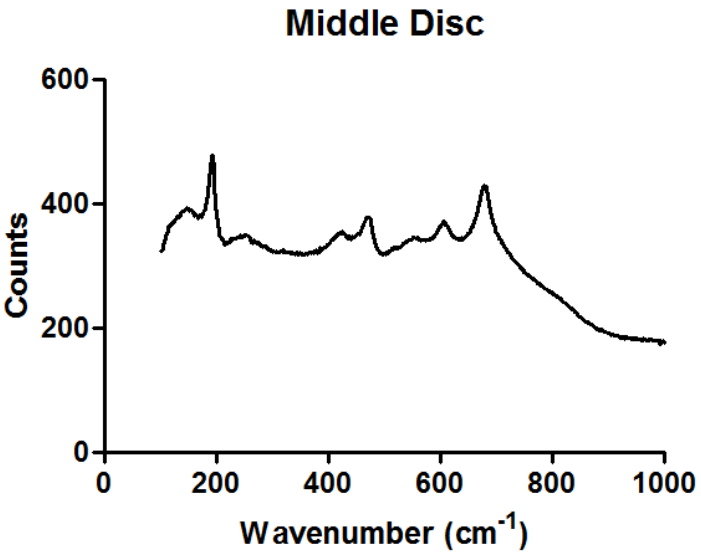

Figure 74 Raman spectra of TiO_2 on CoCrMo disc located in the middle of the deposition chamber.

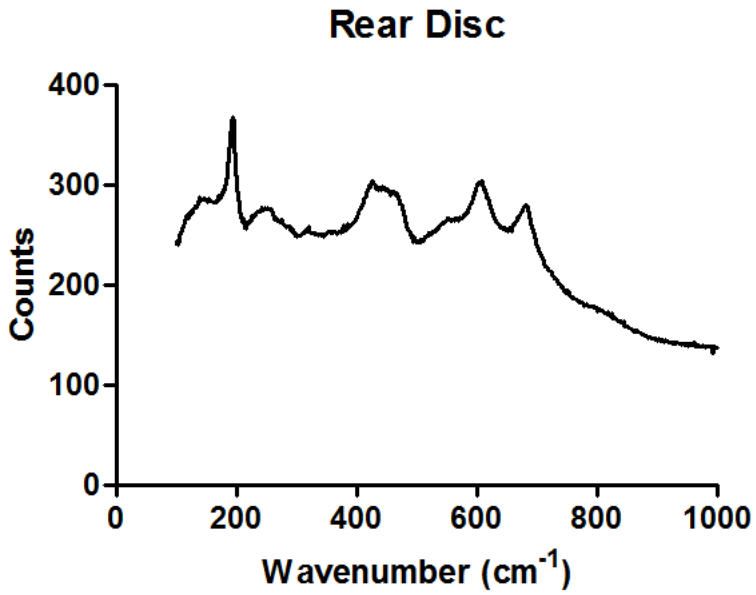

Figure 75 Raman spectra of TiO_2 on CoCrMo disc located at the rear of the deposition chamber.

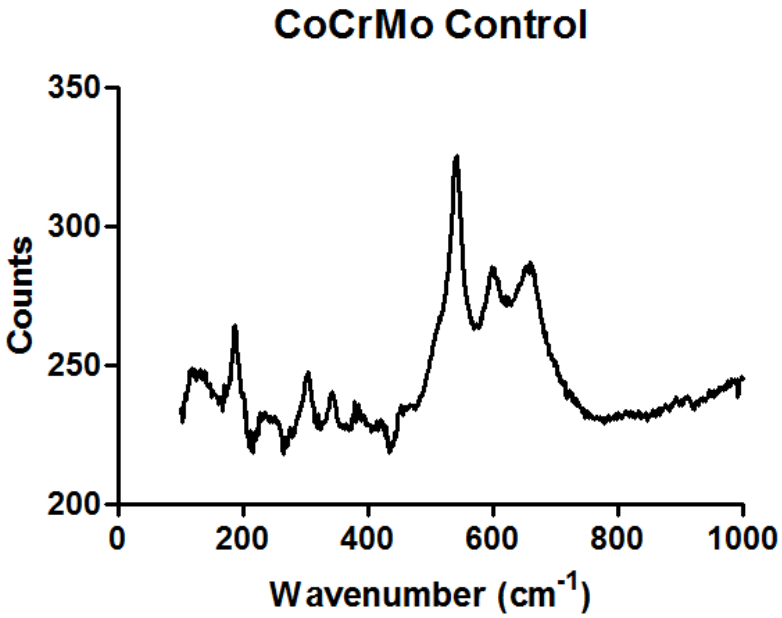

Figure 76 Raman spectra of CoCrMo SLA disc.

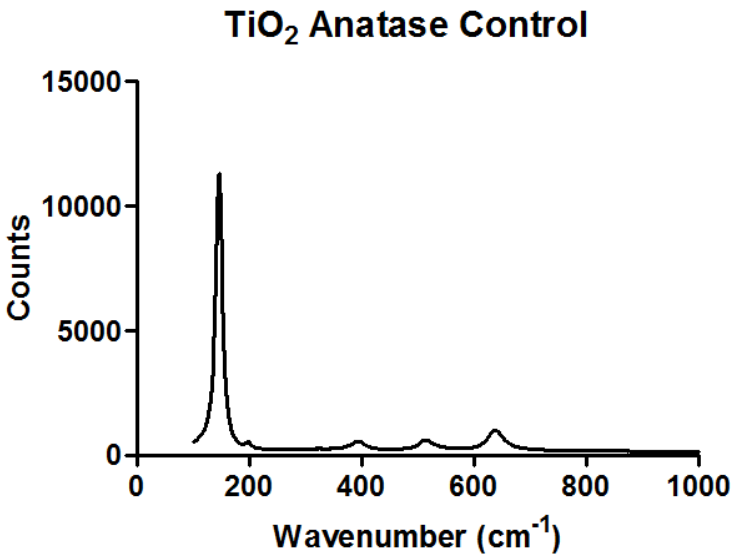

Figure 77 Raman spectra of anatase TiO_2 on smooth CoCrMo disc.

9. APPENDIX B – TI SLA MORPHOLOGY

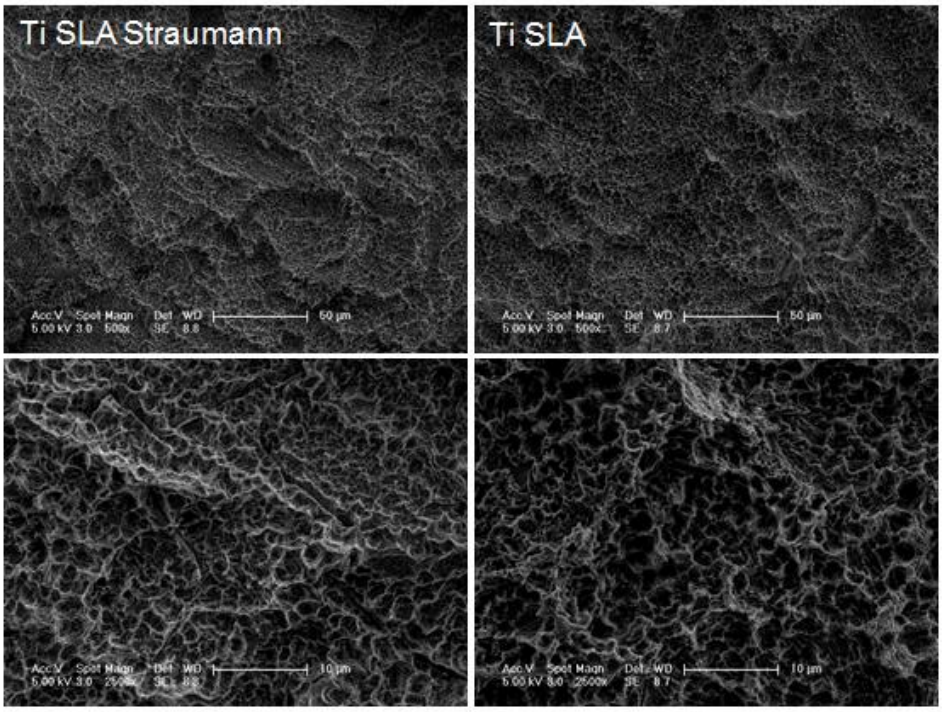

Figure 78 SEM images at low and high magnification showing similar surface morphology on SLA discs supplied by Straumann and those created at the Eastman.